

Fall 2014

# Nanotechnology and additive manufacturing platforms for clinical medicine: An investigation of 3D printing bioactive constructs and halloysite nanotubes for drug delivery and biomaterials

Jeffery A. Weisman  
*Louisiana Tech University*

Follow this and additional works at: <https://digitalcommons.latech.edu/dissertations>

 Part of the [Biomedical Engineering and Bioengineering Commons](#), [Nanoscience and Nanotechnology Commons](#), and the [Other Medicine and Health Sciences Commons](#)

---

## Recommended Citation

Weisman, Jeffery A., "" (2014). *Dissertation*. 223.  
<https://digitalcommons.latech.edu/dissertations/223>

This Dissertation is brought to you for free and open access by the Graduate School at Louisiana Tech Digital Commons. It has been accepted for inclusion in Doctoral Dissertations by an authorized administrator of Louisiana Tech Digital Commons. For more information, please contact [digitalcommons@latech.edu](mailto:digitalcommons@latech.edu).

**NANOTECHNOLOGY AND ADDITIVE MANUFACTURING  
PLATFORMS FOR CLINICAL MEDICINE: AN  
INVESTIGATION OF 3D PRINTING BIOACTIVE  
CONSTRUCTS AND HALLOYSITE NANOTUBES FOR  
DRUG DELIVERY AND BIOMATERIALS**

by

Jeffery A. Weisman J.D., M.S.

A Dissertation Presented in Partial Fulfillment  
of the Requirements of the Degree  
Doctor of Philosophy

COLLEGE OF ENGINEERING AND SCIENCE  
LOUISIANA TECH UNIVERSITY

November 2014

UMI Number: 3662483

All rights reserved

INFORMATION TO ALL USERS

The quality of this reproduction is dependent upon the quality of the copy submitted.

In the unlikely event that the author did not send a complete manuscript and there are missing pages, these will be noted. Also, if material had to be removed, a note will indicate the deletion.



UMI 3662483

Published by ProQuest LLC 2015. Copyright in the Dissertation held by the Author.

Microform Edition © ProQuest LLC.

All rights reserved. This work is protected against unauthorized copying under Title 17, United States Code.



ProQuest LLC  
789 East Eisenhower Parkway  
P.O. Box 1346  
Ann Arbor, MI 48106-1346

LOUISIANA TECH UNIVERSITY

THE GRADUATE SCHOOL

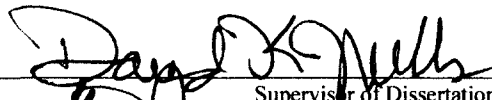
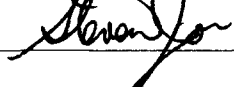
October 3, 2014

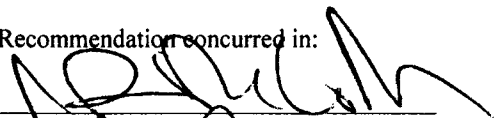
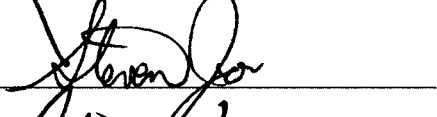

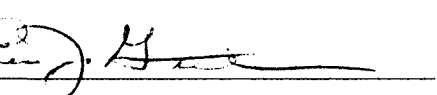
Date

We hereby recommend that the dissertation prepared under our supervision by Jeffery A. Weisman

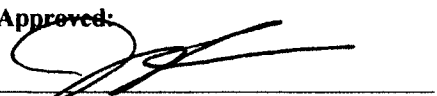
entitled NANOTECHNOLOGY AND ADDITIVE MANUFACTURING PLATFORMS FOR CLINICAL MEDICINE: AN INVESTIGATION OF 3D PRINTING BIOACTIVE CONSTRUCTS AND HALLOYSITE NANOTUBES FOR DRUG DELIVERY AND BIOMATERIALS


be accepted in partial fulfillment of the requirements for the Degree of Doctor of Philosophy in Engineering


  
\_\_\_\_\_  
Supervisor of Dissertation Research  
  
\_\_\_\_\_  
Head of Department  
Biomedical Engineering  
\_\_\_\_\_  
Department

Recommendation concurred in:  
  
\_\_\_\_\_  
  
\_\_\_\_\_  
  
\_\_\_\_\_  
  
\_\_\_\_\_

Advisory Committee

Approved:  
  
\_\_\_\_\_  
Director of Graduate Studies

Approved:  
  
\_\_\_\_\_  
Dean of the Graduate School

  
\_\_\_\_\_  
Dean of the College



## **ABSTRACT**

Personalized medicine requires the development of new technologies for controlled or targeted drug delivery. Three-dimensional (3D) printing and additive manufacturing techniques can be used to generate customized constructs for bioactive compound delivery. Nanotechnology in the form of nanoparticles, used as a stand-alone construct or for material enhancements, can significantly improve established biomaterials such as PMMA based bone cements or enable new technology to have enhanced capabilities. Combinations of the technologies can be used in such applications as infectious disease treatments, chemotherapeutic targeted drug delivery or targeted delivery of nearly any bioactive compound.

Chemotherapeutic or antibiotic enhanced 3D printing filaments were invented and designed to allow for the fabrication of antibiotic beads, drug eluting catheters, drains, stents, screws or any bioactive construct. Halloysite nanotubes (HNTs) were investigated as a modular platform and solely or in combinations were coated in metals including: iron for magnetic targeted delivery including hyperthermia, gold for laser targeted hyperthermia or barium as a contrast agent for visualization. The particles were test loaded with antibiotics or chemotherapeutics as well as coated in biocompatible coatings containing lipids or layered polyelectrolytes. Nanoparticles were added to 3D printing filaments or bone cements to test increases in strength, contrast or pore size.


3D print filaments and bioactive constructs that eluted gentamicin sulfate were tested using clinical microbiology lab standards and were shown to inhibit bacterial growth. 3D print filaments that eluted methotrexate were shown to inhibit proliferation of osteosarcoma cells and also provided a means for sustained drug release. Halloysite was successfully shown as a modular platform that could be highly customized for patient specific uses. Single coatings or combinations of magnetically susceptible iron coatings, gold coatings, drug loading of multiple bioactive compounds and biocompatible coatings were also developed. Bone cements with barium-coated particles were shown to have enhanced contrast.

The first ever ability to create and use bioactive 3D printing filaments on consumer printers was realized and HNTs were developed as proof of principle for multi-functional and real time customizable nanoparticle platforms. Nanoparticles as additives showed ways to modify established biomaterials or 3D printing filaments with enhanced features and properties.

## APPROVAL FOR SCHOLARLY DISSEMINATION

The author grants to the Prescott Memorial Library of Louisiana Tech University the right to reproduce, by appropriate methods, upon request, any or all portions of this Dissertation. It is understood that "proper request" consists of the agreement, on the part of the requesting party, that said reproduction is for his personal use and that subsequent reproduction will not occur without written approval of the author of this Dissertation. Further, any portions of the Dissertation used in books, papers, and other works must be appropriately referenced to this Dissertation.

Finally, the author of this Dissertation reserves the right to publish freely, in the literature, at any time, any or all portions of this Dissertation.

Author  \_\_\_\_\_

Date 10/03/2014

## **DEDICATION**

To my parents Sherwin Weisman and Phyllis Stern-Weisman, sister Courtney Weisman, grandparents Martin Stern, Lillian Stern, Yale Weisman and Betty Weisman.

## TABLE OF CONTENTS

ABSTRACT.....	iii
DEDICATION.....	vi
LIST OF TABLES.....	xvi
LIST OF FIGURES.....	xvii
ACKNOWLEDGMENTS.....	xxvii
CHAPTER 1 INTRODUCTION.....	1
1.1 Introduction.....	1
1.2 Grand Challenges for Engineering.....	3
1.3 Objectives.....	4
1.3.1 Creation of a Modular Nanoparticle Platform.....	5
1.3.2 Enhancing PMMA Bone Cements and 3D Printing Bone Cements.....	6
1.3.3 3D Printing Bioactive Constructs.....	6
1.4 Organization of Dissertation.....	7
CHAPTER 2 BACKGROUND.....	9
2.1 Introduction.....	9
2.2 Oncology.....	10
2.2.1 Literature Review: Osteosarcoma.....	10
2.2.2 Epidemiology.....	11
2.2.3 Presentation and Diagnosis.....	11
2.2.4 Treatment of Osteosarcoma.....	12
2.3 Infectious Disease.....	14

2.3.1	Osteomyelitis .....	14
2.3.2	Pathology .....	15
2.3.3	Acute vs. Chronic.....	15
2.3.4	Treatment Modalities .....	16
2.4	Additive Manufacturing.....	16
2.5	Halloysite Nanotechnology and Sintering.....	19
2.5.1	Halloysite Nanotubes .....	19
2.5.2	Metal Acetylacetonates .....	21
2.6	PMMA Bone Cements.....	21
<b>CHAPTER 3 HALLOYSITE NANOTUBES AS A MODULAR PLATFORM FOR NANOPARTICLE CREATION.....</b>		<b>24</b>
3.1	Introduction.....	24
3.2	Design and Objectives .....	26
3.2.1	Metal Coating Objective .....	26
3.2.2	Modular Metal Coating Objective .....	26
3.2.3	Biocompatible Coating Objective.....	26
3.2.4	Imaging and EDAX Objective.....	27
3.2.5	Magnetically Susceptible Particle Objective .....	27
3.2.6	Cytotoxicity Study Objective.....	27
3.2.7	Loading and Elution Objective .....	27
3.2.8	Improved Materials Property Objective.....	28
3.3	Materials .....	28
3.3.1	Metal Acetates and Acetylacetonates .....	29
3.3.2	Lipid Coatings.....	30
3.3.3	Polyelectrolyte LBL Coatings.....	30
3.3.4	SEM, TEM, MRI and EDAX.....	31

3.4	Fabrication and Methods .....	31
3.4.1	Metal Acetylacetonate Sintering.....	32
3.4.2	Lipid Coating .....	33
3.4.3	LBL Polyelectrolyte Coating .....	34
3.4.4	Cytotoxicity Testing.....	35
3.4.5	Vacuum Loading.....	35
3.4.6	Elution Testing.....	36
3.5	Testing and Controls .....	36
3.5.1	Nanoparticle Creation .....	37
3.5.2	Nanoparticle Imaging and Verification.....	37
3.5.3	Cell Culture Controls and Control Materials .....	37
3.5.4	Elution Testing Controls .....	37
3.5.5	MRI Imaging.....	38
3.6	Results and Discussion .....	38
3.6.1	Coating Halloysite Nanotubes .....	38
3.6.1.1	Control halloysite.....	39
3.6.1.2	Iron Acetate and Iron Acetylacetonate .....	40
3.6.1.3	Gold Acetate .....	42
3.6.1.4	Barium Acetylacetonate.....	46
3.6.1.5	Copper Acetylacetonate .....	48
3.6.1.6	Nickel Acetylacetonate .....	50
3.6.1.7	Lithium Acetylacetonate.....	52
3.6.2	Multiple and Modular Metal Coatings.....	54
3.6.2.1	Iron and gold coatings.....	55
3.6.3	Cytotoxicity Testing.....	56

3.6.4	Lipid and LBL Coatings .....	59
3.6.4.1	Lipid Bioactive Coatings .....	59
3.6.4.2	LBL Polyelectrolyte Biocompatible Coatings .....	61
3.6.5	Release Profiles.....	62
3.6.6	Barium Nanoparticle Enhanced Bone Cements.....	64
3.7	Conclusion .....	67
CHAPTER 4 3D PRINTING ANTIBIOTIC CONSTRUCTS.....		69
4.1	Introduction.....	69
4.2	Design and Objectives .....	71
4.2.1	Thermal Stability Objective .....	71
4.2.2	Filament Extrusion Objective .....	71
4.2.3	3D Printing and Additive Manufacturing Objective.....	72
4.2.4	Bacterial Testing Objective.....	72
4.2.5	Elution Testing Objective .....	72
4.2.6	Comparison With Current Standards Objective.....	72
4.2.7	Scanning Bone Defects Then Printing Plugs Objective.....	73
4.3	Materials .....	73
4.3.1	Bioplastics and Polymers .....	74
4.3.2	PMMA Bone Cements .....	75
4.3.3	Bioactive Materials .....	76
4.3.4	Halloysite Nanotubes .....	77
4.3.5	Bacterial Culture Supplies .....	78
4.3.6	Computer Modeling.....	79
4.3.7	Filament Extruder .....	79
4.3.8	3D Printers .....	80



4.3.9	3D Scanners .....	82
4.4	Fabrication and Methods .....	83
4.4.1	Bioactive Coating of Pellets.....	84
4.4.2	Layer-By-Layer Coatings .....	87
4.4.3	Atomizer Based Coating.....	88
4.4.4	Filament Extrusion.....	89
4.4.5	Construct Design and Printing.....	91
4.4.6	Bone Cement Fabrication and Molds.....	92
4.4.7	Halloysite Preparation.....	94
4.4.8	Bacterial Culture Methods .....	94
4.4.9	Imaging and Measurements of Filaments and Cultures.....	95
4.4.10	Spectrophotometry and Reagents.....	95
4.5	Testing and Controls.....	96
4.5.1	Pellet Coating and Extrusion Process .....	97
4.5.2	Printer Testing and Controls .....	98
4.5.3	Heat of Decomposition Testing .....	98
4.5.4	Bone Cement Standards.....	98
4.5.5	Bacterial Testing Controls .....	99
4.5.6	Elution Testing Controls.....	100
4.6	Results and Discussion .....	100
4.6.1	Control Bacterial Plates and Broths.....	101
4.6.2	Heated Antibiotics.....	104
4.6.2.1	Gentamicin Sulfate.....	105
4.6.2.2	Tobramycin .....	107
4.6.2.3	Nitrofurantoin .....	109

4.6.3	Pellets.....	111
4.6.3.1	Manufacturing.....	111
4.6.3.2	Control and oil-coated pellets .....	112
4.6.3.3	Gentamicin pellets .....	115
4.6.3.4	Tobramycin pellets.....	119
4.6.3.5	Nitrofurantoin pellets .....	122
4.6.3.6	HNT and HNT-GS pellets .....	123
4.6.3.7	Atomizer-coated GS Pellets.....	127
4.6.4	Extruded Filaments .....	129
4.6.4.1	Control filaments .....	130
4.6.4.2	Gentamicin filaments.....	133
4.6.4.3	Tobramycin filaments .....	138
4.6.4.4	Nitrofurantoin filaments.....	144
4.6.4.5	Halloysite filaments .....	147
4.6.4.6	Atomizer fabricated GS filaments .....	150
4.6.5	3D Fabricated Discs.....	153
4.6.5.1	Control discs .....	154
4.6.5.2	Gentamicin discs.....	157
4.6.5.3	Tobramycin discs.....	161
4.6.5.4	Nitrofurantoin discs .....	165
4.6.5.5	Halloysite discs .....	169
4.6.5.6	Atomizer-fabricated GS discs.....	172
4.6.6	Bioactive Constructs .....	174
4.6.6.1	Bio-square .....	175
4.6.6.2	Catheters .....	177

4.6.6.3	Antibiotic beads .....	182
4.6.6.4	Antibiotic beads with nanotubes.....	188
4.6.6.5	Scanning defects and printing custom inserts.....	190
4.7	Conclusion .....	194
CHAPTER 5 3D PRINTING CHEMOTHERAPEUTICS AND BONE CEMENTS....		196
5.1	Introduction.....	196
5.2	Design and Objectives .....	197
5.2.1	Thermal Stability Objective .....	198
5.2.2	Filament Extrusion Objective .....	198
5.2.3	3D Printing and Additive Manufacturing Objective.....	198
5.2.4	Cell Testing Objective .....	198
5.2.5	Elution Testing Objective .....	198
5.2.6	Optimizing Existing Materials for 3D fabrication.....	198
5.3	Materials .....	199
5.3.1	Bioplastics and Polymers.....	200
5.3.2	Bioactive Materials .....	201
5.3.3	XTT and Live/Dead assay.....	201
5.3.4	Plate Reader .....	202
5.4	Fabrication and Methods .....	203
5.4.1	PCL Extrusion and Methotrexate Printing.....	203
5.4.2	Osteosarcoma Cell Cultures.....	204
5.4.3	XTT Assay .....	204
5.4.4	Live/Dead Cytotoxicity Assay.....	204
5.4.5	Cell Culture Well Inserts.....	205
5.5	Testing and Controls.....	206

5.5.1 Pellet Coating and Extrusion Process .....	206
5.5.2 Printer Testing and Controls .....	206
5.5.3 Heat of Decomposition Testing .....	207
5.5.4 Cell Culture Controls and Control Materials .....	207
5.5.5 Elution Testing Controls .....	208
5.6 Results and Discussion .....	208
5.6.1 3D Printing Bone Cements .....	208
5.6.1.1 Bone cement filaments.....	209
5.6.1.2 3D printing bone cement filaments.....	210
5.6.1.3 Cell viability assays with bone cement filaments.....	211
5.6.2 Fabricating Methotrexate Laden Constructs.....	213
5.6.2.1 Methotrexate thermal stability testing .....	214
5.6.2.2 Methotrexate enhanced filaments .....	215
5.6.2.3 Methotrexate elution profiles.....	219
5.6.2.4 Fabrication of 3D printed methotrexate constructs.....	220
5.6.2.5 Cell assays with methotrexate enhanced filaments.....	223
5.7 Conclusion .....	227
CHAPTER 6 CONCLUSIONS AND FUTURE WORK.....	229
6.1 Conclusions.....	229
6.2 Future Work.....	231
APPENDIX A IMAGEJ ANALYSIS LIVE/DEAD ASSAYS.....	232
APPENDIX B SURFACE AREA RATIOS.....	236
APPENDIX C EDGE EFFECTS BASIC MODEL.....	237

BIBLIOGRAPHY..... 242

## LIST OF TABLES

Table 3-1: Table of bone cements' contrast level in Hounsfield Units .....	66
Table A-1: ImageJ analysis of Live/Dead assay with metal-coated HNT categories.....	232
Table A-2: ImageJ analysis of Live/Dead assay with heated MTX categories .....	234
Table A-3: ImageJ analysis of Live/Dead assay with MTX filament categories .....	235

## LIST OF FIGURES

Figure 3-1: A) iron acetate B) iron acetylacacetate [110] .....	29
Figure 3-2: DOTAP lipid structure [111] .....	30
Figure 3-3: A) PVP structure B) PAA structure [112] .....	31
Figure 3-4: Unprocessed iron-coated halloysite .....	33
Figure 3-5: Lipid coating of particles. 1) A DOTAP and chloroform/methanol solution is heated 2) The solution is vacuumed overnight to deposit the lipids 3) The nanoparticles to be coated are added and vortexed.....	34
Figure 3-6: SEM control halloysite nanotubes .....	39
Figure 3-7: TEM control halloysite nanotubes .....	39
Figure 3-8: EDAX control halloysite.....	40
Figure 3-9: SEM iron-coated halloysite.....	41
Figure 3-10: TEM iron-coated halloysite .....	41
Figure 3-11: EDAX of iron-coated halloysite .....	42
Figure 3-12: Sintering with gold acetate.....	43
Figure 3-13: SEM image of gold-coated HNTs .....	44
Figure 3-14: TEM image of gold-coated HNTs .....	44
Figure 3-15: TEM gold-coated HNTs .....	45
Figure 3-16: TEM gold-coated HNTs .....	45
Figure 3-17: EDAX gold-coated HNTs 2:1 ratio .....	46
Figure 3-18: SEM barium-coated HNTs .....	47
Figure 3-19: TEM barium-coated HNTs .....	47
Figure 3-20: EDAX barium-coated HNTS .....	48

Figure 3-21: SEM copper-coated HNTs .....	49
Figure 3-22: TEM copper-coated HNTs .....	49
Figure 3-23: EDAX copper-coated HNTs .....	50
Figure 3-24: SEM nickel-coated HNTs .....	51
Figure 3-25: TEM nickel-coated HNTs .....	51
Figure 3-26: EDAX nickel-coated HNTs .....	52
Figure 3-27: SEM lithium-coated HNTs .....	53
Figure 3-28: TEM image of lithium-coated HNTs .....	53
Figure 3-29: EDAX lithium-coated HNTs .....	54
Figure 3-30: TEM of iron/gold-coated HNT .....	55
Figure 3-31: Live/Dead assay of particles with osteoblasts in order of green live stain, red dead stain and light microscopy image at 40X. A-C) Control cells D-F) Control HNTs G-I) Lithium-coated HNTs J-L) Iron-coated HNTs .....	57
Figure 3-32: Live/Dead assay of particles with osteoblasts in order of green live stain, red dead stain and light microscopy image at 40X. A-C) Barium-coated HNTs D-F) Copper-coated HNTs G-I) Nickel-coated HNTs .....	58
Figure 3-33: TEM of lipid-coated iron sintered HNTs .....	59
Figure 3-34: TEM of lipid-coated gold sintered HNTs .....	60
Figure 3-35: TEM image of lipid-coated iron/gold sintered HNTs .....	60
Figure 3-36: TEM LBL polyelectrolyte-coating iron HNTs .....	61
Figure 3-37: A) gold-coated HNTs and B) LBL polyelectrolyte-coated, gold-coated HNTs loaded with methotrexate .....	62
Figure 3-38: Elution profile of HNTs loaded with gentamicin sulfate .....	63
Figure 3-39: Elution profile of HNTs loaded with methotrexate .....	63
Figure 3-40: Elution profile of HNTs loaded with nitrofurantoin .....	64
Figure 3-41: A) Low viscosity commercial bone cement B) High viscosity commercial bone cement C) PMMA only bone cement.....	65



Figure 3-42: A) HNT enhanced plain PMMA bone cement B) Barium-coated HNT enhanced plain PMMA bone cement.....	66
Figure 4-1: Polylactic acid structure and bag of Polylactic acid pellets[118] .....	74
Figure 4-2: Bone cement kit liquid monomer/powder and PMMA structure[120].....	75
Figure 4-3: Structures A) Gentamicin B) Tobramycin C) Nitrofurantoin[121] .....	76
Figure 4-4: SEM pictures of halloysite nanotubes.....	77
Figure 4-5: Mueller-Hinton plate, package of plates and broth bottles .....	78
Figure 4-6: Solidworks 3D CAD program interface[123].....	79
Figure 4-7: First generation Extrusionbot filament extruder[118] .....	80
Figure 4-8: A) Original Makerbot Replicator B) Makerbot Filament C) Makerbot Replicator 5 <sup>th</sup> Generation D) Makerbot Replicator 2X[124] .....	81
Figure 4-9: Roland LP-250 desktop 3D scanner.....	82
Figure 4-10: Process of coating beads with additives.....	85
Figure 4-11: Results of failure to change coating tube (left) or too much oil (right) .....	86
Figure 4-12: Individual and batch coating of beads A-B) Nitrofurantoin-PLA coat C-D) Gentamicin sulfate-PLA coat .....	86
Figure 4-13: Atomizer based coating setup A) atomizer B) syringe pump C) Erlenmeyer flask D) atomizer probe.....	88
Figure 4-14: Small batch filament extrusion with ramp .....	90
Figure 4-15: .STL files of constructs A) disc B) bead and C) catheter .....	92
Figure 4-16: PMMA bone cement molds A) 6mm Beads B) 5 mm Discs.....	93
Figure 4-17: A-B) Negative control plate C-D) Positive control plate showing bacterial lawn plates.....	102
Figure 4-18: A) Test tube broth cultures with negative control on left and positive inoculated control on right B) Close up of sterile broth C) Inoculated broth.....	103
Figure 4-19: Mueller Hinton <i>E.coli</i> plate with 100 µg gentamicin antibiotic-impregnated wafer .....	104
Figure 4-20: A) Heated gentamicin sulfate plate B) Control gentamicin plate .....	105

Figure 4-21: A) Sterile broth B) <i>E. coli</i> inoculated broth C-E) Control gentamicin powder added to inoculated broth.....	106
Figure 4-22: A) Sterile broth B) <i>E. coli</i> inoculated broth C-E) Heated gentamicin powder added to broth .....	106
Figure 4-23: A) Heated tobramycin sulfate plate B) Control tobramycin plate .....	107
Figure 4-24: A) Sterile broth B) <i>E. coli</i> inoculated broth C-E) Control tobramycin powder added to inoculated broth.....	108
Figure 4-25: A) Sterile broth B) <i>E. coli</i> inoculated broth C-E) Heated tobramycin powder added to broth .....	108
Figure 4-26: A) Control nitrofurantoin plate B) Heated nitrofurantoin plate.....	109
Figure 4-27: A) Sterile broth B) <i>E. coli</i> inoculated broth C-E) Control nitrofurantoin powder added to inoculated broth.....	110
Figure 4-28: A) Sterile broth B) <i>E. coli</i> inoculated broth C-E) Heated nitrofurantoin powder added to broth .....	110
Figure 4-29: SEM of control pellet surface .....	112
Figure 4-30: Mueller Hinton plate with PLA control pellet on left and a PLA oil-coated pellet on right.....	113
Figure 4-31: A) Sterile broth B) <i>E. coli</i> inoculated broth C-E) PLA control pellet in broth culture .....	114
Figure 4-32: A) Sterile broth B) <i>E. coli</i> inoculated broth C-E) PLA oil-coated pellet in broth culture.....	115
Figure 4-33: A) 1 wt% PLA-coated pellet B) 2.5 wt% PLA-coated pellet C) SEM of gentamicin sulfate powder D) SEM of gentamicin sulfate-coated pellet. ....	116
Figure 4-34: A) 1 wt% gentamicin-coated pellet B) 2.5 wt% gentamicin-coated pellet.....	117
Figure 4-35: A) Sterile broth B) <i>E. coli</i> inoculated broth C-E) PLA 1 wt% gentamicin-coated pellet in broth culture .....	118
Figure 4-36: A) Sterile broth B) <i>E. coli</i> inoculated broth C-E) PLA 2.5 wt% gentamicin-coated pellet in broth culture .....	118
Figure 4-37: A) SEM of tobramycin) 1 wt% tobramycin PLA-coated pellet C) 2.5 wt% tobramycin PLA-coated pellet.....	119
Figure 4-38: A) 1 wt% tobramycin-coated pellet B) 2.5 wt% tobramycin-coated pellet	120

Figure 4-39: A) Sterile broth B) <i>E. coli</i> inoculated broth C-E) PLA 1 wt% tobramycin-coated pellet in broth culture .....	121
Figure 4-40: A) Sterile broth B) <i>E. coli</i> inoculated broth C-E) PLA 2.5 wt% tobramycin-coated pellet in broth culture .....	121
Figure 4-41: A) nitrofurantoin powder B) 1 wt% PLA pellet coated in nitrofurantoin..	122
Figure 4-42: A) sterile broth B) <i>E. coli</i> inoculated broth C-E) PLA 1 wt% nitrofurantoin-coated pellet in broth culture F) PLA pellet coated in 1 wt% nitrofurantoin .....	123
Figure 4-43: A) 1.5 wt% gentamicin loaded HNT-coated PLA pellet B) 10 wt% HNT-coated PLA pellet C) SEM of HNT-coated pellet.....	124
Figure 4-44: A) 10 wt% HNT-coated PLA pellets on Mueller Hinton plate B) 1.5 wt% gentamicin loaded HNT-coated PLA pellets on Mueller Hinton plate .....	125
Figure 4-45: A) Sterile broth B) <i>E. coli</i> inoculated broth C-E) 10 wt% HNT-coated PLA pellet in broth culture .....	126
Figure 4-46: A) sterile broth B) <i>E. coli</i> inoculated broth C-E) 1.5 wt% gentamicin loaded HNT-coated PLA pellet in broth culture.....	126
Figure 4-47: A) Photograph of atomizer-coated PLA pellet B) SEM of atomizer- coated PLA pellet.....	127
Figure 4-48: A) Atomizer-coated pellet B) Atomizer-coated pellet.....	128
Figure 4-49: A) Sterile broth B) <i>E. coli</i> inoculated broth C-E) 1 wt% gentamicin atomizer-coated PLA pellet in broth culture.....	128
Figure 4-50: A) PMMA filament B) SEM of PMMA filament C) Control PLA filament D) SEM of control PLA filament .....	130
Figure 4-51: A) PMMA control top B) PMMA control bottom C) PLA and oil-coated PLA controls top D) PLA and oil-coated PLA controls bottom.....	131
Figure 4-52: A) Sterile broth B) <i>E. coli</i> inoculated broth C-E) PMMA control filament in broth culture.....	132
Figure 4-53: A) Sterile broth B) <i>E. coli</i> inoculated broth C-E) PLA filament in broth culture .....	132
Figure 4-54: A) Sterile broth B) <i>E. coli</i> inoculated broth C-E) Oil-coated PLA filament in broth culture.....	133

Figure 4-55: Photographs and SEM images for A) 1 wt% gentamicin PMMA filament B) 1 wt% gentamicin PLA filament C) 2.5 wt% gentamicin PLA filament D) SEM 1 wt% gentamicin PLA filament E) SEM 2.5 wt% gentamicin PLA filament.....	134
Figure 4-56: Agar plate with A) 2.5 wt% gentamicin PLA filament B) control PLA filament C) control PMMA filament D) 2.5 wt% gentamicin PMMA filament .....	135
Figure 4-57: Agar plate with A-C) 1 wt% gentamicin PLA filament D) 1 wt% gentamicin PMMA filament .....	136
Figure 4-58: Broth cultures for A) Sterile broth B) <i>E. coli</i> inoculated broth C) Control PMMA D) Control PLA E) 2.5 wt% gentamicin-doped PMMA F) 2.5 wt% gentamicin-doped PLA .....	137
Figure 4-59: Broth cultures for A) Sterile broth B) <i>E. coli</i> inoculated broth C-E) 1 wt% gentamicin-doped PLA filaments.....	137
Figure 4-60: Broth cultures for A) Sterile broth B) <i>E. coli</i> inoculated broth C-E) 1 wt% gentamicin-doped PMMA filaments .....	138
Figure 4-61: Photographs and SEM images of A) 1 wt% tobramycin-doped PMMA B) 1 wt% tobramycin-doped PLA C) SEM 1 wt% tobramycin-doped PLA.....	139
Figure 4-62: A) 2.5 wt% tobramycin PLA filament B) 1 wt% tobramycin PLA C) 2.5 wt% tobramycin PLA filament D) 1 wt% tobramycin PLA filament .....	140
Figure 4-63: A) 1 wt% tobramycin PMMA filament B) 2.5 wt% tobramycin PMMA filament .....	141
Figure 4-64: A) Sterile broth B) <i>E. coli</i> inoculated broth C-E) 1 wt% tobramycin doped PLA filaments .....	142
Figure 4-65: A) Sterile broth B) <i>E. coli</i> inoculated broth C-E) 1 wt% tobramycin doped PMMA filaments.....	142
Figure 4-66: A) Sterile broth B) <i>E. coli</i> inoculated broth C-E) 2.5 wt% tobramycin doped PLA filaments .....	143
Figure 4-67: A) Sterile broth B) <i>E. coli</i> inoculated broth C-E) 1 wt% tobramycin doped PMMAA filaments.....	143
Figure 4-68: A) Nitrofurantoin filament.....	144
Figure 4-69: Plates are divided into quadrants with filament with top left being control PMMA, top right being nitrofurantoin 1 wt% PMMA, bottom left nitrofurantoin 1 wt% PLA and bottom right control PLA and oil-coated PLA filaments.....	145

Figure 4-70: A) Sterile broth B) <i>E. coli</i> inoculated broth C-E) 1 wt% nitrofurantoin doped PLA filaments .....	146
Figure 4-71: A) Sterile broth B) <i>E. coli</i> inoculated broth C-E) 1 wt% nitrofurantoin doped PMMA filaments.....	147
Figure 4-72: A) 7.5 wt% HNT loaded with gentamicin PLA filament B) 1.5 wt% HNT loaded with gentamicin PLA filament C) 10 wt% HNT PLA filament D) SEM 1.5 wt% HNT loaded with gentamicin filament.....	148
Figure 4-73: A) 10 wt% HNT-PLA filament B-C) 1.5 wt% HNT loaded with gentamicin PLA filament.....	148
Figure 4-74: A) Sterile broth B) <i>E. coli</i> inoculated broth C-E) 10 wt% HNT doped PLA filaments .....	149
Figure 4-75: A) Sterile broth B) <i>E. coli</i> inoculated broth C-E) 1.5 wt% gentamicin loaded HNT doped PLA filaments .....	150
Figure 4-76: A) Atomizer based gentamicin PLA filament B) SEM of atomizer manufacturing method filament.....	151
Figure 4-77: A-D) 1 wt% atomizer-coated gentamicin doped PLA filaments .....	152
Figure 4-78: A) sterile broth B) <i>E. coli</i> inoculated broth C-E) 1 wt% atomizer-coated gentamicin doped PLA filaments.....	152
Figure 4-79: PMMA bone cement test disc mold.....	154
Figure 4-80: A) PLA control disc B) PMMA control disc .....	155
Figure 4-81: A) Control PMMA disc B) Control PLA disc .....	155
Figure 4-82: A) Sterile broth B) <i>E. coli</i> inoculated broth C-E) Control PMMA discs...	156
Figure 4-83: A) Sterile broth B) <i>E. coli</i> inoculated broth C-E) Control PLA discs .....	156
Figure 4-84: A) 1 wt% gentamicin PMMA disc B) 1 wt% gentamicin PLA disc.....	157
Figure 4-85: PMMA 1 wt% gentamicin disc b) PLA 1 wt% gentamicin disc .....	158
Figure 4-86: A) PMMA 2.5 wt% gentamicin disc B) PLA 2.5 wt% gentamicin disc C) Control PMMA disc D) Control PLA disc .....	159
Figure 4-87: A) Sterile broth B) <i>E. coli</i> inoculated broth C-E) 1 wt% gentamicin PMMA discs .....	159
Figure 4-88: A) Sterile broth B) <i>E. coli</i> inoculated broth C-E) 1 wt% gentamicin PLA discs .....	160

Figure 4-89: A) Sterile broth B) <i>E. coli</i> inoculated broth C-E) 2.5 wt% gentamicin PMMA discs .....	160
Figure 4-90: A) Sterile broth B) <i>E. coli</i> inoculated broth C-E) 2.5 wt% gentamicin PLA discs .....	161
Figure 4-93: A) Sterile broth B) <i>E. coli</i> inoculated broth C-E) 1 wt% tobramycin PMMA discs .....	164
Figure 4-94: A) Sterile broth B) <i>E. coli</i> inoculated broth C-E) 1 wt% tobramycin PLA discs .....	164
Figure 4-95: A) Sterile broth B) <i>E. coli</i> inoculated broth C-E) 2.5 wt% tobramycin PMMA discs .....	165
Figure 4-96: A) Sterile broth B) <i>E. coli</i> inoculated broth C-E) 2.5 wt% tobramycin PLA discs .....	165
Figure 4-97: Bacterial plates of nitrofurantoin discs divided in quadrants. Top left: control PMMA; Top right: 1 wt% nitrofurantoin-laden PMMA disc; Bottom left: 1 wt% nitrofurantoin-laden PLA disc; Bottom right: control PLA disc .....	166
Figure 4-100: A) Sterile broth B) <i>E. coli</i> inoculated broth C-E) 1 wt% nitrofurantoin PLA discs .....	168
Figure 4-101: A) 1.5 wt% HNT loaded with gentamicin disc B) 7.5 wt% HNT loaded with gentamicin disc .....	170
Figure 4-102: A) Sterile broth B) <i>E. coli</i> inoculated broth C-E) 1.5 wt% HNT loaded with GS PLA discs .....	170
Figure 4-103: A) Sterile broth B) <i>E. coli</i> inoculated broth C-E) 7.5 wt% HNT loaded with GS PLA discs .....	171
Figure 4-105: A) 1 wt% gentamicin PLA test disc made with atomizer-coated pellets .....	173
Figure 4-106: A) Sterile broth B) <i>E. coli</i> inoculated broth C-E) 1 wt% gentamicin disc made by atomizer method .....	173
Figure 4-107: 1 wt% gentamicin PLA construct .....	174
Figure 4-108: A) Bio-square print file B) 1 wt% nitrofurantoin bio-square.....	175
Figure 4-109: A) Control 100 µg gentamicin wafer B) 1 wt% gentamicin-laden PLA bio-square C) control PLA bio-square .....	176
Figure 4-110: Partial HNT enhanced PLA dog bone print.....	177

Figure 4-111: A) .STL file catheter B-C) 1 wt% gentamicin laden PLA catheter .....	178
Figure 4-112: A-B) SEM of catheter and embedded antibiotics .....	178
Figure 4-113: Top row) Control PLA catheters; Bottom row) 1 wt% gentamicin PLA catheters.....	179
Figure 4-114: A) Control PLA catheters B) 1 wt% gentamicin PLA catheters.....	180
Figure 4-115: A) Sterile broth B) <i>E. coli</i> inoculated broth C-E) Control PLA catheters .....	180
Figure 4-116: A) Sterile broth B) <i>E. coli</i> inoculated broth C-E) 1 wt% gentamicin PLA catheters.....	181
Figure 4-117: Elution profile 1wt% GS-PLA catheter .....	182
Figure 4-118: A) 3D printed mold B) Silicone rubber mold .....	183
Figure 4-119: A) Printing antibiotic bead B) Antibiotic bead compared to coin .....	183
Figure 4-120: A) Control PLA 3D printed bead B) 1 wt% gentamicin PLA 3D printed bead.....	184
Figure 4-121: A-B) SEM 1 wt% gentamicin PLA 3D printed bead.....	184
Figure 4-122: A) Control beads B) 1 wt% gentamicin PLA 3D printed bead C) 1 wt% PMMA-molded bead .....	185
Figure 4-123: A) Sterile broth B) <i>E. coli</i> inoculated broth C-E) control PMMA- molded bead .....	185
Figure 4-124: A) Sterile broth B) <i>E. coli</i> inoculated broth C-E) 1 wt% gentamicin PMMA molded bead.....	186
Figure 4-125: A) Sterile broth B) <i>E. coli</i> inoculated broth C-E) control PLA 3D- fabricated beads .....	186
Figure 4-126: A) Sterile broth B) <i>E. coli</i> inoculated broth C-E) 1 wt% gentamicin PLA 3D fabricated bead.....	187
Figure 4-127: 7.5 wt% HNT loaded with gentamicin PLA 3D-printed bead.....	188
Figure 4-128: A) 7.5 wt% HNT loaded gentamicin PLA 3D-fabricated bead .....	189
Figure 4-129: A) Sterile broth B) <i>E. coli</i> inoculated broth C-E) 7.5 wt% HNT loaded gentamicin PLA 3D-fabricated bead.....	189
Figure 4-130: A) Irregular shaped bone defect B) 6mm hole defects .....	190

Figure 4-131: Bone 360 degree scan with all four defects .....	191
Figure 4-132: A) 6 mm bone defect B) Entire femur portion.....	191
Figure 4-133: Irregular bone defect computer model .....	192
Figure 4-134: Printed irregular defect gentamicin (gray) control (white) .....	192
Figure 4-135: A) Femur with irregular defect B) Femur with 1 wt% gentamicin-PLA fitted insert C) Femur with control PLA fitted insert.....	193
Figure 4-136: A) 6 mm control plug B) 6 mm control plug fitted into cow femur .....	193
Figure 5-1: PCL container, pellet and molecular structure[125] .....	200
Figure 5-2: Methotrexate structure and powder [126] .....	201
Figure 5-3: XTT Reagent Salt.....	202
Figure 5-4: Thermo Scientific Plate Reader .....	203
Figure 5-5: 96 well with inserted pellets, filaments and discs .....	205
Figure 5-6: A) Bosworth PMMA only powder B) Commercial PMMA bone cement ..	209
Figure 5-7: A) Kyphos bone cement filament B) Bosworth PMMA powder only filament C) SEM of Kyphos bone cement filament D) SEM of Bosworth PMMA powder only filament .....	210
Figure 5-8: A) Bosworth PMMA-only disc B) Bosworth PMMA-only bead .....	211
Figure 5-9: Live/Dead Assay A) Control well B) PLA filament well C) Bosworth PMMA-only filament well D) Kyphos commercial bone cement well .....	212
Figure 5-11: XTT table showing percent activity.....	214
Figure 5-12: Live/Dead cytotoxicity assays (A) Control well (B) Control methotrexate (C) Heated methotrexate .....	215
Figure 5-13: A) 2.5 wt% PLA pellet B) 1 wt% PCL-coated pellets.....	215
Figure 5-14: A-B) Methotrexate powder SEM.....	216
Figure 5-15: A) PLA pellet B) 2.5 wt% MTX-coated PLA pellet C) 1 wt% PCL pellet D) MTX-coated PCL pellet.....	217
Figure 5-16: (A) 2.5 wt% methotrexate PLA filament (B) SEM of 2.5 wt% methotrexate PLA filament.....	218



Figure 5-17: A) Control PCL filament B) SEM control PCL filament .....	218
Figure 5-18: A) 1 wt% MTX PCL filament B) SEM of 1 wt% MTX PCL filament .....	219
Figure 5-19: Elution Profile of 2.5wt% MTX-PLA filament .....	220
Figure 5-20: A) 2.5 wt% MTX PLA stent B) 2.5 wt% MTX PLA disc .....	221
Figure 5-21: Comparison between gentamicin and methotrexate laden beads. Left: gentamicin-laden bead; Right: methotrexate-laden bead.....	222
Figure 5-22: SEM of methotrexate laden 6 mm bead.....	223
Figure 5-24: Live/Dead assay green live component A) Control B) PLA control pellet C) PLA pellet oil-coated D) PLA pellet coated MTX E) PLA filament F) 2.5 wt% MTX-PLA filament .....	225
Figure 5-25: Live/Dead assay red dead component A) Control B) PLA control pellet C) PLA pellet oil-coated D) PLA pellet coated MTX E) PLA filament F) 2.5 wt% MTX-PLA filament .....	226
Figure C-1: Model of square sides and corners .....	238
Figure C-2: Test Disc Elution Field.....	239
Figure C-3: Biosquare Elution Field.....	240

## ACKNOWLEDGMENTS

First and foremost, I have to thank Dr. David Mills, my mentor, for providing me this opportunity and his guidance. Dr. Mills has always believed in the potential of his students and encourages them to chart their own course. He allowed me the proper space in which to develop my own ideas and grow as a scientist.

None of this would have been possible without the love and support of my family. I am truly lucky to have an amazing family that has always encouraged my extended journey as a student. Without the extensive support of my parents, Phyllis Stern-Weisman and Sherwin Weisman, none of this would have been possible. They have always encouraged my interest in the sciences and I cannot put into words the amount of assistance they have given me during my research. My sister Courtney Weisman, grandparents Martin and Lillian Stern as well as Yale and Betty Weisman have always shown a great amount of interest, love and support in my endeavors. I also have to thank my cousin, Dr. Nancy Pleshko, who has always been available to help answer my many questions.

The success of my work was only due to being part of a skilled team and great lab group. We accomplished much. I have to especially thank Udayabhanu Jammalamadaka, Karthik Tappa and Connor Nicholson for their hard work, late nights and rapid pace we kept on this project.

# CHAPTER 1

## INTRODUCTION

### 1.1 Introduction

There is a need in clinical medicine for the development of new patient specific technologies for the treatment of illness using controlled drug delivery systems or replacement of damaged tissue with biocompatible alternatives. Researchers have discovered drugs that can treat many clinical conditions but challenges remain in targeting them at the proper concentrations, and to the proper location, *in-vivo*. Surgeons need improved biomaterials to repair the body or to reduce the risk of infection. Physicians note the need for both patient specific medicine and improved drug targeting.

Numerous medical conditions require treatments delivered to specific areas of the body. Localized infectious diseases include bacterial or fungal infections such as *Staphylococcus* or *Aspergillus*. One specific example of this problem is in orthopedics. Hip and knee replacements have a 1% failure by infection rate.[1] Additionally, up to 40,000 prosthetic failures annually require hospitalizations and additional procedures costing from \$30,000 to \$100,000 per patient.[2] Cancer can be localized or metastasize and become systemic. Certain populations of cells within the body can have a mutation that prevents proper functioning as in the case of cystic fibrosis.[3] There are many ways to treat these conditions. Chemotherapeutics can stop or eliminate cancer growth.[4]

Antibiotics can kill a bacterial infection or slow bacterial growth to allow the body's immune system to mobilize.[5] Gene therapy can modify the DNA of damaged cells and allow for proper proteins to be created.[6] The challenges involve proper delivery. Many current treatments are systemic. In systemic delivery a compound is delivered to the entire body. A much larger amount than is needed must be introduced resulting in such negative side effects as nephrotoxicity or hepatotoxicity.[7] A localized dosage or ability to target a treatment with a specific compound can prevent systemic damage.

Additionally, targeted drug delivery provides the capability for compounds that were previously found to be ineffective due to toxicity and efficacy levels to be re-investigated for treatment. There is current research into targeted drug delivery and many results have been achieved using such techniques as antibodies, carrier proteins or lipid coats.

Biomaterials are another area of medical interest that has seen recent innovations. The original materials such as bone cement, Plexiglass®, or titanium screws have given way to new smart materials.[8] These materials include resorbable screws made from bioplastics and tissues grown from a patient's cells.[9] There are additional possibilities to use biomaterials for localized drug delivery or in sensor systems to monitor a patient's health.

Nanotechnology is becoming quickly integrated into the medical field to more precisely target drug delivery or create biomaterials with novel properties.[10] Carbon nanotubes have been heavily investigated and new technologies as well as methods to adapt them are relevant areas of research.[11] These technologies can be costly to work with.[12] Halloysite shows promise as an adaptable platform for controlled drug delivery and creation of biomaterials with increased strength.[13]

Additive manufacturing is an emerging field in biomedicine that is developing new fabrication techniques.[14] Recent advances in additive manufacturing are focusing on biomedical applications.[15] Old biomaterials have the potential to be repurposed with new manufacturing processes. Novel capabilities may be achieved by applying 3D fabrication to create smart biomaterials.

The questions that this type of research seeks to answer involve looking to new possibilities for targeted treatments, developing novel nanotechnology platforms that can be adapted, enhancing existing biomaterials as well as developing new additive manufacturing techniques that can work with new or existing biomaterials.

## **1.2 Grand Challenges for Engineering**

The United States National Academy for Engineering looked at several key challenges facing humanity at the turn of the century.[16] The Academy evaluated how engineering and scientific research over the previous century had led to the betterment of society. Based on the needs of humanity and the current level of technology fourteen key areas of need or “Grand Challenges” were developed in 2008 that could help to define the next century.[16] These challenges covered a wide range of engineering disciplines and require interdisciplinary collaborations in many cases. The challenges include such needs as creating viable fusion technology, making solar power economical, new technologies to handle urban infrastructure and universal access to clean water.

Two of these challenges related to clinical medicine in the need for 1) better health informatics and 2) engineering better medicines. These two challenges are highly related and have the potential to lead to a higher quality of and more personalized care.

Health informatics is a diverse challenge. It covers the creation of electronic and universally accessible health records that can provide real time information to any health care professional. This additionally creates the possibility for systems that can monitor individual patient health and make suggestions to prevent disease. On a societal level this can lead to the tracking of epidemics to large-scale regional or demographic issues in health. To reach this point specialized computer systems that can process the data will be needed. Personalized data may need to be collected in more efficient manners that require specialized sensors or monitoring technology. This could be wearable technology or implantable nano-sensors that can provide real time data feeds.

Engineering better medicines or those that are personalized will be required to implement the knowledge of improved health informatics. Technologies will be needed for delivering patient specific drugs to regions of the body where a disease exists or to prevent one from developing. Nanotechnologies that could be custom built and directed to a targeted area could give localized drug dosages. Monitoring antibiotic usage and only using it in directed manners could reduce bacterial resistance. Building medical devices or implants by custom compounding drugs for a specific patient could fulfill this need.

The creation of custom nanoparticles and combinations of novel additive manufacturing processes can provide pathways for these two linked challenges to effect real changes in the quality of care received by patients.

### **1.3 Objectives**

This project will have a diverse range of objectives with a unified goal of advancing personalized medicine by focusing on targeted drug delivery and the

optimization of biomaterials. The follow three objectives will be the core focus of this project:

- Objective 1: The creation of a modular nanoparticle platform for drug delivery using halloysite nanotubes
- Objective 2: Using halloysite as a modular platform to enhance poly(methyl methacrylate) (PMMA) bone cements as well as 3D printing bone cements
- Objective 3: The 3D printing of a biocompatible composite material with bioactive additives

These objectives will advance the fields of controlled drug delivery and biomaterials to result in more patient specific medical treatments.

### 1.3.1 Creation of a Modular Nanoparticle Platform

Halloysite nanotubes will be used as a model for the creation of modular nanoparticle platforms for drug delivery and biomaterial enhancements. Various metals and compounds will be used to coat the surface or lumen of the tubes. The coatings will be done solely or in combination. The goal will be to create novel material properties such as responsiveness to magnetic fields or gold particles for potential laser induced hyperthermia. Bioactive compounds or dyes will be loaded into the lumen or on the surface of these particles. They will then be coated in biocompatible lipid or polyelectrolyte shells.

It is hypothesized that based upon the unique properties of halloysite that the nanotubes will act as a modular platform that can be fabricated to desired specifications.

This objective will be tested through the creation of nanoparticles with different coatings, nanoparticles doped with compounds or nanoparticles encased in biocompatible coatings. Imaging will be done to confirm construction of the particles with transmission electron or scanning electron microscopy. Elution studies will be done to compare

bioactive compound release over time. Cytotoxicity studies will be done on certain particle types as necessary.

### 1.3.2 Enhancing PMMA Bone Cements and 3D Printing Bone Cements

PMMA bone cements will be enhanced with nanoparticles or additives to enhance their material or drug eluting properties. Barium coated halloysite nanotubes will be created and tested when added to PMMA bone cements to show both increased strength and contrast on imaging. Halloysite nanotubes will also be tested as a potential solution to losses in strength shown by commercial bone cements when mixed with chemotherapeutics.

It is hypothesized that increased contrast for imaging or strength for drug delivery can be achieved in bone cements by the addition of halloysite nanotubes. Creating novel halloysite particles and mixing them with bone cements will test these hypotheses. All materials will be imaged by magnetic resonance imaging or scanning electron microscopy.

### 1.3.3 3D Printing Bioactive Constructs

Methods of 3D printing and additive manufacturing technology will be researched with the objective of developing a method to 3D print a bioactive construct using any consumer 3D printer. Methods of extruding printable bioactive filaments will be developed and demonstrated that have a uniform dispersion of additives. This goal will focus on antibiotic and chemotherapeutic based filaments. The goal will include the capability to print any 3D construct including but not limited to test discs, beads and catheters. Additionally, this project will look at methods to 3D scan bone defects to print a filler construct with bioactive compounds. A focus will be made on biodegradable



materials such as bioplastics that can be resorbed by the body but will also look at established materials such as PMMA bone cements.

It is hypothesized that it is possible to use 3D fabrication methods to print constructs without the thermal degradation of antibiotic or chemotherapeutics. Creating a filament extrusion device and extrusion method will test this hypothesis. Bioactive compounds will be heated to the extrusion and or 3D print temperature as necessary to show continued bioactivity or lack of degradation. Antibiotic filaments will be tested in bacterial broth or plate cultures to International Organization for Standardization (ISO) testing standards. Cell culture testing will be done to show the toxicity of extruded PMMA bone cement filaments or those with chemotherapeutic additives. Bioactive constructs will be printed and then tested as necessary. Imaging of all filaments and constructs will occur.

#### **1.4 Organization of Dissertation**

This dissertation comprises six chapters. Chapter One is a brief introduction of current issues in drug delivery and additive manufacturing that states the objectives of the project. Chapter Two is a detailed review of prior literature and the state of technology in nanoparticle creation, PMMA bone cements or related biomaterials and additive manufacturing methods. Chapter Three focuses on halloysite nanotubes as a potential modular platform for custom nanoparticle creation including properties such as magnetic control, contrast or bioactive substance loading. Chapter Four focuses on novel additive manufacturing techniques that involve creating custom 3D printing filaments with bioactive antibiotic additives and testing them with bacterial or cell cultures. Chapter

Five investigates 3D printing chemotherapeutics and bone cements. Chapter Six draws conclusions on these technologies and discusses future work.

## **CHAPTER 2**

### **BACKGROUND**

#### **2.1 Introduction**

It has been said that we are currently in the third industrial revolution.[17] Materials and technologies that were theoretical only a few decades ago can now be fabricated in small laboratory facilities. From nanotubes to 3D printing a car, the progress is increasing exponentially. The same progress can be seen in some areas of medicine. The survival rate for several types of childhood leukemia has gone from 10% in the 1960's to 90% since 2000.[18] Despite these advancements, some areas in medicine have improved slowly or have moved backwards. Pancreatic cancer still has a high mortality rate.[19] Additionally, even with antibiotics and sterile operating rooms, 1% of orthopedic surgeries still results in infection.[20] Novel manufacturing techniques, the ability to use off-the-shelf technology in new ways, and the modular capabilities of new treatments may give rise to great advances in personal medicine that can overcome these challenges.

A review and understanding of recent advances in additive manufacturing and modular capabilities in nanotechnology are necessary to understand the areas of medicine that they may be able to yield advancements in. This review will begin by covering cancer and infectious disease in orthopedics. The review will look at how advances in

methods of additive manufacturing or novel modular nanotechnologies as well as biomaterials could help to treat these diseases.

## 2.2 Oncology

The issue in how to manage oncology is complicated and would take more pages than a brief review provides. The general issue is unregulated cell growth and how to control it. The concepts of systemic drug delivery (chemotherapy) and radiation oncology are fairly well known. They involve bringing a destructive force or cytotoxic compound into contact with the cells to reduce growth. Novel approaches such as gene therapies or antibody approaches to reprogram the body are currently being developed.[21] However, these technologies will take time to develop and may not apply to all cancers. A common issue in cancer involves metastases that spread to the bones.[22] This can cause great discomfort in patients. Many times the tumor can be removed if clean margins can be found. However, this often is not possible and palliative treatments must be initiated. An understanding of bone cancers can lead to potential concepts for treatments.[23]

### 2.2.1 Literature Review: Osteosarcoma

Osteosarcoma is the most common primary tumor of the bone in children and a source of morbidity and mortality.[24] Osteosarcoma has a bimodal age distribution, affecting younger children and elderly adults.[24] The main treatment option is surgical resection of the tumor with adjuvant chemotherapy.[25]

### 2.2.2 Epidemiology

Osteosarcoma is most common in children and ranks eighth among childhood cancers.[26] A number of inheritable genetic syndromes increase the risk for developing osteosarcoma. These syndromes include hereditary retinoblastoma, Li-Fraumeni syndrome, and Rothmund-Thomson syndrome.[27, 28] In adults, populations at risk for developing osteosarcoma are those who underwent radiation therapy for a solid tumor in childhood and adults who develop Paget's Disease of the bone.[29, 30] Adults typically have a poorer prognosis than children.[25]

### 2.2.3 Presentation and Diagnosis

The clinical presentation of osteosarcoma is often a constellation of findings that include pain around a focal bone mass that is present for several months.[31] The initial work-up in diagnosis includes imaging and hematologic studies. Initial imaging includes radiographs of the suspected area, magnetic resonance imaging for better resolution, and other imaging studies to look for metastatic disease.[32] Several hematologic markers such as alkaline phosphatase may be elevated in osteosarcoma although none are particularly sensitive or indicative of prognosis.[33] A much more definitive diagnosis requires a biopsy, which is performed by an interventional radiologist or orthopedic surgeon.[34] Interventional radiologists can perform image-guided biopsies such as computed tomography, fluoroscopy, or ultrasound. Interestingly, ultrasound has been shown to be a sensitive imaging modality to obtain definitive diagnosis.[35] Orthopedic surgeons often perform an open surgical biopsy. Typically, the same surgeon who performs the biopsy will perform the definitive resectional procedure.[25] Osteosarcomas often occur on the metaphysis of long bones in children and the most common locations

include the distal femur, proximal tibia, and proximal humerus.[28] A portion of the initial patient work-up is to investigate for the presence of metastatic disease. There is often subclinical metastatic disease at the time of clinical presentation and the most common site is the lungs.[25] Radionucleotide bone scans and positron emission tomography scans are the two more common imaging modalities used to assess for metastatic disease.[36] These can also be helpful in monitoring the tumor's response to presurgical chemotherapy.

#### 2.2.4 Treatment of Osteosarcoma

Surgery and chemotherapy are both recommended for successful treatment of osteosarcoma.[25] Surgical options may include amputation procedures or limb-sparing surgeries.[37] Surgery alone can rarely be curative but with the additional adjuvant or neoadjuvant chemotherapeutics there is a dramatic improvement in survival rates.[38-40] Any metastatic disease that is evident on investigative imaging, such as radio-nucleotide bone scans and positron emission tomography scans, often requires surgical resection along with the primary tumor.[28]

The chemotherapeutic regimens most often used in the neoadjuvant and adjuvant treatment of osteosarcoma include the following four agents: methotrexate, doxorubicin, cisplatin, and ifosfamide.[41] Before surgical resection of the primary tumor, these agents are administered for up to three months and for up to six months following resection.[25, 42] These agents can be delivered intravenously, intra-arterially, or by trans-catheter arterial chemoembolization.[43] Preoperative intra-arterial chemotherapy can be performed less than a week before the surgical resection and often forms a capsule around the tumor which helps in removal.[44] The efficacy of the neoadjuvant therapy as

in many cancers is often not in decreasing the size or number of malignant cells but to decrease the vascularity of the tumor bed and the potential for angiogenesis.[45] The body's response to the drug therapy can be measured with serial arteriography, which has a high sensitivity in detecting decreases in vascularity of the tumor.[46] Positron emission tomography with 2-deoxy-(18F) fluoro-D-glucose is another imaging modality that has been shown to be efficacious in detecting osteosarcoma's response to neoadjuvant chemotherapy.[46]

As was previously noted, surgery is required for definitive cure. A variety of modern surgical techniques are broadly categorized into amputational or limb-sparing procedures.[47] Limb-sparing surgery is ideal for the patient to spare them the necessity for a prosthesis and are performed in approximately 80% of osteosarcoma resections.[48] The rate of local recurrence is likely related to the adequacy of surgical margins during the resection. There is no consensus on the width of a surgical margin and this is an area of current research. However, for bone cancers both narrow and wide margins have shown similar rates of recurrence assuming the margins are negative for malignant cells.[40] Regardless of the margin or employed surgical technique, an orthopedic implant is often placed on the edge of an osteosarcoma limb resection. Drug-eluting capabilities in these orthopedic implants have been the focus of several *in vivo* and *in vitro* investigations.

Novel surgical implants for the prevention of local recurrence in osteosarcoma has been the focus of several studies. The Miura study demonstrated in rat osteosarcoma cell cultures that cisplatin implanted in various polymers could deliver a sustained, slow release of the agent.[49] The Natsugoe study imbedded cisplatin into biodegradable

plastics, injected them into rats, and showed good concentration of the drug 10 days following administration.[50] The Withrow study demonstrated in dogs with osteosarcoma, that biodegradable cisplatin polymers implanted at the time of tumor resection decreased the local recurrence rate by over 50%.[51]

Others have investigated the feasibility of different drug-eluting or structurally supporting materials in osteosarcoma models. The Gulati study showed favorable results with drug-eluting titanium nanotubes that showed good drug delivery and adhesion to osteoblastic cells.[52] There is a clear need for new treatments and technologies for osteosarcoma and related bone cancers.

## 2.3 Infectious Disease

Infectious disease can be particularly problematic as it pertains to bone and joint infections. It was once thought that infectious disease from common bacteria that cause bone infections had been conquered.[53] Unfortunately, antibiotic resistance is changing the seriousness of hospital acquired infections. Bacteria such as methicillin-resistant *Staphylococcus aureus* (MRSA) are becoming common place in many American hospitals.[53] Even a low 1% incident of surgical infection is now far too high when there is no easy treatment option. This is of particular concern in deep surgical procedures as the bacteria can easily reach the blood stream then travel to hard to treat areas of the body or cause septicemia.[54]

### 2.3.1 Osteomyelitis

Osteomyelitis by definition is an infection that is localized to bone tissue. It is caused by an infectious organism and associated with an inflammatory process that can then result in bone destruction.[55] This inflammation can involve the marrow and bone



cortex. The infection can also reach the joint and surrounding soft tissue and result in joint destruction. The healing process could cause the formation of scar tissue and mobility issues.[56] Osteomyelitis is more prevalent in males than females in all age groups.[57]The infection is becoming increasingly more common in younger age groups with approximately 85% of cases occurring in patients under the age of 17.[57] The annual incidence of osteomyelitis in the United States is 13 per 100,000.[58] The use of antibiotics has reduced mortality but the morbidity of this disease is clearly high.

### 2.3.2 Pathology

Osteomyelitis can occur through several mechanisms. The most common cause for infection is from trauma, surgery or spread of a localized infection.[58] Contiguous spread would logically not be primarily age correlated and in the case of trauma could involve any area of bone due to the nature of the infection. It is common for this type of osteomyelitis to be polymicrobial.[59] Osteomyelitis can also occur through a blood-based infection that can allow seeding to occur in the bone. This most commonly occurs in the metaphysis portion of the long bone.[56] This type of osteomyelitis is commonly monomicrobial.[60] Osteomyelitis is also a common complication in diabetes mellitus due to the vascular insufficiency seen in the disease. The infection can begin as an ulcer in the dermis and then spread to the bone.[61]

### 2.3.3 Acute vs. Chronic

Osteomyelitis can be either acute or chronic. Acute osteomyelitis occurs over the course of days or weeks.[62] Patients would note the pain at the site and later find complications. Chronic osteomyelitis is defined as the persistent infection over an

extended period of time. The chronic infection can be caused by drug resistant microorganisms, necrotic tissue or recurring infections.

As in most infectious diseases, the age of the patient and method of infection is highly organism specific. The most common organism is *Staphylococcus aureus* due to the virulence factors and the ability to form a biofilm.[63] The more common organisms in infants are *Escherichia coli* and *Streptococcus agalactiae*. [64] This compares to MRSA, *Enterococcus*, *Streptococcus* and *Pseudomonas aeruginos* in adults.[64]

#### 2.3.4 Treatment Modalities

Treatment of osteomyelitis has evolved substantially over the years, especially since the discovery of antibiotics. Treatments vary substantially based on the timeframe of a particular patient's disease, their response to treatment, and the nature of the microbial pathogen causing the infection. There is a need for both more effective and patient specific treatments.

## 2.4 Additive Manufacturing

Additive manufacturing may be able to solve some of the previously discussed issues in medicine. Additive manufacturing is the fabrication of an object using information from a computer-aided design (CAD) file that is converted to a stereolithography (.STL) file to physically fabricate an object through a machine.[65] Although this method is useful in rapid prototyping, additive manufacturing techniques such as 3D printing, are only now coming to the forefront of public knowledge.[66-68] The majority of basic additive manufacturing techniques use readily moldable materials such as plastics. It is also possible to additively manufacture metals and ceramics; however, fabrication methods must evolve to enable printing of all three categories of

materials interchangeably.[69] Additive manufacturing falls into three categories depending on the state of the material used: solid based, liquid based, and powder based. Liquid-based additive manufacturing uses either a substance that is melted, deposited, and then solidified through cooling, or a liquid polymer that is deposited and then solidified through curing.[70] However, with liquid polymer, the current layer must be polymerized to maintain the shape before the next layer can be deposited.[71-73] Solid additive manufacturing is primarily restricted to the manufacture of laminated objects, wherein sheets of material are fused through pressure and heat, then cut to the desired shape using a carbon dioxide laser.[74] Though this method is applicable to metals and ceramics, it generates large amounts of waste materials once the object is made. Powder-based additive manufacturing consists of sequentially layering powdered material and either melting or binding the material before the next successive layer is deposited.[75-77][78] Although wide varieties of this method exist, one technology that is widely known is selective laser sintering wherein each successive layer of powder is first deposited, then sintered using a laser before the next layer is applied.[79]

In response to marketplace demand, 3D printing technology has rapidly advanced in recent years.[80, 81] A typical printing set-up uses the user generated .STL file to generate nearly any desired shape so long as the volume of the object is less than the printer's capability.[82, 83] As researchers seek to further customize this manufacturing method for rapid prototyping, wider arrays of materials and the ability to specially tailor the properties of those materials are required.[84] Also needed is a method to ensure consistent dispersion in the host polymer without requiring industrial grade equipment that maintains printability through commercially available devices.

Fused deposition modeling printers normally use a plastic or polymer filament to build a three-dimensional construct in a layered manner. The most common types of plastic used are polylactic acid (PLA) and acrylonitrile butadiene styrene (ABS). The consumer versions of these printers operate at resolutions ranging from 50 to 400 microns. Most printers move a plastic filament of 1.75 mm to 3 mm diameter through a heated print head with a narrow nozzle around 0.4 mm, melting the plastic and passing it through the nozzle as the print head continues to move along the print path. Plastics such as PLA or ABS rapidly cool, enabling subsequent layers to be sequentially built without loss of resolution, resulting in highly customizable properties of the construct. As the print head temperature, percentage fill, and resolution are easily modified, highly variable designs of the same construct can be obtained. Both PLA and ABS are printed at temperatures normally ranging from 220-230 °C.

The fabrication process can be further customized by using designer filaments with tailored material properties. One filament for cosmetic purposes is called “Laywood” and is a PLA-saw dust mix. It allows for printing of constructs that appear to be made of wood.[85] Temperature can be controlled to change wood tones and coloring. A material property-based filament called Carbomorph can be used to print low cost sensors using conductive carbon in the plastic.[83] A 3D printer with multiple heads can be used to then fabricate a construct with selected portions of the device conductive or nonconductive.

The push for custom filament creation has led to the design of personalized filament extruders. These devices combine a hopper or feed mechanism with a metal pipe that has an internal auger system. The pipe is heated to a desired temperature and

the material that enters the system melt-flows to the distal portion at which a metal die is in place. The metal die has a hole drilled into it that is equal to the desired filament diameter. The temperature for extrusion must be set to provide a proper material flow and to allow rapid cooling and hardening upon extrusion. A temperature that is too high will result in a thinner filament that will not function with a 3D printer's feed mechanism. If the temperature is too low or the material expands, the filament will not be able to pass through a feed mechanism such as the M6X26 extruder pipe screws seen in many consumer printers.

Most extrusion systems use plastic pellets of the desired material with a diameter of 3 mm to 6 mm. It is challenging to mix an additive with these pellets and to achieve dispersion in the polymer. The additive can be placed as a powder with the pellets in the hopper at the percentage mix required, but the extruded filament will be non-uniform. The filament can be cut up and re-extruded but this will lead to additional heating of the additive, time, and cost in wasted materials, as well as loss of confidence in doping percentages.

## **2.5 Halloysite Nanotechnology and Sintering**

A key to the success of recent 3D fabrication technology is the ease of use. It may be possible to do this at a nano scale level. A modular system could be developed using a cheap affordable nanotechnology.

### **2.5.1 Halloysite Nanotubes**

Halloysite nanotubes are naturally occurring nanotubes composed of silica and alumina.[86-91] The outside of the tube has a net negative charge due to the silica, while the inside has a net positive charge attributed to the alumina.[86-91] This charge

difference is due to the bonding pattern of the aluminum and silicon atoms relative to each other. The typical inner diameter, outer diameter, and length of these tubes are 1-30 nm, 30-50 nm, and 100-200 nm, respectively.[86-91]

Since halloysite nanotubes are hydrophilic and have opposite surface polarizations for the inner and outer lumen, they can be easily filled and/or coated.[89] This capability and the natural availability of these particles have made them practical for many nanotechnology applications.[89] They are particularly suited for time controlled release of chemicals, mainly in drug delivery and material enhancement.[92] Halloysite also has thermal and mechanical properties that are highly desirable in polymer composite areas, primarily for the reinforcement of low-density polymers.[93] By varying the amount of halloysite and selecting applicable coatings, the thermal and mechanical properties of given polymers can be specifically tailored to the desired application.

The hollow cylindrical geometry of halloysite nanotubes allows them to be loaded with a variety of chemicals through vacuum cycling, which in turn leads to a time release of the loaded chemical agent.[94] The most often researched application of this approach is extended delivery of drugs due to the biocompatibility of halloysite.[95] During loading of chemical agents under pressure, the lumen is filled, however the particles can also be externally coated. For drug delivery, the drug is first rapidly released through desorption of the active agent from the outer lumen and the ends of the tube, and then more slowly released through pore diffusion from the loaded inner lumen.[89] HNT loaded particles demonstrate a 5-10% initial burst release, followed by a much slower release.[89]

Mechanical properties of various materials can also be enhanced through the addition of halloysite. The tensile strength and tensile modulus increase when halloysite is used as a filler.[96] In comparison to carbon nanotubes, halloysite nanotubes are much cheaper and far less toxic.

### 2.5.2 Metal Acetylacetonates

Metal acetate or metal acetylacetonates are unique complexes that are commonly used in chemistry. The metal acetylacetonates are coordination complexes made up of a metal ion and acetylacetonate anion.[97] Iron and gold are more commonly known complexes but many other metals are used, such as barium, copper, nickel, zinc, chromium, cobalt, lithium, and titanium, are readily manufactured by the chemical industry. Metal acetylacetonates are used in industry as catalysts or NMR shift reagents. Lithium acetate is used in DNA gel electrophoresis solutions as a buffer.[98] These compounds degrade between 200 °C to 300 °C. Due to their thermal degradation, they make ideal candidates for coatings via sintering.[99]

## 2.6 **PMMA Bone Cements**

Bone cement is generally composed of polymethylmethacrylate (PMMA), and has been used by orthopedic surgeons for more than six decades.[100] The first use of PMMA bone cement was in 1958 when British orthopedic surgeon Sir John Charnley implanted a hip endoprosthesis using PMMA.[100] PMMA allows for the implantation and fixation of prostheses to the bone and has been the subject to continuous development in parallel with improvements of surgical techniques.

Bone cement tends to consist of 90% polymer.[100] The remaining material consists of barium or zirconium oxide powders that make the resulting product radio-

opaque.[100] The chemical structure of bone cement consists of two compounds glued together. The first consists of pre-polymerized PMMA, supplied as “spheres.” These “spheres” are the white powder.[101] To prepare bone cement, powdered PMMA (the “sphere” mixture) is mixed with a liquid containing monomeric methylmethacrylate (MMA) in the presence of a catalyst. The powder quickly dissolves in the monomer and undergoes a polymerization reaction at room temperature to form putty-like cement.[101] The polymerizing fluid bonds together the spheres into a strong, but brittle mass. As the liquid monomer polymerizes, the bone cement hardens. The individual PMMA spheres are entrapped and bonded within the polymerized monomer. The spheres and the polymerized monomer do not bond chemically.[102]

The term “cement” may not be entirely accurate. The word cement is often used to describe something that bonds two items. Cement implies that the PMMA adheres the implant into the bone. Bone cement instead acts as a filler, like grout. It fills the void between the implant and surrounding bone by creating a constricted space for the implant to be held firmly against the bone. Plexiglas or Lucite are materials that consist of nearly pure PMMA.

Bone cements for primary arthroplasty are widely used by orthopedists and other surgeons. Bone cement is a substance commonly used for fixation of artificial joints in bone, and it is extensively used in hip and knee replacement surgery. Various types of bone cements are available to surgeons that vary in regard to viscosity, processing, content, and application properties.[102] Many surgeons mix prophylactic antibiotics into the bone cement while mixing the components together.[103] Many types of antibiotics can be used in the mixing process, the typical antibiotics used consist of gentamicin,



tobramycin or vancomycin.[104] Worldwide, tobramycin is commonly used.[105] Gentamicin and tobramycin are aminoglycoside antibiotics used to treat many common bacterial infections, particularly gram-negative infections.[106] Vancomycin is a glycopeptide antibiotic used in the treatment of infections caused by many common gram-positive bacteria.[107] Surgeons in the United States predominantly use gentamicin.[105] These antibiotics are available in a powdered form that can easily be mixed into the PMMA. Once PMMA is mixed with antibiotics and used in a procedure the antibiotics will leach from the bone cement into the surrounding areas. The local concentration of antibiotics is usually sufficient to initially kill the bacteria left in the operative wound.

However, addition of antibiotics to bone cement leads to a weakening of the cement.[108] Sustained release of the antibiotics from the PMMA over a longer time period is also limited. Previous experiments have shown that limited release could be less than 10% of the loaded antibiotics. Mixing the antibiotics uniformly can be difficult even when done with a sonicator. PMMA is not a porous material. Close to 70% of the antibiotics which are released will elute within the first 24 hours in standard commercially viable bone cements.[109] This release also only constitutes a low percentage of the total available antibiotic. The non-porous nature of PMMA bone cement causes limited release of the antibiotics that are widely (and unevenly) distributed throughout the cement sample.

## CHAPTER 3

# HALLOYSITE NANOTUBES AS A MODULAR PLATFORM FOR NANOPARTICLE CREATION

### 3.1 Introduction

Nanotechnology holds great promise for drug delivery in clinical medicine. The ability to generate a unique particle that can deliver a drug or gene can allow for novel treatments. Techniques to generate nanoparticles can be complicated and costly. There is also cost and time involved in making modifications to an existing particle. A need exists for a modular platform to test new technologies or compounds for drug delivery both cheaply and quickly.

Halloysite nanotubes are alumina-silica composites with the structure  $(Al_2Si_2O_5(OH)_4 \cdot 2H_2O)$ . The tubes have a unique charge structure. The silica on the outside gives the structure a net negative charge. The inner lumen has a net positive charge from the alumina. The mineral rolled into a tube positions the silicon and aluminum atoms to achieve this unique charge profile. The length of the tubes varies between 100 to 2,000 nm. The outer diameter can run 30 to 50 nm but the inner lumen runs 10 to 30 nm.

The ease of coating or loading has led to halloysite being used in many different industries. The low cost and naturally occurring tube is hydrophilic and has both positive and negative charges when in reference to the lumen and surface, respectively. The

nature of the nanotube allows for controlled release of compounds and strengthening of materials. The controlled release capabilities can be used as a stand-alone particle or as a composite of for example a polymer. This nature of the halloysite tubes allows for customization that then yields polymers or particles with special capabilities.

Halloysite loading is typically done under vacuum. However, the tubes can also adsorb compounds from solution under room temperature conditions. A core area of halloysite research is delivery of drugs based upon the biocompatibility of the halloysite nanotube. Outer coatings can be involved in halloysite drug delivery. In this case a coating such as a polyelectrolyte can dissolve over time or with a trigger that allows a release to occur. This typically occurs in a burst release that is then sustained over time. The initial burst is 5% to 10% of the load. It has been demonstrated that both hydrophobic and hydrophilic agents can be loaded into halloysite.

Material mechanical properties improve with halloysite as an additive. These properties can include tensile strength or compression. Halloysite can be added as additional wt% filler to the material to notice these gains with little modification made to the fabrication process.

Specialized coatings added to the halloysite could give enhanced material properties as a stand-alone particle or as a composite material. A magnetically susceptible particle for example could allow for the generation of hyperthermia in a magnetic field. These magnetic properties could also allow for the halloysite to remain stationary while a drug is released. A gold coating would also generate hyperthermia via a proper frequency laser.

The present work demonstrates a method to use halloysite nanotubes as a modular platform for custom nanoparticle creation. The nanotubes are coated with gold, iron, barium, copper, nickel and lithium. Additionally, lipid and polyelectrolyte coatings are added to show modular bioactive coatings. Preliminary cytotoxicity studies were run to gather initial data on potential uses in *in vitro* or *in vivo* drug delivery studies.

### **3.2 Design and Objectives**

This study examines the capabilities of fabricating custom metal coatings onto the halloysite nanotubes, adding bioactive external coatings to the nanotubes, loading the nanotubes with bioactive substances, imaging the nanotubes, running elemental analysis on the nanotubes, checking for magnetic properties and preliminary cell cytotoxicity testing of the nanotubes. The following sections break down the design objectives into specific areas.

#### **3.2.1 Metal Coating Objective**

The first objective is to create a low cost and quick method to coat a nanoparticle with a metal. A method to coat halloysite nanotubes in metals such as gold, iron and copper will be developed.

#### **3.2.2 Modular Metal Coating Objective**

The second objective is to create a nanoparticle that is tunable. A method of coating the halloysite nanotubes with multiple metal compounds in a desired order will be developed.

#### **3.2.3 Biocompatible Coating Objective**

The third objective is to apply biocompatible coatings to the nanoparticle. Biocompatible coatings allow enhanced functioning in an organism. The nanoparticles

will be coated with lipid or polyelectrolyte coating to demonstrate the capability of a modular platform that can have biocompatible coating options.

#### 3.2.4 Imaging and EDAX Objective

The fourth objective is to confirm that the coatings are present and to quantify the number of nanoparticles. Scanning electron microscopy (SEM), transmission electron microscopy (TEM) and energy dispersive X-ray analysis (EDAX) will be used.

#### 3.2.5 Magnetically Susceptible Particle Objective

The fifth objective is to coat the particles with iron, which will allow them to react to magnetic fields. This magnetic property will be useful in medical treatments for hyperthermia in which a laser or oscillating magnetic field is used to generate temperatures that can damage or kill cancer cells. Iron coated halloysite particles will be created such that they react to magnetic fields.

#### 3.2.6 Cytotoxicity Study Objective

The sixth objective is to test the cytocompatibility of the nanoparticles. It can be desirable to have particles that are cytocompatible or cytotoxic depending on the goal of use.

#### 3.2.7 Loading and Elution Objective

The seventh goal is to confirm the ability of the particles to carry compounds of interest. One goal of a modular particle is that it can carry a compound of interest. The particles will be loaded with gentamicin, nitrofurantoin, methotrexate and alizarin red dye, and the release of these compounds will be measured as a function of time.

### 3.2.8 Improved Materials Property Objective

The final objective is to create a modular platform that can interact as a particle or enhance the properties of a biomaterial. Barium-coated halloysite nanotubes will be added to PMMA bone cement, and the material properties of the composite will be measured.

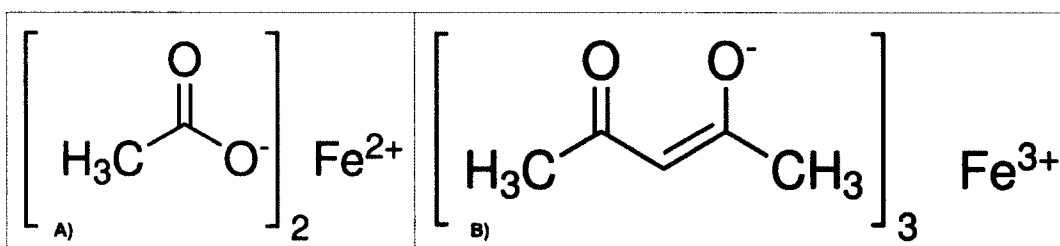
## 3.3 Materials

All treatment compounds used in this study were purchased from Sigma Aldrich (St. Louis, MO) including gentamicin sulfate (GS), tobramycin, methotrexate, alizarin red dye and nitrofurantoin. The Nanodrop spectrophotometer was from Thermo Scientific (Wilmington, DE). Heating of biomaterials was done with a Vulcan® A550 Series Benchtop Muffle Furnaces from Thomas Scientific (Swedesboro, NJ). All gentamicin visualizing reagents including sodium tetraborate, 2-mercaptoethanol and phthalaldehyde were ordered from Sigma Aldrich (St. Louis, MO). Halloysite nanotubes were also obtained from Sigma Aldrich (St. Louis, MO). The SEM and EDAX was a Hitachi S-4800 (Schaumburg, IL). Additional imaging was done by a FEI Tecnai G2 F30 Twin (Hillsboro Oregon), and a Libra 120 Transmission Electron Microscope made by ZEISS (Peabody, MA). Iron (III) acetylacetonate, iron (II) acetate, copper (II) acetylacetonate, lithium acetylacetonate and nickel (II) acetylacetonate were purchased from Sigma Aldrich (St. Louis MO). Gold acetate was ordered from VWR International (Radnor, PA). Barium acetylacetonate was ordered from Fischer Scientific Company (Hampton, NH). The polyelectrolytes for coatings were polyvinylpyrrolidone (PVP, MW~1,300,000) and Poly(acrylic acid) (PAA, MW~250,000) from Sigma Aldrich (St. Louis, MO). Lipids used were 18:1 TAP (DOTAP) 1,2-dioleoyl-3-trimethylammonium-

propane (chloride salt) from Avanti Polar Lipids (Alabaster, AL). Cell culture plates and other lab plastics were purchased from MidSci, (St. Louis, MO). Dulbecco's Phosphate Buffered Saline (DPBS), Dulbecco's Modified Eagle's Medium (DMEM), fetal bovine serum (FBS), penicillin-streptomycin-amphotericin (PSA) antibiotics, and Live/Dead Viability/Cytotoxicity kit were obtained from Life Technologies, (Carlsbad, CA). Osteosarcoma cell line (CRL 2836) and Osteoblast cell line (MC3T3-E1 subclone 4 (ATCC CRL-2593) was purchased from ATCC (Manassas, VA).

### 3.3.1 Metal Acetates and Acetylacetonates

Metal acetate or metal acetylacetonates are unique complexes that are commonly used in chemistry. The metal acetylacetonates are coordination complexes made up of a metal ion and acetylacetonate anion. Iron and gold are more commonly known complexes but many other metals are used such as barium, copper, nickel, zinc, chromium, cobalt, lithium and titanium. These metals are readily manufactured by the chemical industry. Iron acetate and iron acetylacetonate are structurally shown in Figure 3-1, demonstrating the anion and cation components.



**Figure 3-1:** A) iron acetate B) iron acetylacetonate [110]

Metal acetylacetonates are used in industry as catalysts or NMR shift reagents. Lithium acetate is used in DNA gel electrophoresis solutions as a buffer. These

compounds degrade between 200 °C to 300 °C. Their thermal degradation makes them ideal candidates for coatings via sintering.

### 3.3.2 Lipid Coatings

Lipid coatings are commonly given to nanoparticles. Coatings can allow a particle to merge with a cell lipid membrane or disperse further into an organism. All lipid coatings were done to simulate a biocompatible lipid-coated particle. The DOTAP lipid was used (Figure 3-2).

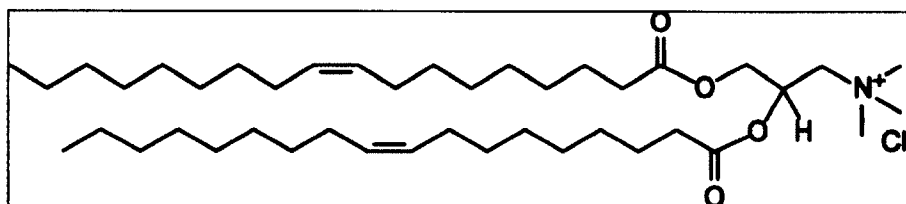
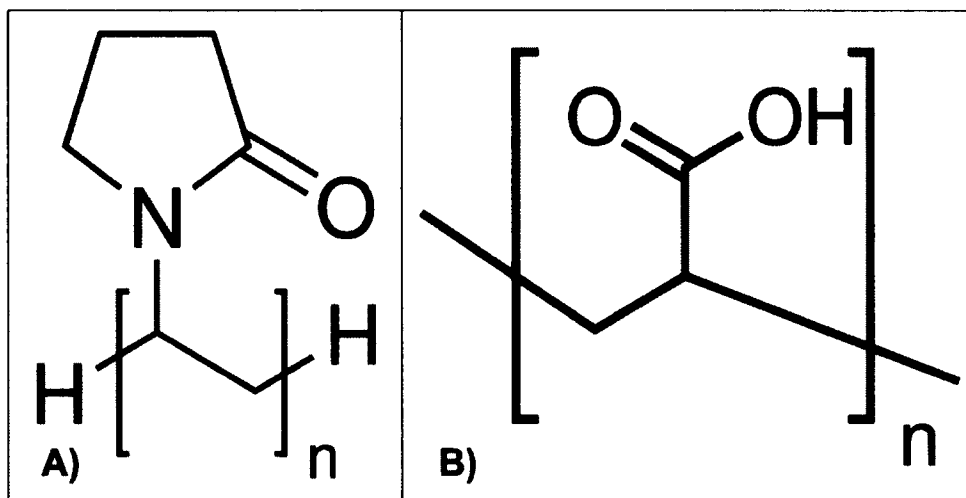


Figure 3-2: DOTAP lipid structure [111]

### 3.3.3 Polyelectrolyte LBL Coatings

The concept of layer-by-layer (LBL) assembly is based on the consecutive deposition of oppositely charged polyelectrolytes on surfaces. LBL allows for the formation of multiple layers of shells of different polymers. The layering can be done with nanometer precision. The polyelectrolytes used were positively charged polyvinylpyrrolidone (PVP) and negatively charged poly(acrylic acid) (PAA) (Figure 3-3).





**Figure 3-3:** A) PVP structure B) PAA structure [112]

#### 3.3.4 SEM, TEM, MRI and EDAX

The imaging was done by a scanning electron microscopy (SEM), transmission electron microscopy (TEM) and energy-dispersive X-ray spectroscopy (EDAX). EDAX gives an elemental analysis of a sample. An x-ray source excites the electrons, which emit photons as they return to the K and L shell. A percent composition can then be determined. SEM scans a sample with a focused beam of electrons. The electrons interact with the sample's surface topography and allow an image to be translated from the signal. TEM sends a beam of electrons through a thin specimen. Magnetic Resonance Imaging (MRI) applies a strong magnetic field to the sample, then applies an electromagnetic pulse to excite hydrogen atoms and then detects the radio frequency signal they emit.

### 3.4 Fabrication and Methods

The basic fabrication methods for modifying the nanotubes by either sintering or bioactive coatings, cell culturing and MRI imaging are described. Modifications to these methods are described in individual subsections.

### 3.4.1 Metal Acetylacetonate Sintering

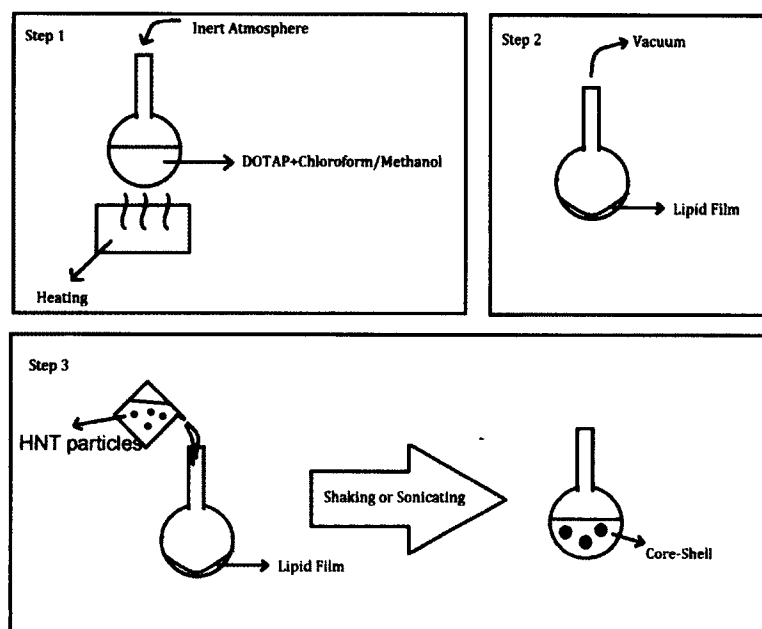
Most metal acetylacetonates degrade completely at 300 °C, outgassing acetone and carbon dioxide and leaving behind positively charged metal ions. The negatively charged outer lumen of the halloysite causes these metal ions to readily bond to the outer surface, allowing for a one step sintering coating. Most of the metal acetate and acetyl acetates were mixed with halloysite in a 1:1 ratio by weight. The mixing was done in 100 mg to 250 mg batches of halloysite to allow for a more uniform sintering. Halloysite was dried overnight at 60 °C. The halloysite was then weighed and mixed with an equal amount of a metal acetate or metal acetylacetonate. Powders were moderately mixed in a mortar and pestle whenever possible. The powders were then placed into 5 mL VWR borosilicate glass containers and vortexed vigorously for a minute. Containers were then placed in a Vulcan oven. The oven was programmed to heat to 300 °C at a rate of 5 °C/min. The program was then set to stay at this temperature for 4 hours. The program then cooled to room temperature at 5 °C/min. This resulted in a sintering reaction which coated the halloysite nanotube in a metal shell or deposited metal clusters onto portions of the nanotube. Temperatures were varied for certain reactions. After sintering the glass tubes were vortexed or ground by mortar and pestle to break up any clumps of material. The raw materials are moderately clumped but breaks down to a fine powder with minimal vortexing or additional processing (Figure 3-4).



**Figure 3-4:** Unprocessed iron-coated halloysite

#### 3.4.2 Lipid Coating

The lipid coating process is shown in Figure 3-5. The DOTAP was dissolved in a chloroform:methanol (4:1 v/v) solution while heated at 60 °C in a glass flask. The flask was then put under vacuum overnight to evaporate any remaining organic solvent and deposit a lipid film on the surface. Particles were loaded into a solution in syringe and loaded into the flask using a drop-by-drop method that caused the drops to roll down the surface. The solution was then sonicated or vortexed (Figure 3-5).



**Figure 3-5:** Lipid coating of particles. 1) A DOTAP and chloroform/methanol solution is heated 2) The solution is vacuumed overnight to deposit the lipids 3) The nanoparticles to be coated are added and vortexed

### 3.4.3 LBL Polyelectrolyte Coating

PVP/PAA multilayers were organized on halloysite/gold nanocomposites at pH 3 through the LBL technique described in the literature and specifically adapted as follows.[113] Vials with 25 mg of HNT/Au were filled with 1 mL of water at pH 3, shaken, centrifuged, and decanted. The vials were washed and filled with 1 mL of PVP (1 mg/mL at pH 3). Tubes were mixed for five minutes and centrifuged. The PVP solution was decanted and the vials were filled with 1 mL of water, which were adjusted to pH 3. The tubes were mixed for five minutes and centrifuged, and water was decanted. Next, the vials were filled with 1 mL of PAA (3 mL/100 mL at pH 3). Tubes were mixed for five minutes, centrifuged, and decanted. The cycling of PVP and PAA coatings were repeated until the desired polyelectrolyte architectures were created. Lastly, 1 mL of methotrexate (MTX) 0.5mg/mL in water at pH 3 was added to the vials and mixed for ten

minutes. Finally, the polyelectrolyte drug-coated HNT/Au composites were dried for analysis.

#### 3.4.4 Cytotoxicity Testing

Osteosarcoma cell line (CRL 2836) and osteoblast cell line (CRL-2593) were purchased from ATCC (Manassas, VA). Cells were plated in 25 cm<sup>2</sup> tissue culture flasks and incubated at 37 °C under humidified 5% CO<sub>2</sub> and 95% air in complete DMEM containing 10% FBS and 1% PSA. Subconfluent cells were passaged with 0.25% Tryple-E then collected by centrifugation, re-suspended in complete DMEM and subcultured at a 3:1 split into 25 cm<sup>2</sup> tissue culture flasks.

Confluent cultures were passaged and seeded into wells at uniform cell density. Particles were then added and after one day or three days test wells were tested for toxicity using the Live/Dead assay.

A Live/Dead cytotoxicity kit was used for testing. The protocol supplied by the manufacturer was used for the assay. The dyes were diluted to 2 μM solutions and were added to the test wells. Fluorescence microscopy was used to image live and dead cells after they were incubated for 30 minutes in the dye solutions.

#### 3.4.5 Vacuum Loading

Halloysite nanotubes were loaded with bioactive compounds under vacuum. A glass vacuum chamber or bell jar was used with a lab vacuum. Halloysite nanotubes were placed in a test tube of a solution of a compound to be loaded. The halloysite was either left statically or with a magnetic stir bar overnight to load. The concentration of the solution or halloysite was modified as necessary to achieve proper loading concentrations.

#### 3.4.6 Elution Testing

Elution studies were conducted on some of the loaded nanotubes. The method of static elution at 37 °C was chosen for ease of replication. The testing occurred in 1 mL Eppendorf tubes that were tinted to prevent degradation of eluted products by light. Deionized water was used as a medium for ease of replication. Solution was removed from tube to tube at a specified time interval. This allowed for all elution testing of the solutions for the same construct to be analyzed at a later date on the same machine. The time intervals that were run for elution testing were: 1 minute, 2 minutes, 5 minutes, 10 minutes, 20 minutes, 40 minutes, 1 hour, 2 hours, 4 hours, 8 hours, and then daily for 7-10 days. All solutions were run on a NanDrop spectrophotometer at an appropriate wavelength for the bioactive substance. The micro-cuvette option was used, which involved a 500 ml cuvette. The spectrophotometer was set with a base level using control deionized water. Elution curves were additively plotted to show a drug's release profile from either the filament or construct. Absorbance levels for a substrate were used to determine concentrations. Control curves were plotted using substrates of interest by using solutions of known concentration.

### 3.5 Testing and Controls

This testing required positive, negative, and material controls to achieve reliable data. Statistical analysis was also done to confirm differences or similarities between experimental groups.

### 3.5.1 Nanoparticle Creation

Multiple batches of each nanoparticle type were made to verify the consistency of the process. Conditions were kept as sterile as possible, and new borosilicate glass containers were used for different metal coatings of particles.

### 3.5.2 Nanoparticle Imaging and Verification

All nanoparticles were imaged with SEM and TEM. The sintering of the metal particles was visually confirmed. EDAX was also used to confirm sintering via elemental analysis. Lipid coatings and LBL polyelectrolyte coatings were also visually confirmed by imaging.

### 3.5.3 Cell Culture Controls and Control Materials

During the cell culture testing process controls were always used. These controls included control media wells and control cell wells, which provided a negative and positive control for basic growth, respectively. Additionally, all modified and tested materials were compared to halloysite and barium controls. When possible, differing steps of the fabrication process were tested. This testing allowed proper conclusions to be drawn from the data.

### 3.5.4 Elution Testing Controls

Spectrophotometry must be checked with controls and properly calibrated. This must especially be done when using very low concentrations of a substrate of interest. The spectrophotometer was checked with a control of plain deionized water regularly to verify that the absorbance was zero. Absorbance curves were calculated using known levels of a substrate.

### 3.5.5 MRI Imaging

MRI images were collected from bone cements with halloysite and halloysite coated in barium to check for the amount of contrast provided by the barium-coated halloysite. Control PMMA-only cements, commercial barium-enhanced cements, halloysite-only enhanced cements and combinations were imaged on the MRI machine to act as positive and negative controls for each additive. Additionally the machine was calibrated using international methods of control water and air-filled blocks. The MRI facility at the Biomedical Research Institute in Shreveport, Louisiana was used.

## 3.6 **Results and Discussion**

The method to modularly create custom nanoparticles involved trials of alternative methods before the optimization of the process using metal acetate and metal acetylacetonates. This process was completed in phases. First, different materials were sintered onto the halloysite nanotubes. The modular nature of the particles was tested with multiple layers done. The coated particles were analyzed to confirm the success of the coating process. Preliminary cytotoxicity testing was then done on these particles. Next, lipid or LBL coatings were added to particles. Finally, barium-coated particles were added to bone cements to test the enhanced contrast and other material properties.

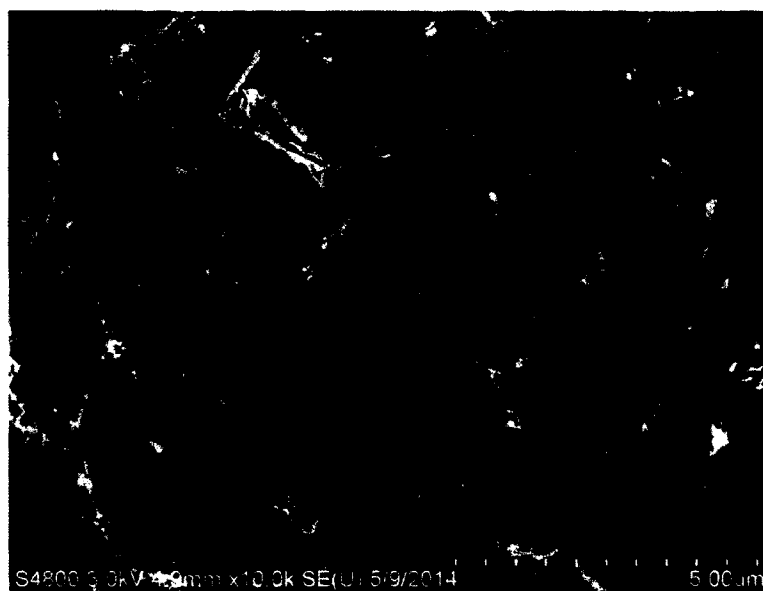
### 3.6.1 Coating Halloysite Nanotubes

The metal acetates and metal acetylacetonates were used in a sintering process to create custom depositions of metals on the halloysite nanotubes. The particles were analyzed using SEM, TEM and EDAX. The particles had to be secured by carbon tape to prevent damage to the SEM. The tape resulted in the carbon peaks seen in the EDAX. Particles were coated with iron, gold, barium, lithium, copper and nickel.



### 3.6.1.1 Control halloysite

Control halloysite was imaged for later comparison to coated nanotubes. SEM (Figure 3-6), TEM (Figure 3-7) and EDAX (Figure 3-8) were applied to the control halloysite nanotubes.



**Figure 3-6:** SEM control halloysite nanotubes



**Figure 3-7:** TEM control halloysite nanotubes

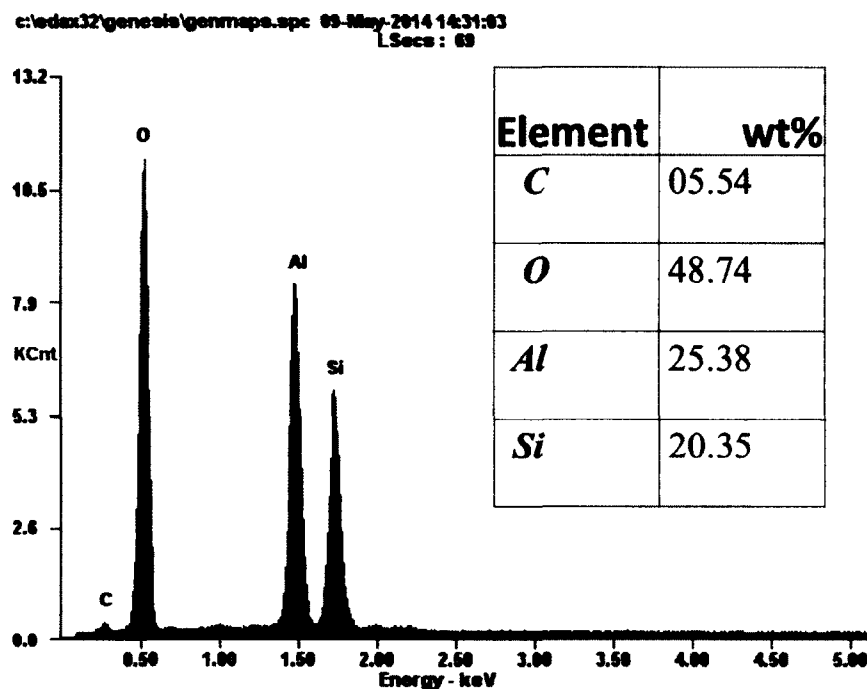


Figure 3-8: EDAX control halloysite

The ability of the halloysite to clump can be seen in the SEM. The TEM shows the hollow lumen and differences in size among the tubes. The EDAX confirms the alumina-silicate elemental structure of the nanotubes. The surfaces on control HNTs are smooth and no artifacts exist around the outer edges.

### 3.6.1.2 Iron Acetate and Iron Acetylacetonate

Iron acetate and iron acetylacetonate were used to sinter the halloysite and coat it in iron. The reactions were run in 100 mg 1:1 batches of HNTs and either an acetate or acetylacetonate. The sintered powders were then vortexed or ground by mortar and pestle. The iron (iii) acetylacetonate sintered HNTs were found to be magnetically susceptible while the iron (ii) acetate did not create a magnetically susceptible particle. The iron (iii) acetylacetonate created a highly paramagnetic particle that would stand on

end and rotate in a magnetic field. The iron acetylacetonate-coated HNTs that were magnetic were imaged and analyzed with EDAX. However, SEM imaging was done of the iron acetate to prevent damage to the SEM. This work is shown in Figure 3-9, Figure 3-10 and Figure 3-11.



**Figure 3-9:** SEM iron-coated halloysite



**Figure 3-10:** TEM iron-coated halloysite

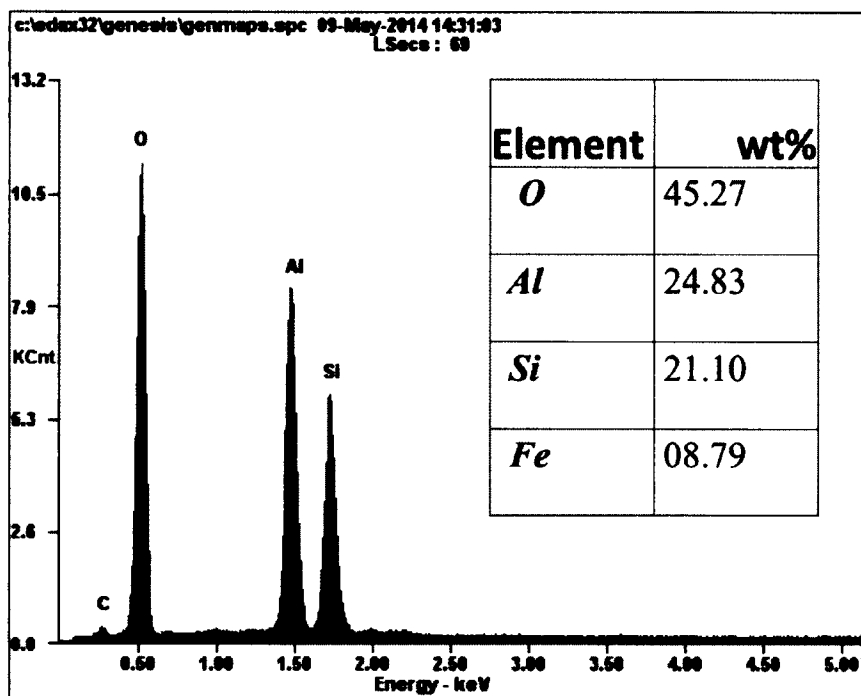


Figure 3-11: EDAX of iron-coated halloysite

The imaging and EDAX shows a coating that is confirmed to be iron. The iron tends to clump into spheroids as it deposits and seems to have a preference for deposition on the ends of the nanotube. Multiple layers of coating of 2:1 iron-heavy ratios were applied, which increased the response to a magnetic stimulus. The ability to create a nanoparticle that can be controlled with an electromagnetic probe or similar device could yield value in drug delivery or for hyperthermia based treatments.[114] A combination of both in terms of chemosensitization could exponentially increase the effects.

### 3.6.1.3 Gold Acetate

The gold nanotubes were coated in 100 mg batches in 1:1 or 2:1 ratios of gold acetate to HNTs. This reaction began to occur at a lower temperature and was more volatile at 300 °C, so it was run at 220 °C to 250 °C. The energetic nature of the reaction

at higher temperatures or heating speeds is shown by the powder coating the outside of the 5 mL beakers and bottom of external larger beaker (Figure 3-12).



**Figure 3-12:** Sintering with gold acetate

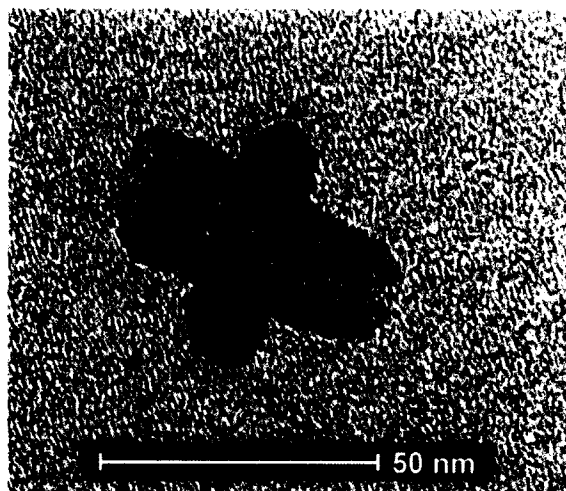
The gold-coated HNTs are spread all over the 5 mL beakers and cover slips. The gold-coated nanotubes were a fine powder and were vortexed to further disperse them. Mortar and pestle processing tended to create thin sheets of material. This is similar to properties seen in working with gold and gold particles. The gold-coated HNTs were imaged and EDAX was run. This is shown in Figure 3-13, Figure 3-14, Figure 3-15, Figure 3-16 and Figure 3-17.



**Figure 3-13:** SEM image of gold-coated HNTs



**Figure 3-14:** TEM image of gold-coated HNTs



**Figure 3-15:** TEM image of gold-coated HNTs



**Figure 3-16:** TEM gold-coated HNTs

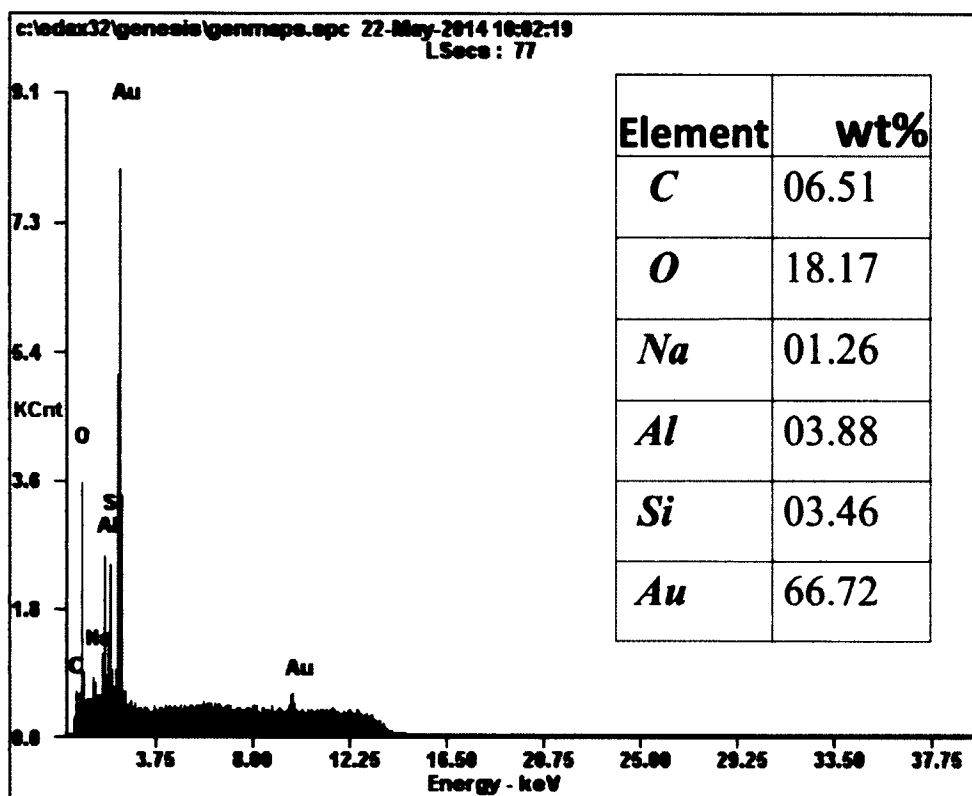


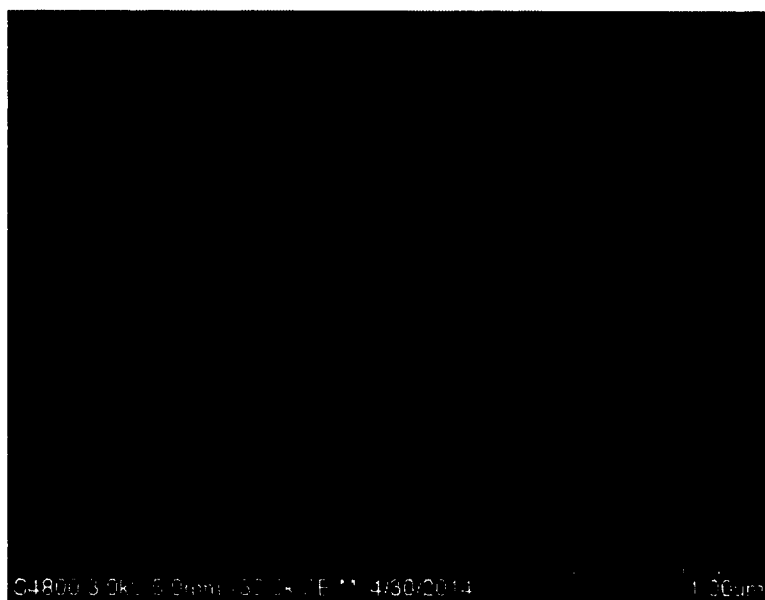
Figure 3-17: EDAX gold-coated HNTs 2:1 ratio

The imaging and EDAX confirmed that gold was present on the sintered halloysite. The gold acted as a thin coating of spheroids that collected on the surface. Differing ratios of gold were used to confirm the modular nature of the technique. Gold nanoparticles are currently under investigation for many novel medical treatments. The ability to create a custom nanoparticle that could react to a laser for a hyperthermia-based treatment is a valuable aspect of this technology.

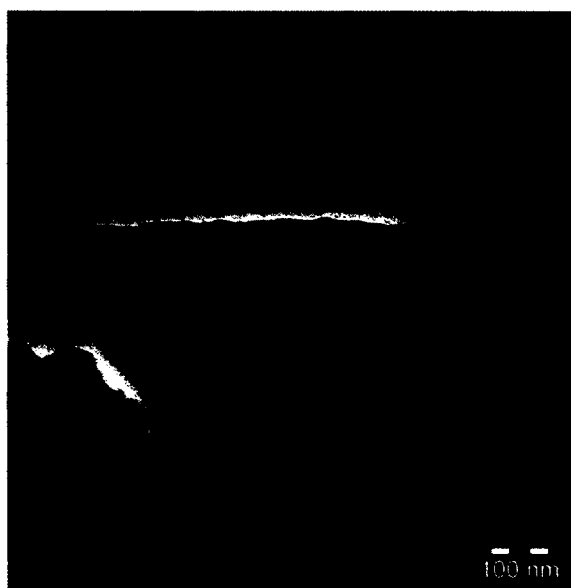
#### 3.6.1.4 Barium Acetylacetonate

Barium acetylacetonate was mixed in 100 mg or 250 mg batches with halloysite. The material was sintered at 300 °C and then ground by mortar and pestle. Imaging and EDAX was done. This is shown in Figure 3-18, Figure 3-19 and Figure 3-20.





**Figure 3-18:** SEM barium-coated HNTs



**Figure 3-19:** TEM barium-coated HNTs

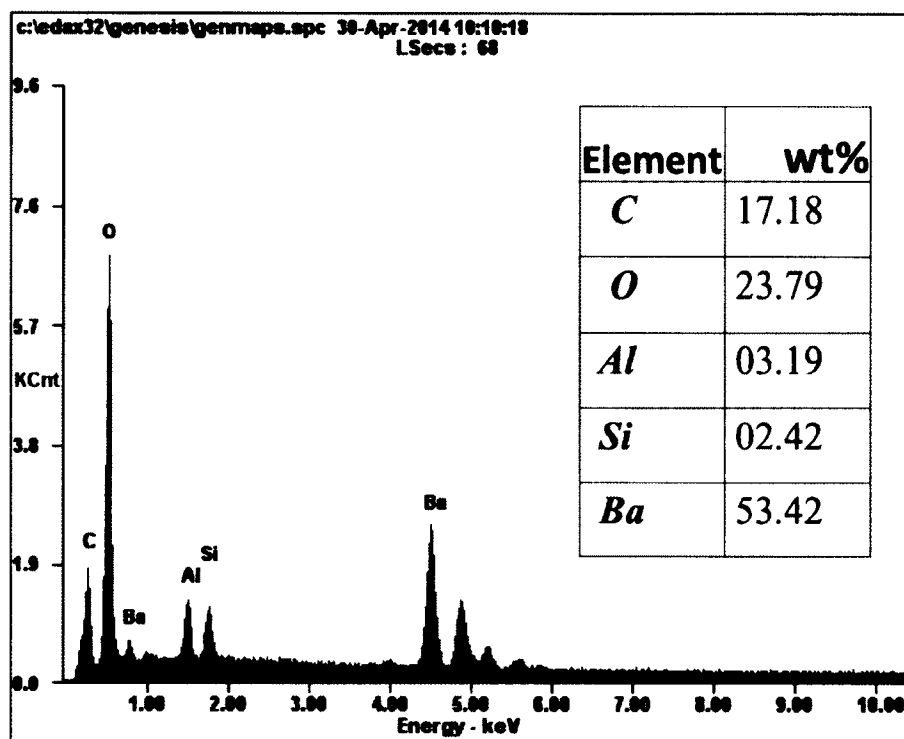
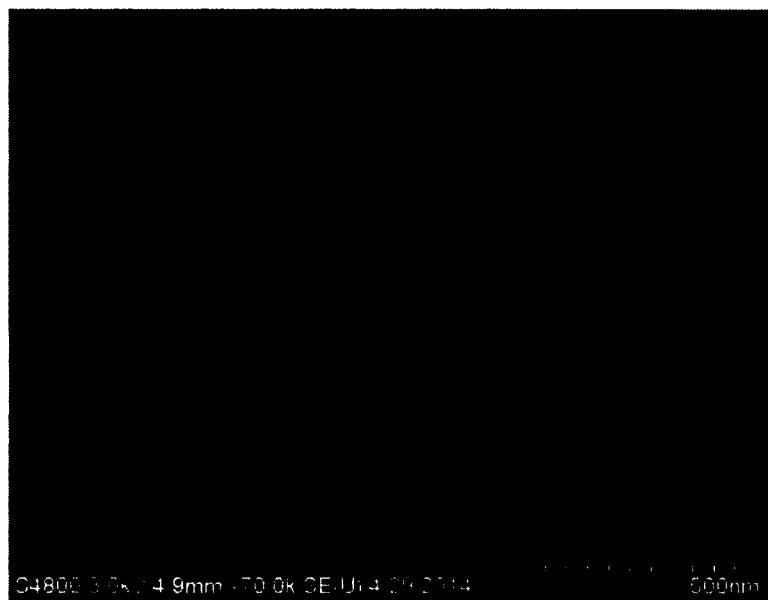


Figure 3-20: EDAX barium-coated HNTS

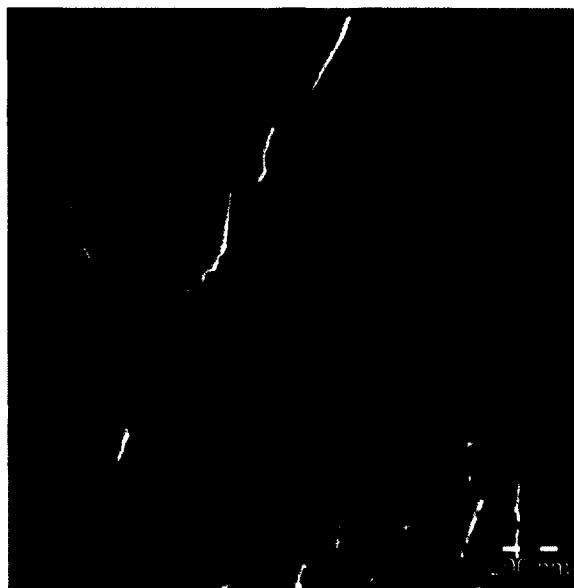
Both SEM and TEM showed that barium coated the nanotubes. EDAX also exhibited a barium peak. The barium seemed to create strong shell-like layers and spheroid depositions. Barium is commonly used as a contrast agent. The ability to create custom nanoparticles with contrast has many potential medical uses.

#### 3.6.1.5 Copper Acetylacetonate

Copper acetylacetonate was mixed in 100 mg batches in a 1:1 ratio with HNTs. Imaging and EDAX was done to confirm that the HNTs had been sintered and coated with the copper. This is shown in Figure 3-21, Figure 3-22 and Figure 3-23.



**Figure 3-21:** SEM copper-coated HNTs



**Figure 3-22:** TEM copper-coated HNTs

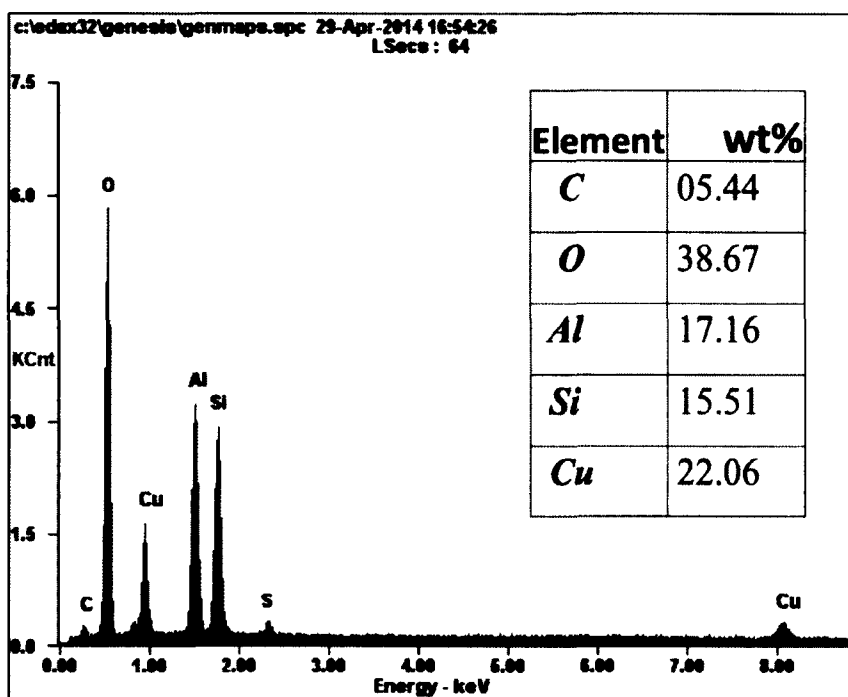
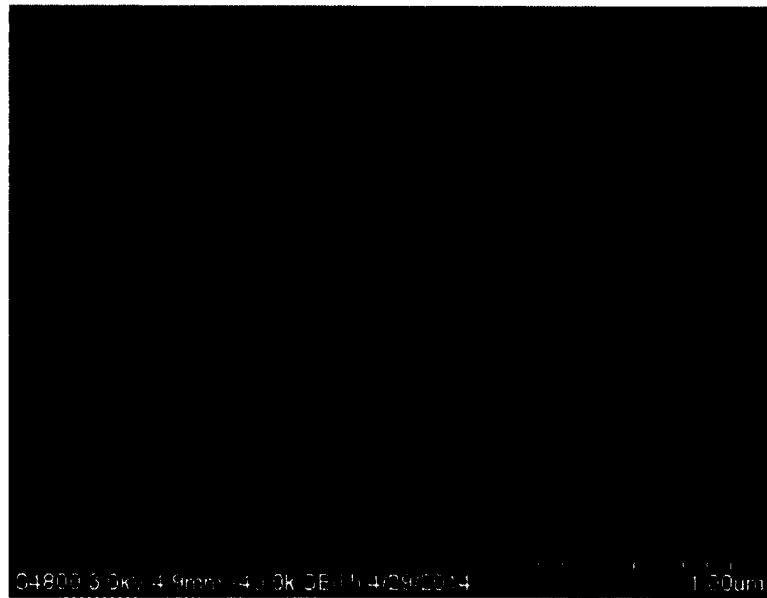


Figure 3-23: EDAX copper-coated HNTs

Both imaging and EDAX confirm copper coatings on the HNTs. The copper coated less in spheroids than the iron and gold. Some of the surface shapes were more irregular. However, sheet coatings still appear on several tubes. Copper can act as a cytotoxic additive in cell culturing and nanotubes with copper as a component could be used for targeted cytotoxic effects for use as controls in cell culture studies.[115, 116] Additionally, this technology could be valuable in other scientific fields such as sensors based on the conductivity of copper.

#### 3.6.1.6 Nickel Acetylacetonate

Nickel acetylacetonate was mixed in 100 mg batches in a 1:1 ratio with HNTs. Imaging and EDAX was done to confirm that the HNTs had been sintered and coated with the nickel. This is shown in Figure 3-24, Figure 3-25 and Figure 3-26.



**Figure 3-24:** SEM nickel-coated HNTs



**Figure 3-25:** TEM nickel-coated HNTs

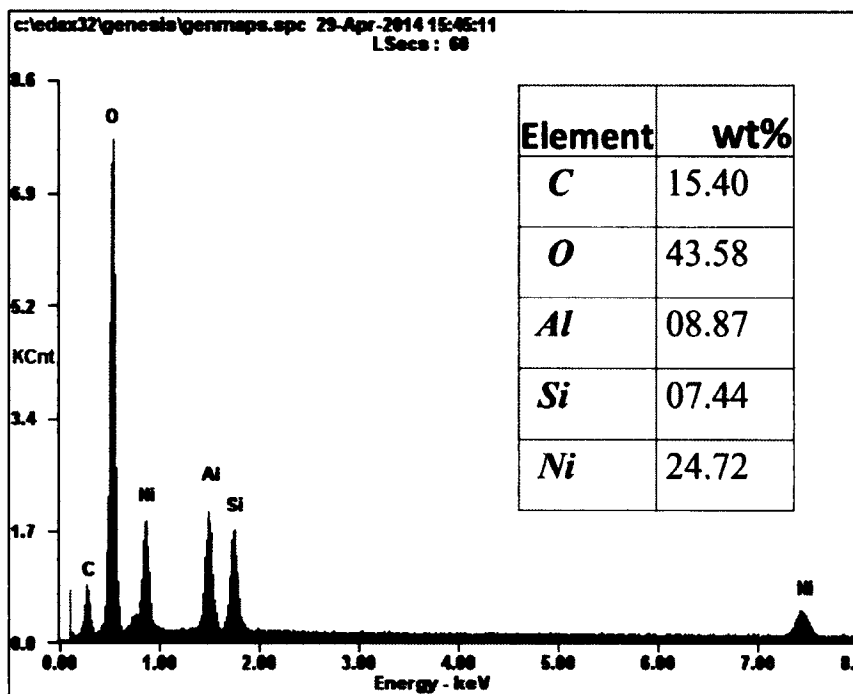


Figure 3-26: EDAX nickel-coated HNTs

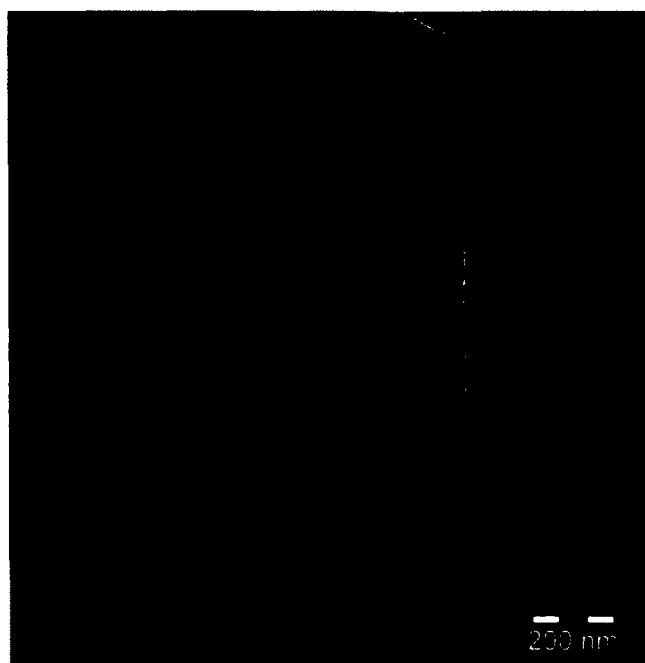
Both imaging and EDAX confirms nickel coatings on the HNTs. The nickel coated in smaller spheroids than the iron and gold. The nickel was not magnetically susceptible or only showed moderate properties. However, it is possible that other variations of this reaction could be developed to create a particle which could be strongly influenced by a magnetic field.

#### 3.6.1.7 Lithium Acetylacetonate

Lithium acetylacetonate was mixed in 100 mg batches in a 1:1 ratio with HNTs. Imaging and EDAX was used to confirm that the HNTs had been sintered and coated with the lithium. This is shown in Figure 3-27, Figure 3-28 and Figure 3-29.



**Figure 3-27:** SEM lithium-coated HNTs



**Figure 3-28:** TEM image of lithium-coated HNTs

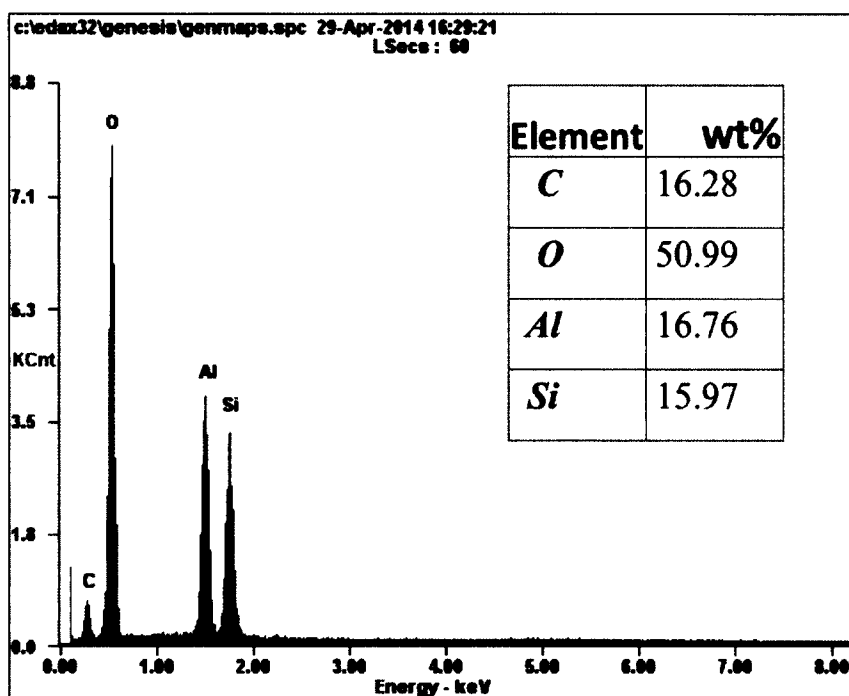


Figure 3-29: EDAX lithium-coated HNTs

Imaging confirms lithium coatings on the HNTs. The coatings are smoother and smaller than the other elements. The smaller size of the atom may make imaging more difficult. EDAX does not show the lithium even though it is present. The signal from lithium is masked by the signal from the beryllium material of the window used in the EDAX machine because the atomic number for beryllium (4) is too close to the atomic number for lithium (3).[117] For this reason EDAX could not detect the following elements: H, He, Li, or Be. Lithium-coated nanoparticles have substantial applications to sensors.

### 3.6.2 Multiple and Modular Metal Coatings

Changes in the ratio of metal acetylacetonate to HNT altered the coating thickness. This effect allowed for a system to create custom coatings. The ability to coat layers of different materials could create unique capabilities. A particle coated with iron



first and then gold would be magnetically susceptible. It hypothetically could be held in place by a magnetic field while a laser is used to target the gold shell and generate hyperthermia. While this work will demonstrate iron and gold combinations of coatings, iron and barium combinations of coatings were also generated.

#### 3.6.2.1 Iron and gold coatings

Iron acetylacetonate was mixed with HNTs in a 100 mg batch at a 1:1 ratio. They were heated in a Vulcan oven to sinter the iron onto the HNTs. The particles were then ground in a mortar and pestle. Finally, gold acetate was mixed with the iron particles in a 100 mg batch at a 1:1 ratio. The standard reaction for gold sintering was run. The final particles were found to be magnetic. Only TEM imaging was used because of the constraint of the magnetic nature of the particles (Figure 3-30).

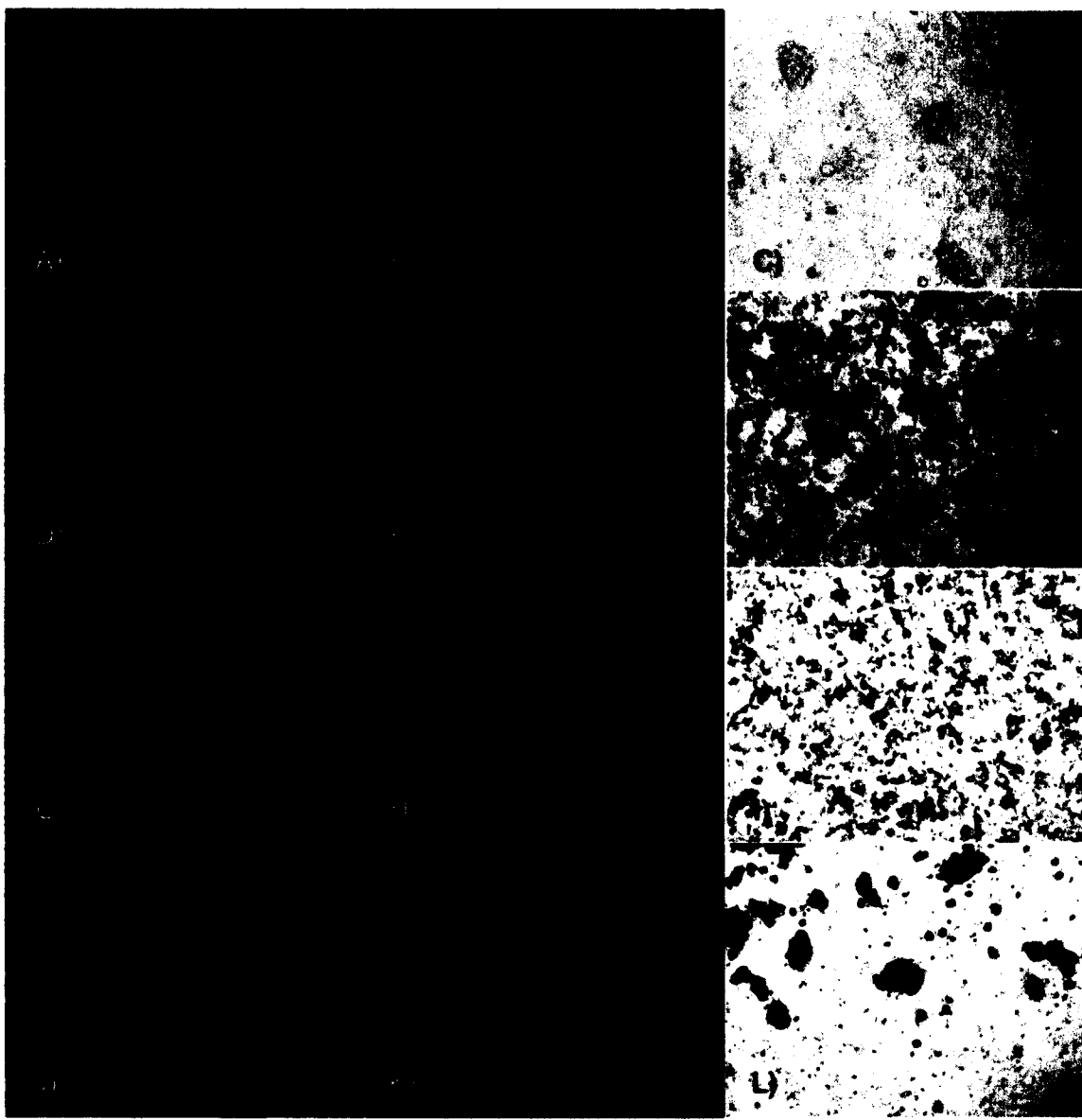


**Figure 3-30:** TEM of iron/gold-coated HNT

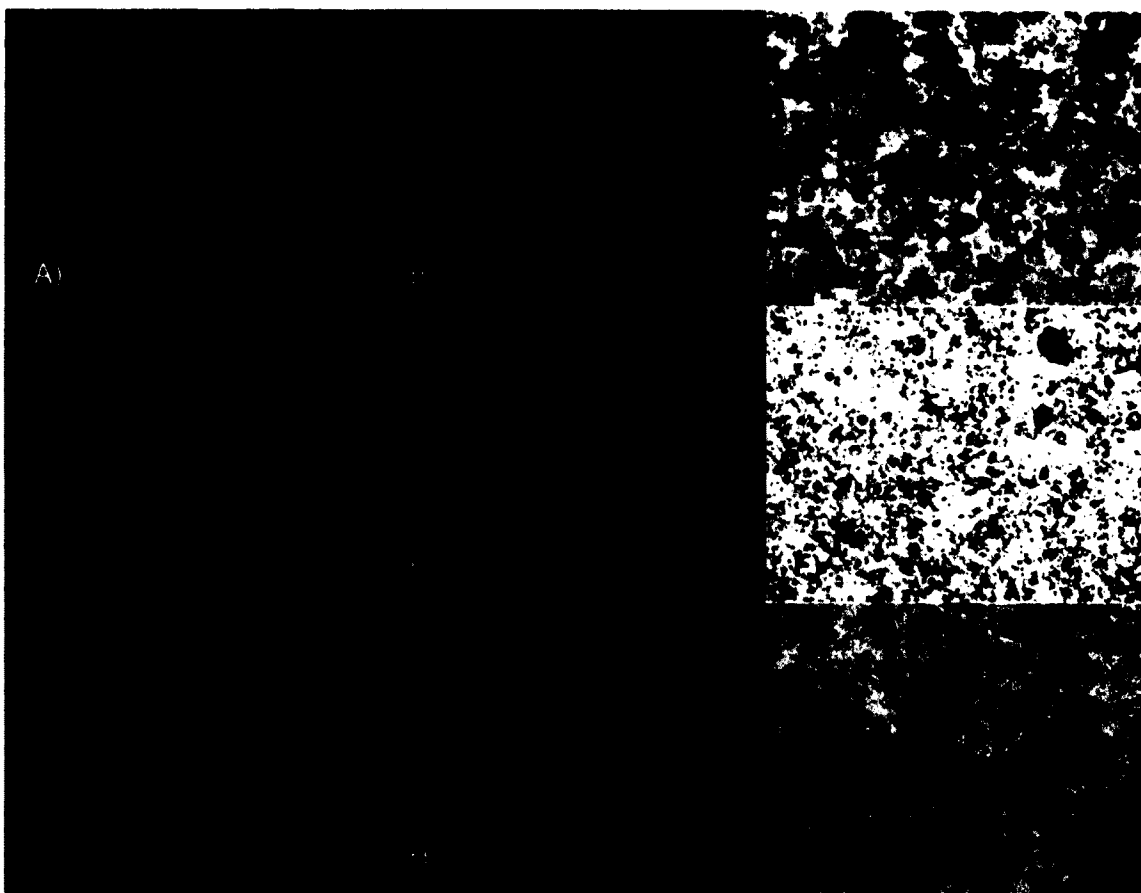
The particles had final coloring similarities to the gold particles. The particle reacted to a magnetic field. The particles had handling properties similar to both the iron and gold-coated particles.

### 3.6.3 Cytotoxicity Testing

Preliminary cytotoxicity testing was run. Osteoblast cells were plated in a 96 well plate with 1 w/v% of control HNTs and HNTs coated with iron, barium, copper and nickel. Six wells of each particle and appropriate controls were plated. After two days they were imaged by a Live/Dead assay as shown in Figure 3-31 and Figure 3-32. These images were quantified using the ImageJ analysis software in Appendix A.



**Figure 3-31:** Live/Dead assay of particles with osteoblasts in order of green live stain, red dead stain and light microscopy image at 40X. A-C) Control cells D-F) Control HNTs G-I) Lithium-coated HNTs J-L) Iron-coated HNTs



**Figure 3-32:** Live/Dead assay of particles with osteoblasts in order of green live stain, red dead stain and light microscopy image at 40X. A-C) Barium-coated HNTs D-F) Copper-coated HNTs G-I) Nickel-coated HNTs

The osteoblast Live/Dead assays provided strong preliminary indicators about the particles. Control wells had more confluence and cell growth. Control HNTs, iron-coated HNTs, barium-coated HNTs, and lithium-coated HNTs all had substantial cell growth. The cell viability suggests that these particles should be further investigated for drug delivery applications in cell culture studies. Copper-coated HNTs and nickel-coated HNTs almost completely killed all cells in the wells where they were placed. This cytotoxicity does not necessarily indicate that these particles are not useful. Copper is commonly added to cell culture wells to guarantee inhibition of cell growth or death.[115, 116] A copper nanoparticle that can be targeted could act to kill a cell

without being loaded with any drugs. There is clear potential for future research to investigate applications of these classes of particles.

#### 3.6.4 Lipid and LBL Coatings

To allow for *in vivo* uses, such as drug delivery, nanoparticles need to stay in the blood stream or not damage areas of the body as they pass through. The iron and gold-coated nanotubes were coated in lipids and polyelectrolytes that are known to act as biocompatible coatings to demonstrate the modular nature of the technology.

##### 3.6.4.1 Lipid Bioactive Coatings

DOTAP lipids were used to coat the iron-coated HNTs, gold-coated HNTs, and iron/gold-coated HNTs. The results were imaged by TEM (Figure 3-33, Figure 3-34 and Figure 3-35).



**Figure 3-33:** TEM of lipid-coated iron sintered HNTs



**Figure 3-34:** TEM of lipid-coated gold sintered HNTs



**Figure 3-35:** TEM image of lipid-coated iron/gold sintered HNTs

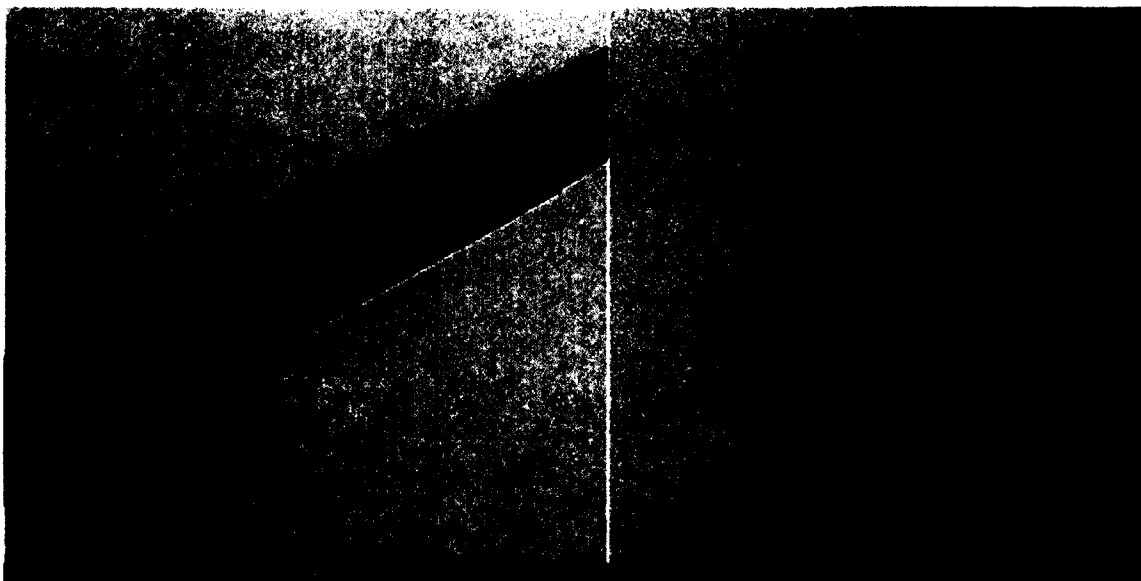
These images act as preliminary results, showing the capability to coat the particles in lipid coatings. Based on substantial usage in the literature, DOTAP lipids are likely to be biocompatible. Thus, this result acts as a proof of principle showing the creation of a modular nanoparticle fabrication system that can have biocompatible coatings.

#### 3.6.4.2 LBL Polyelectrolyte Biocompatible Coatings

The polyelectrolyte PVP and PAA were used to create a LBL coating of the iron-coated HNTs and gold-coated HNTs. The results were imaged to confirm coating (Figure 3-36 and Figure 3-37).



**Figure 3-36:** TEM LBL polyelectrolyte-coating iron HNTs



**Figure 3-37:** A) gold-coated HNTs and B) LBL polyelectrolyte-coated, gold-coated HNTs loaded with methotrexate

The polyelectrolyte coating can clearly be seen. One advantage of a polyelectrolyte system over a lipid based one is that the coating can be tuned to slowly dissolve over time. A particle with magnetic susceptibility properties can maintain position in a localized area, giving a coating time to dissolve.

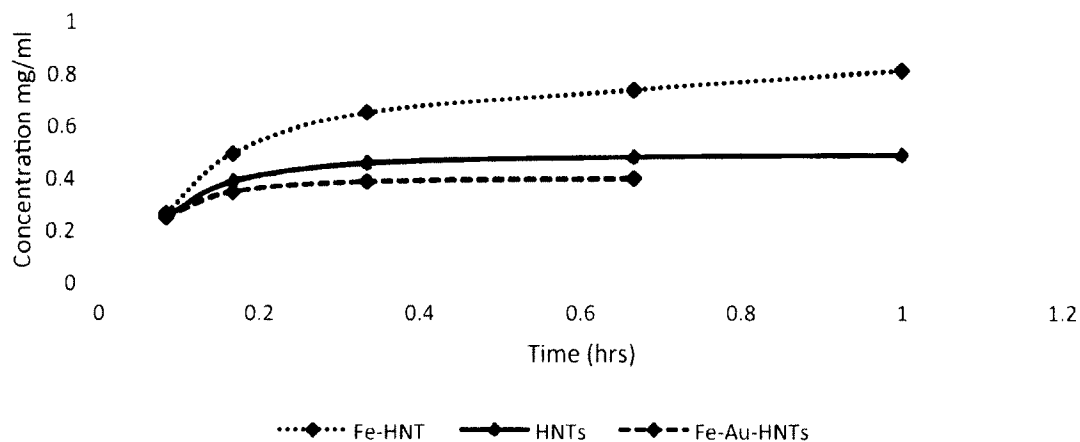
### 3.6.5 Release Profiles

Halloysite can be loaded with compounds of interest and will release them in a sustained manner.[88] Substances of interest can be vacuum loaded into the lumen of HNTs. The charge of the substrate to be absorbed is also highly relevant. The outer surfaces of HNTs are negatively charged while the lumen is positively charged. It is highly relevant to determine how coating with iron or gold will affect the release profile.

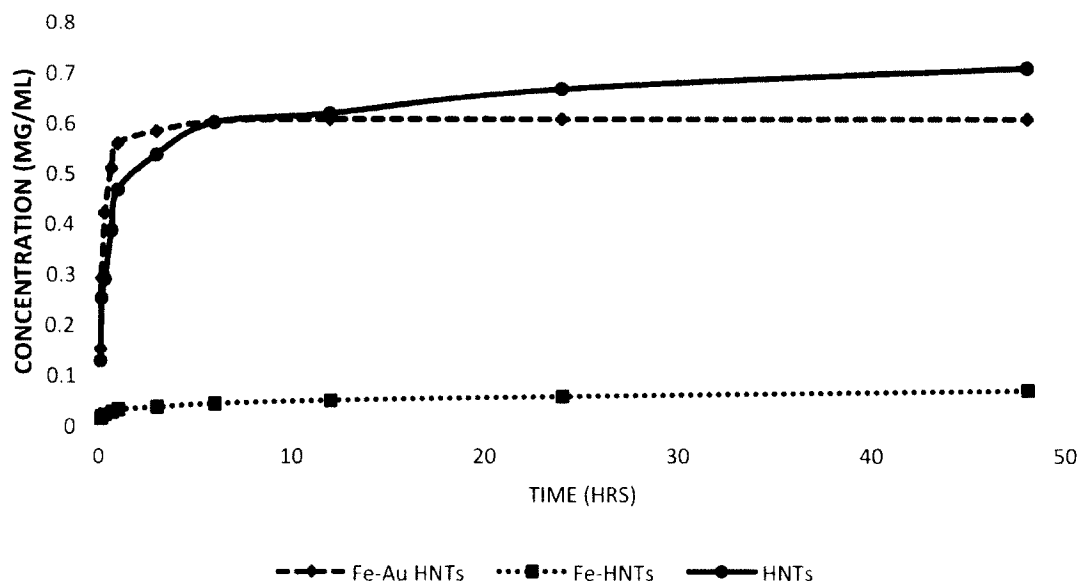
Gentamicin sulfate, methotrexate and nitrofurantoin were vacuum loaded into HNTs. Maximum solubility solutions of the substances were made. Gentamicin was dissolved in deionized water at 50 mg/mL. Methotrexate was dissolved in dimethyl



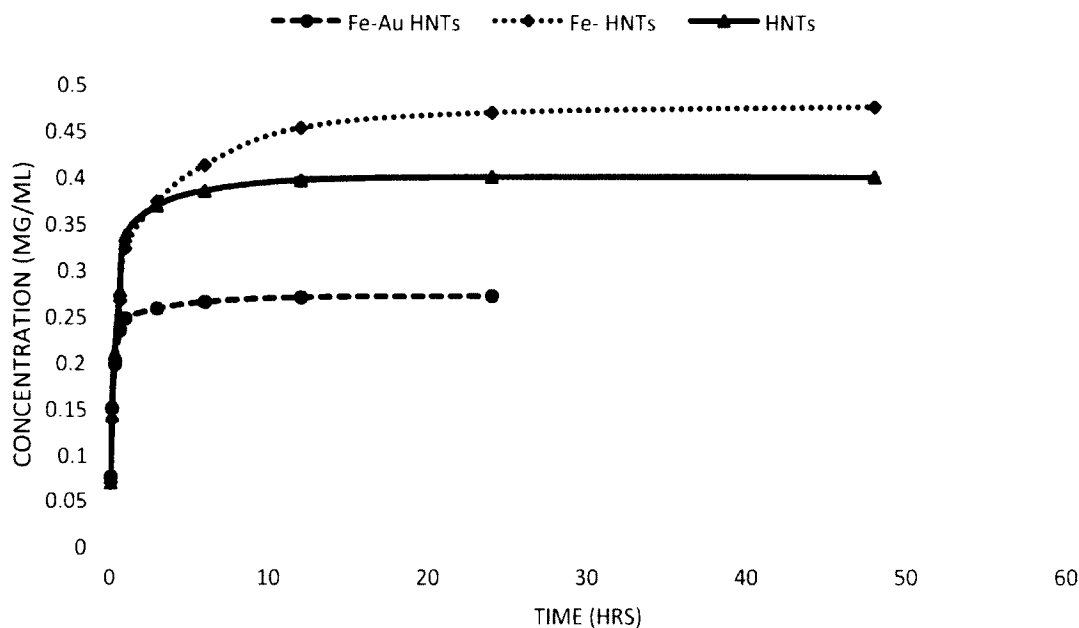
sulfoxide at 90 mg/mL. Nitrofurantoin was dissolved in acetone at 5 mg/mL. A test tube was filled with 5 mL of a solution and enough halloysite to approximately load the amount in the solution, assuming 10% loading by weight. Control halloysite, iron-coated halloysite and iron/gold-coated halloysite were used. Static elution profiles were run as shown in Figure 3-38, Figure 3-39 and Figure 3-40.



**Figure 3-38:** Elution profile of HNTs loaded with gentamicin sulfate



**Figure 3-39:** Elution profile of HNTs loaded with methotrexate



**Figure 3-40:** Elution profile of HNTs loaded with nitrofurantoin

In the gentamicin sulfate release profile the control halloysite showed a release profile similar to that of other experimental protocols. The iron/gold-coated particles likely loaded and released less gentamicin. The iron-coated halloysite had the strongest release profile. The charges of the different metal coatings and locations likely played a large part in the release profile. A similar effect was seen with the nitrofurantoin release profiles. However, the methotrexate release profiles showed the control HNTs and iron/gold-coated HNTs having a more sustained release profile than the iron-coated HNTs. It should be noted that due to solubility effects in water that the nitrofurantoin and methotrexate loaded HNTs had substantially longer release profiles than the gentamicin loaded HNTs.

### 3.6.6 Barium Nanoparticle Enhanced Bone Cements

A core objective was to demonstrate that nanoparticle modification could also enhance biomaterials. HNTs can enhance the material properties of biomaterials such as

bone cements.[96] The sintering process creates even more customization opportunities. Barium-coated HNTs were tested by MRI to determine the amount of contrast that they added to the bone cements in Hounsfield units. Control bone cements were mixed and molded from low viscosity and high viscosity commercial cements that contained barium. Additionally, plain PMMA powder was obtained to be able to create bone cement molded constructs without barium (Figure 3-41).



**Figure 3-41:** A) Low viscosity commercial bone cement B) High viscosity commercial bone cement C) PMMA only bone cement

Three experimental group categories were made using the PMMA-only bone cements. These were control HNTs, barium-coated HNTs, and barium. Additives were added to the virgin PMMA cements by wt% in 5 wt% intervals. The control HNT group had 5 wt%, 10 wt%, 15 wt% and 20 wt% concentrations. The barium-coated HNT group had 5 wt%, 10 wt% and 15 wt% mixed into the cement. These groups are shown in Figure 3-42.



**Figure 3-42:** A) HNT enhanced plain PMMA bone cement B) Barium-coated HNT enhanced plain PMMA bone cement

A 30 mm long rectangular bar sample of each cement was run through a MRI machine set to 120 KV. The three-dimensional scan was manually observed. Fifty to one hundred 1 mm point regions of interest (ROI) were calculated in each sample for contrast in Hounsfield Units. The ROIs from the samples were averaged in Table 3-1.

Table 3-1: Table of bone cements' contrast level in Hounsfield Units

Control Groups	Hounsfield Units	HNTs	Hounsfield Units	Barium coated HNTs	Hounsfield Units
Low Viscosity	1473	5wt%	140	5wt%	382
High Viscosity	1443	10wt%	164	10wt%	652
PMMA only	68	20wt%	164	15wt%	1029

The PMMA-only cement has very low contrast and visibility at 68 Hounsfield units. HNTs per the literature can add strength but add little contrast compared to commercial low or high viscosity cements. In fact 20 wt% HNTs added to the cement only increase the Hounsfield units to 164 from 68 of plain PMMA. Barium-coated HNTs at 15 wt% are 1029 Hounsfield units. The barium-coated HNTs were 6.3x's the contrast level of the control HNTs. The barium coated HNTs at 15wt% were 15.1x's the contrast level of plain PMMA. The 15wt% barium-coated HNTs had roughly 70% of the contrast

level of the commercial bone cements. Each 5 wt% increase in barium-coated HNTs resulted in a 300 Hounsfield unit increase in contrast. It should be noted that multiple layers of barium coatings could be done to further enhance the contrast level of the barium-coated HNTs. This could allow for a commercial level of contrast with the optimal level HNTs added to the bone cement for strength increases. This simple study shows the potential for even further customized HNTs as biomaterial enhancers.

### 3.7 Conclusion

A method for making modular nanoparticles with custom coatings was created. The metal acetates and metal acetylacetonates were used to coat HNTs. A wide variety of coatings was accomplished. SEM, TEM and EDAX were used to verify the coating of HNTs with iron, gold, barium, lithium, copper and nickel. The coatings allow for the creation of nanoparticles with a wide range of properties. Iron coatings were proven to be magnetically susceptible. Barium coatings added contrast to biomaterials. Lithium and copper have unique properties that show potential for sensors or cytotoxic particles in the case of copper.

The ability to alter the percent coating by increasing or decreasing the ratio of metal acetylacetonate to HNTs was also demonstrated. For example, gold-coated HNTS at a 2:1 instead of a 1:1 ratio showed more gold coatings on SEM. The ability to use coatings of different metals was also demonstrated. Iron/gold and iron/barium particles were fabricated.

Biocompatibility is an issue in the use of nanoparticles. DOTAP lipid coatings and LBL polyelectrolyte coatings were added to iron-coated HNTs, gold-coated HNTs, and iron/gold-combination coated HNTs.

Preliminary cytotoxicity studies were run on the basic particles to provide information for future work. Control HNTs, iron-coated HNTs and barium-coated HNTs had similar effects on osteoblast cultures. In contrast, copper- and nickel-coated HNTs led to almost universal cell death.

Particles eluted loaded drugs differently based on their unique structure and charge profiles. The MRI contrast findings showed that halloysite additives used to strengthen the PMMA polymer can provide enhanced properties, such as contrast.

## CHAPTER 4

### 3D PRINTING ANTIBIOTIC CONSTRUCTS

#### 4.1 Introduction

Additive manufacturing and 3D printing provide the potential for highly personalized medicine and will have many implications for patient care. This chapter demonstrates the first methods of 3D printing as a method of controlled drug delivery for medical treatment. Recent advances in biofabrication and bioprinting, such as microcontact printing or 3D printing, may enable unique universal and on-demand medical treatments.

Developed in the early 1990's by Sachs *et al.*, 3D printing technology then was a powder-based fabrication method that was focused towards rapid tool production using metals and ceramics. A typical printing set-up produces a 3D model based on a digital file through an additive process that lays down successive layers in almost any shape. Three-dimensional printing is most well-known for creating plastic prototypes, objects and structures rapidly, cheaply, and with an amazing degree of accuracy. The most common consumer method of fabrication is called fused deposition modeling (FDM), a term that has recently become nearly synonymous with 3D printing. For this method, a plastic filament is melted and laid down in a layer-by-layer process to build a construct. 3D printing has found its place in medicine, biotechnology and nanotechnology, thus

paving the way for the rapid printing of medicines, artificial devices, prosthetics, and even human tissue. Currently, an intense research effort is focused on the application of 3D printing for the development of blood vessels, bioengineered tissues, and functional biomedical materials and devices for dental and orthopedic applications.

Osteomyelitis is an intractable condition affecting both the young and the elderly. It is generally treated with local or systemic antibiotic therapy and often multiple surgical interventions. Osteomyelitis is difficult to treat, and for the patient that is unresponsive to antibiotic treatment, it can lead to limb amputation or death. Chronic osteomyelitis can require surgical debridement and local antibiotic treatment.

Antibiotic-impregnated beads delivered during debridement have numerous advantages over systemic therapy. These advantages include ease of placement, application with different antibiotics, decreased systemic toxicity, reduced hospital stays and patient cost.

The disadvantages of currently used non-biodegradable (PMMA) beads include low biocompatibility, poor antibiotic release with slow residual antibiotic release for unknown periods, necessity of surgical removal, and cytotoxic effects due to thermal damage during PMMA polymerization. In contrast, biodegradable antibiotic carriers offer many advantages. They do not require a second surgery to remove the carrier material, are gradually replaced by ingrowing tissue, and may even support new bone growth.

Additionally, antibiotic release during degradation could increase the antibacterial efficacy compared to non-biodegradable carriers. Unsolved issues include inadequate mechanical properties and processability, rapid release of antibiotics, cytotoxicity of degradation products, and no current FDA approval of these methods as of this paper.



Systemic delivery of antibiotics affects the intended site as well as unaffected tissues, and for some patients, raises the risks of cytotoxicity, nephrotoxicity, and an increase in antibiotic resistance. It is clinically advantageous to have direct treatment without unnecessary and widespread harmful effects. A key goal in this field is to combine the key features of 3D printing (accuracy, speed, tunability) into a system that enables on-demand, customized, and patient-specific antibiotic treatments, and has the potential to address many of the disadvantages with current antibiotic carrier systems.

In the present work, a new class of bioactive 3D printing filaments using gentamicin sulfate, tobramycin and nitrofurantoin were created. It was found that through the manufacturing process, these compounds retained their effective antimicrobial or cell growth inhibiting properties despite the heat required in this method of fabrication.

## **4.2 Design and Objectives**

The experimental design will look at proving the basic capabilities of filament extrusion, bioactive construct fabrication and bacterial or material testing of filaments and constructs. The following sections break down the design objectives into specific areas.

### **4.2.1 Thermal Stability Objective**

The first objective should be to test thermal stability of different bioactive compounds. These should be compared to known bioplastics or polymer melt and melt-flow temperatures. A search for optimal combinations should occur.

### **4.2.2 Filament Extrusion Objective**

A method of uniformly mixing bioactive additives with materials for 3D printing filaments will be developed. This method can be tested with a custom built or newly

commercially available filament extruder. The ability to fabricate 3D printing filament that is the proper diameter and is usable on either a commercial or consumer fused deposition modeler 3D printer will be developed.

#### 4.2.3 3D Printing and Additive Manufacturing Objective

The ability to 3D print a custom extruded bioactive filament will be demonstrated. This objective will involve either designing a custom 3D printing machine or developing a method that allows for a custom extruded filament to be used in an already available 3D printing device. A consumer or tabletop 3D printing device is used to prove the universal capabilities of this technology. Of the many types of 3D fabrication methods available, the design will focus on fused deposition modeling, one of the more common methods.

#### 4.2.4 Bacterial Testing Objective

The functionality of antibiotic-loaded bioactive constructs will be tested *in vitro* with living bacteria. These tests would be done to ISO or ASTM standards in both broth and plate cultures. The ability to verify results with outside laboratories such as the clinical microbiology lab at LSU Health Shreveport will also be tested.

#### 4.2.5 Elution Testing Objective

The ability to quantify the amount of bioactive material or antibiotic eluted from an extruded filament or printed construct will be tested. This test will yield valuable information in determining the effects of the selectable percentage fill in constructs and how it will affect elution profiles.

#### 4.2.6 Comparison With Current Standards Objective

All extruded filaments and constructs will be tested with comparable PMMA-based materials to act as a control. The current gold standard in implant material is

PMMA bone cement. Knowing how well the bioactive constructs compare to current materials will be critical in determining the value of continued research.

#### 4.2.7 Scanning Bone Defects Then Printing Plugs Objective

A method will be developed to allow a surgeon to scan a bone defect in real time and to create a drug eluting implant that can fill an existing or surgically created defect. This method will extend current technology that uses a MRI or CT scan to create 3D-printed constructs of a body part.

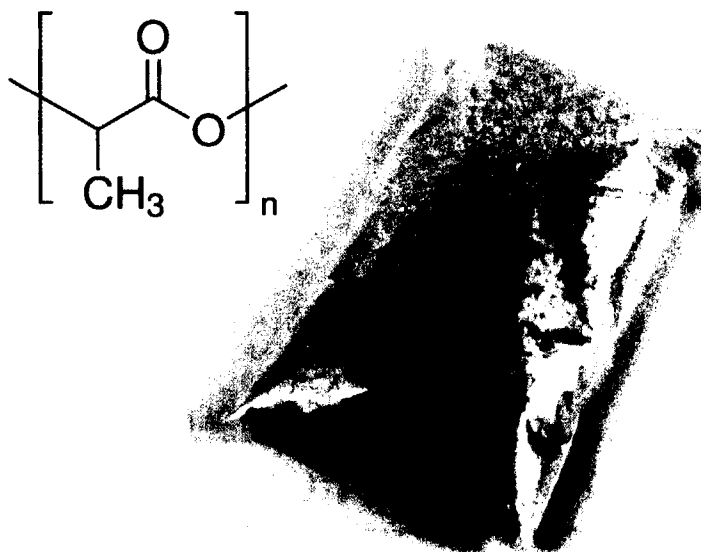
### 4.3 Materials

All treatment compounds used in this study were purchased from Sigma Aldrich (St. Louis, MO), including gentamicin sulfate (GS), tobramycin and nitrofurantoin. PMMA bone cement was a low viscosity ORTHOSET® 3 radiopaque bone cement from Wright Medical (Warsaw, IN). The polylactic acid (PLA) beads used for the printing media were obtained from NatureWorks, LLC (Minnetonka, MN). For bacterial culture, *E. Coli* vitroids Escherichia coli ATCC® 11775 Vitroids™ 1000 CFU were purchased from Sigma Aldrich (St. Louis, MO). Bacterial culture supplies, including 100 mm Hinton Mueller agar plates and Hinton Mueller liquid broth 1 L were purchased from Fischer Scientific (Hampton, NH). KJLC 705 silicon oil used for coating the beads prior to extrusion was purchased from Kurt J. Lesker Company (Jefferson Hills, PA). The 3D printing set-up consisted of an ExtrusionBot extruder purchased from ExtrusionBot, LLC (Phoenix, AZ) and a MakerBot 2X or Replicator 3D printer (Brooklyn, NY). The atomizer setup used a Sonics® brand atomizer (Newton, CT). The nanodrop spectrophotometer was from Thermo Scientific (Wilmington, DE). Biomaterials were heated with a Vulcan® A550 Series Benchtop Muffle Furnaces from Thomas Scientific

(Swedesboro, NJ). All gentamicin visualizing reagents, including sodium tetraborate, 2-mercaptoethanol and phthalaldehyde were ordered from Sigma Aldrich (St. Louis, MO). Halloysite nanotubes were also obtained from Sigma Aldrich (St. Louis, MO). The Solidworks 2014 student edition 3D CAD program Dassault Systèmes (Waltham, MA) was used for modeling. A Roland Corporation LP-250 desktop 3D scanner (Osaka, Japan) was used for scanning constructs. The SEM was a Hitachi S-4800 (Schaumburg, IL).

#### 4.3.1 Bioplastics and Polymers

Plastic polymers have been developed with many properties. For this study a focus was on polylactic acid bioplastics. This common bioplastic is used in many 3D printing filaments and world wide in manufacturing. The PLA chemical structure and PLA pellets are shown in Figure 4-1.



**Figure 4-1:** Polylactic acid structure and bag of Polylactic acid pellets[118]

The polymer structure shown in Figure 4-1 allows for use in a wide range of temperatures. The melting point is roughly 150 °C with a melt flow normally achieved in

the 190 °C to 220 °C ranges.[119] This melt flow allows for use in 3D printing applications. The lower melting point allows for usage in pressurized filament extrusion devices at proper temperatures that do not degrade select bioactive compounds. Most PLA pellets for injection molding or extrusion are 3-5 mm in size.

#### 4.3.2 PMMA Bone Cements

PMMA bone cement was a low viscosity ORTHOSET® 3 Radiopaque Bone Cement from Wright Medical (Warsaw, IN). Bone cement is normally sold in a kit that comprises a forty-gram powder pouch and vial of liquid monomer. Bone cement is used by mixing a powdered PMMA polymer with a liquid monomer. It is then allowed to set for several minutes. A bone cement kit is shown in Figure 4-2.

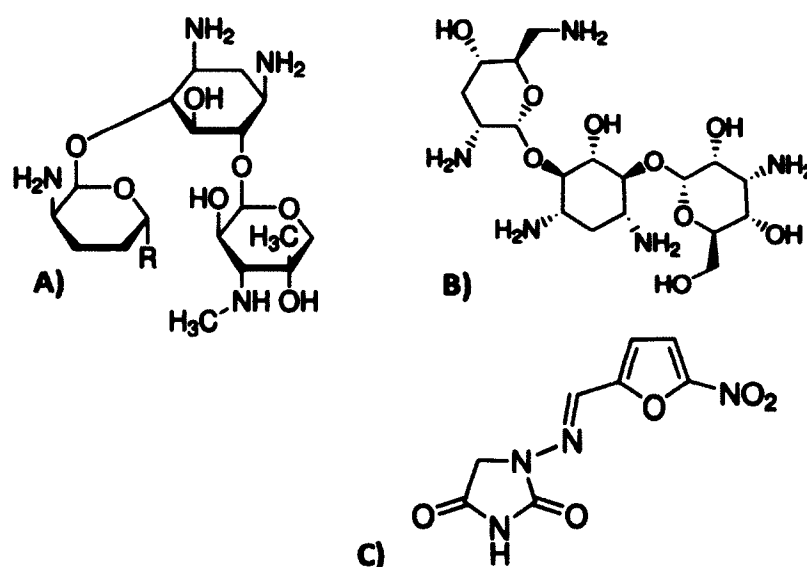


**Figure 4-2:** Bone cement kit liquid monomer/powder and PMMA structure[120]

During the setting process temperatures of 80-90 °C were recorded on the ORTHOSET cements. These cements are available with antibiotics already mixed into the powders. The pre-mixed versions were not used in this study to allow for controls on antibiotic sources.

### 4.3.3 Bioactive Materials

All treatment compounds used in this study were purchased from Sigma Aldrich (St. Louis, MO) including gentamicin sulfate (GS), tobramycin and nitrofurantoin. These antibiotics were chosen for predicted thermal stability properties. The chemical structure of these antibiotics allows them to survive thermal degradation at higher temperatures as can be seen by Figure 4-3.



**Figure 4-3:** Structures A) Gentamicin B) Tobramycin C) Nitrofurantoin[121]

The expected degradation point of the aminoglycoside antibiotics such as GS and tobramycin is higher than other classes of antibiotics. They are commonly mixed with bone cements to make antibiotic beads and used by orthopedic surgeons. This means they are already exposed to temperatures in excess of 90 °C when clinically used. The expected degradation point is in excess of 240 °C. Aminoglycoside antibiotics have high water solubility. GS is soluble up to 50 mg/mL and tobramycin is also soluble up to 50

mg/mL. The melting points differ, however, with tobramycin melting at 160 °C and GS melting ranging from 220 °C-240 °C.[122] The aminoglycosides dissolve clearly into water and need to be visualized with a reagent. Aminoglycoside powders are white on visual inspection. Nitrofurantoin in contrast is yellow on visual inspection. It can be visualized with peaks at 260 nm and 375 nm with spectrophotometry. Nitrofurantoin is only minimally soluble in water, with a 0.19 mg/mL solubility. The melting point is around 270 °C.[122]

#### 4.3.4 Halloysite Nanotubes

Halloysite nanotubes were obtained from Sigma Aldrich (St. Louis, MO). Halloysite has been characterized in many studies and used as a model nanoparticle for material property enhancements or drug delivery. Halloysite nanotubes are shown in Figure 4-4.

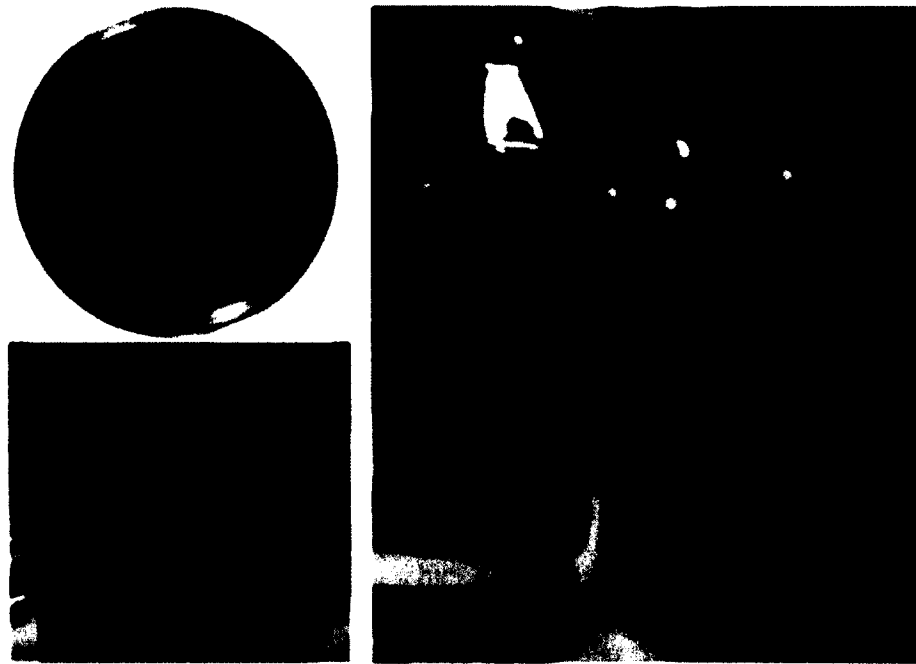


**Figure 4-4:** SEM pictures of halloysite nanotubes

The nanotubes have lengths of a few hundred nanometers with hollow inner lumens ranging from 10-50 nm. They are a proven and modifiable nanotechnology platform.

#### 4.3.5 Bacterial Culture Supplies

Bacterial culture supplies of 100 mm Hinton Mueller agar plates, and Hinton Mueller liquid broth 1 L bottles were purchased from Fischer Scientific (Hampton, NH). These packages of plates and broths are shown in Figure 4-5.



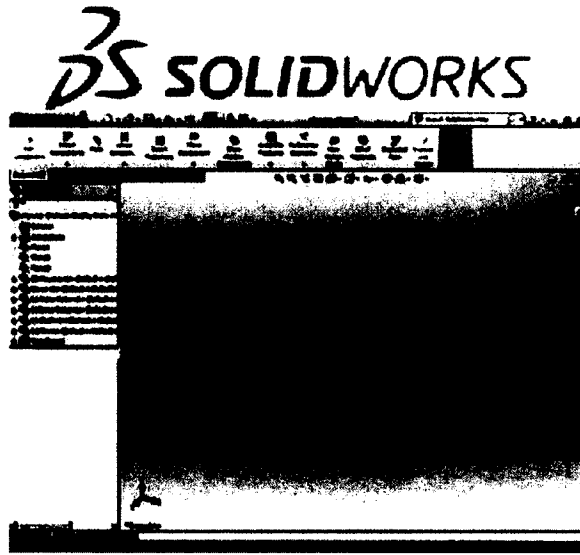
**Figure 4-5:** Mueller-Hinton plate, package of plates and broth bottles

Both plates and bottles were re-shipped from the manufacturer Remel and made to clinical microbiology laboratory standards.



#### 4.3.6 Computer Modeling

The Solidworks 2014 student edition 3D CAD program by Dassault Systèmes (Waltham, MA) was used for modeling. The program interface with a part is shown in Figure 4-6.

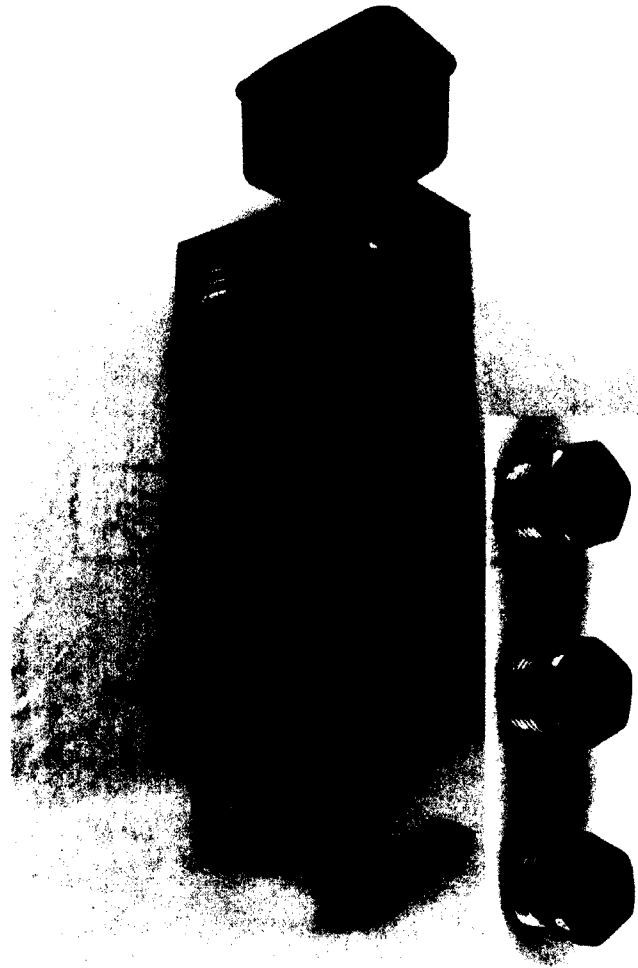


**Figure 4-6: Solidworks 3D CAD program interface[123]**

Program constructs were saved in .STL file format for easy interaction with 3D printers.

#### 4.3.7 Filament Extruder

Filament extrusion was done by an ExtrusionBot extruder purchased from ExtrusionBot, LLC (Phoenix, AZ). This instrument is shown in Figure 4-7.

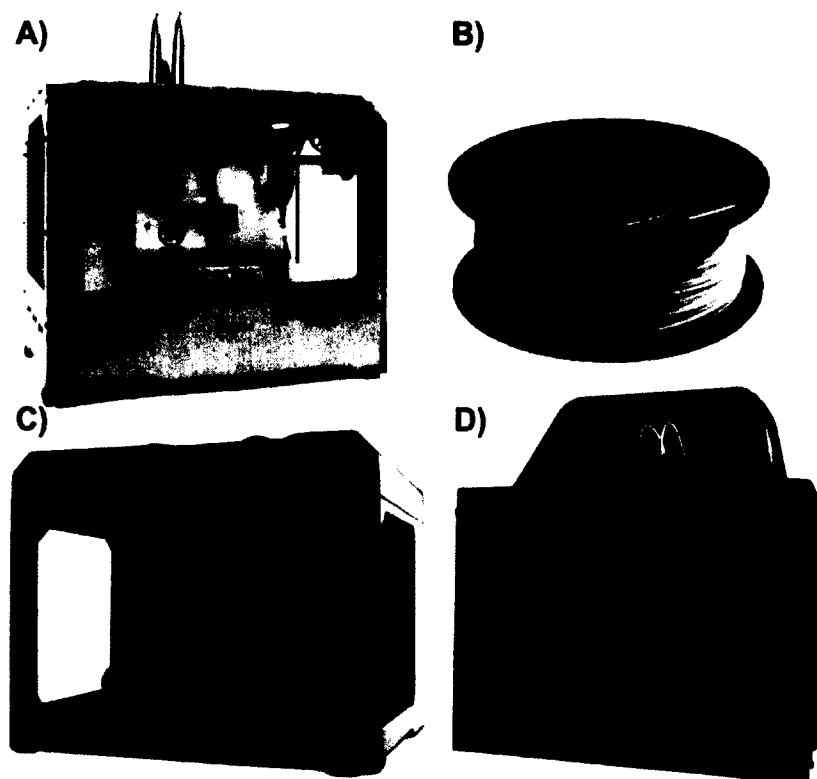


**Figure 4-7:** First generation Extrusionbot filament extruder[118]

The device includes a hopper for pellets that feeds into a pipe. The pipe has an auger and is heated by a heating mechanism. The temperature can be set and is maintained by sensors. The pellets are melted and pushed into the distal portion of the pipe. The distal portion has a metal die with a hole drilled into it of desired extrusion diameter. The filament that is extruded is cooled above melting by a fan attached on the back of the unit.

#### 4.3.8 3D Printers

The MakerBot 2X or Replicator 3D printer made by Makerbot Inc (Brooklyn, NY) was used for fabrication. These units are shown in Figure 4-8.



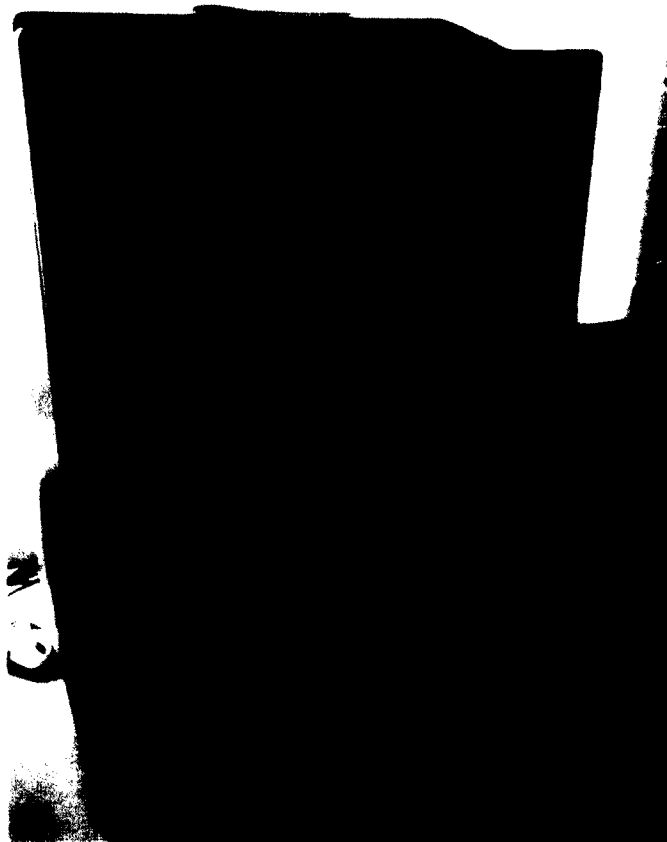
**Figure 4-8:** A) Original Makerbot Replicator B) Makerbot Filament C) Makerbot Replicator 5<sup>th</sup> Generation D) Makerbot Replicator 2X[124]

The original Makerbot Replicator has two print heads and a heated build platform. This configuration is similar to the Makerbot 2X which also has two print heads and a heated platform. Both of these units are recommended for use with ABS plastic filaments. The Makerbot Replicator 5<sup>th</sup> Generation uses a novel detachable print head that unclips by a magnet. All units function by fused deposition modeling. They run on various versions of the Makerware software that can use .STL file formats. The printers are able to fabricate any construct in the .STL file format. The constructs can be rotated in three dimensions and resized. The 3D printers use a software program called Makerware, which allows for several customizable fabrication options. The temperature they use to print is typically 220 °C for PLA or ABS plastics. This temperature can be

modified. The resolution on these printers typically ranges from 50 to 400 microns. This resolution can be considered the width of the slice used in the fabrication process. The percentage fill of the file can also be modified. Most prints are done at a low percentage fill of 10% - 20%.

#### 4.3.9 3D Scanners

A Roland LPX-250 3D desktop laser scanner was used to scan any larger components into SolidWorks that had to be modeled. This was located in the basement of Bogard Hall, Louisiana Tech University. A part to be scanned is placed on the rotating scanner bed then automatically turned 360 degrees while the scanning takes place. This device is shown in Figure 4-9.



**Figure 4-9:** Roland LP-250 desktop 3D scanner

#### 4.4 Fabrication and Methods

To understand the steps required in 3D printing antibiotic eluting constructs a wide range of fabrication techniques and general experimental methods must be reviewed. These range from extruding PLA polymers into 3D printing filaments to creating 3D fabricated constructs with them. In general different methods of bacterial testing and measuring drug elution must also be used. Once fabrication methods have been described a working knowledge of these techniques can allow for replication of these studies.

Several fabrication techniques for the coating of pellets and filament extrusion will be discussed. The knowledge of proper temperatures and materials is necessary for the creation of a uniform bioactive filament. This discussion will primarily focus on polymers and bioactive additives.

Once filaments can be created then constructs can be modeled for fabrication. The Solidworks modeling program will be used to create various constructs for fabrication. The setups involved in the 3D printing will be discussed in terms of printer type and setting.

Controls of the PMMA bone cement will need to be fabricated for comparison testing. The techniques to create PMMA bone cement filaments in the same size and similar PMMA constructs for comparison testing will be discussed.

The setup of bacterial plate or broth culturing testing will be discussed. The ISO clinical microbiology standards for this testing will be explained with any modifications that were made to them.

The drug release profile of both the filaments and 3D printed constructs will need to be monitored. The setup to design this will be discussed as well as the protocols for generating visualizing agents needed to do spectrophotometry of certain bioactive compounds.

Finally, several prototype technologies or techniques for the surgical use of these technologies will be discussed. This discussion will include the scanning and printing of defects as well as the fabrication setup for a 3D surgical printing pen or gun.

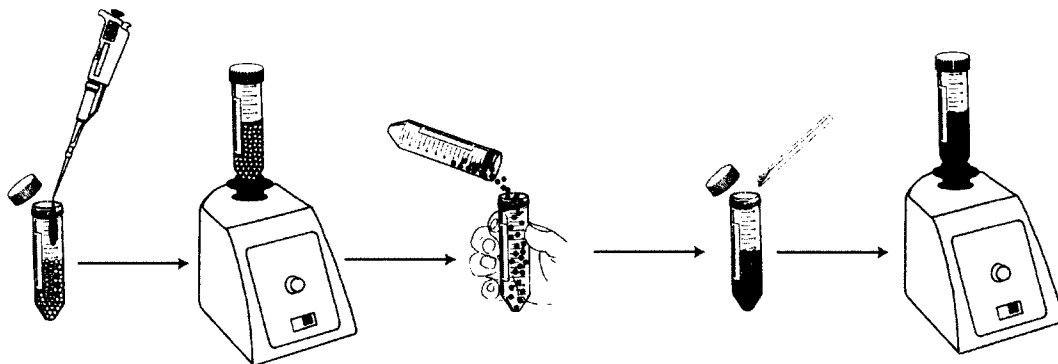
#### 4.4.1 Bioactive Coating of Pellets

One of the main challenges in extruding a bioactive 3D printing filament involves creating a uniform distribution of the bioactive compound or particle. No PLA fine powders are commercially available. Freeze-fracturing of pellets into fine powders is expensive and difficult. Once done, there are still challenges in the extrusion process. Almost all commercial filament extruders use an auger for continuous flow. A piston-based system could resolve this for small batch filament extrusion but to use existing technology requires the ability to modify standard injection molding pellets.

To enable an even dispersion of added particulate through the use of commercially available PLA/ABS beads, a coating method using KJL 705 silicone oil was chosen. The silicone oil showed thermal stability in the extrusion ranges required for the beads (170-180 °C for PLA, 205-215 °C for ABS) and enabled surface suspension of particulate on the pellets to ensure both a minimal loss of the product through the extrusion process and ensure even dispersion. This coating material was chosen arbitrarily, and whereas any material that enables the surface suspension of particulate

will work, additional considerations may exist, such as material properties or, in the case of bioactive compounds, biocompatibility.

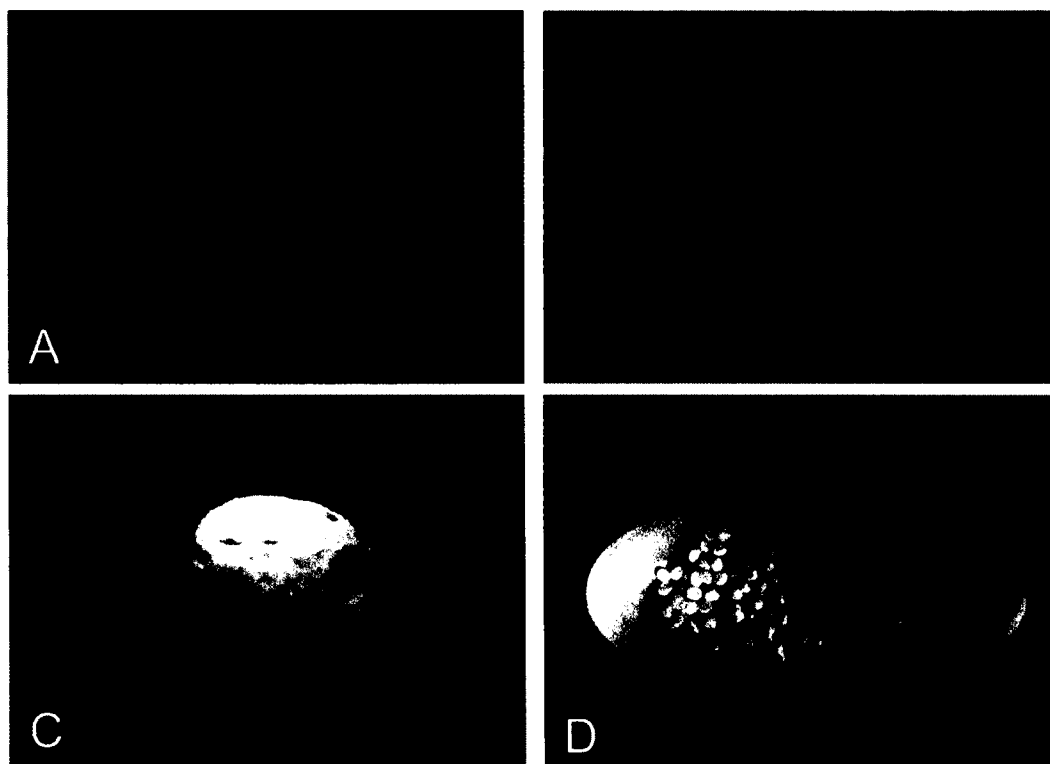
The coating process was comprised of five basic steps. To demonstrate the process, an example of a 20 gram batch of beads using the KJL 705 silicone oil was used. The beads must first be coated in the silicone oil, and vortexed to ensure complete coating of the beads. A proper amount of oil must be used, however, as excessive amounts of oil will lead to clumping of the pellets and extrusion problems due to improper melt flow. For example, a batch of 20 grams of pellets with 15  $\mu\text{L}$  of oil was used to fully coat the beads. Once vortexed, but prior to the introduction of additives, the beads must be placed in a new container as losses of additive material will occur on the surface of the container. After the containers are switched and the additive is introduced, the mixture is again vortexed to allow for complete coating of the beads. Uptake of additives will vary through this method due to particle size. This process is pictured in Figure 4-10, errors in the process are shown in Figure 4-11 and the results are shown in Figure 4-12.



**Figure 4-10:** Process of coating beads with additives



**Figure 4-11:** Results of failure to change coating tube (left) or too much oil (right)



**Figure 4-12:** Individual and batch coating of beads A-B) Nitrofurantoin-PLA coat C-D) Gentamicin sulfate-PLA coat



In considering additives for the silicone coating method, particle size is a constraint that must be considered. For materials such as nanoparticles or halloysite nanotubes that are already of a fine particulate nature, this method is readily applicable; however, for large particles, preprocessing may be necessary. A ball mill can be used to reduce particle size, assuming that the material of the balls used is denser than the material being milled. While milling may yield some contamination to the product, sufficiently high doping percentages in the filament (~5% by weight or greater) should overcome any concerns with the contaminating product. Other methods such as chemical processing may also be used to generate the desired particle size.

This method was used to create antibiotic coatings of 1%, 2.5% or 5% on PLA pellets. The pellets were coated in 10-15  $\mu\text{L}$  of silicone oil in 20 gram batches using 50 mL sterile and disposable plastic test tubes. These values meant that a 1% by weight addition used 200 mg of powder, 2.5 %wt used 500 mg and 5% wt used 1 g of an additive. Gentamicin was used to coat pellets at 1%, 2.5% and 5%. Tobramycin was used to coat pellets at 1% and 2.5%. Nitrofurantoin was used to create coatings at 1%. Antibiotics were ground with a mortar and pestle to ensure uniform powder size and help the coating process.

#### 4.4.2 Layer-By-Layer Coatings

The standard coating method discussed in Section 4.4.1 works well for coatings of up to 5% of many substances without loss of additive. Should greater weight percentages be desired, this process may be repeated, following the form of a layer-by-layer deposition onto the surface of the beads. The layering method has been repeated

successfully using iron nanoparticles in other testing to achieve a 25% coating that could be extruded into a usable filament.

#### 4.4.3 Atomizer Based Coating

One concern with using an additive such as coating oil involves the unknowns of *in vivo* testing. Other methods were developed to allow for pellets to be coated with only the bioactive substrate and no filler material. A bioactive substance of interest was dissolved or suspended in solution. That solution can then be sprayed via an atomizer onto the pellets to create a nano-film or coating on each pellet. An example of this method is shown in Figure 4-13.



**Figure 4-13:** Atomizer based coating setup A) atomizer B) syringe pump C) Erlenmeyer flask D) atomizer probe

The atomizer is placed vertically into an Erlenmeyer flask with two openings. A syringe is connected to the atomizer via the horizontal opening. The syringe pump can be connected to the syringe to slowly push the solution into the atomizer for uniform spray. The flask can also be placed on a hot plate at a low setting to aid in evaporation of

any excess liquid. The hot plate was set between 50 °C-60 °C to evaporate excess liquids without affecting material or bioactive coat properties.

This method was used with a 5 mL syringe that had been loaded with 5 mL of a solution comprising 200 mg of gentamicin. The Erlenmeyer flask had 20 grams of pellets and allowed for a 1% coating to occur.

#### 4.4.4 Filament Extrusion

The Extrusionbot filament extruder was used to extrude PLA pellets into filaments. The metal die chosen for the extrusion nozzle had a 1.75 mm diameter nozzle. This is a common filament size used in many 3D printers. Pellets were used in 20 gram batches to allow for custom manufacturing. The proper PLA extrusion point is roughly 170 °C for the filament to maintain a  $1.75\text{mm} \pm 0.1\text{mm}$  diameter. This temperature allows for an extrusion of a few feet of filament per minute. Temperatures below 170 °C can be used for extrusion but may have a very slow extrusion speed. These lower temperatures may also result in increased filament diameter that does not fit a standard 3D printer. The cooling fan located on the back of the unit can help to more rapidly harden the extruded filament. A common problem in filament extrusion is stretching or thinning of small sections of filaments during small batch manufacturing. These effects typically decrease pellet load, which lowers backpressure. The lower pressure causes sections of filament to stay heated around the metal die for longer periods of time. The weight of the already extruded portions can cause stretching. A metal ramp can allow for additional cooling, reduce the weight of the already extruded filament and act as a cold sink. This setup is shown in Figure 4-14.



**Figure 4-14:** Small batch filament extrusion with ramp

The filament can be created in small batches and gathered manually as shown in Figure 4-14. To maintain backpressure it may be necessary to use a plunger to push pellets in the hopper into the auger system. The beginning and ends of extruded filament batches may have irregular mixing or diameter sizes and should be discarded.

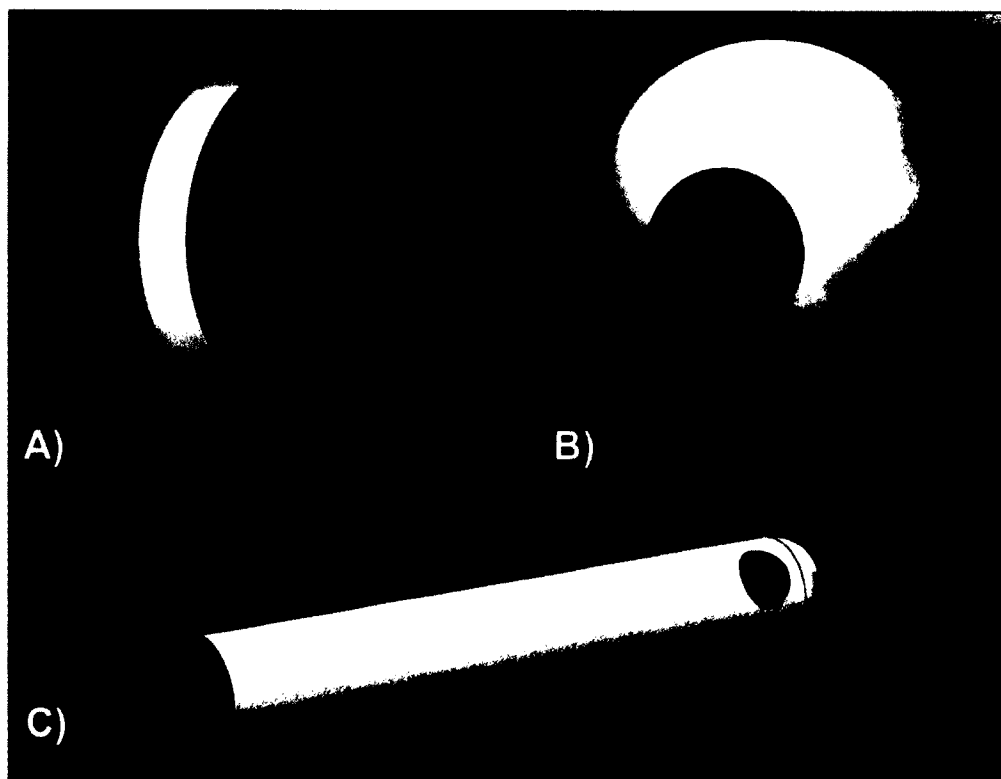
Excess temperatures might cause a “thermal run away.” This effect will cause the bioplastic to have an increased flow rate and can create issues with the filament diameter. It can be particularly noticed in an almost liquid-like extrusion rate and water-like flow out of the metal die at increased temperatures. Additives may cause issues with extrusion temperatures and may necessitate real-time adjustments to maintain a proper extrusion diameter. The coating oils amount must be particularly monitored. Excess oil for a

bioactive coating can cause filament bubbling at the extrusion point. This bubbling will result in an irregular surface that causes great discrepancies in diameter. Temperatures should be checked by individual machine as the heating sensors can slightly vary and effect extrusion rate and or diameters.

Filament should be stored in sterile containers or bags and kept refrigerated until printing. After filaments are extruded the machine should be purged with plain PLA pellets. This purging must be done with the metal die both on and off. When the metal die is removed, a large amount of material will pass out at a much larger diameter and rate. However, addition of the metal die will change the level of backpressure and help to clean any remaining coating material from the extruder.

#### 4.4.5 Construct Design and Printing

Constructs for printing were designed in Solidworks and saved as .STL files. They were opened in the Makerware software program and fabricated on the 3D printers as needed. Three core constructs were created for testing and shown in Figure 4-15.



**Figure 4-15:** .STL files of constructs A) disc B) bead and C) catheter

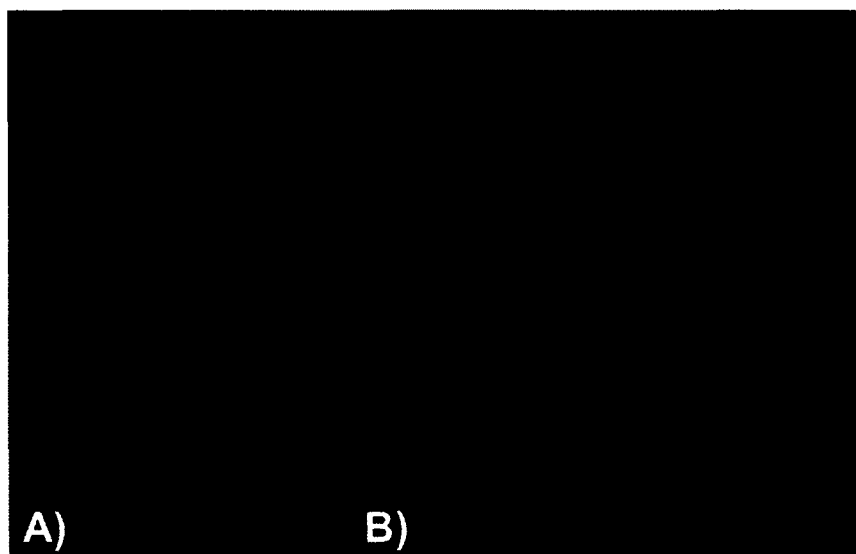
The test disc was a simple shape that could be resized to fit in a variety of bacterial culture plates or cell culture wells. For bacterial cell studies it was fabricated at a 5 mm diameter with 1 mm height and 100% fill. The printing temperature was 220 °C. The bead was fabricated at 6 mm, a standard size for antibiotic beads, with a 3 mm lumen. The beads were printed at 220 °C and a 10% fill. The catheter was printed and modeled as the distal tip for a single port 14 French catheter. The length was roughly 30 mm. The print temperature was 220 °C and the percent fill was set at 10%.

#### 4.4.6 Bone Cement Fabrication and Molds

The fabrication of bone cement controls can be made using plain PMMA bone cements or PMMA bone cements mixed with antibiotics. Loading the mixed bone cements into a standard syringe with a Luer Lock tip can be used to mold a filament. The

diameter of the syringe tube lumen is 1.9 mm. Quick extrusion with added rolling can allow for a thinner filament to be created. To create a similar percent by weight additive similar to PLA bead percentages, the bone cement powders were weighed and a percentage of additives of that weight were mixed in with the powder.

To compare the bone cements to the 3D printed constructs molds were generated. The disc construct and bead construct were modeled. A negative of the 5 mm disc was made and custom two-piece bead mold was made. Based on the difficulty the literature noted in removal from molds, two different types of molds were created. The first was 3D printed 6 mm bead mold and the second was a silicon putty based mold. These beads differed from the 3D fabricated ones in that the lumen was not hollow and they were spheres 100% full of the bone cement material. Antibiotic beads were made of 1% gentamicin. The PMMA bone cement mold files can be seen in Figure 4-16.



**Figure 4-16:** PMMA bone cement molds A) 6mm Beads B) 5 mm Discs

#### 4.4.7 Halloysite Preparation

Plain halloysite nanotubes were added to PLA pellets for filament fabrication and printing. They were added using the oil coat fabrication method. A 1wt% and 10wt% filament were fabricated using the standard and layer-by-layer fabrication methods.

Halloysite has been used as a particle for controlled and extended drug release.

Halloysite nanotubes were vacuum loaded in 1 gram batches in a saturated gentamicin sulfate solution of 10 mL containing 500 mg of dissolved substrate. After vacuum loading, the tubes were dried, then washed, and re-dried. The tubes were added to PLA pellets using the oil coating method to obtain a 1.5wt% HNT-loaded with gentamicin filament. A layer-by-layer method was used twice to obtain a 7.5% by weight addition to PLA pellets. The pellets were extruded from a clean filament extruder to create 1.5wt% and 7.5wt% HNT-loaded filaments. The filaments were used for bacterial and drug elution studies.

#### 4.4.8 Bacterial Culture Methods

All the samples were tested for antimicrobial activity by two methods, agar diffusion and liquid nutrient broth. In addition to the experimental groups, negative controls were also tested for antimicrobial activity. A set of positive controls was used and included the antibiotic powder of respective categories. Plain PLA samples and oil-coated samples were taken as negative controls. *E. coli* vitroids were used to raise bacterial colonies and one colony was picked to make 0.5 McFarland Standard bacterial suspensions.

Agar diffusion assays were run in accordance with ISO standard 17025 for measuring bacterial zones of inhibition. Hinton Mueller agar was taken, and to this 50  $\mu$ L



of bacterial culture was added. The liquid was distributed evenly on the plate using sterile glass beads. To this inoculated plate, fabricated antibiotic groups were tested. Filaments were cut into 1 cm sections and 3D-fabricated constructs were used. Zones of inhibition were measured for the groups after 24 hours of incubation at 37 °C. Every group was tested in 5 plates for reliability and reproducibility.

Liquid broth cultures were generated using Hinton Mueller broths. Sterile test tubes were loaded with 3 mL of broth, inoculated with 50 µL of bacterial cultures, and vortexed. Specimens of each group were then added. The filaments were cut into 1 cm sections and 3D printed constructs were used. These cultures were incubated for 24 hours at 37 °C on a rocker. Triplicates of each group were tested and compared to controls.

#### 4.4.9 Imaging and Measurements of Filaments and Cultures

The extruded filaments, 3D printed discs or bone cement controls were imaged using S4800 Field Emission SEM, Hitachi (Schaumburg, IL) at 35X, 2kX and 15kX magnifications. Bacterial plates and cultures were photographed with a Canon camera. The kill zone of the agar diffusion test was measured with a caliper at 3 different locations for each filament or disc.

#### 4.4.10 Spectrophotometry and Reagents

Elution studies were conducted on some of the antibiotic filaments and some printed constructs. The method of static elution at 37 °C was chosen for ease of replication. For filament, 1 cm sections were run, and 3D printed constructs were tested. The testing occurred in 1 mL Eppendorf tubes that were tinted to prevent degradation of eluted products by light. Deionized water was used as a medium for ease of replication. The filament or construct was moved from tube to tube at a specified time interval. This

movement allowed for all elution testing of the solutions for the same construct to be analyzed at a later date on the same machine. The time intervals were 1 minute, 2 minutes, 5 minutes, 10 minutes, 20 minutes, 40 minutes, 1 hour, 2 hours, 4 hours, 8, hours, and then daily for 7-10 days. All solutions were run on a NanoDrop spectrophotometer at an appropriate wavelength for the bioactive substance. The micro-cuvette option was used which involved a 500  $\mu$ l cuvette. The spectrophotometer was set to a base level using control deionized water. Elution curves were additively plotted to show a drug's release profile from either the filament or construct. Absorbance levels for a substrate were used to determine concentrations. Control curves were plotted using substrates of interest by using solutions of known concentration.

Gentamicin required a visualizing reagent to be mixed. This solution was OPTA reagent made by 2.5 gm OPT mixed with 62.5 mL methanol mixed with 3 mL beta mercapto-ethanol. The solution sat for 24 hours in a tin foil-covered container. It was used within 72 hours. The mixture used was 2 ml GS + 2 ml isopropanol + 2 ml OPTA reagent.

#### **4.5 Testing and Controls**

This project required the use of a wide range of equipment and experimental protocols. It was critical to plan both positive and negative controls in advance of experiments. Equipment usage had to be planned in advance to create control constructs before any experimental ones were made to prevent cross contamination. Experimental components were made in fume hoods and experiments were run in as sterile conditions as possible. At all points analysis was done to confirm statistical differences between

tested groups. The equipment and experimental setup basic calibration testing and controls are described below.

#### 4.5.1 Pellet Coating and Extrusion Process

It was critical to determine if a uniform coating was on each pellet. The batches of pellets were visually inspected to check for uniform coating and lack of powder remaining in mixing tubes. Methods for pellet coating were checked by weight and scanning electron microscopy. Coated pellets were placed on bacterial plates and zones of inhibition were measured and checked for uniformity of size.

Extruded filaments were visually checked for uniformity and consistent coloring based upon the bioactive additive. An electronic caliper was used to check for a uniform diameter. The beginning and ending portion of a filament was discarded to avoid the risks of improper mixing. SEM was taken of each filament to check for uniform fabrication and find bioactive powders on the surface coatings. Zones of inhibition measurements were taken and compared from filaments of the same extrusion to check for uniformity. Additionally, elution testing was done.

Three Extrusionbot filament extruders were used during this project. Control plain PLA and control oil-only-coated PLA pellets were created first on the machines to avoid any contamination. Bioactive coats of similar compounds were run initially on the same machines and in an increasing concentration. Gentamicin 1%-coated pellets were run before 2.5%-coated pellets. Additionally, after each batch of bioactive-coated pellets were run the equipment was cleaned. This procedure resulted in substantial and sustained purges of the Extrusionbots with plain PLA pellets. The hoppers and tubing that led to the auger system were cleaned and vacuumed to pick up any loose particles. Specialized

purges were done with more or less backpressure that was achieved by removing the metal die. Additionally, the machines were run at much higher temperatures up to 220 °C or with other polymers that are known to extrude more viscously and pick up leftover particulate.

#### 4.5.2 Printer Testing and Controls

The 3D printers were carefully calibrated and returned to factory setting. The Makerbot 2X and Makerbot Replicator 5<sup>th</sup> generation were new and from the manufacturer. All control constructs were printed on them before printing any bioactive constructs. The printer heads were purged for substantial periods of time between different filaments with control PLA filaments. Filaments of different levels of a bioactive compound were used from least to most concentrated. Before printing of bioactive constructs the printers were used to make small random constructs and the weights were compared. The difference in construct weight was within 1%-5% when repetitive small prints were done.

#### 4.5.3 Heat of Decomposition Testing

The 3D printers run at a temperature of 220 °C. The gentamicin, tobramycin and nitrofurantoin antibiotics were heated with Vulcan ovens for five minutes at 220 °C. They were then checked for effectiveness on bacterial plates in 1 mg batches and compared with control antibiotics to show that there was no significant loss of antibacterial properties during the heating process.

#### 4.5.4 Bone Cement Standards

There is a large value in comparing a new technology to an established one. PMMA-based bone cements are the gold standard in medical implant materials. Bone

cement controls were made using antibiotics to act as a control and demonstrate a comparison of effectiveness. Bone cements were compared to antibiotic filaments by extruding mixed bone cement from a syringe of a diameter that was approximately 1.75 mm. Different batches of the bone cement contained gentamicin at 1% and 2.5%, tobramycin at 1% and 2.5% and nitrofurantoin at 1%. Additionally, bone cement beads with 1% gentamicin were created in molds and compared to the printed ones. Elution studies compared the amount of antibiotics eluted from filaments and beads with both PLA prints and PMMA bone cements.

#### 4.5.5 Bacterial Testing Controls

The bacterial plate and broth cultures were mixed to ISO 17025 or related standards using manufacturer created Mueller-Hinton broth and plates. This standardization was meant to aid in the recreation of any experiments. Bacteria were ordered from Sigma-Aldrich for the ability to repeat studies identically. The bacterial studies always include plates or broths with no bacteria or plain bacteria only as negative and positive controls respectively. Special control gentamicin-eluting discs were used to test the bacteria susceptibility. The plates and broths used to test heated and control antibiotics also served as an additional control to show that the bacteria were susceptible to the antibiotics.

The manufacturing and printing process involved multiple steps. The produced material was tested at the end of each step. These controls checked all steps of the process to conclusively prove that any antibacterial results were legitimate. For the pellets, plain PLA, oil-coated PLA and bioactive-coated PLA of each category were tested in both broths and on plates. The filaments that were extruded were tested with the

controls of plain-PLA filament, oil-coated PLA filament and bioactive PLA filament. Constructs were tested using plain PLA and bioactive coatings. The PMMA bone cements were also used as controls to compare to the current gold standard for antibiotic implant.

#### 4.5.6 Elution Testing Controls

Spectrophotometry must be checked with controls and properly calibrated. This process must especially be done when using very low concentrations of a substrate of interest. The spectrophotometer was checked with plain deionized water regularly. This test verified that the absorbance was zero with a control. Absorbance curves were calculated using known levels of a substrate. Diluting the substrate of interest allowed for the creation the of calibration curves. For gentamicin the calibration curves were made using the visualizing reagent. To control for degradation of the visualizing reagent over time, all elution samples were saved and run the same day.

### **4.6 Results and Discussion**

Methods to create and the manufacturing of 3D printable antibiotic filaments were developed in phases to prove the concept. The thermal stability of antibiotics was proven. Methods of coating pellets were developed and filaments were extruded. Modified coating methods were researched. Pellets and filaments were checked for uniformity and were tested with bacterial cultures. Discs, beads, and catheters were fabricated with the 3D printer. These constructs were also tested with cultures. Elution testing was done. Nanoparticles were loaded with antibiotics to test additional and sustained drug elution properties.

The results and discussion of this novel work will be covered. First, results on the antibiotics of gentamicin, tobramycin and nitrofurantoin will be presented and discussed in relation to their thermal stability. Next, the silicone oil coating method and the testing of pellets for uniformity and antibacterial properties with controls will be reviewed. The extrusion and testing of these coated pellets will then be discussed in terms of filament antibacterial capabilities. They will be compared to control filaments made with bone cements. The discussion will then carry to printing filaments into 5mm discs. These discs will be compared to bone cement controls. The 1% gentamicin filaments will be printed into antibiotic beads and compared to bone cements molded into beads. The basic printing method and the creation of 1% gentamicin catheters will be examined and tested. Finally, elution testing will be discussed.

Nanoparticles in the form of halloysite loaded with gentamicin were created. They were used to fabricate 1% and 7.5% antibiotic filaments, which were compared to a 10% HNT control filament.

Additionally, this section will discuss the outcome of scanning a defect and printing an antibiotic plug. This method will be compared to the additional method of using a 3D printing pen or gun for filling a defect.

#### 4.6.1 Control Bacterial Plates and Broths

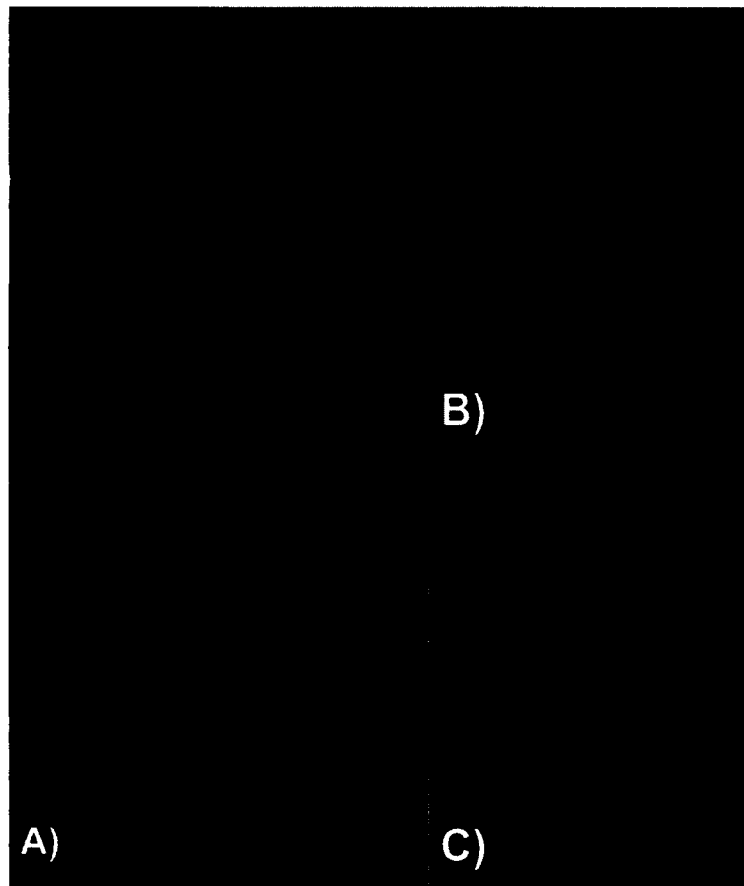
Bacterial plates and broths were created in accordance with ISO 17025 and related standards. A 0.5 McFarland standard was used to generate 50 uL of *E. coli* that inoculated each Mueller Hinton plate or broth. Positive and negative control plates were generated for testing, as shown in Figure 4-17.



**Figure 4-17:** A-B) Negative control plate C-D) Positive control plate showing bacterial lawn plates

All broth culture testing was also done with a positive and negative control. The positive control turbidity level can be compared to experimental cultures to show an equal level of growth or differing levels of inhibition of growth. The broth culture controls can be seen as shown in Figure 4-18.

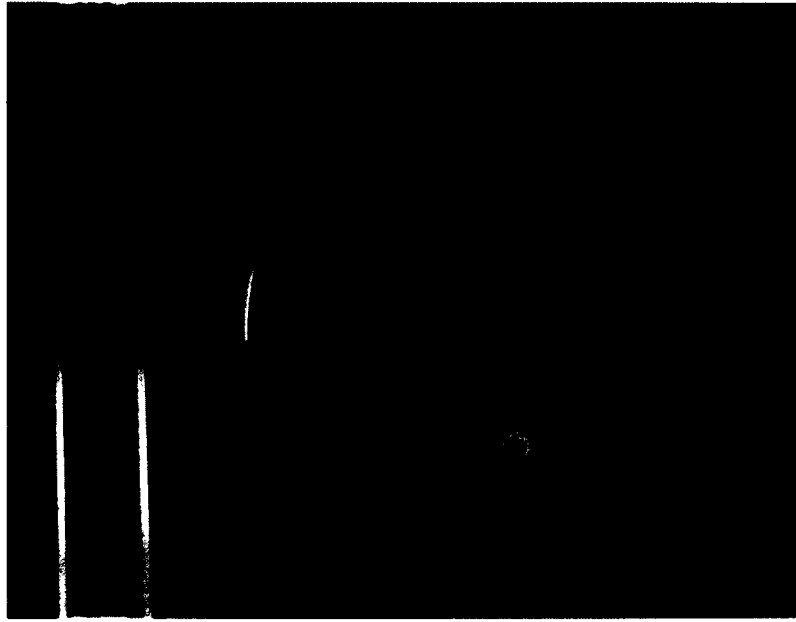




**Figure 4-18:** A) Test tube broth cultures with negative control on left and positive inoculated control on right B) Close up of sterile broth C) Inoculated broth

The bacterial plates were also tested with 100  $\mu\text{g}$  antibiotic-impregnated wafers.

This test was used to verify that that the *E. coli* was susceptible to gentamicin using a certified eluting disc. The result is shown in Figure 4-19.



**Figure 4-19:** Mueller Hinton *E.coli* plate with 100 µg gentamicin antibiotic-impregnated wafer

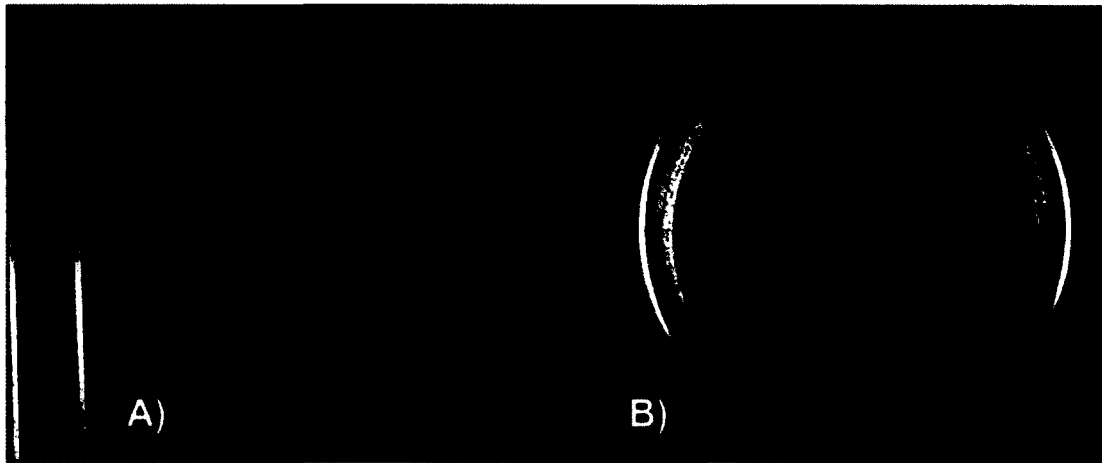
Three plates with wafers were made. Each wafer's zone of inhibition was measured with a digital caliper at three points and averaged. The wafers had an average zone of inhibition of 29.83 mm (+/- 0.34mm).

#### 4.6.2 Heated Antibiotics

The extrusion temperature for PLA bioplastic filament manufacturing is 170 °C and for 3D printing the material is 220 °C. Samples of the antibiotics comprising gentamicin, nitrofurantoin and tobramycin were heated in 100 mg batches and then 1 mg of each was placed onto three Mueller Hinton plates and broths. Control unheated antibiotics were used as well. The plates and broths were inoculated with *E. coli* per the methods section.

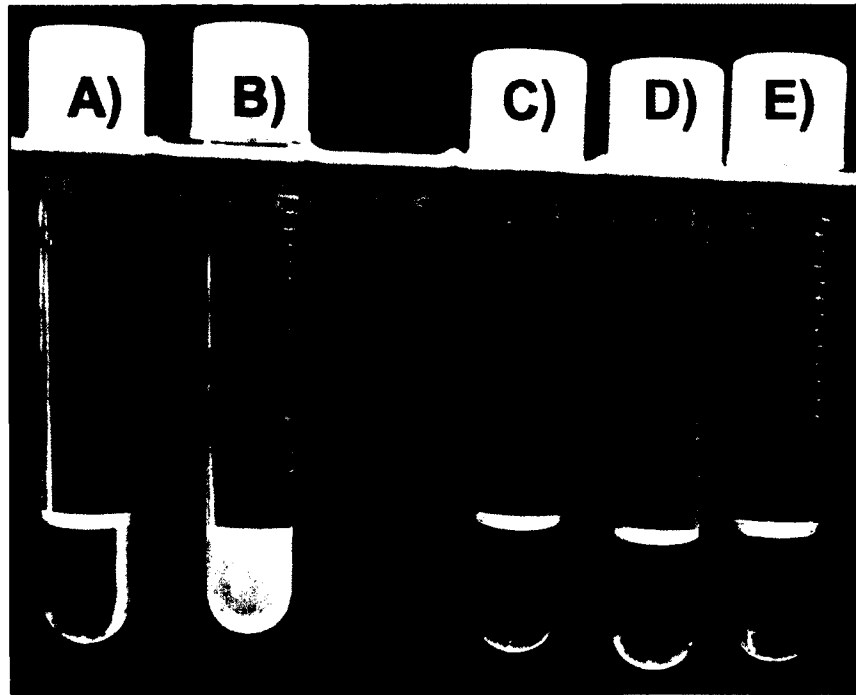
#### 4.6.2.1 Gentamicin Sulfate

Three plates were prepared to test both control gentamicin and heated gentamicin. Testing was done with the addition of 1 mg of the powders to the plates. The control and cooked gentamicin powders on plates can be seen in Figure 4-20.

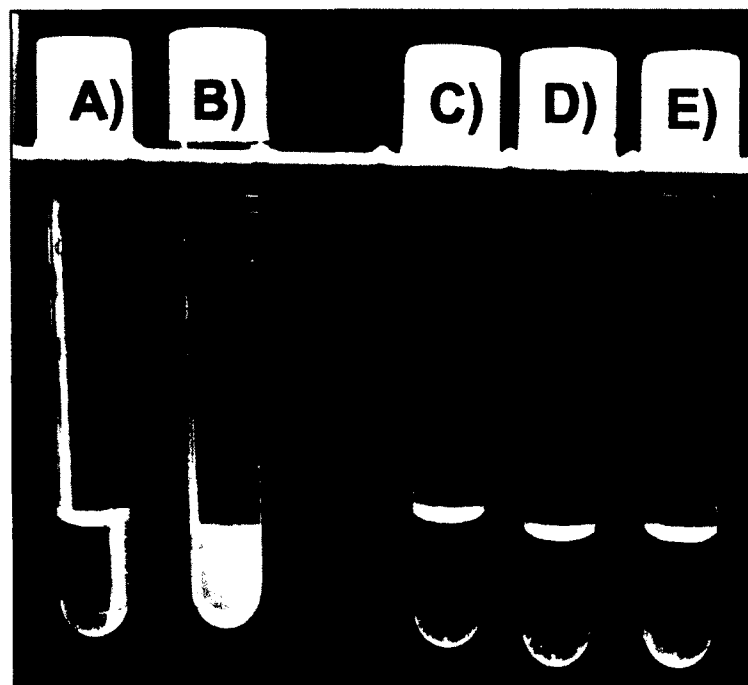


**Figure 4-20:** A) Heated gentamicin sulfate plate B) Control gentamicin plate

The zones of inhibition were measured at three points by a digital caliper for each of the three plates in the group and averaged. The average zone of inhibition in control gentamicin was 37.4 mm (+/- 0.55 mm) compared to a zone of inhibition of 36.6 mm (+/- 1.56 mm) for heated. Statistical analysis shows no difference between the two groups. The broth cultures can be seen in Figure 4-21 and Figure 4-22.



**Figure 4-21:** A) Sterile broth B) *E. coli* inoculated broth C-E) Control gentamicin powder added to inoculated broth

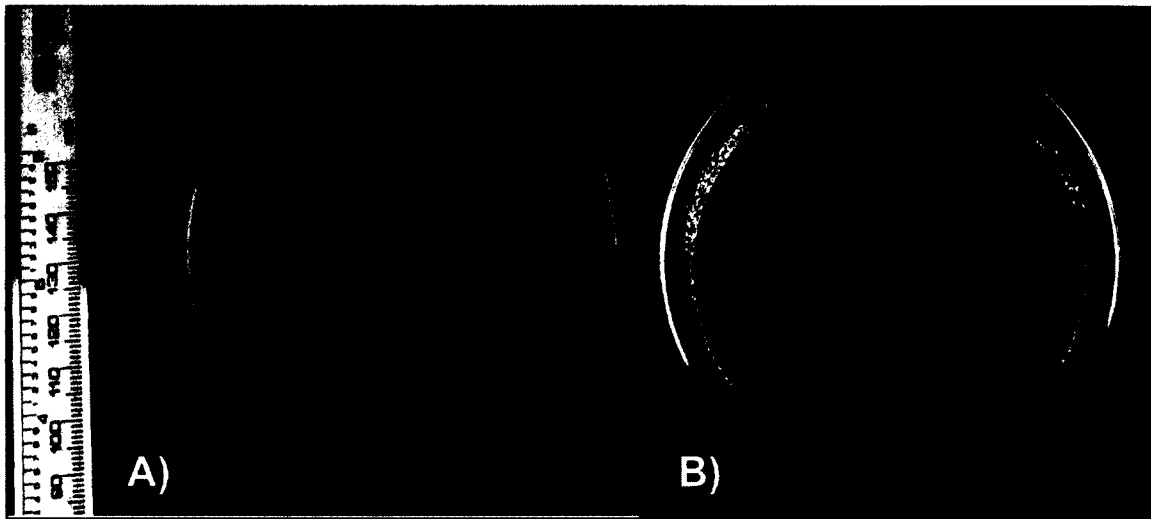


**Figure 4-22:** A) Sterile broth B) *E. coli* inoculated broth C-E) Heated gentamicin powder added to broth

The broth cultures had no bacterial growth compared to controls. Gentamicin that was heated to the temperatures used for 3D fabrication was able to prevent bacterial growth.

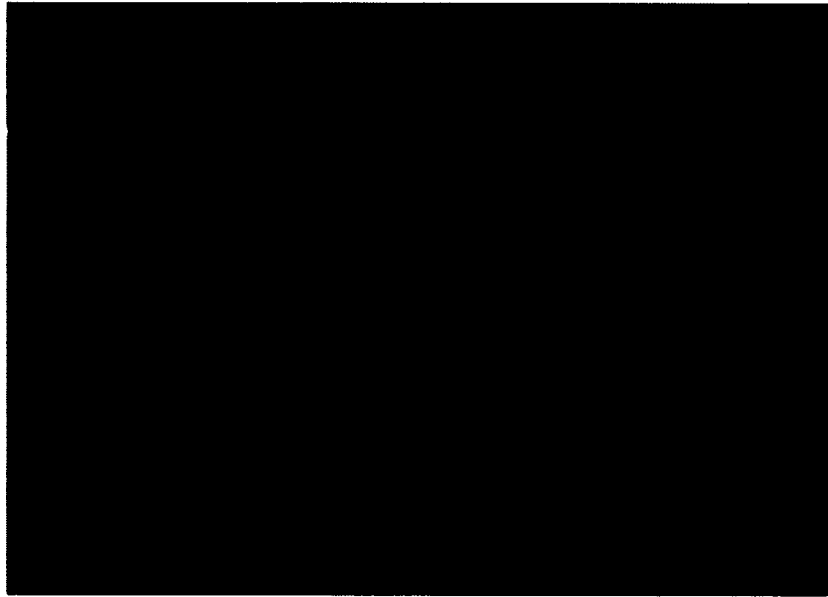
#### 4.6.2.2 Tobramycin

Three plates were prepared to test both control tobramycin and heated tobramycin. To test the samples, 1 mg of the powders was added to the plates. The control and cooked tobramycin powders on plates can be seen below in Figure 4-23.



**Figure 4-23:** A) Heated tobramycin sulfate plate B) Control tobramycin plate

The zones of inhibition were measured at three points by a digital caliper for each of the three plates in the group and averaged. The average zone of inhibition in control tobramycin was 37.2 mm (+/- 3.48 mm), compared to a zone of inhibition of 35.7 mm (+/- 1.34 mm) for heated. Statistical analysis shows no difference between the two groups. The broth cultures can be seen in Figure 4-24 and Figure 4-25.



**Figure 4-24:** A) Sterile broth B) *E. coli* inoculated broth C-E) Control tobramycin powder added to inoculated broth



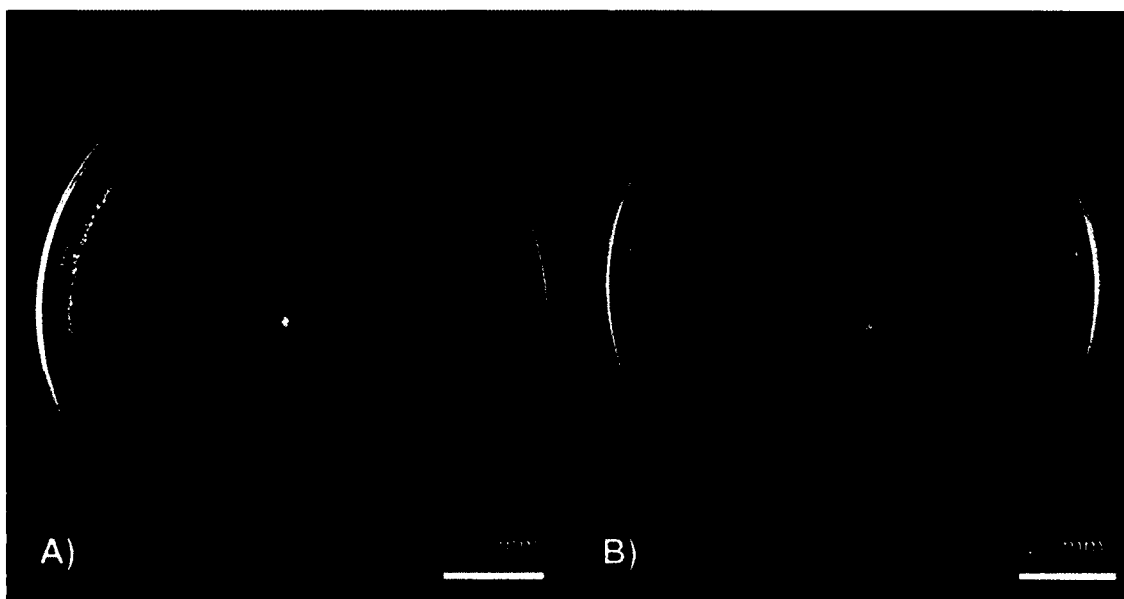
**Figure 4-25:** A) Sterile broth B) *E. coli* inoculated broth C-E) Heated tobramycin powder added to broth

No bacterial growth occurred in any broth culture compared to controls.

Tobramycin that was heated to temperatures used for 3D fabrication prevented bacterial growth.

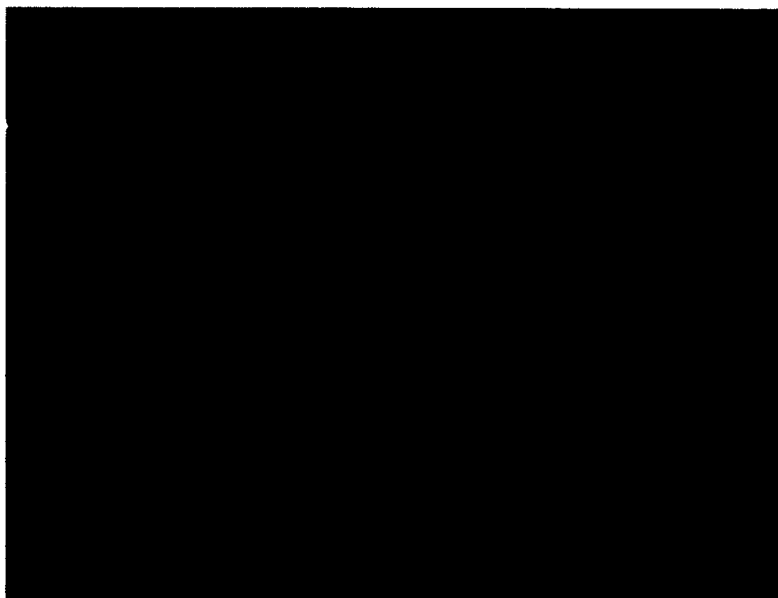
#### 4.6.2.3 Nitrofurantoin

Three plates were prepared to test both control nitrofurantoin and heated nitrofurantoin. A 1 mg sample of the powders was added to the plates. The control and cooked tobramycin powders on plates can be seen below in Figure 4-26.



**Figure 4-26:** A) Control nitrofurantoin plate B) Heated nitrofurantoin plate

The average zone of inhibition in control nitrofurantoin was 30.9 mm (+/- 1.74 mm) compared to a zone of inhibition of 29.5 mm (+/- 1.21 mm) for heated. Analysis shows no difference between the two groups. The broth cultures can be seen in Figure 4-27 and Figure 4-28.



**Figure 4-27:** A) Sterile broth B) *E. coli* inoculated broth C-E) Control nitrofurantoin powder added to inoculated broth



**Figure 4-28:** A) Sterile broth B) *E. coli* inoculated broth C-E) Heated nitrofurantoin powder added to broth

No bacterial growth occurred in any broth culture compared to controls. The orange/yellow color of the broth is from the colored powder. Nitrofurantoin that was



heated to comparable temperatures for 3D fabrication was able to prevent bacterial growth.

#### 4.6.3 Pellets

Pellet coating is a critical step in the fabrication process. To achieve a consistent bioactive compound dispersion, the pellets should be as evenly coated as possible. The oil coating method was used either singly or in a layer-by-layer fashion for groups consisting of 1% gentamicin, 2.5% gentamicin, 1% tobramycin, 2.5% tobramycin, 1% nitrofurantoin, 1% HNT loaded with gentamicin, and 7.5% HNT loaded with gentamicin. The atomizer spray coating method was also used.

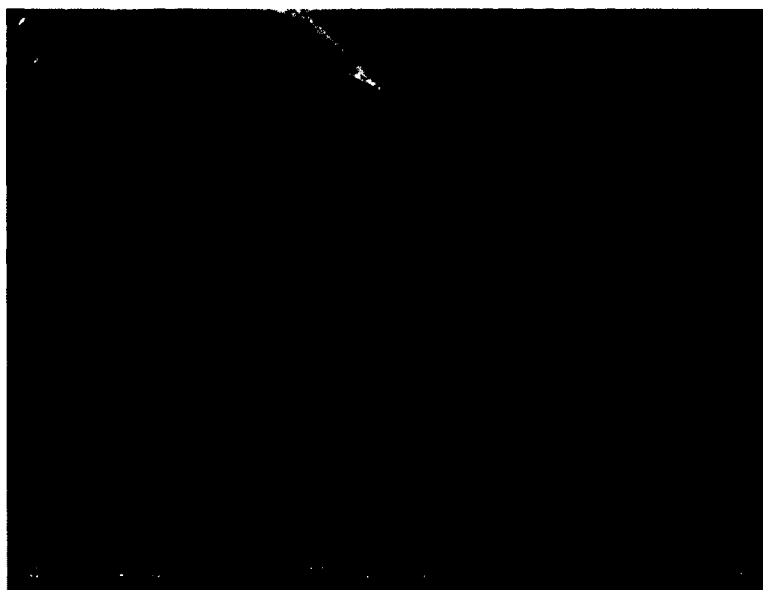
##### 4.6.3.1 Manufacturing

The basic manufacturing process described in detail in Section 4.4.1 was used for each material, and the associated figures lay out the results. The coating materials were ground with a mortar and pestle as much as possible. Using proper amounts of coating material is critical to prevent clumping during fabrication or later problems in the extrusion process. The optimal oil amount per layer of coating ranged from 10  $\mu\text{L}$  to 20  $\mu\text{L}$ . Initial attempts that used higher amounts between 100  $\mu\text{L}$  and 500  $\mu\text{L}$  resulted in substantial clumping of the pellets, coating material sticking to the 50 mL mixing tube, and clogging of the internal workings of the filament extruder. The low amount of oil would allow pellets to hold only 1% to 5% of their weight in powdered material. To add additional powdered material to the pellets, a layer-by-layer coating method was successfully used to go as high as 15%-20%. Additional methods for alternative materials have been used to go as high as 25% for iron nanoparticles with cutting up filaments, coating, and then re-extrusion of materials. Excess oil or oils with lower

boiling points would also cause bubbling or warping of the filament later on during filament extrusion. These anomalies would cause blockages of the filament during the 3D fabrication process. It was also critical to change the oil coated 50 mL tube to prevent powdered materials from sticking to the side of mixing containers. A proper pellet-coating process was highly correlated to the success of later 3D fabrication.

#### 4.6.3.2 Control and oil-coated pellets

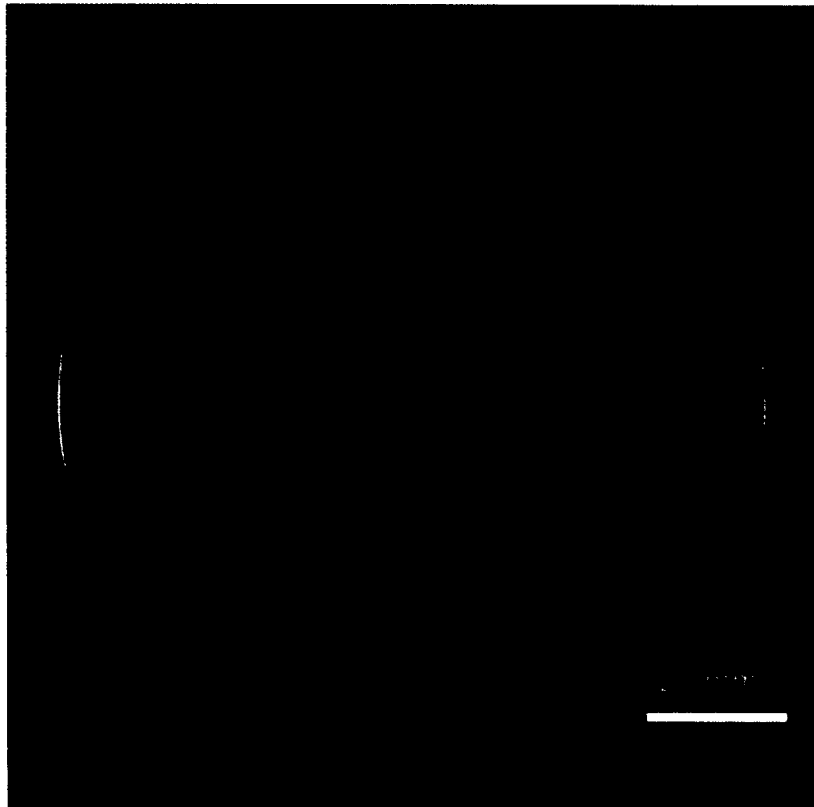
PLA pellets were coated with 20  $\mu\text{L}$  of coating oil. Control pellets were imaged using SEM as shown in Figure 4-29. Oil-coated pellets were not imaged by SEM out of concern for volatility in the vacuum chamber. The round pellets would roll on the double-sided carbon tape floor used for SEM so an additional piece of tape had to be placed over them to prevent movement. This restricts the view of the entire round pellet in images.



**Figure 4-29:** SEM of control pellet surface

The basic pellet SEM will be relevant in relation to demonstrations of coatings of additional bioactive powders in other sections.

The control PLA pellet and oil-coated pellet were tested in both Mueller Hinton plate and broth cultures that had been inoculated with *E. coli*. Three pellets of the control PLA were chosen for broth and another three pellets were chosen for plating. A control PLA pellet is shown in Figure 4-30 and control PLA pellets in broth cultures are shown in Figure 4-31.



**Figure 4-30:** Mueller Hinton plate with PLA control pellet on left and a PLA oil-coated pellet on right



**Figure 4-31:** A) Sterile broth B) *E. coli* inoculated broth C-E) PLA control pellet in broth culture

The three broth cultures and the bacterial plates show no inhibition of bacterial growth. The broth cultures have the same turbidity as the positive control *E. coli*.

Oil-coated pellets were also placed on three plates and in three broth cultures. The results for the PLA oil-coated pellet plate can be seen in Figure 4-30 and in Figure 4-32.

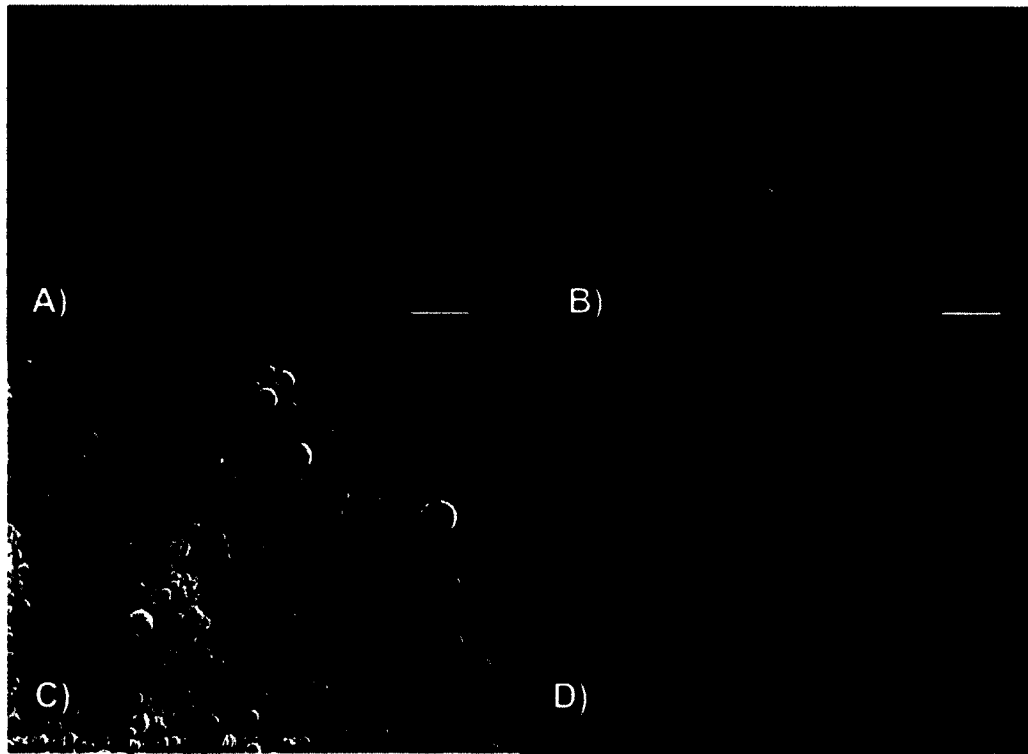


**Figure 4-32:** A) Sterile broth B) *E. coli* inoculated broth C-E) PLA oil-coated pellet in broth culture

The oil coating had no inhibition of bacterial growth or antimicrobial properties in either the bacterial plate or broth cultures. The turbidity level of the positive inoculated control is equivalent to that of the oil-coated beads in broth cultures.

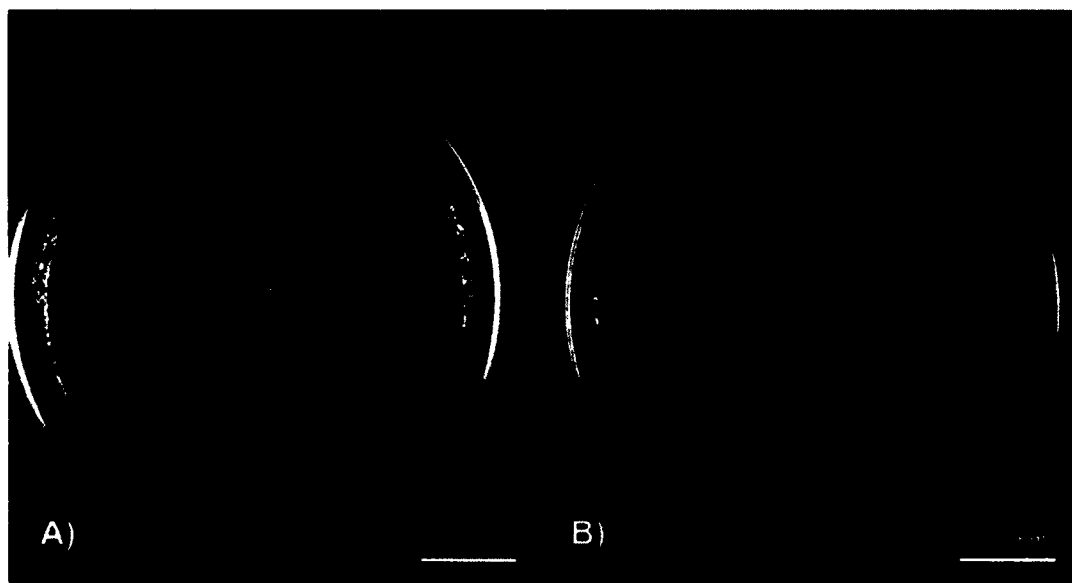
#### 4.6.3.3 Gentamicin pellets

PLA pellets were coated in 1 wt%, 2.5 wt% and 5 wt% gentamicin. Photographic and then SEM images are shown in Figure 4-33.



**Figure 4-33:** A) 1 wt% PLA-coated pellet B) 2.5 wt% PLA-coated pellet C) SEM of gentamicin sulfate powder D) SEM of gentamicin sulfate-coated pellet.

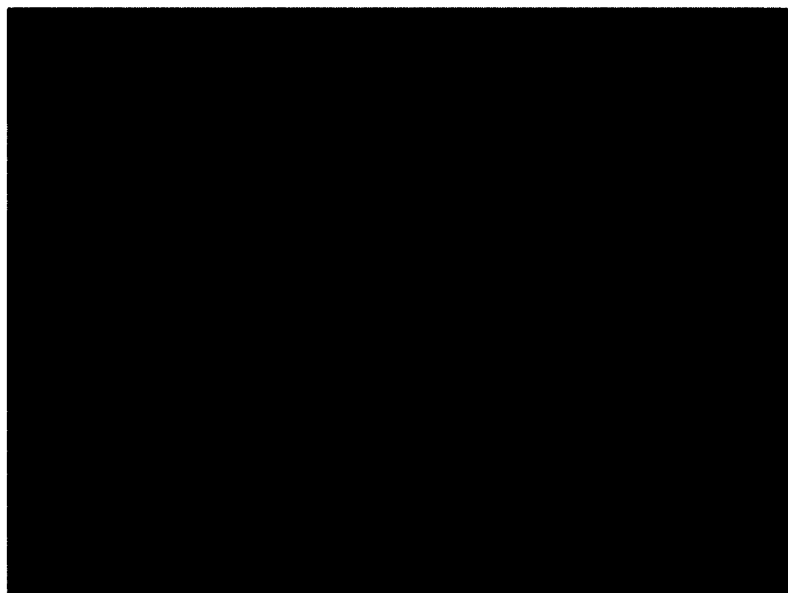
Visual inspection indicated that the process of placing the pellet on the carbon tape and using compressed air to remove any loose powder disturbed a more uniform coating. This process was necessary to prevent powder from damaging the SEM. The coated pellets were plated on Mueller Hinton plates. Five 2.5 wt%-coated pellets and three 1%-coated pellets were tested on individual plates, and the result is shown in Figure 4-34.



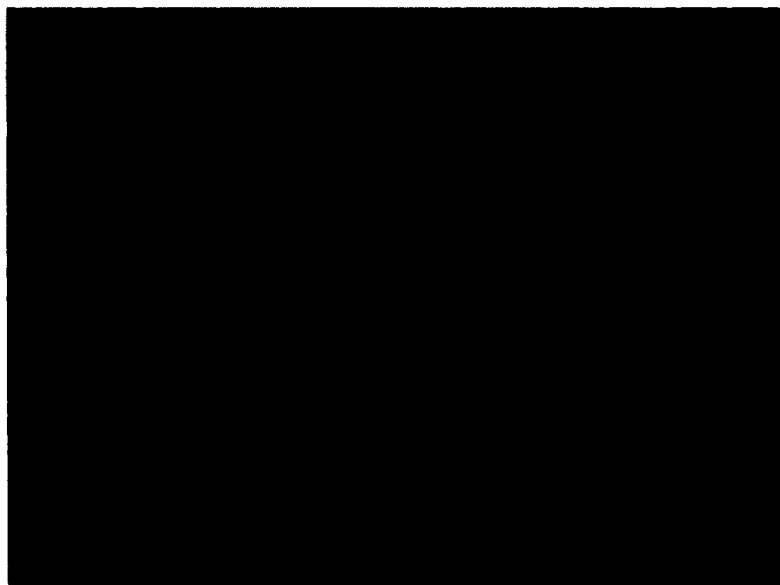
**Figure 4-34:** A) 1 wt% gentamicin-coated pellet B) 2.5 wt% gentamicin-coated pellet

The zones of inhibition were measured with a digital caliper at three points and averaged. The 1 wt%-coated pellet had a zone of inhibition of 26.14 mm (+/- 1.69 mm) and the 2.5 wt%-coated pellet had a zone of inhibition of 29.0 mm (+/- 2.78 mm).

ANOVA analysis showed no statistical difference. The lack of significance was likely caused by diffusion in the agar during the testing. Additionally broth culture testing was done for each of the coated pellets, as shown by Figure 4-35 and Figure 4-36.



**Figure 4-35:** A) Sterile broth B) *E. coli* inoculated broth C-E) PLA 1 wt% gentamicin-coated pellet in broth culture



**Figure 4-36:** A) Sterile broth B) *E. coli* inoculated broth C-E) PLA 2.5 wt% gentamicin-coated pellet in broth culture

There is no growth in any of the broth cultures. The broth cultures and bacterial plates exhibit inhibition of bacterial growth. The broth cultures have the same turbidity as the negative control *E. coli*. Both the broth and plate cultures confirm that the coating

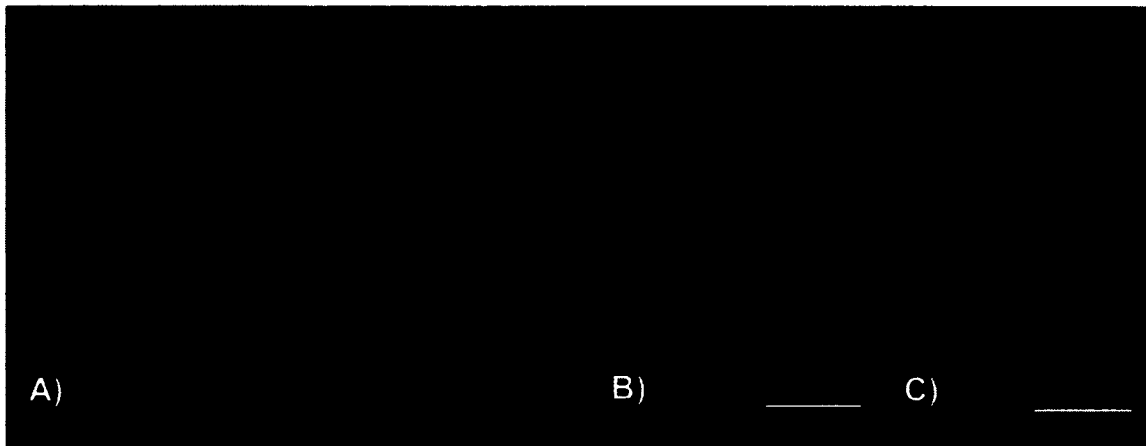


oil has no effect on bacterial growth. This allows us to conclude that the antimicrobial effect is from the gentamicin at this point in the manufacturing process.

#### 4.6.3.4 Tobramycin pellets

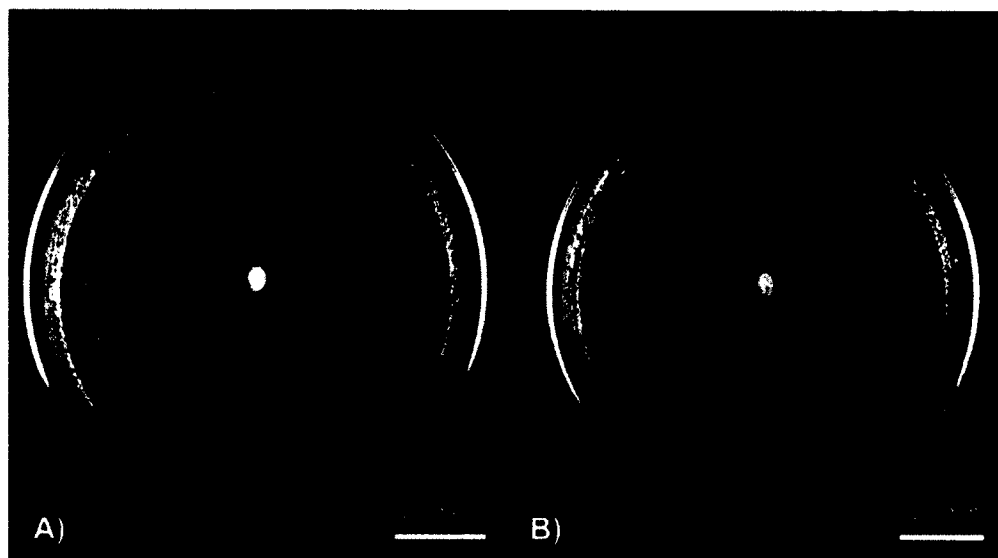
PLA pellets were coated in 1 wt% and 2.5 wt% tobramycin powdered antibiotic.

Photographs and SEM of the pellets were taken as shown in Figure 4-37.



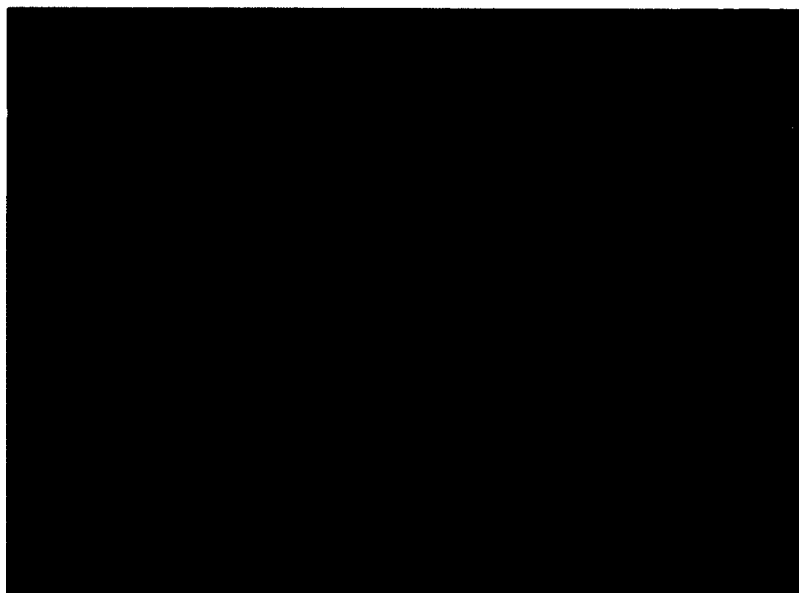
**Figure 4-37:** A) SEM of tobramycin) 1 wt% tobramycin PLA-coated pellet C) 2.5 wt% tobramycin PLA-coated pellet

The tobramycin-coated pellets were plated on Mueller Hinton plates. Three 1 wt%-coated pellets and three 2.5 wt%-coated pellets were tested on individual plates, as shown in Figure 4-38.

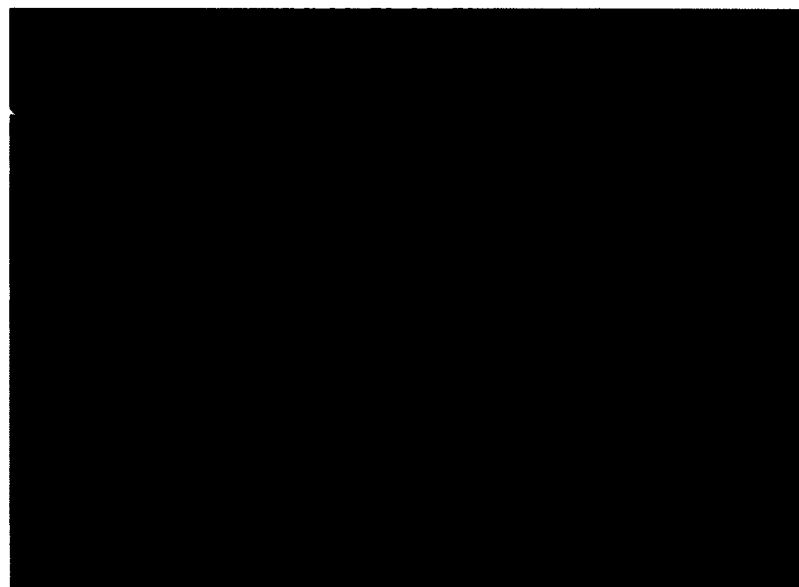


**Figure 4-38:** A) 1 wt% tobramycin-coated pellet B) 2.5 wt% tobramycin-coated pellet

The zones of inhibition were measured with a digital caliper at three points and averaged. The 1 wt%-coated pellet had a zone of inhibition of 26.0 mm ( $\pm$  1.02 mm) and the 2.5 wt%-coated pellet had a zone of inhibition of 25.9 mm ( $\pm$  1.63 mm). Analysis showed no statistical difference. This was likely due to the limiting nature of the diffusion in the agar during the testing. Additionally, broth culture testing was done for each of the coated pellets as shown by Figure 4-39 and Figure 4-40



**Figure 4-39:** A) Sterile broth B) *E. coli* inoculated broth C-E) PLA 1 wt% tobramycin-coated pellet in broth culture



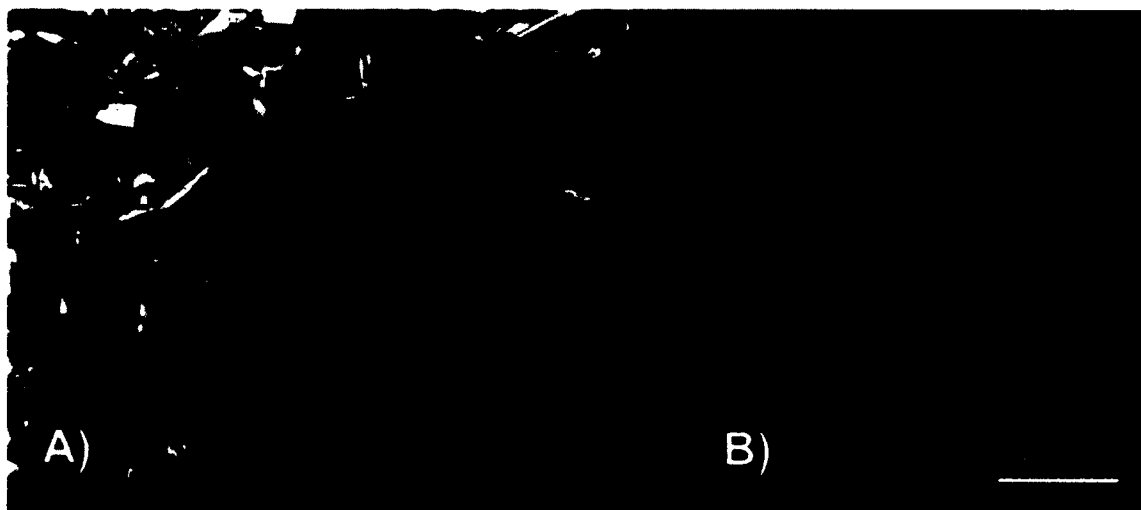
**Figure 4-40:** A) Sterile broth B) *E. coli* inoculated broth C-E) PLA 2.5 wt% tobramycin-coated pellet in broth culture

The broth-only cultures exhibited no growth, while the tobramycin-coated plates inhibited bacterial growth in both the broth cultures and bacterial plates. The broth cultures have the same turbidity as the negative control. Both the broth and plate cultures

confirm that the coating oil did not affect bacterial growth and tobramycin did affect it at this point in the manufacturing process.

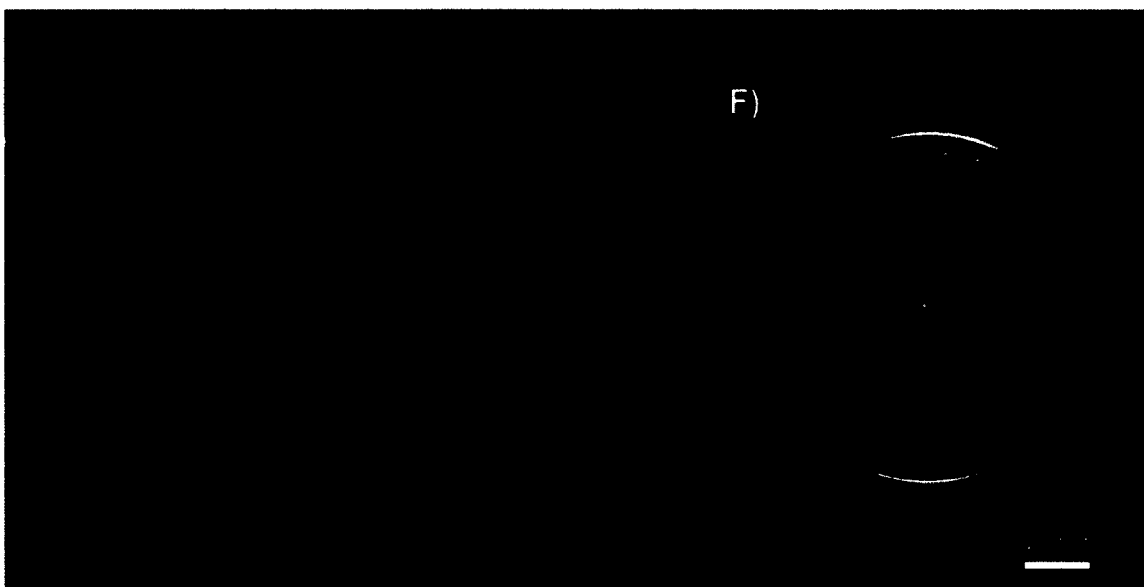
#### 4.6.3.5 Nitrofurantoin pellets

PLA pellets were coated in 1 wt% nitrofurantoin. Photographic and SEM images of the pellets are shown in Figure 4-41.



**Figure 4-41:** A) nitrofurantoin powder B) 1 wt% PLA pellet coated in nitrofurantoin

The nitrofurantoin-coated pellets were plated on Mueller Hinton plates and in broth cultures. Three pellets were placed on both broth and plates, as shown in Figure 4-42.

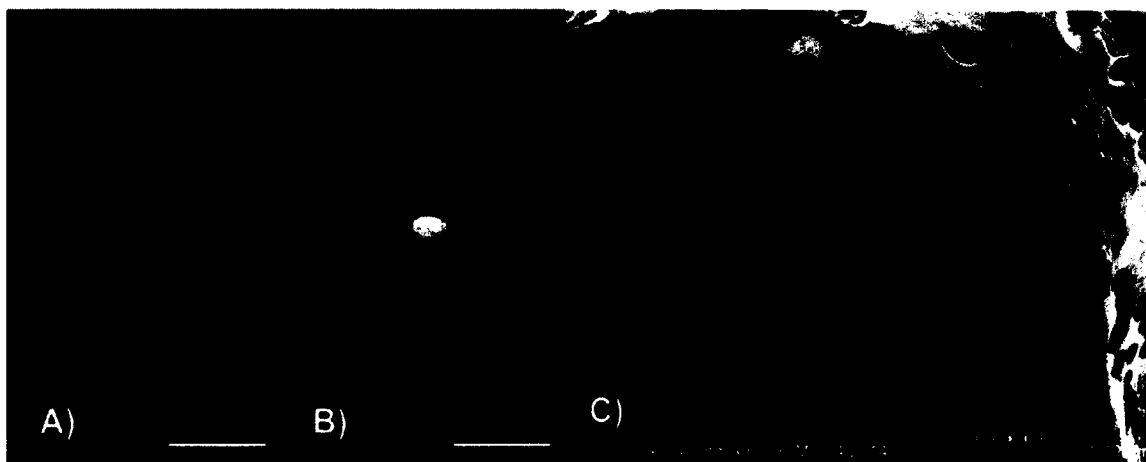


**Figure 4-42:** A) sterile broth B) *E. coli* inoculated broth C-E) PLA 1 wt% nitrofurantoin-coated pellet in broth culture F) PLA pellet coated in 1 wt% nitrofurantoin

No growth occurred in any of the broth cultures. Bacterial growth was inhibited by the nitrofurantoin-coated pellets in both the broth cultures and the bacterial plates. The broth cultures have the same turbidity as the negative control. The yellow color is from the dissolved nitrofurantoin. The zones of inhibition were measured with a digital caliper at three points and averaged. The 1 wt%-coated pellet had an average zone of inhibition of 22.1 mm (+/- 0.53 mm). Both the broth and plate cultures confirm that the coating oil has no effect on bacterial growth and tobramycin does affect bacterial growth at this point in the manufacturing process.

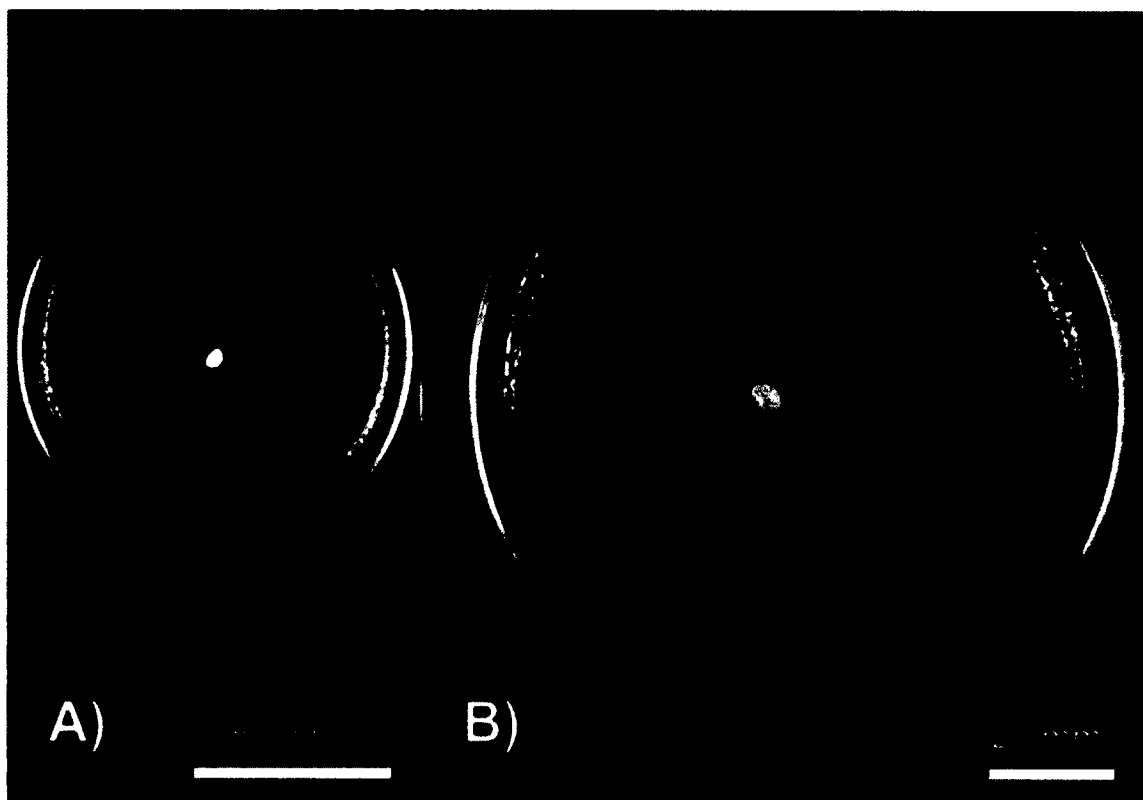
#### 4.6.3.6 HNT and HNT-GS pellets

Halloysite nanotubes can be loaded with a variety of bioactive substances. Testing was done as a proof of principle and to provide a foundation for future work. Photographs and SEM of control 10 wt% HNT-coated PLA pellets are shown in Figure 4-43.



**Figure 4-43:** A) 1.5 wt% gentamicin loaded HNT-coated PLA pellet B) 10 wt% HNT-coated PLA pellet C) SEM of HNT-coated pellet

In the SEM figure, particulate was blown off of the pellet before imaging, and the coating was substantially more consistent. Three plates were made for control 10 wt% HNT-coated PLA pellets, and three plates were made for 1.5 wt% gentamicin-loaded HNT-coated PLA pellets. This is shown in Figure 4-44.

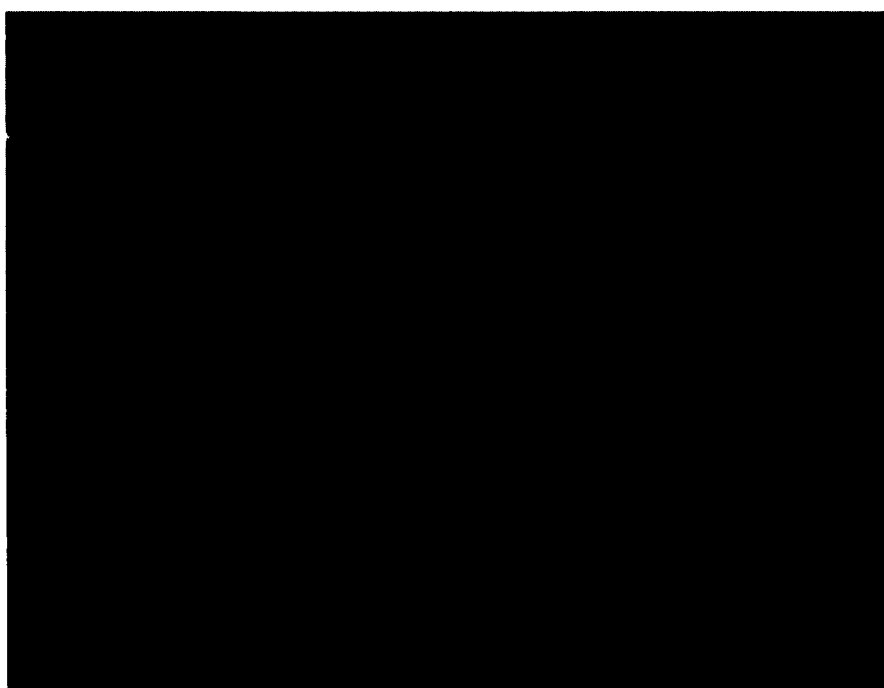


**Figure 4-44:** A) 10 wt% HNT-coated PLA pellets on Mueller Hinton plate B) 1.5 wt% gentamicin loaded HNT-coated PLA pellets on Mueller Hinton plate

All three of the 10 wt% HNT-coated PLA pellets had no bacterial inhibition on the plates. The 1.5 wt% gentamicin loaded HNT-coated PLA pellets all had zones of inhibition. The zones were each measured three times with a digital caliper and the average zone of inhibition was 12.45 mm ( $\pm$  1.26 mm). Halloysite typically loads 10% by weight of a target substance so this is comparable to 0.15% by weight gentamicin. This can be compared to the 1% by weight gentamicin in relation to the initial antibiotic-coated studies. Broth cultures were conducted on 10 wt% HNT-coated PLA pellets and PLA pellets 1.5 wt%-coated in gentamicin loaded HNT as seen in Figure 4-45 and Figure 4-46.



**Figure 4-45:** A) Sterile broth B) *E. coli* inoculated broth C-E) 10 wt% HNT-coated PLA pellet in broth culture



**Figure 4-46:** A) sterile broth B) *E. coli* inoculated broth C-E) 1.5 wt% gentamicin loaded HNT-coated PLA pellet in broth culture

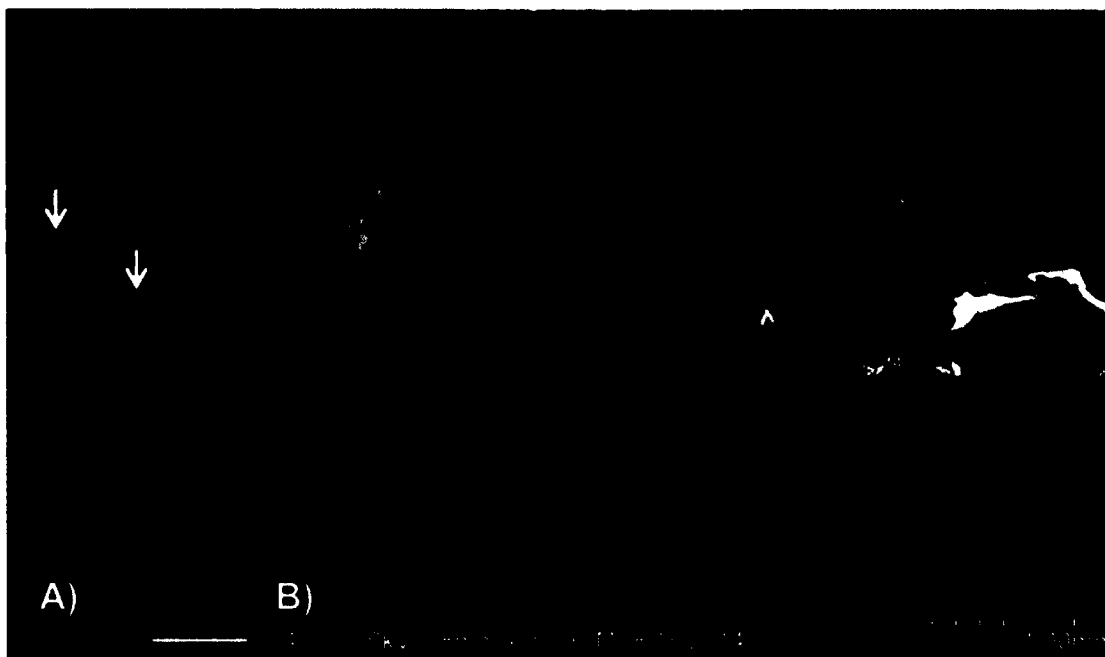
The control HNT-coated pellets showed no antimicrobial activity in the broth culture. The 1.5 wt% gentamicin loaded HNT-coated pellets prevented growth in both



cultures. These studies provide confirmation that a loaded halloysite and bioactive substance can withstand the first step of the manufacturing process.

#### 4.6.3.7 Atomizer-coated GS pellets

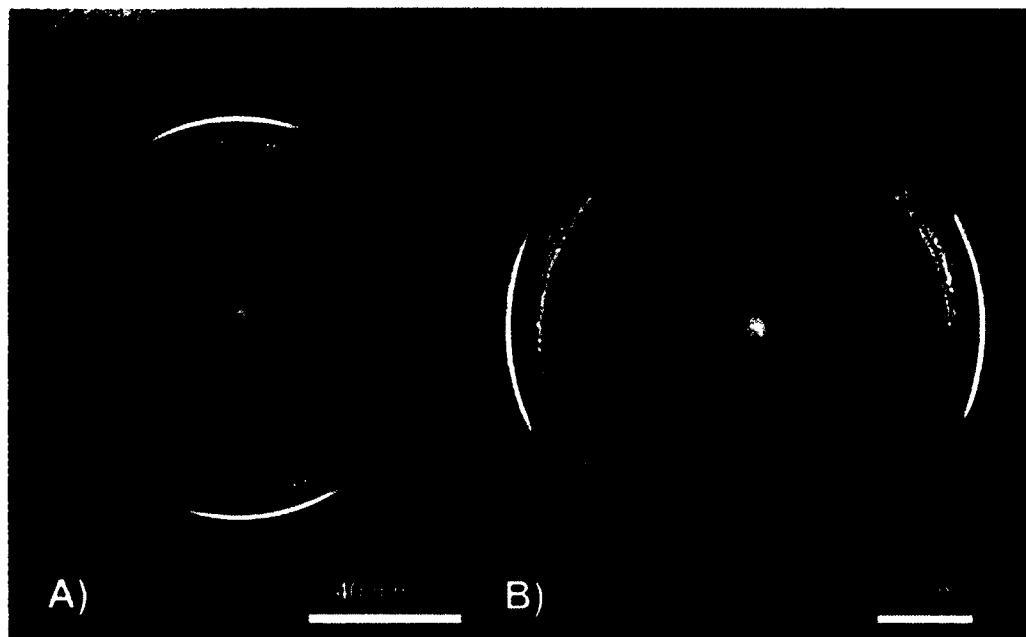
Additional coating processes and methods are possible that can avoid the use of a coating substance or oil. One example demonstrated is that of using an atomizer-based method with the substance of interest dissolved in a solvent. The atomizer coating process described in Section 4.4.3, Atomizer Based Coating, was applied to 20 grams of PLA pellets with gentamicin. Photographs and SEM images were taken of one of those pellets as shown in Figure 4-47.



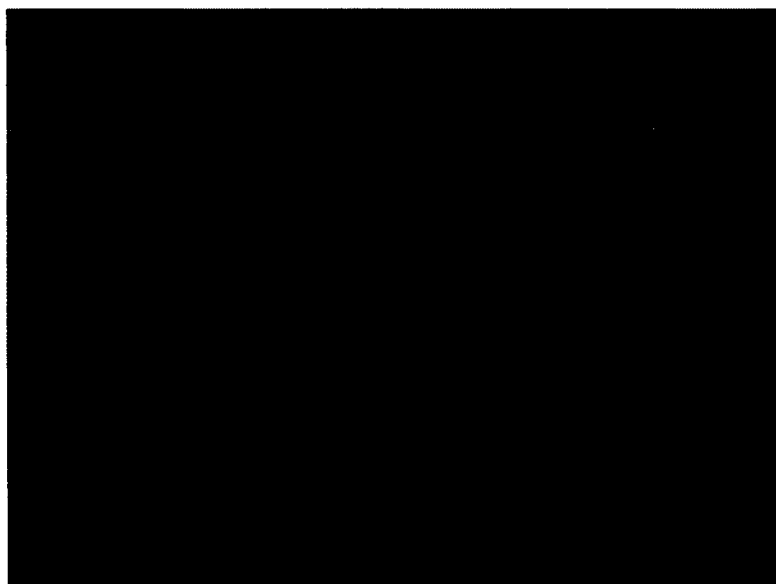
**Figure 4-47:** A) Photograph of atomizer-coated PLA pellet B) SEM of atomizer-coated PLA pellet

The atomizer-coated pellets had some large crystals of gentamicin that formed and could be broken off during routine handling as shown in Figure 4-47. While the surface SEM at lower resolution appeared to show larger crystals only, at higher

resolutions it was possible to see coatings across the surface of the pellet. Three of those pellets were tested on Mueller Hinton plates and three in Mueller Hinton broth. The results of these tests are shown below in Figure 4-48 and Figure 4-49.



**Figure 4-48:** A) Atomizer-coated pellet B) Atomizer-coated pellet



**Figure 4-49:** A) Sterile broth B) *E. coli* inoculated broth C-E) 1 wt% gentamicin atomizer-coated PLA pellet in broth culture

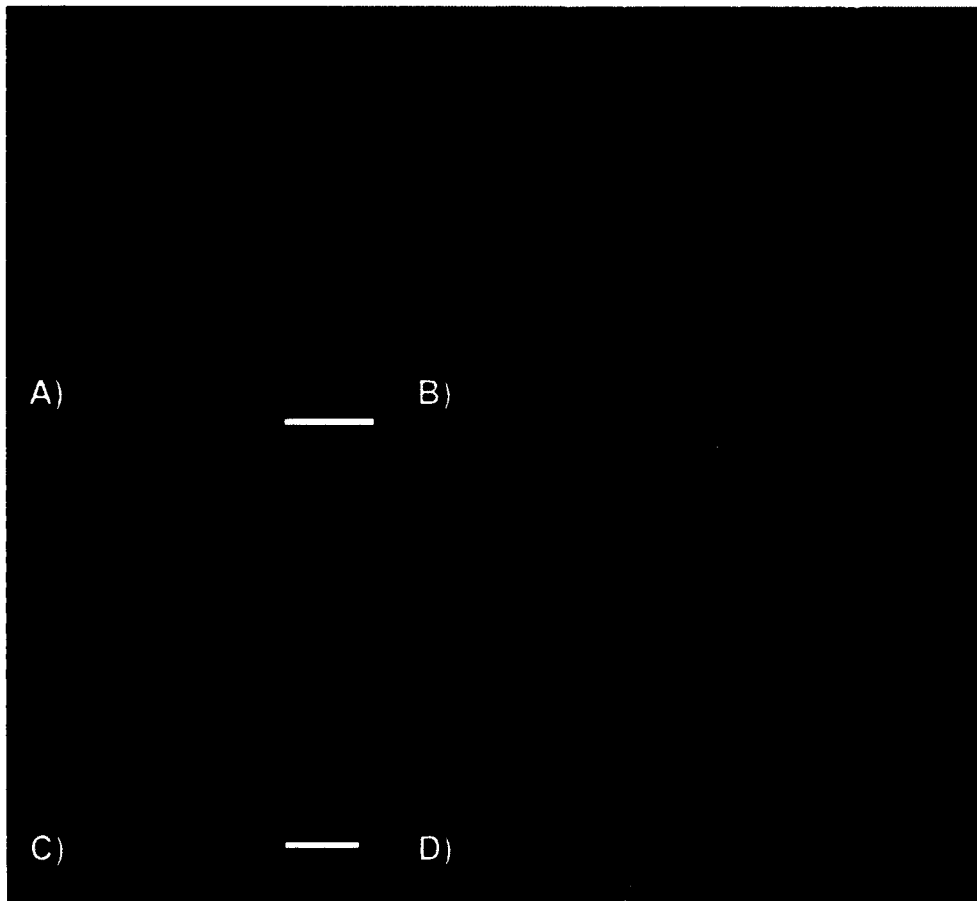
Each pellet was measured at three points with a digital caliper and the average zone of inhibition was 24.3 mm ( $\pm 0.23$  mm N=2,  $\pm 14.05$  mm N=3). As shown in Figure 4-48, one pellet's zone of inhibition varied greatly from the other two. Two pellets had average zones of 32 mm and one had a zone of 8 mm. The wide variation was likely caused by uneven coating as the coating flask bottom had several pellets stacked on top of others. It could have also been that the crystals that precipitated on the pellets were fragile and could shatter which would remove most of the coating. Coating a single layer of pellets at a time, using a tumbler to keep the pellets moving or exercising greater care during handling could solve this problem. An additional solution would be to use pellets of a smaller diameter. All pellets stopped bacterial growth in broth cultures.

#### 4.6.4 Extruded Filaments

The controls and coated pellets were extruded into 1.75 mm diameter 3D printing filaments for fused deposition modeling. An Extrusionbot filament extruder was used, and slight modifications were made to different filament types as necessary. The majority of extrusion was done between 170° to 175 °C. Several meters of each type of filament were extruded. PMMA bone cement filaments were also made to compare to the PLA filaments. These filaments were created by loading the bone cements into a syringe with a tip of similar diameter. The filaments were cut into 1 cm pieces for testing. Small pieces of the filaments were photographed, imaged by SEM, and cultured in both plate and broth cultures. Controls required filaments to be run on the same plate with the plate divided into quadrants. This requirement led to a need for partial plate images of the quadrants. The surface area of the filament touching the surface of the plate was calculated in Appendix B.

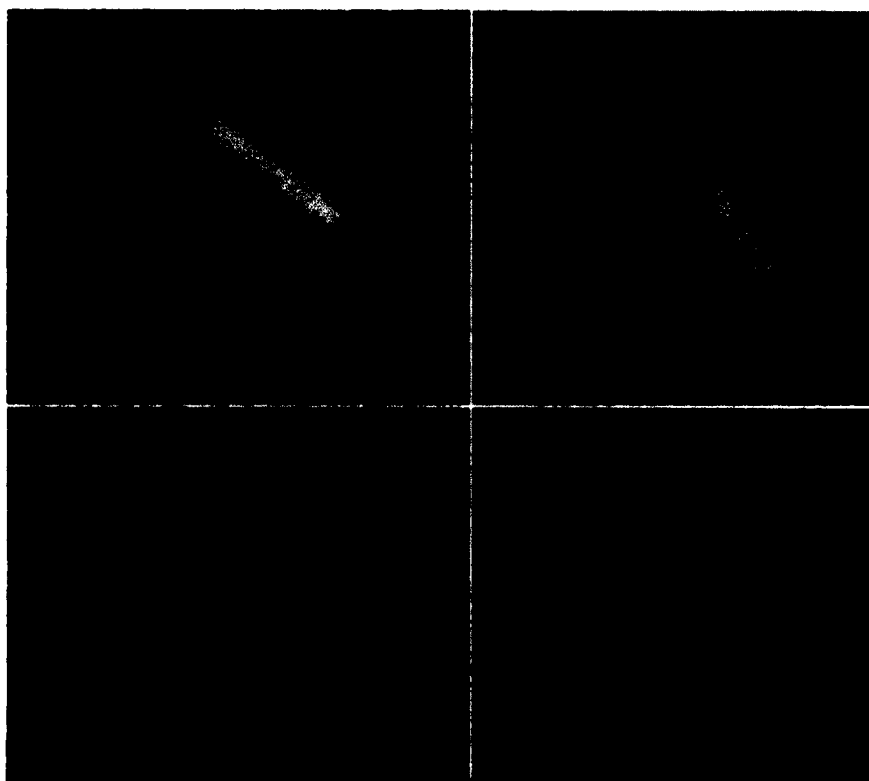
#### 4.6.4.1 Control filaments

Control PLA filaments using plain PLA and oil-coated PLA pellets were extruded. Wright low viscosity Orthoset® bone cement was mixed and syringe molded into filaments. Photographs and SEM of the filaments are shown in Figure 4-50.



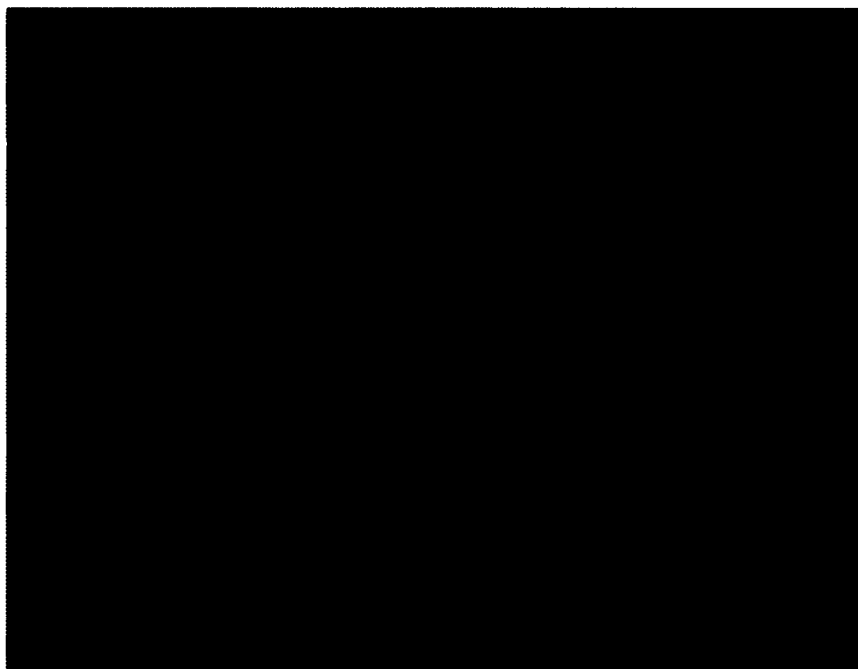
**Figure 4-50:** A) PMMA filament B) SEM of PMMA filament C) Control PLA filament D) SEM of control PLA filament

The PLA filament has a smoother surface than the PMMA filament. This difference may be caused by differences in the extrusion temperature, which was 170 °C as opposed to 90 °C for PMMA. The control PLA filament, oil-coated PLA filament and control PMMA filament were run on bacterial plates as shown in Figure 4-51.

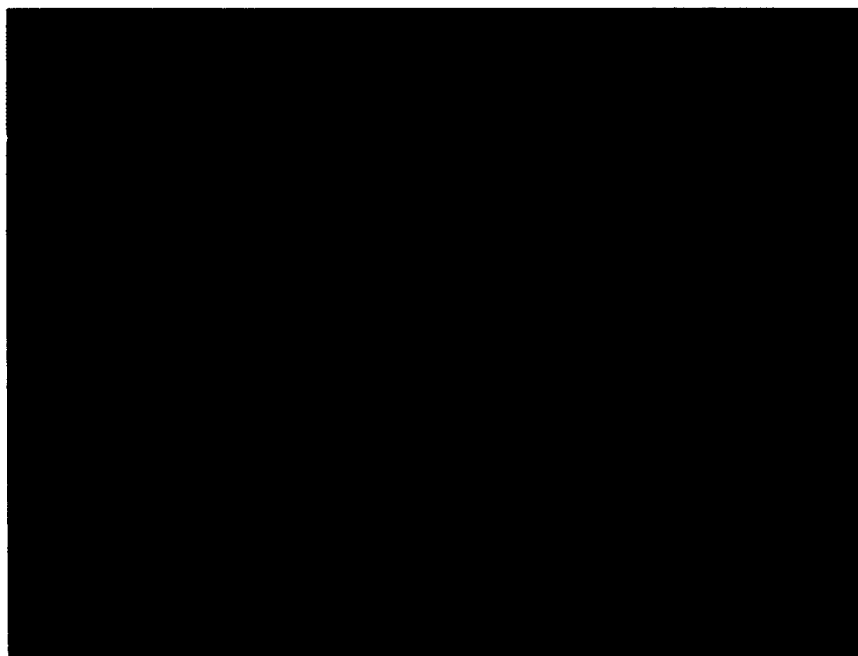


**Figure 4-51:** A) PMMA control top B) PMMA control bottom C) PLA and oil-coated PLA controls top D) PLA and oil-coated PLA controls bottom

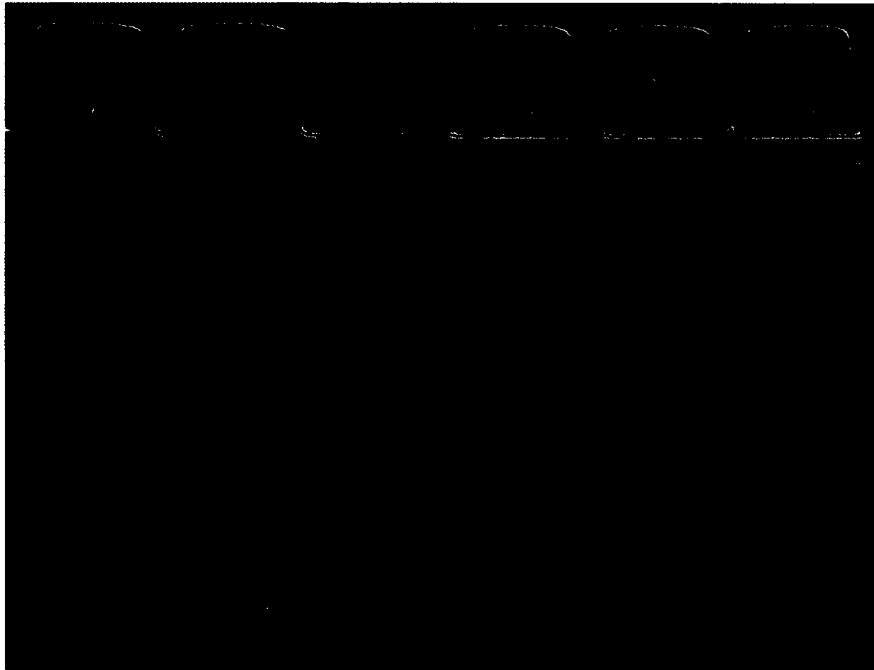
There is no bacterial zone of inhibition or inhibition of bacterial growth that prevents colonies from growing on the surface of the filaments. The filaments were then run in broth cultures as shown in Figure 4-52, Figure 4-53 and Figure 4-54.



**Figure 4-52:** A) Sterile broth B) *E. coli* inoculated broth C-E) PMMA control filament in broth culture



**Figure 4-53:** A) Sterile broth B) *E. coli* inoculated broth C-E) PLA filament in broth culture

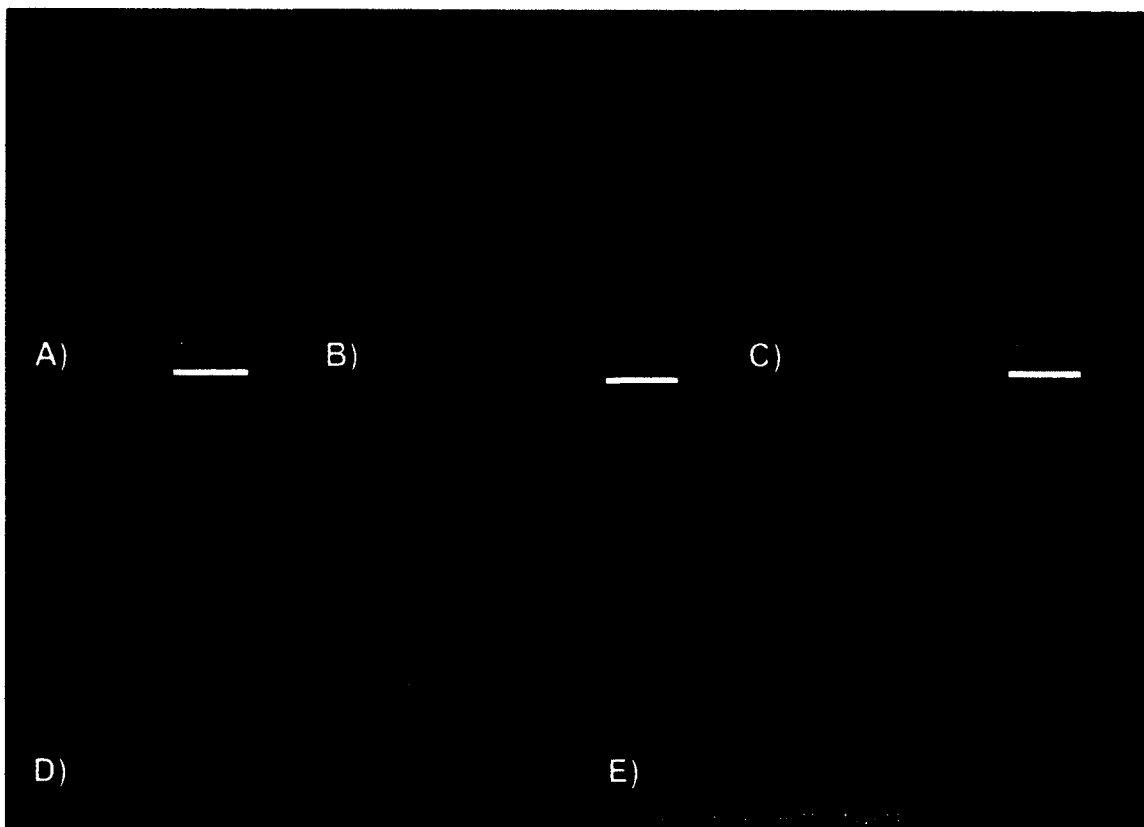


**Figure 4-54:** A) Sterile broth B) *E. coli* inoculated broth C-E) Oil-coated PLA filament in broth culture

There is no bacterial inhibition in any of the broth cultures. These control PLA and PMMA standards can be used for comparison to all other filaments used in this study.

#### 4.6.4.2 *Gentamicin filaments*

PLA and PMMA filaments were fabricated that had an addition of 1 wt% or 2.5 wt% gentamicin sulfate by weight. The filaments were photographed and imaged by SEM, as seen in Figure 4-55.

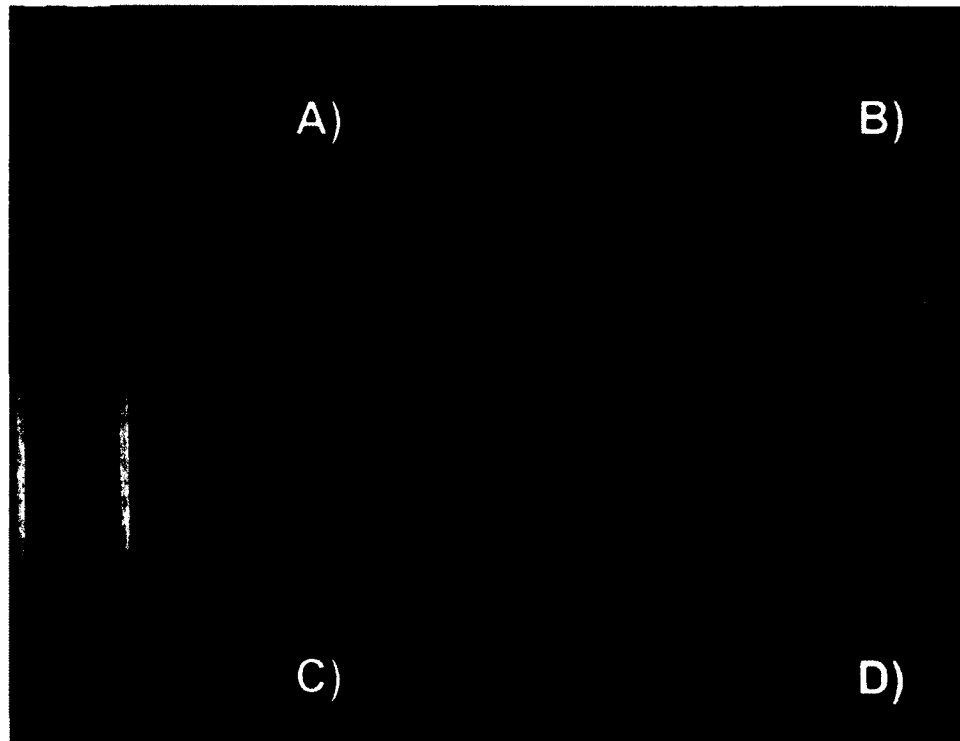


**Figure 4-55:** Photographs and SEM images for A) 1 wt% gentamicin PMMA filament B) 1 wt% gentamicin PLA filament C) 2.5 wt% gentamicin PLA filament D) SEM 1 wt% gentamicin PLA filament E) SEM 2.5 wt% gentamicin PLA filament

PLA and PMMA filaments that were doped with gentamicin were fabricated.

Care was taken to use coating oil levels that would not prevent expansion of the extruded filaments. The 1 wt% and 2.5 wt% gentamicin-doped PLA and PMMA filaments were tested on bacterial plates. Five samples were tested on plates (Figure 4-56).





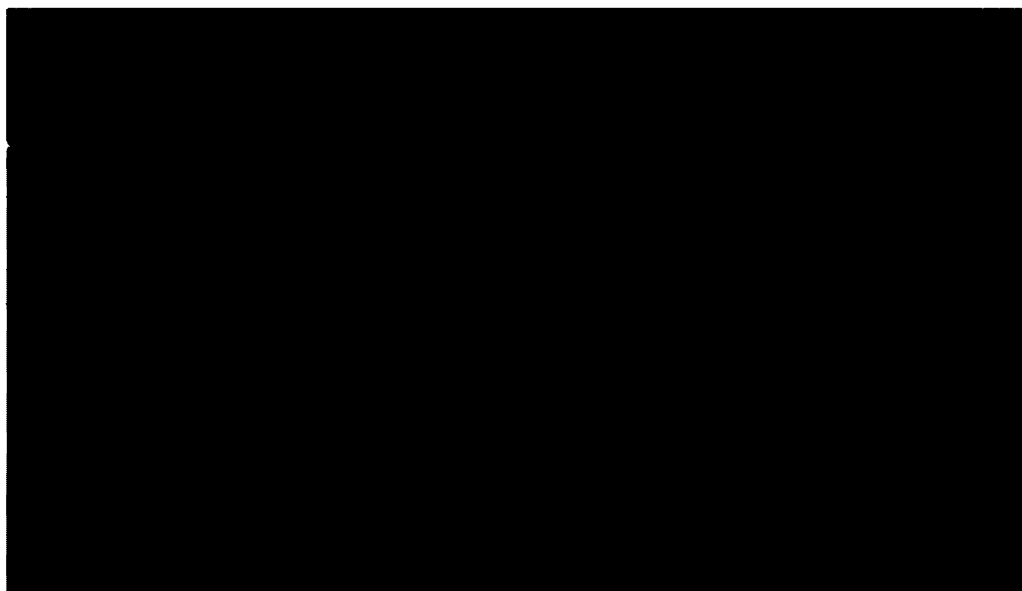
**Figure 4-56:** Agar plate with A) 2.5 wt% gentamicin PLA filament B) control PLA filament C) control PMMA filament D) 2.5 wt% gentamicin PMMA filament

The first group of filament extruded using cleaner extruders and longer purges between extrusions was the 2.5 wt% gentamicin doped PLA. The average zone of inhibition was 23.1 mm ( $\pm$  2.78 mm), based on two digital caliper measurements. This zone was similar to the 2.5 wt% doped PMMA, which had a zone of inhibition of 22.6 mm ( $\pm$  0.79 mm). Statistical analysis showed no difference between these two groups. This result differed with the 1 wt% gentamicin-doped PLA. Full cleaning purges were not done and resulted in initial filament batches that were either not consistent or were consistent but had too low a level of antibiotic. Only three of the five samples inhibited growth, with an average 8.52 mm ( $\pm$  4.3 mm), while all hand made PMMA-gentamicin 1 wt% controls inhibited an average of 13.91 mm ( $\pm$  1.49 mm). These results are shown in Figure 4-57.

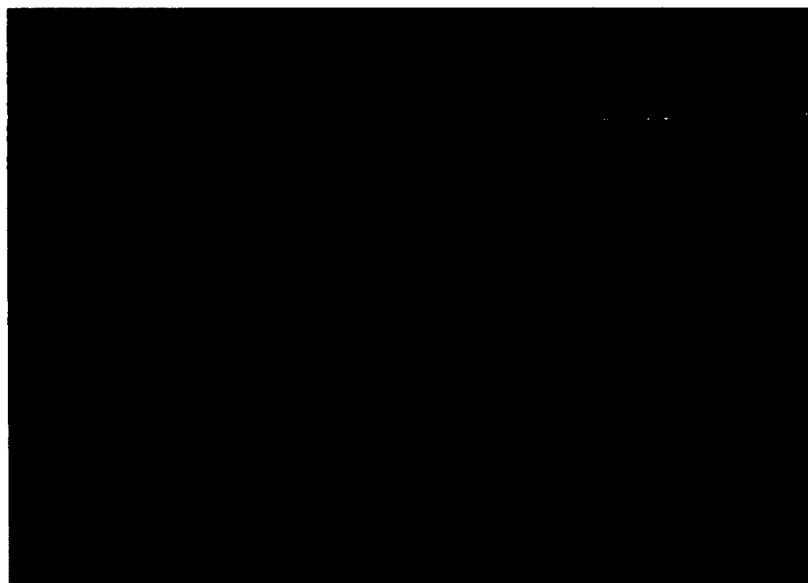


**Figure 4-57:** Agar plate with A-C) 1 wt% gentamicin PLA filament D) 1 wt% gentamicin PMMA filament

The 1 wt% gentamicin-doped PMMA had uniformity across all five samples due to hand mixing with mortar and pestle. Greater care could have been taken to clean the extruder and not test filament from the very beginning of a batch. This was done in further printing of discs and constructs with 1 wt% gentamicin filaments and avoided further issues. The broth cultures for the 1% and 2.5% groups of PLA and PMMA are shown in Figure 4-58, Figure 4-59 and Figure 4-60.



**Figure 4-58:** Broth cultures for A) Sterile broth B) *E. coli* inoculated broth C) Control PMMA D) Control PLA E) 2.5 wt% gentamicin-doped PMMA F) 2.5 wt% gentamicin-doped PLA



**Figure 4-59:** Broth cultures for A) Sterile broth B) *E. coli* inoculated broth C-E) 1 wt% gentamicin-doped PLA filaments



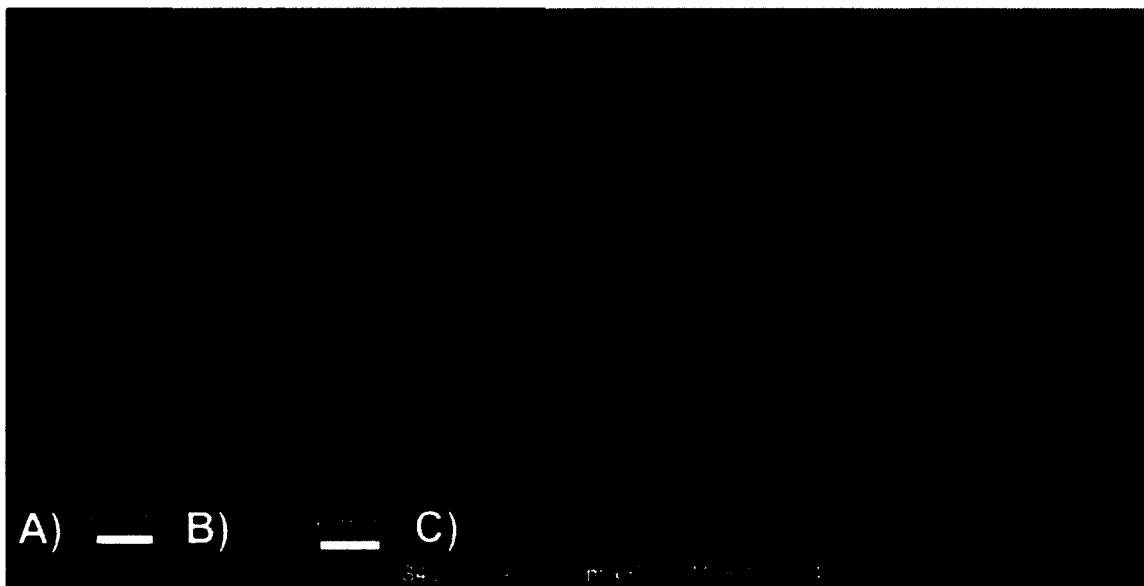
**Figure 4-60:** Broth cultures for A) Sterile broth B) *E. coli* inoculated broth C-E) 1 wt% gentamicin-doped PMMA filaments

The broth cultures show consistent antimicrobial activity for 2.5 wt% gentamicin doped PLA and PMMA. The 1 wt% PLA stopped bacterial growth in only two out of three broth cultures. This inconsistency is again likely to be caused by non-consistent mixing of the filament or too low a level of antibiotic. The 1 wt% gentamicin doped PMMA exhibited no growth. Consistency in the initial extrusion portion from leftover material in the auger is a concern and alternative extrusion methods to overcome limitations of the method may need to be developed.

#### 4.6.4.3 Tobramycin filaments

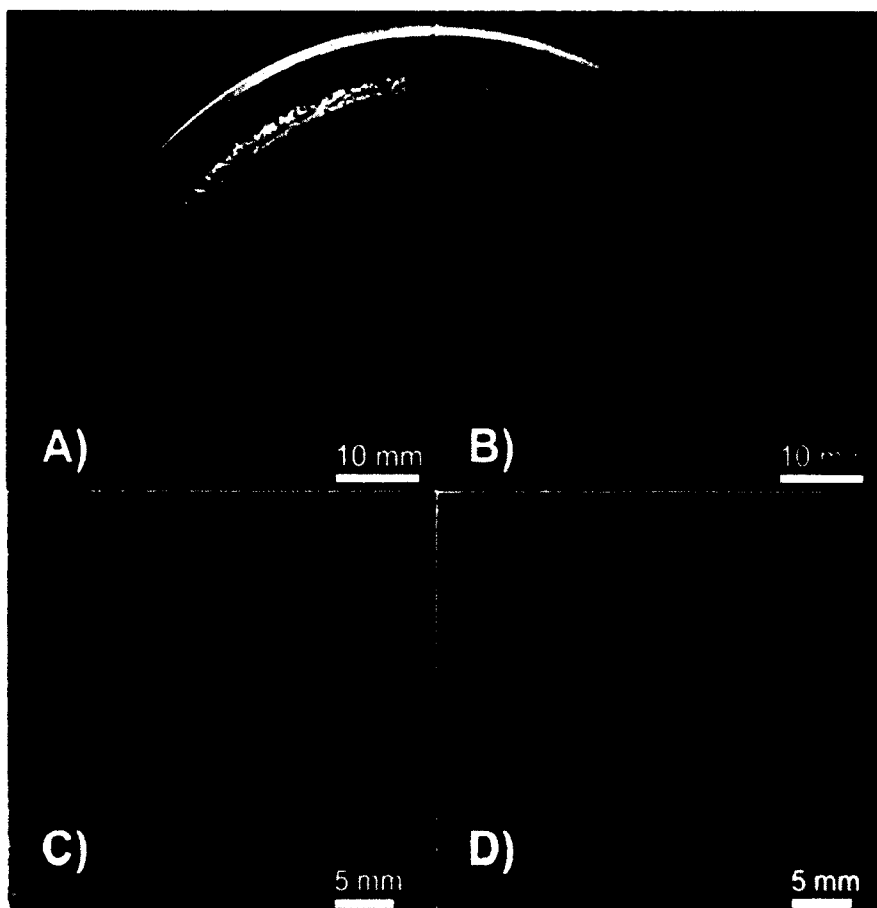
Filaments were fabricated that had an addition of 1% or 2.5% tobramycin by weight. While the decomposition point of tobramycin is over 200 °C, the melting point is 160 °C. The extrusion point was 175 °C. This temperature resulted in a glass or melted sugar-like coating. The fabrication was done for both extruded PLA and molded PMMA

filaments of the same dopant percentages. The filaments were photographed and imaged by SEM, as seen in Figure 4-61.



**Figure 4-61:** Photographs and SEM images of A) 1 wt% tobramycin-doped PMMA B) 1 wt% tobramycin-doped PLA C) SEM 1 wt% tobramycin-doped PLA

The tobramycin filament is silver. The melting of the tobramycin resulted in a color change. Some filament was extruded under the 160 °C point and did not exhibit the color change. There is no clearly visible powders in the filament on SEM. The 160 °C filament was not bacterial tested since the printing process would need to be above 200 °C. The filament was tested to see how heating with the PLA bioplastic above the melt point affected the ability for tobramycin to release. Five Mueller Hinton plates and three broth cultures were tested for 1 cm filaments of PLA mixed with 1.5 wt% tobramycin, 2.5 wt% tobramycin, and PMMA mixed with 1.5 wt% and 2.5 wt% tobramycin. This is shown in Figure 4-62 and Figure 4-63.



**Figure 4-62:** A) 2.5 wt% tobramycin PLA filament B) 1 wt% tobramycin PLA C) 2.5 wt% tobramycin PLA filament D) 1 wt% tobramycin PLA filament



**Figure 4-63:** A) 1 wt% tobramycin PMMA filament B) 2.5 wt% tobramycin PMMA filament

The tobramycin-PMMA filaments had nearly uniform zones of inhibition within each group (Figure 4-63). The 1 wt% tobramycin PMMA zone of inhibition size was 17.2 mm (+/- 1.31 mm) and the 2.5 wt% tobramycin PMMA zone of inhibition PMMA size was 18.7 mm (+/- 1.49 mm). These zones contrasted with the lack of zones of inhibition in the extruded PLA that was mixed with tobramycin. However, some portions of the tobramycin filaments exhibited antimicrobial properties on the plates, as shown in Figure 4-62. The different effect from gentamicin was likely due to the melting point of the tobramycin and interaction with the polymer. Similar effects were shown in the broth cultures as shown in Figure 4-64, Figure 4-65, Figure 4-66 and Figure 4-67.



**Figure 4-64:** A) Sterile broth B) *E. coli* inoculated broth C-E) 1 wt% tobramycin doped PLA filaments

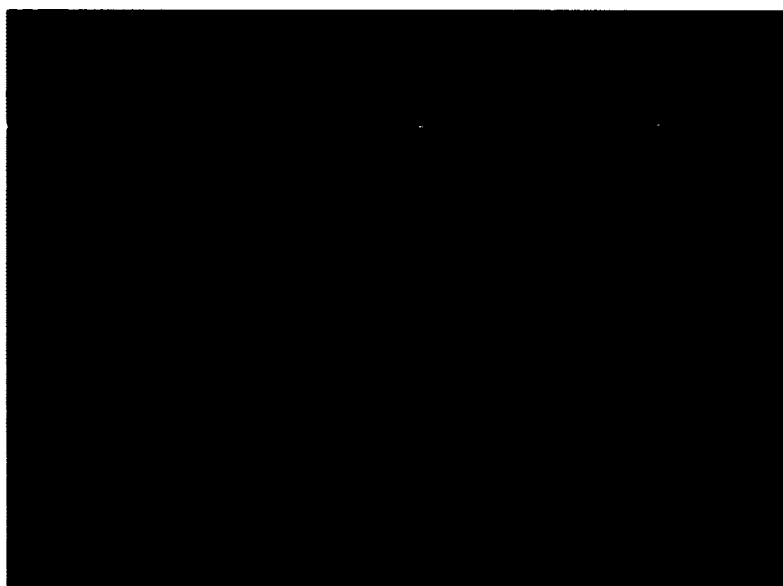


**Figure 4-65:** A) Sterile broth B) *E. coli* inoculated broth C-E) 1 wt% tobramycin doped PMMA filaments





**Figure 4-66:** A) Sterile broth B) *E. coli* inoculated broth C-E) 2.5 wt% tobramycin doped PLA filaments



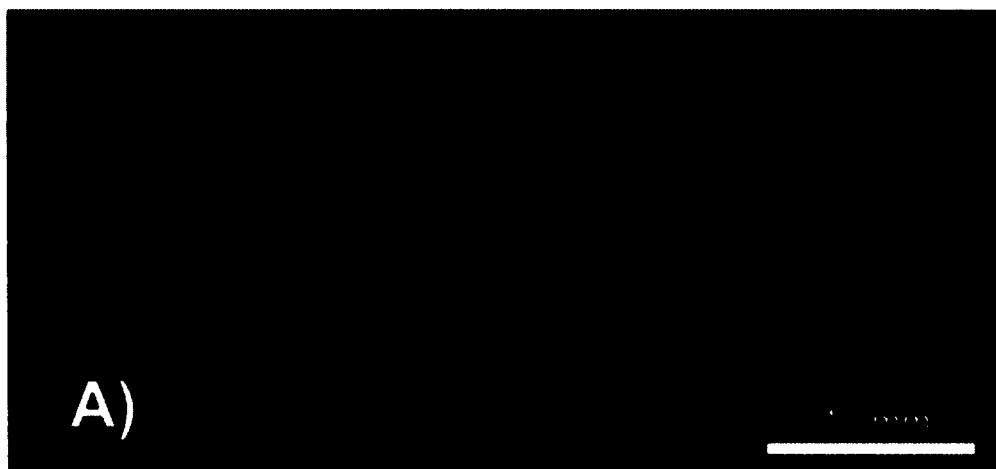
**Figure 4-67:** A) Sterile broth B) *E. coli* inoculated broth C-E) 1 wt% tobramycin doped PMMA filaments

The PMMA broth cultures had no bacterial growth. This result was similar to that from the PMMA bacterial plate cultures. The exothermic PMMA reaction only reaches up to 90 °C, so it is below the melting point of tobramycin. The PLA broth cultures for

both 1% and 2.5% each only had one broth culture where growth was inhibited. The PLA extrusion point was above the 160 °C melting point and even placement in a liquid broth did not allow the tobramycin to disperse from the filaments regularly in high enough levels to consistently inhibit bacteria.

#### 4.6.4.4 Nitrofurantoin filaments

Filaments were made by extruding nitrofurantoin-coated pellets at 175 °C. Nitrofurantoin has a melting point/degradation point in excess of 240 °C. Only filaments with 1 wt% were generated, as a proof of concept, since nitrofurantoin has very low solubility in water. Antimicrobial activity of nitrofurantoin would be viewed as an option for more combinatorial therapy. A construct that combined a highly soluble substance such as gentamicin for an initial burst and also a much more insoluble compound could be desirable. The filament was extruded as shown by a section in Figure 4-68.



**Figure 4-68:** A) Nitrofurantoin filament

The yellow nitrofurantoin powder can be seen within the filament. PMMA filament was also made with 1 wt% nitrofurantoin. The PMMA filament has a yellow coloring as well. Five plates were made as shown in Figure 4-69.



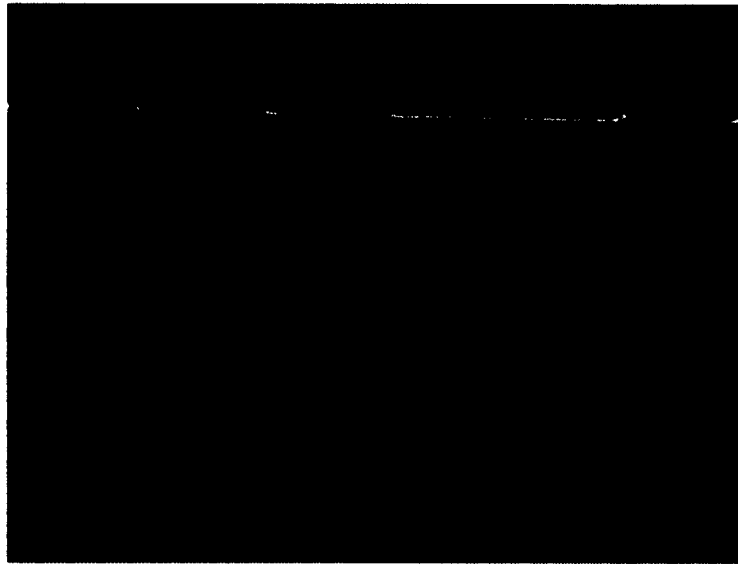
**Figure 4-69:** Plates are divided into quadrants with filament with top left being control PMMA, top right being nitrofurantoin 1 wt% PMMA, bottom left nitrofurantoin 1 wt% PLA and bottom right control PLA and oil-coated PLA filaments.

Zones of inhibition were photographed and measured on multiple points with a digital caliper. Results for nitrofurantoin plates were inconclusive. All five nitrofurantoin doped PLA filaments had inhibitory properties but they were variable. For example, the zone of inhibition sizes of gentamicin 2.5 wt% filament was consistent in size across plates. The zone of inhibition size with the nitrofurantoin filaments was variable. Three plates had similar partial zone sizes of 5.25 mm. The overall average was a 4.67 mm zone of inhibition ( $\pm$  2.78 mm). However, of the other two, the largest outlier plate had a zone of 13.5 mm and the lowest had a 0.5 mm zone of inhibition. This large zone could have been because the doping percent was too low. The gentamicin 1 wt% exhibited similar inconsistencies that were thought to be from improper extrusion. However, the

gentamicin powder extruded clear while the nitrofurantoin extruded yellow. Powder can be seen in these filaments. The cause of the powder may be inconsistent mixing or too low a doping percentage. This antibiotic also has a low solubility. Interactions with the polymer chains are not ruled out. PMMA filaments had no antimicrobial properties on the plates. Two broth cultures were also run and the results are shown in Figure 4-70 and Figure 4-71.



**Figure 4-70:** A) Sterile broth B) *E. coli* inoculated broth C-E) 1 wt% nitrofurantoin doped PLA filaments

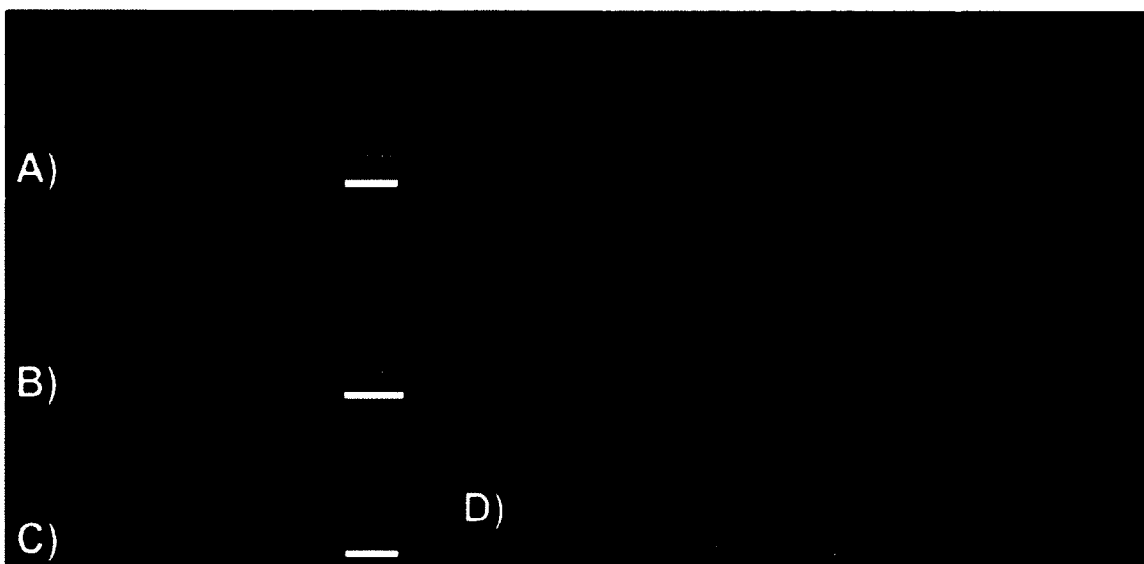


**Figure 4-71:** A) Sterile broth B) *E. coli* inoculated broth C-E) 1 wt% nitrofurantoin doped PMMA filaments

The broth cultures show no inhibition or only minimal inhibition of bacterial growth. Only one nitrofurantoin doped PLA filament was able to inhibit growth in the broth culture. Low dopant percentage, antibiotic low solubility, or polymer interaction may have prevented the desired antimicrobial effect.

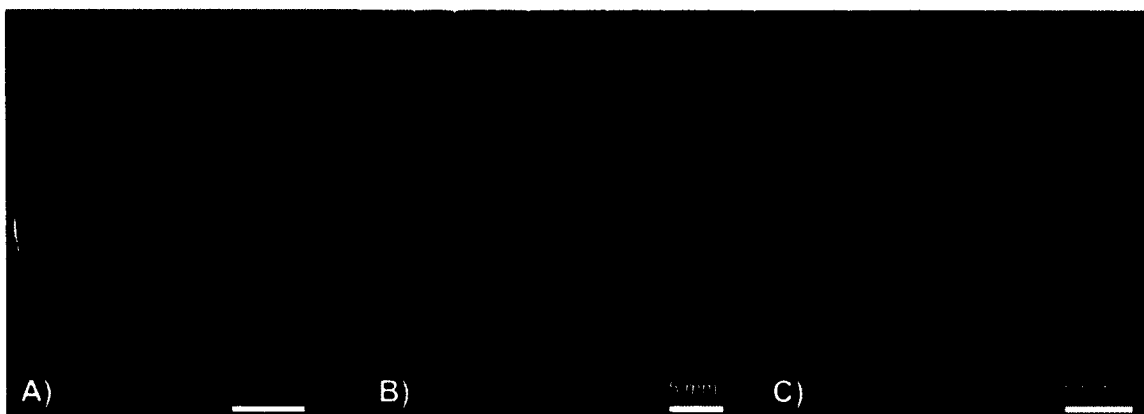
#### 4.6.4.5 Halloysite filaments

Halloysite filaments were created to show the possibility of fabricating constructs with nanotechnology. The HNTs were either control (unloaded) or loaded with gentamicin sulfate. Several feet of 1.5 wt% and 7.5 wt% filament of gentamicin loaded HNT was constructed. A 10% HNT filament was also constructed. A portion of these filaments are shown in Figure 4-72.



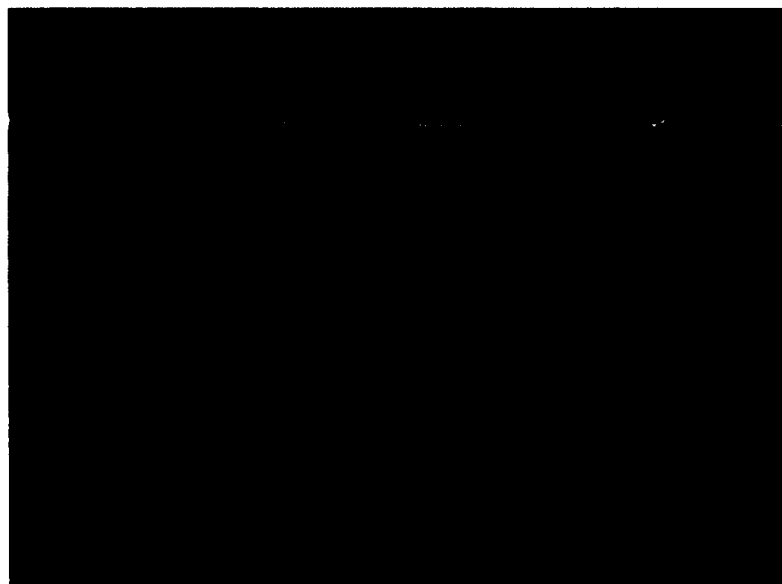
**Figure 4-72:** A) 7.5 wt% HNT loaded with gentamicin PLA filament B) 1.5 wt% HNT loaded with gentamicin PLA filament C) 10 wt% HNT PLA filament D) SEM 1.5 wt% HNT loaded with gentamicin filament

The HNT particles can be seen in all three filaments. They are particularly noticeable in the 10 wt% filament. SEM shows HNTs embedded in the PLA filament. Five samples of each the 1.5 wt% filament doped with gentamicin-loaded HNT and 10 wt% HNT filament was tested on bacterial plates and in broth cultures (Figure 4-73).



**Figure 4-73:** A) 10 wt% HNT-PLA filament B-C) 1.5 wt% HNT loaded with gentamicin PLA filament

The HNT-doped filaments overall showed no bacterial inhibition. One sample of the gentamicin-loaded HNT filament had a partial zone. From a bottom view of the plates there appeared to be slight antimicrobial properties. The vacuum-loaded HNT acts as a carrier of a substrate at 10% to 15% of its weight. The 1.5% HNT filament would have been only 0.15% gentamicin. That gentamicin, once loaded, was set for controlled release. A higher doping percentage of antibiotic-loaded halloysite would likely show a more consistent effect. The HNT doped filaments were testing broth culture ( Figure 4-74 and Figure 4-75).



**Figure 4-74:** A) Sterile broth B) *E. coli* inoculated broth C-E) 10 wt% HNT doped PLA filaments



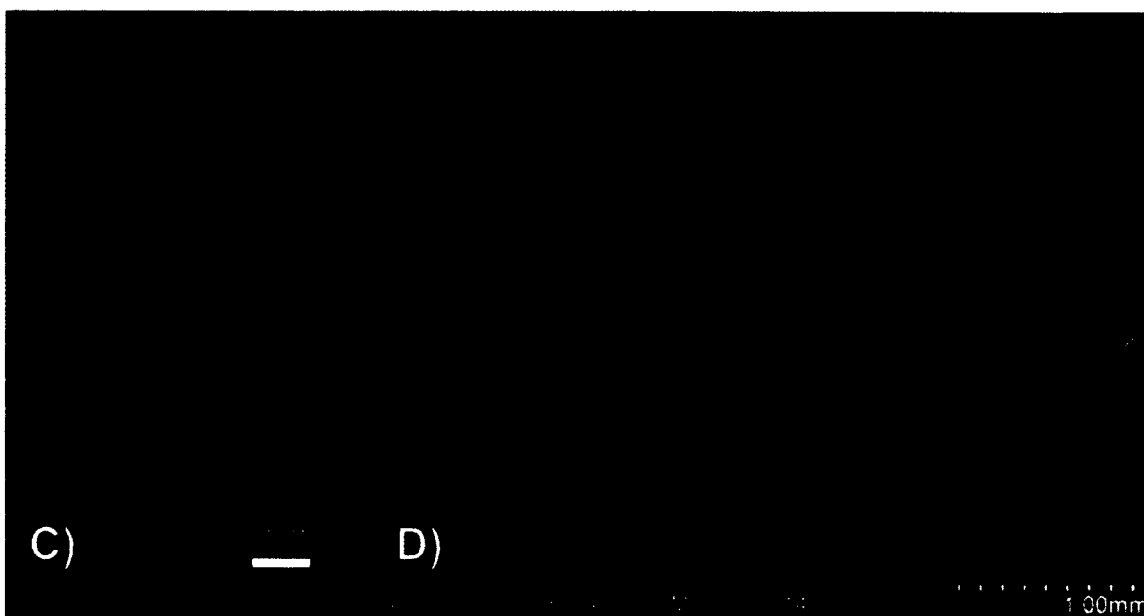
**Figure 4-75:** A) Sterile broth B) *E. coli* inoculated broth C-E) 1.5 wt% gentamicin loaded HNT doped PLA filaments

Overall the HNT filaments did not inhibit bacterial growth in broth cultures (Figure 4-74 and Figure 4-75). Only one of the gentamicin-eluting filaments was able to stop the growth. Even with a liquid medium, the low dopant level or controlled release effect of loading the gentamicin into the halloysite did not allow for release to occur quickly enough.

#### 4.6.4.6 *Atomizer fabricated GS filaments*

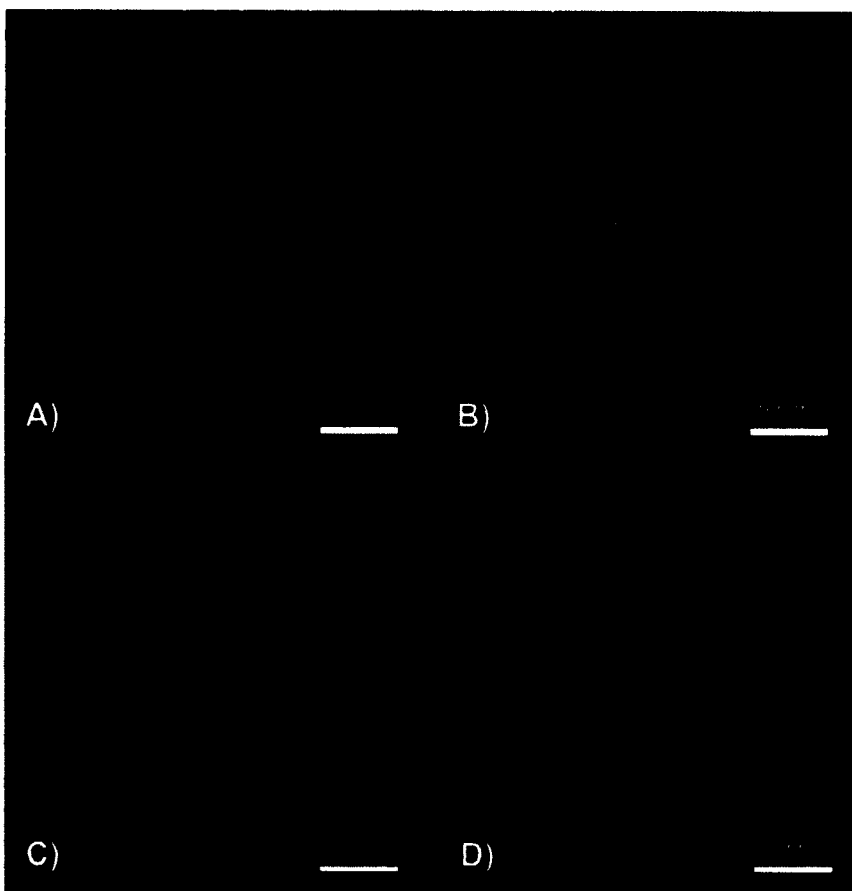
The pellets that were coated in gentamicin by the atomizer were extruded at 175 °C into a 3D printing filament in a 20 gram batch. A small portion of the filament was photographed and an SEM was taken (Figure 4-76).





**Figure 4-76:** A) Atomizer based gentamicin PLA filament B) SEM of atomizer manufacturing method filament

The SEM shows deposits of gentamicin crystals embedded in the PLA. Five of these filaments were cultured on Mueller Hinton plates and three in Mueller Hinton broths. The results are shown in Figure 4-77 and Figure 4-78.



**Figure 4-77:** A-D) 1 wt% atomizer-coated gentamicin doped PLA filaments

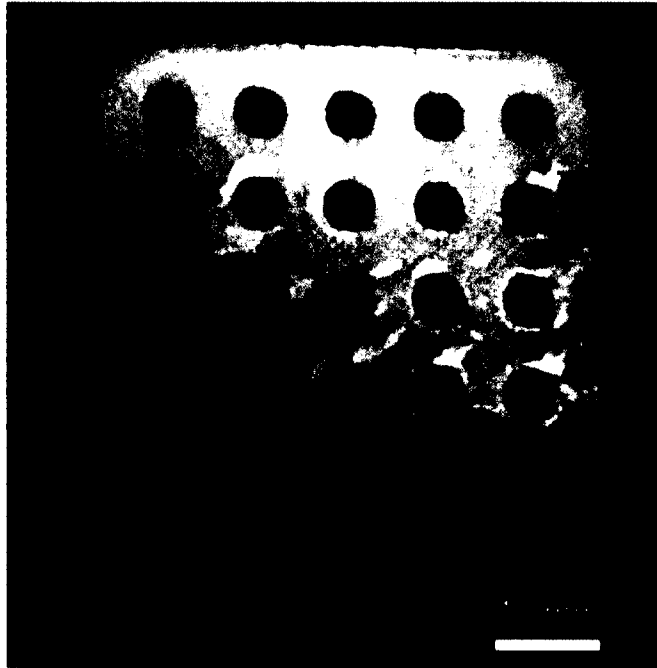


**Figure 4-78:** A) sterile broth B) *E. coli* inoculated broth C-E) 1 wt% atomizer-coated gentamicin doped PLA filaments

The atomizer-coated filaments all showed antimicrobial properties and inhibited growth on the plates to some extent and in the broths. A digital caliper was used to measure each plate at three points. Two of the filaments had similar sized zones of inhibition with an average 14.5 mm and 21.5 mm. The other filaments had either a partial zone of inhibition or antimicrobial properties that had minimal zones of inhibition. The overall average zone of inhibition size was 11.27 mm (+/- 8.29 mm). The broths had no bacterial growth. This lack of growth may have been caused by variable mixing of the antibiotics in the extrusion process. These pellets also had more fragile gentamicin crystal coatings that could break off during the manufacturing process. The plates only have a small portion of the filament touching the agar while the broths allow for full surface and pore area to interact or elute. Modifications to this method in a commercial manner could allow for consistently fabricated filament with uniform elution properties.

#### 4.6.5 3D Fabricated Discs

A fused deposition-modeling printer was used to 3D-fabricate constructs. A Makerbot consumer printer was used to demonstrate the versatility of this method of fabrication. The discs were 5 mm in diameter and 1 mm in height and were modeled in SolidWorks. The bone cements were fabricated into a disc using a mold as shown in Figure 4-79 that was then covered with two glass slides and held under pressure with a c-clamp. The mold was fabricated using a 3D printer and ABS plastic.



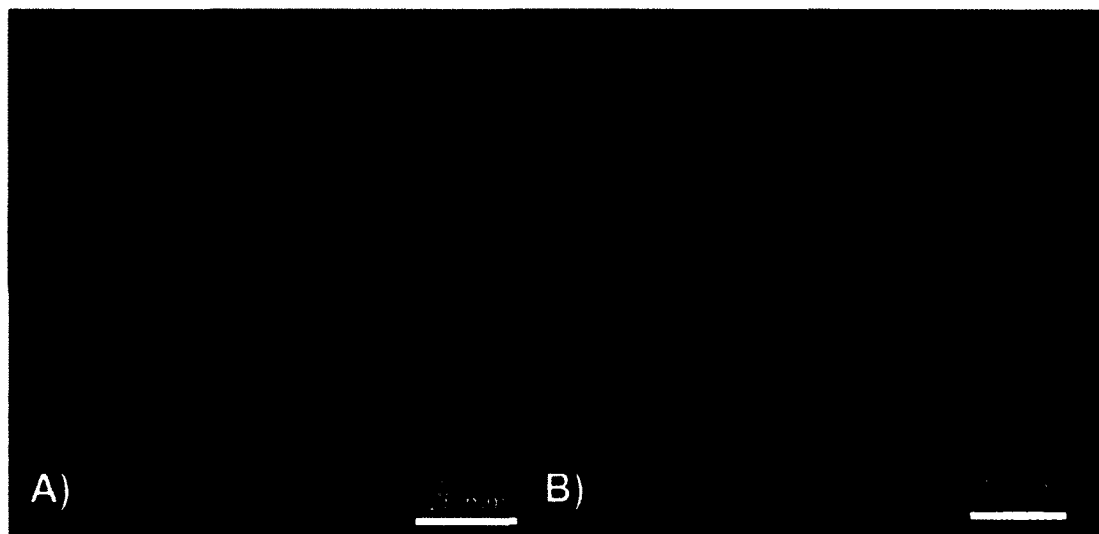
**Figure 4-79:** PMMA bone cement test disc mold

The mold as shown above was used to create the PMMA bone cement test discs.

A single remaining PMMA disc can be seen in the bottom left corner of the mold.

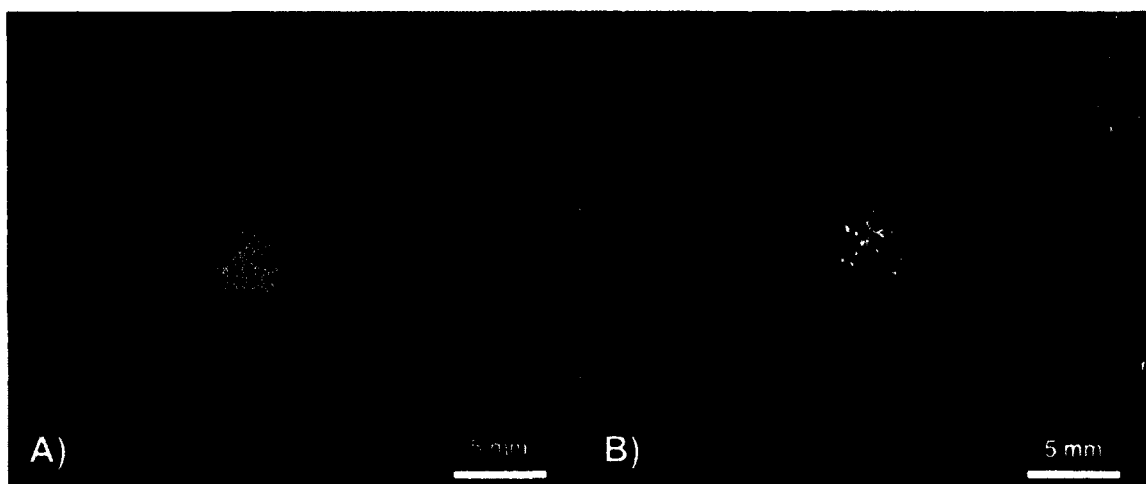
#### 4.6.5.1 Control discs

The Makerbot Replicator 5<sup>th</sup> generation printer with a new printer head was used to fabricate control test discs. The printing temperature was set to 220 °C with a 300 micron resolution and 100% fill. This setup is shown along with a PMMA test disc in Figure 4-80.

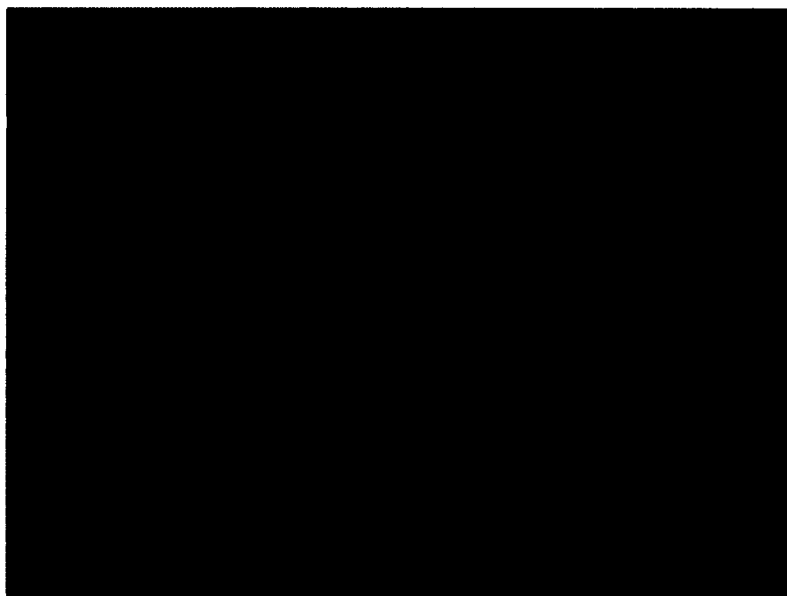


**Figure 4-80:** A) PLA control disc B) PMMA control disc

Five bacterial plate cultures and three broth cultures were run with control PLA and PMMA discs. The results are shown in Figure 4-81, Figure 4-82 and Figure 4-83.



**Figure 4-81:** A) Control PMMA disc B) Control PLA disc



**Figure 4-82:** A) Sterile broth B) *E. coli* inoculated broth C-E) Control PMMA discs

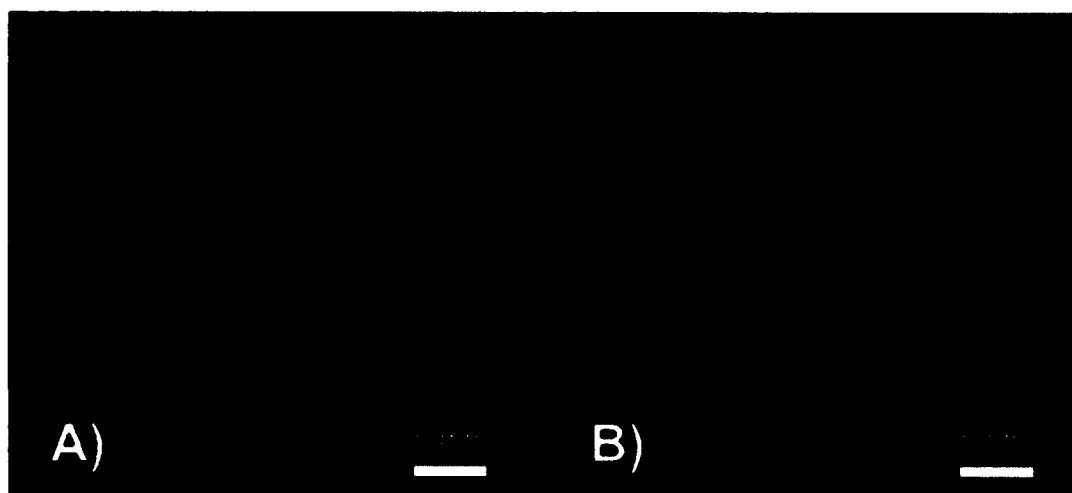


**Figure 4-83:** A) Sterile broth B) *E. coli* inoculated broth C-E) Control PLA discs

In all control disc studies there was no bacterial inhibition. No bacterial plate shows any inhibition of bacterial growth. No broth culture shows any inhibition of bacterial growth.

#### 4.6.5.2 Gentamicin discs

Both PMMA and PLA discs were fabricated with gentamicin as a bioactive additive. Discs were fabricated at 1 wt% and 2.5 wt% gentamicin for both PMMA and PLA. Pictures were taken of the discs to show uniformity of manufacturing as shown in Figure 4-84.

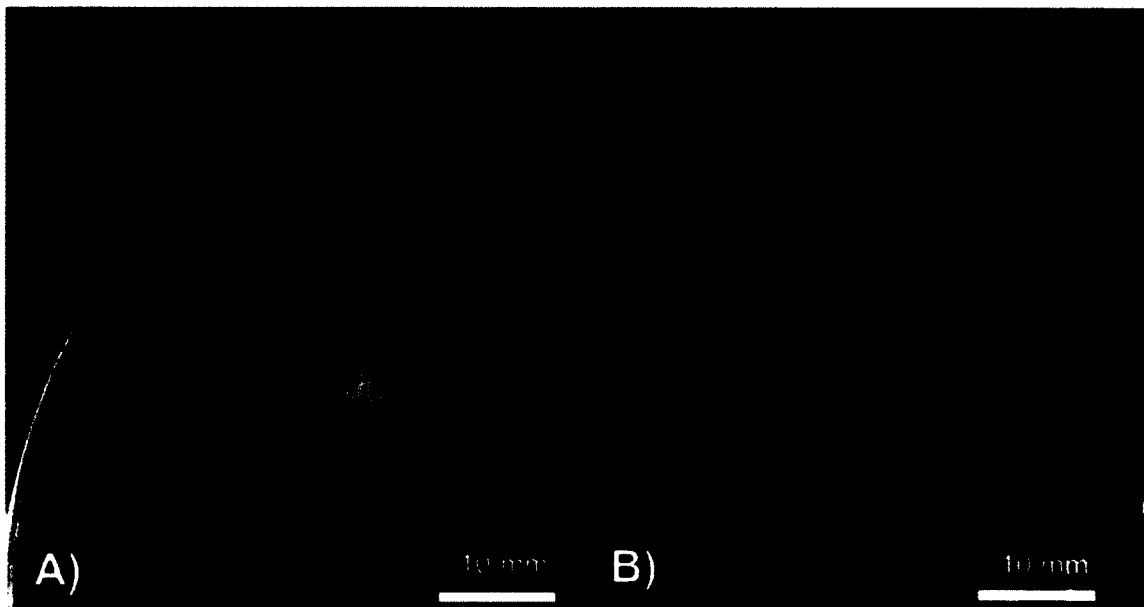


**Figure 4-84:** A) 1 wt% gentamicin PMMA disc B) 1 wt% gentamicin PLA disc

Five plates of each category were tested on Mueller Hinton plates and three discs of each category were tested in Mueller Hinton broth cultures.

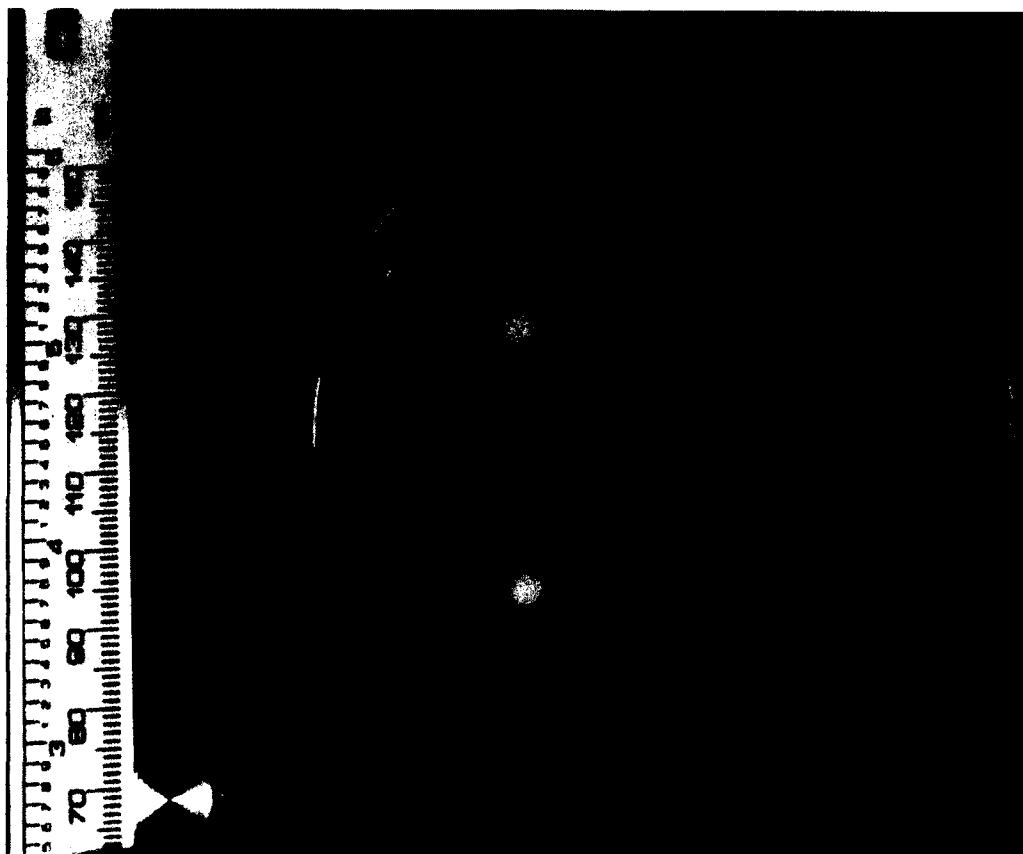
All bacterial plates and broth cultures inhibited bacterial growth. The 1 wt% gentamicin PLA disc had a zone of inhibition of 12.9 mm ( $\pm$  2.56 mm) (Figure 4-85). This compares to a 12.2 mm ( $\pm$  0.39 mm) zone of inhibition from the 1 wt% gentamicin PMMA discs (Figure 4-85). Statistical analysis shows no significant difference between the groups. The 2.5 wt% gentamicin PLA disc had a zone of inhibition of 21.4 mm ( $\pm$  1 mm) (Figure 4-86). This compares to the 22.0 mm ( $\pm$  0.75 mm) zone of inhibition from the 2.5 wt% gentamicin PMMA discs (Figure 4-86). ANOVA shows no significant difference between the groups. All broth cultures

prevented bacterial growth (Figure 4-87, Figure 4-88, Figure 4-89, Figure 4-90). The results show the capability for gentamicin to be used as a bioactive agent in 3D fabrication of simple constructs.

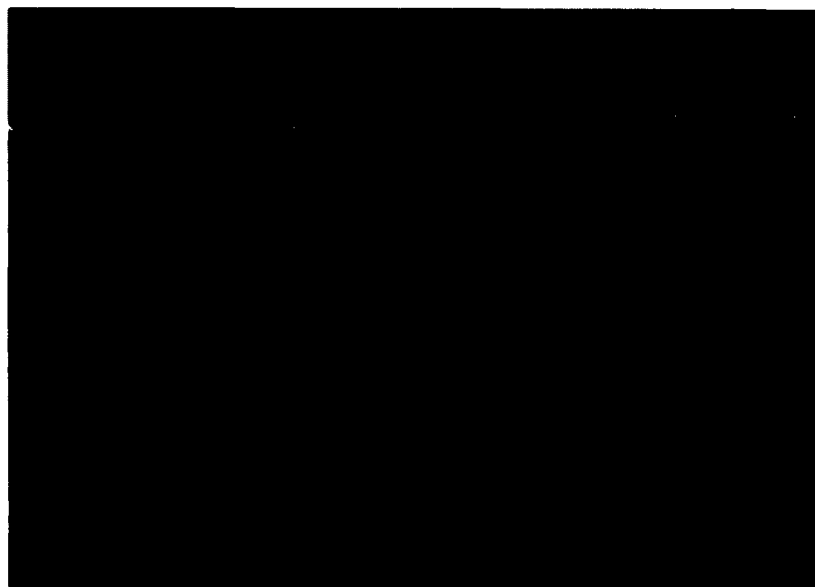


**Figure 4-85:** PMMA 1 wt% gentamicin disc b) PLA 1 wt% gentamicin disc

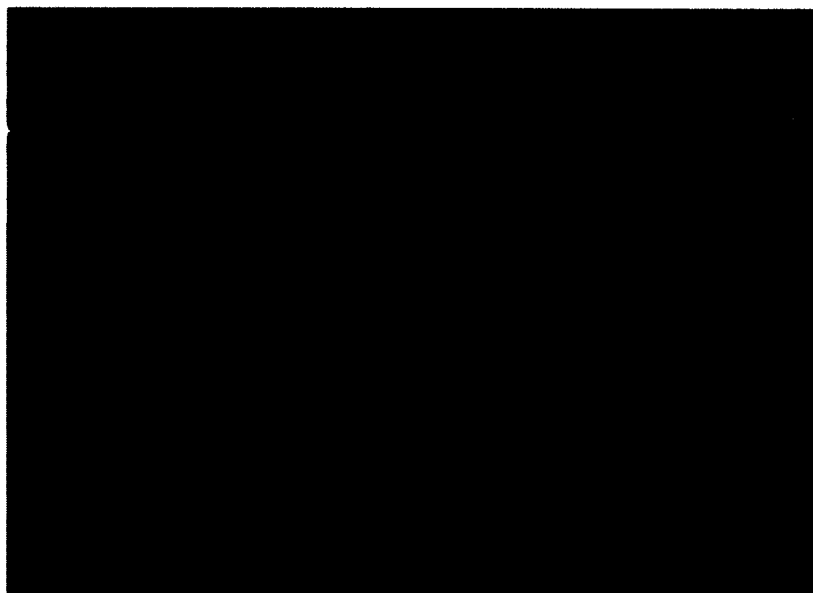




**Figure 4-86:** A) PMMA 2.5 wt% gentamicin disc B) PLA 2.5 wt% gentamicin disc C) Control PMMA disc D) Control PLA disc



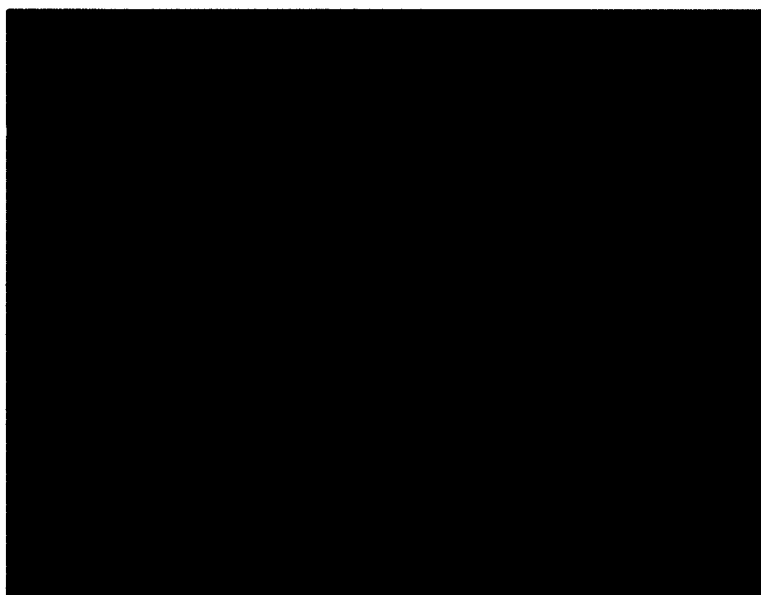
**Figure 4-87:** A) Sterile broth B) *E. coli* inoculated broth C-E) 1 wt% gentamicin PMMA discs



**Figure 4-88:** A) Sterile broth B) *E. coli* inoculated broth C-E) 1 wt% gentamicin PLA discs



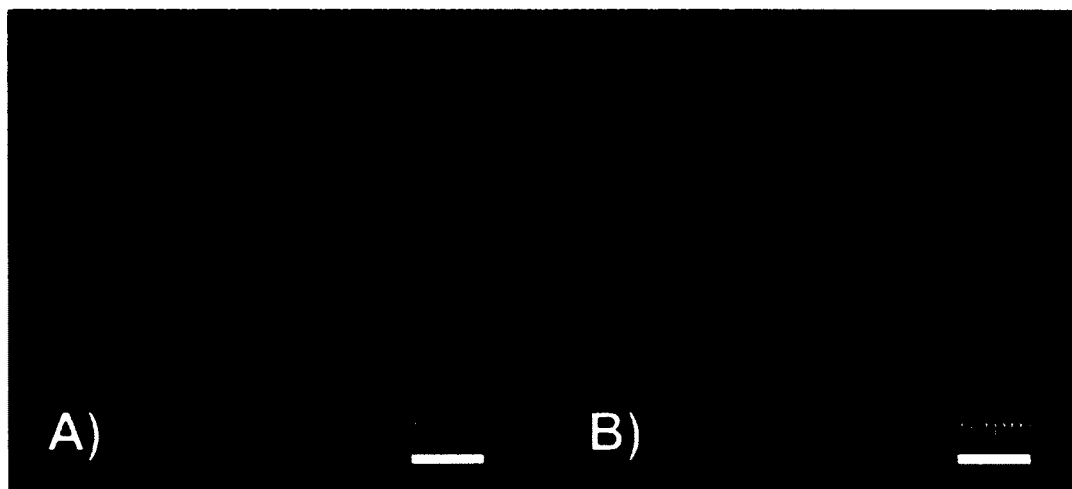
**Figure 4-89:** A) Sterile broth B) *E. coli* inoculated broth C-E) 2.5 wt% gentamicin PMMA discs



**Figure 4-90:** A) Sterile broth B) *E. coli* inoculated broth C-E) 2.5 wt% gentamicin PLA discs

#### 4.6.5.3 Tobramycin discs

Tobramycin-laden discs were fabricated. The groups for testing were 1 wt% and 2.5 wt% of both PMMA and PLA. Pictures of these discs are shown in Figure 4-91.



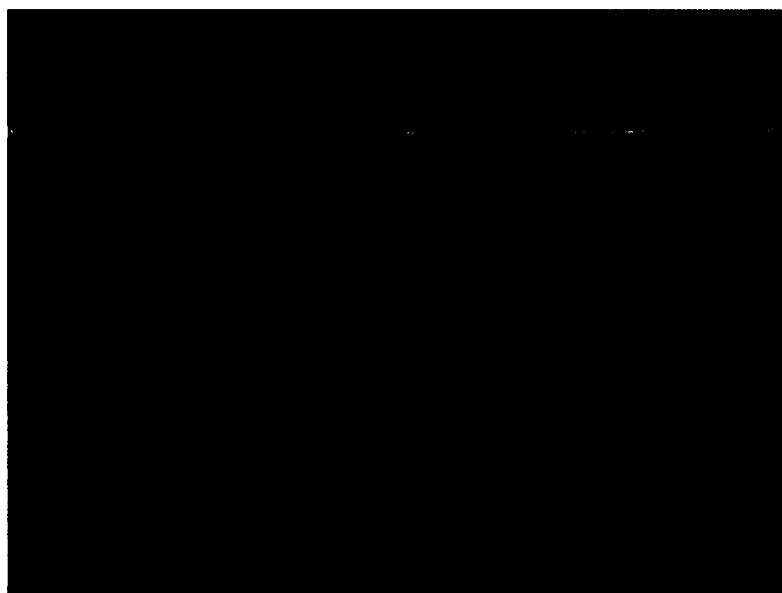
**Figure 4-91:** A) PMMA 1 wt% tobramycin disc b) PLA 1 wt% tobramycin disc

The discs were uniformly manufactured in both feature and weight. Each group of the discs was tested on five Mueller Hinton agar plates as well as three Mueller Hinton broths.

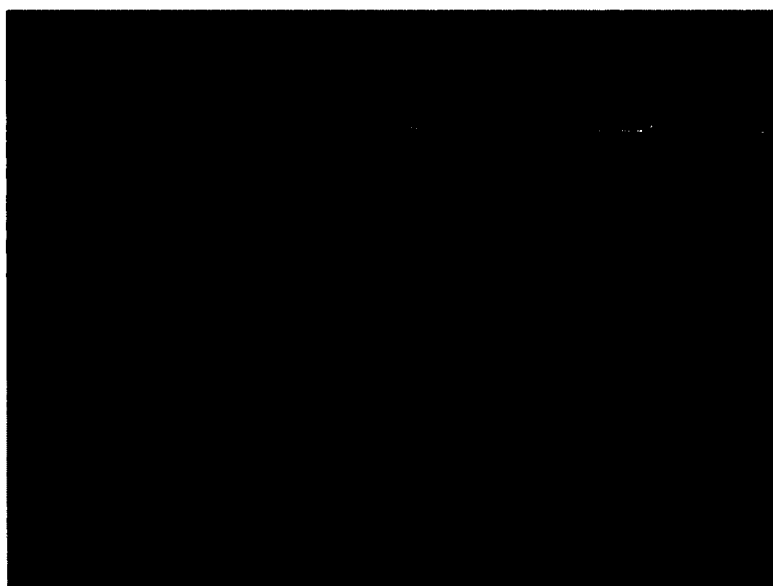
The bacterial plates were measured by digital caliper at three points for each zone of inhibition. The tobramycin-laden PLA discs had no zones of inhibition (Figure 4-92). The PMMA discs of 1 wt% tobramycin and 2.5 wt% tobramycin had zones of inhibition of 13.74 mm (+/- 1.71 mm) and 17.42 mm (2.81 mm), respectively (Figure 4-92). The broth cultures showed similar results with no antibacterial properties in the PLA discs (Figure 4-94, Figure 4-96). The bone cement tobramycin-laden discs showed no bacterial growth (Figure 4-93, Figure 4-95). Again, this was likely due to the low melting point of tobramycin and interaction with the polymer. A more pressurized and lower temperature printer head that could operate below 160 °C would likely overcome these issues. For these reasons no further printing of constructs was done with tobramycin.



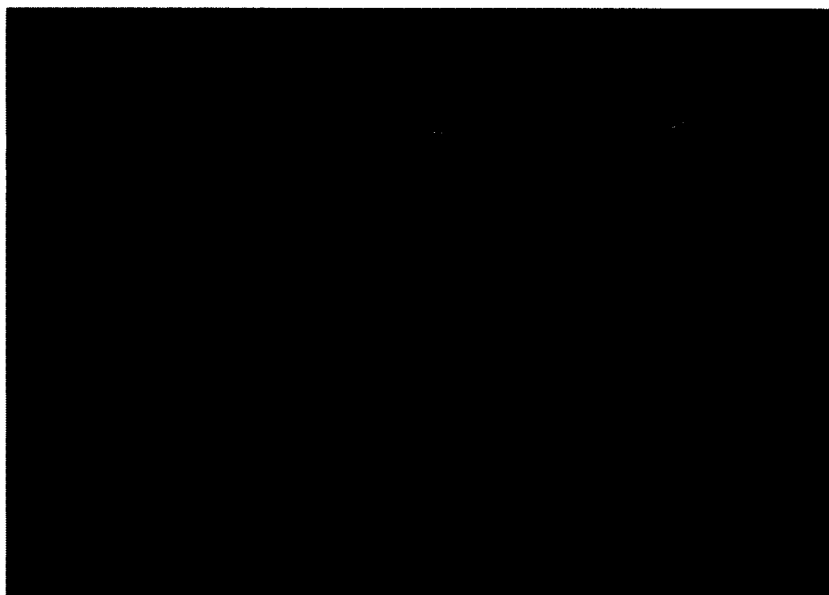
**Figure 4-92:** A) 1 wt% tobramycin PMMA disc B) 1 wt% tobramycin PLA disc C) 2.5 wt% tobramycin PMMA disc D) 2.5 wt% tobramycin PLA disc



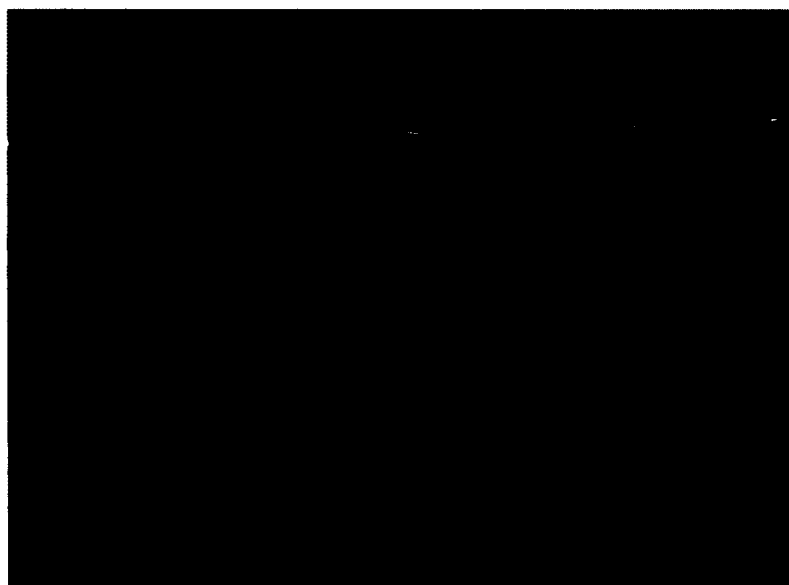
**Figure 4-93:** A) Sterile broth B) *E. coli* inoculated broth C-E) 1 wt% tobramycin PMMA discs



**Figure 4-94:** A) Sterile broth B) *E. coli* inoculated broth C-E) 1 wt% tobramycin PLA discs



**Figure 4-95:** A) Sterile broth B) *E. coli* inoculated broth C-E) 2.5 wt% tobramycin PMMA discs

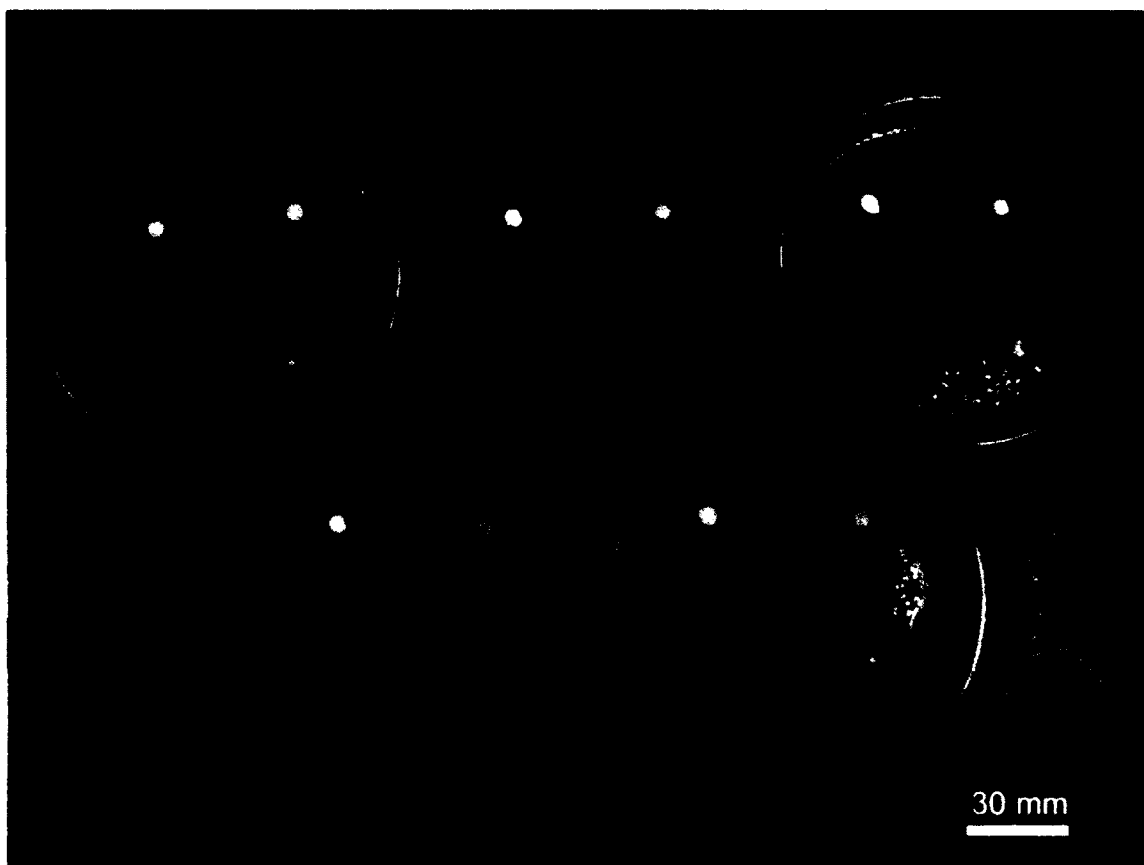


**Figure 4-96:** A) Sterile broth B) *E. coli* inoculated broth C-E) 2.5 wt% tobramycin PLA discs

#### 4.6.5.4 Nitrofurantoin discs

Nitrofurantoin discs were fabricated of 1 wt% PMMA and PLA. Limited results were previously seen in studies involving filaments in both the PMMA and PLA

materials. The low solubility of the antibiotic was likely a primary cause of these results. The lack of antibacterial properties in the control PMMA made further testing challenging. Antibacterial activity might be improved with higher doping percentages. PMMA and PLA discs were fabricated with 1 wt% nitrofurantoin. Mueller Hinton plate cultures were run with five samples from each group as shown in Figure 4-97.



**Figure 4-97:** Bacterial plates of nitrofurantoin discs divided in quadrants. Top left: control PMMA; Top right: 1 wt% nitrofurantoin-laden PMMA disc; Bottom left: 1wt% nitrofurantoin-laden PLA disc; Bottom right: control PLA disc

The PMMA mixed with nitrofurantoin has no zones of inhibition (Figure 4-98). The PLA-nitrofurantoin discs have varying levels of inhibition. Three discs have partial zones around 7 mm (Figure 4-98). Two discs have no zones of inhibition. The overall



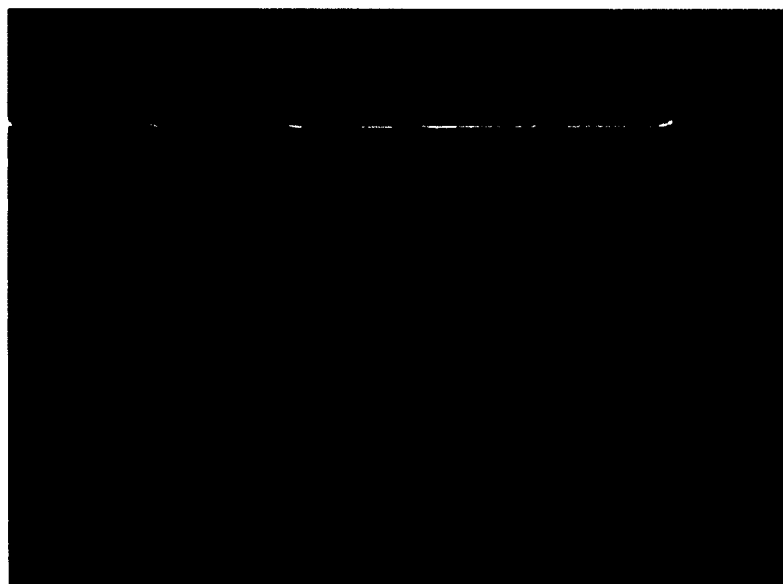
average zone of inhibition is 3.1 mm (+/- 4.13 mm) Broth cultures provided similar results, as shown in Figure 4-99 and Figure 4-100.



**Figure 4-98:** A) 1 wt% nitrofurantoin-laden PMMA disc B-D) 1 wt% nitrofurantoin-laden PLA disc



**Figure 4-99:** A) Sterile broth B) *E. coli* inoculated broth C-E) 1 wt% nitrofurantoin PMMA discs



**Figure 4-100:** A) Sterile broth B) *E. coli* inoculated broth C-E) 1 wt% nitrofurantoin PLA discs

The PMMA broth culture showed no bacterial inhibition (Figure 4-99). Only one of the PLA broth cultures showed inhibition of bacterial growth (Figure 4-100). The results shown could be caused by low dopant percentages or low solubility of the

nitrofurantoin in water. Similar effects were seen in the 1% gentamicin filaments, but they disappeared in the gentamicin discs that had been printed in 300  $\mu\text{m}$  layers and had more surface area. Combinations of antibiotics may be more viable that can use nitrofurantoin filaments. A burst release from gentamicin combined with a longer/lower release of nitrofurantoin or even antibacterial properties could be interesting in creating implantable device shielding.

#### 4.6.5.5 *Halloysite discs*

The HNT filament that contained halloysite loaded with gentamicin was used to fabricate discs for testing. This testing was done for the 1.5 wt% HNT loaded with gentamicin filament as well as a 7.5 wt% HNT loaded with gentamicin filament. No control unloaded halloysite filament was printed into discs and tested, based on substantial results showing a lack of antibacterial properties. Five discs were tested on Mueller Hinton plates (three plates for 7.5 wt% HNT loaded with gentamicin), and three discs were tested in broth cultures, as shown in Figure 4-101, Figure 4-102, and Figure 4-103.



**Figure 4-101:** A) 1.5 wt% HNT loaded with gentamicin disc B) 7.5 wt% HNT loaded with gentamicin disc



**Figure 4-102:** A) Sterile broth B) *E. coli* inoculated broth C-E) 1.5 wt% HNT loaded with GS PLA discs



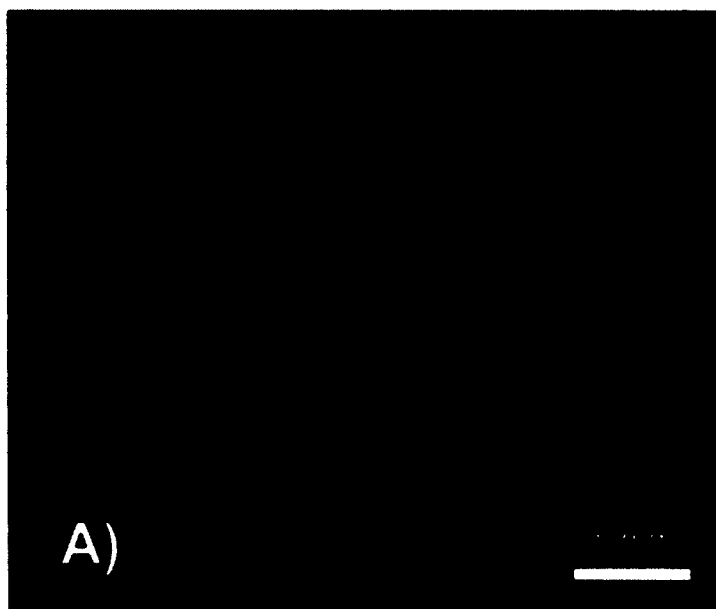
**Figure 4-103:** A) Sterile broth B) *E. coli* inoculated broth C-E) 7.5 wt% HNT loaded with GS PLA discs

The bacterial plates were measured at three points by digital caliper to determine the zone of inhibition. The 1.5 wt% HNT loaded with gentamicin disc had no zone of inhibition. All 7.5 wt% HNT loaded with gentamicin discs had zones of inhibition. The three zones of inhibition were highly variable. The largest zone was 17.6 mm. One was around 10 mm and the other was 7 mm. The overall average was 11.12 mm ( $\pm 5.26$  mm) Halloysite has a tendency to clump. Humidity can cause this. It is very likely that halloysite dispersion within the filaments was not consistent. HNTs only carried 10% of their weight in gentamicin and they have a slow and more sustained release. This low loading and slow release likely led to very low levels of gentamicin considering discs tended to weigh between 16 mg-20 mg and in the 7.5 wt% HNT disc would only carry 150  $\mu$ g dispersed through the entire disc with only a fraction of this on the surface. The 100  $\mu$ g wafer controls that were tested were designed for almost complete release. The broth cultures helped to allow for a more sustained release because of the liquid medium

and high solubility of gentamicin. While the 1.5 wt% HNT-loaded discs had no broth culture inhibition, the 7.5 wt% HNT loaded discs did halt the growth when compared to the controls. These studies show the potential for nanotechnology to be incorporated into this method. This technology could allow for sustained release of highly water-soluble substances or even thermal protection during the manufacturing process.

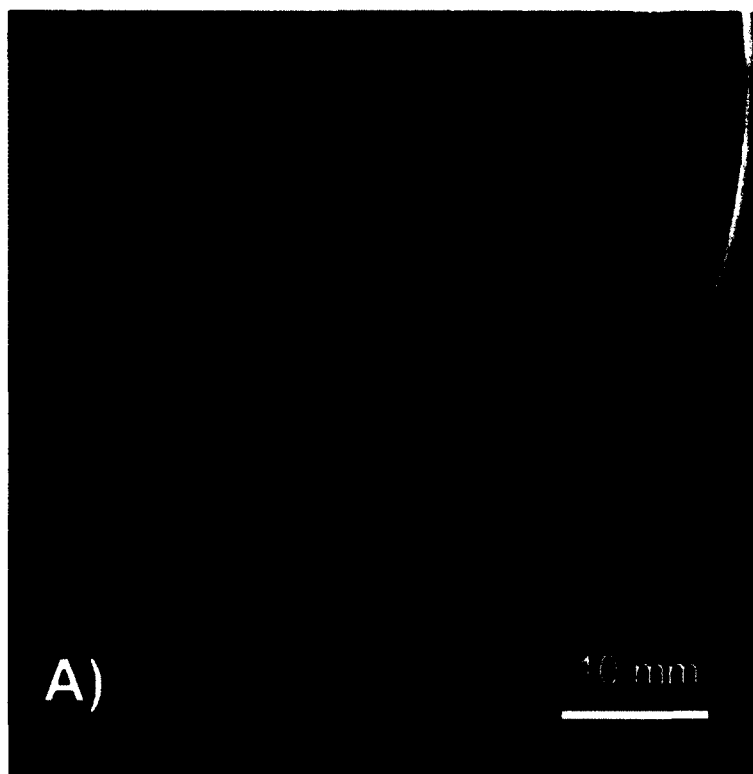
#### 4.6.5.6 Atomizer-fabricated GS discs

The filaments that were manufactured with atomizer-coated pellets were 3D printed into test discs. A picture of the test disc, which is consistent with other discs, is shown in Figure 4-104.



**Figure 4-104:** A) 1 wt% gentamicin test disc fabricated using atomizer-coated pellets

Five test discs were then plated on Mueller Hinton bacterial plates and three in broth cultures. This is shown in Figure 4-105 and Figure 4-106.



**Figure 4-105:** A) 1 wt% gentamicin PLA test disc made with atomizer-coated pellets



**Figure 4-106:** A) Sterile broth B) *E. coli* inoculated broth C-E) 1 wt% gentamicin disc made by atomizer method

The test discs on bacterial plates had their zone of inhibition measured by a digital caliper at three points. All atomizer-based test discs had a zone of inhibition with a 12.2

mm (+/- 3.62 mm) average zone. All broth cultures had no bacterial growth. The success of this method shows alternative methods exist for coating or mixing pellets or powders for extrusion in an attempt to create a consistently bioactive additive laden filament.

#### 4.6.6 Bioactive Constructs

The test discs were simple constructs. They were 5 mm circles with 100% in-fill. They acted to prove the potential and show the resolutions that could be achieved by bioactive filaments. The advantages of this technology involve the hollow nature of constructs or complexity of the fabricated devices. A newly extruded 1 wt% gentamicin filament was primarily used for these tests. The first print ever done was a partial 14 French catheter as proof of principle to act as a bead with a base as shown in Figure 4-107.



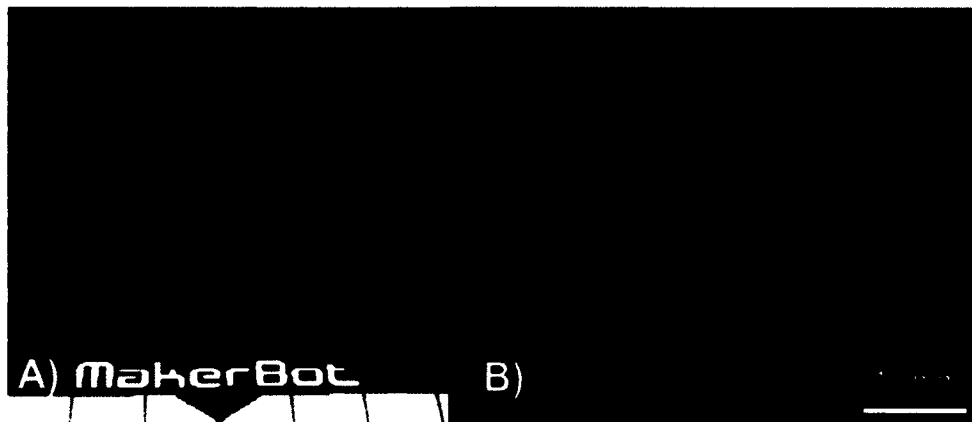
**Figure 4-107: 1 wt% gentamicin PLA construct**

The additional constructs that followed were a large simple one-inch square, full 14 French catheter tip and antibiotic beads. The antibiotic beads were made of PLA and compared to PMMA beads molded to industry standards.



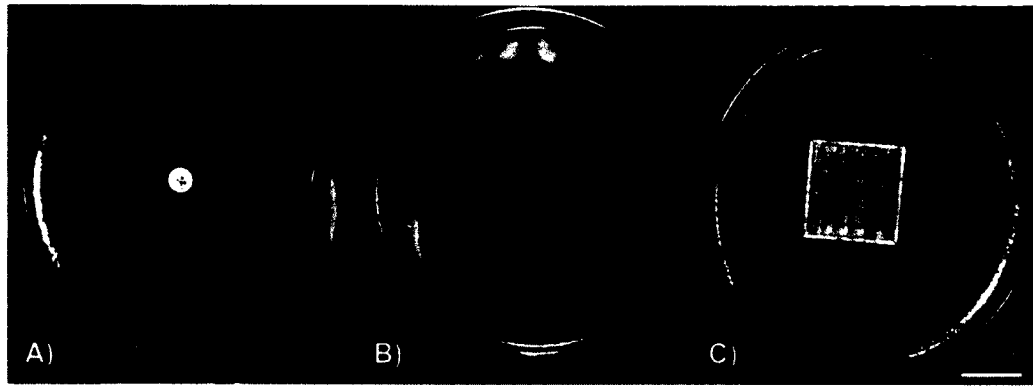
#### 4.6.6.1 Bio-square

A one-inch square was designed to prove the potential for a longer sustained print of a bioactive construct. The square had a 1 mm height and 100% in-fill. The design .STL file and a photograph are shown in Figure 4-108.



**Figure 4-108:** A) Bio-square print file B) 1 wt% nitrofurantoin bio-square

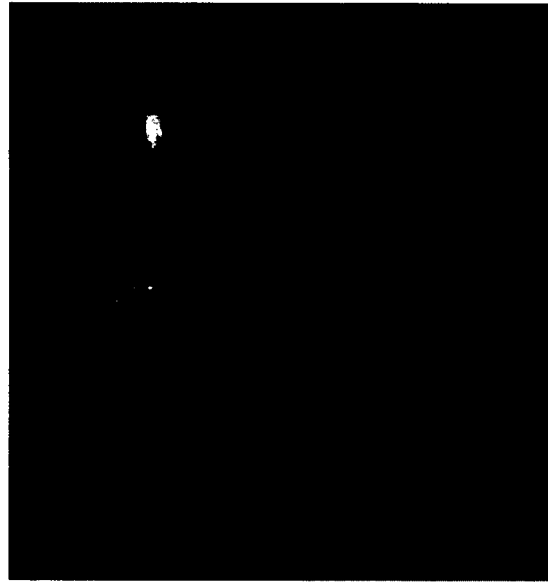
The above print took several minutes and included a raft. The final square was complete and did not have any missing layers. The construct was uniform. The pictured square is made from nitrofurantoin to demonstrate that other antibiotics can have more complex structures, even though the experiments focus on gentamicin. A single 1 wt% gentamicin biosquare was fabricated and tested on bacterial plates and compared to controls. This test is shown in Figure 4-109.



**Figure 4-109:** A) Control 100  $\mu\text{g}$  gentamicin wafer B) 1 wt% gentamicin-laden PLA bio-square C) control PLA bio-square

The test bio-square concept was successful. The zone of inhibition based on two digital caliper measurements was 32.5 mm. This size compared to a zone of inhibition of 20.3 mm of a control wafer and no zone of inhibition in a control bio-square that was only PLA. It should be noted that there is uniformity of the zone of inhibition around the circle. There is not uniformity of the zone of inhibition around the square. The corners are rounded. This is due to edge effects and explained in Appendix C.

Additionally, a HNT laden filament was test printed into a bio-square and into a dog bone shape for potential future strength tests. The bio-square printed successfully. The dog bone print was partially completed (Figure 4-110).



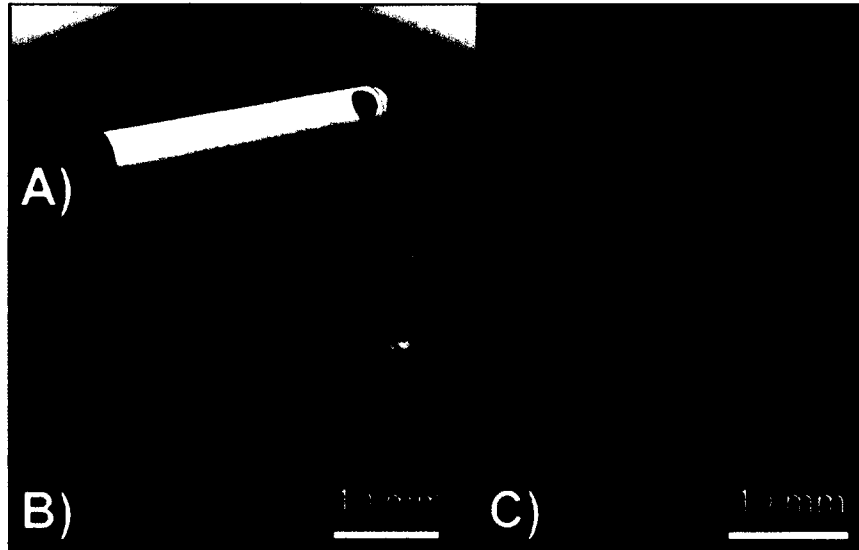
**Figure 4-110:** Partial HNT enhanced PLA dog bone print

These tests were only to show potential proof of principle of the technology and go beyond the scope of the core bioactive nature of this investigation. This proof of principle shows the potential for future studies to investigate not only HNTs as a delivery mechanism but also in terms of strength testing. Strength testing was not investigated at this time since breaks in any 300  $\mu\text{m}$  layering of the filaments would adversely affect the results. The number of breaks or improperly aligned filaments in a layer cannot be confirmed. Additional research and projects should focus on this determination.

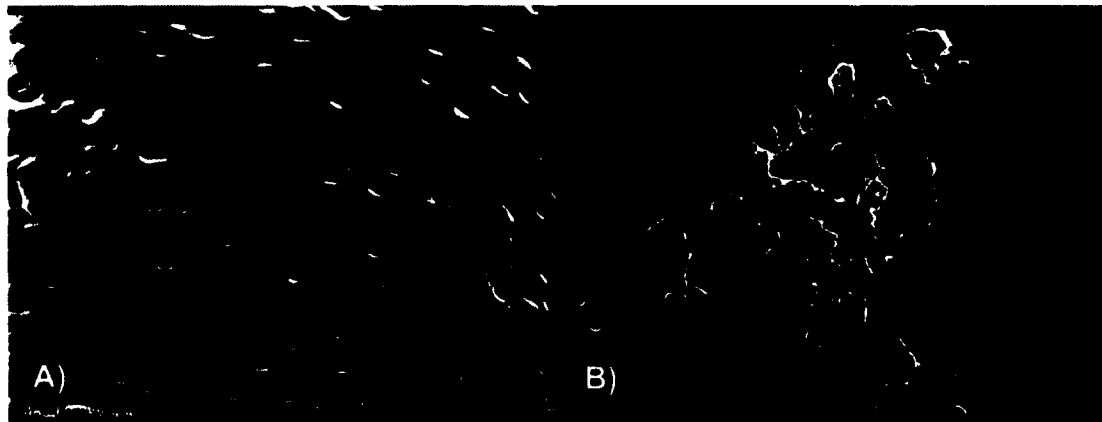
#### 4.6.6.2 Catheters

There is a large potential for disruptive technology in custom surgical or drainage catheters, which can be fabricated, in the surgical suite. The ability to elute a desired bioactive compound and degrade internally is also desirable. To demonstrate this concept a 14 French catheter tip of 3 cm length with a distal single port was fabricated. Both control and 1 wt% gentamicin laden PLA filament were used. The printing temperature was 220  $^{\circ}\text{C}$  and the in-fill was 10%. The lumen and distal port are the same

diameter. Pictures and SEM of the catheters are shown in Figure 4-111 and Figure 4-112.



**Figure 4-111:** A) .STL file catheter B-C) 1 wt% gentamicin laden PLA catheter



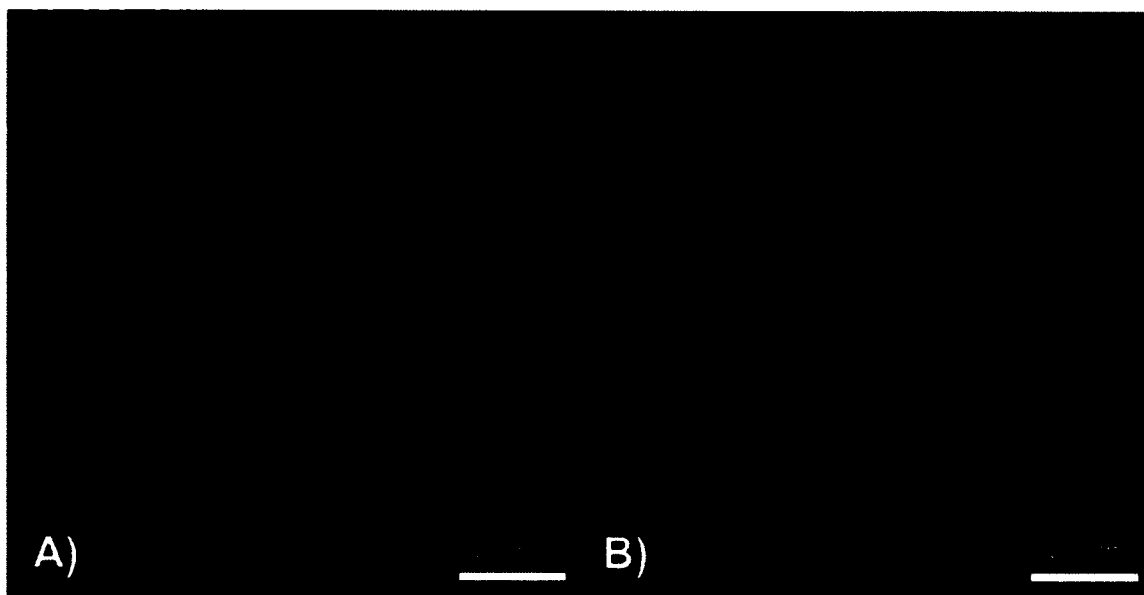
**Figure 4-112:** A-B) SEM of catheter and embedded antibiotics

The photographs confirm a uniform print. The SEM shows the individual layering of the build. The higher resolution of the SEM shows the individual gentamicin powder spheroids. These match the original control gentamicin powder SEM images. A single 7.5wt% halloysite loaded with gentamicin PLA catheter was printed only as a proof of

concept and not further tested. Three control and three 1wt% gentamicin-laden catheters were each tested on both Mueller-Hinton plates and broth cultures. These are shown in Figure 4-113 through Figure 4-116.



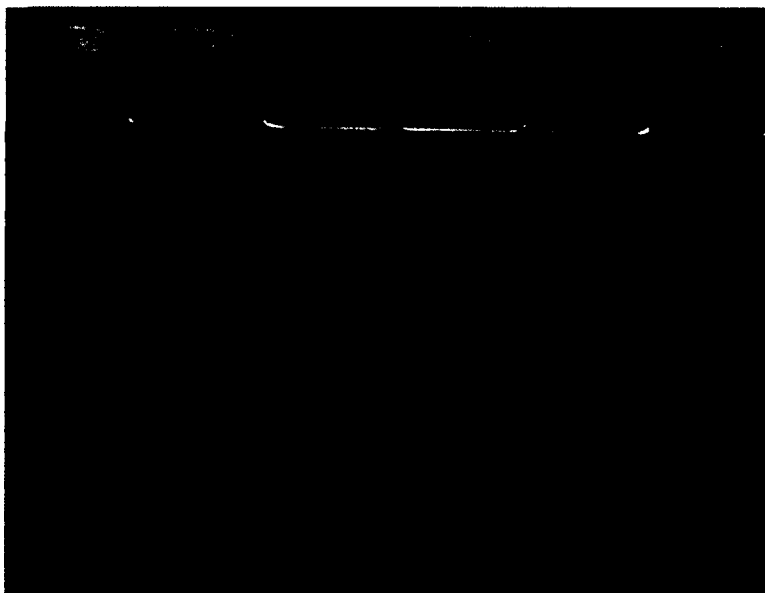
**Figure 4-113:** Top row) Control PLA catheters; Bottom row) 1 wt% gentamicin PLA catheters



**Figure 4-114:** A) Control PLA catheters B) 1 wt% gentamicin PLA catheters



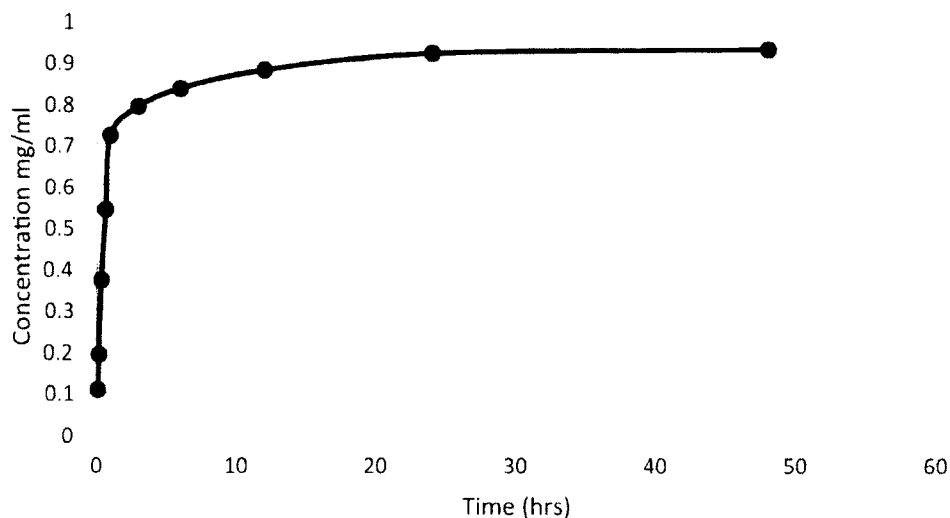
**Figure 4-115:** A) Sterile broth B) *E. coli* inoculated broth C-E) Control PLA catheters



**Figure 4-116:** A) Sterile broth B) *E. coli* inoculated broth C-E) 1 wt% gentamicin PLA catheters

The bacterial plates show no inhibition with control PLA catheters. The 1 wt% gentamicin PLA catheters have a strong and uniform zone of inhibition. Digital calipers were used at multiple points to measure the rectangular shaped zone of inhibition that had an average length of 43.2 mm and an average width of 19.8 mm. Broth cultures containing the 1 wt% gentamicin catheters led to complete inhibition of bacterial growth. This inhibition compares to the control catheters that had substantial bacterial growth equal to the positive control. These results add substantial evidence to the potential of this technology to create constructs, which can prevent bacterial growth and biofilms in common medical devices such as catheters.

A catheter gentamicin elution profile was run as a proof of principle using the gentamicin visualizing methodology and timing of samples noted in the materials and methods section. The image is shown below as Figure 4-117.



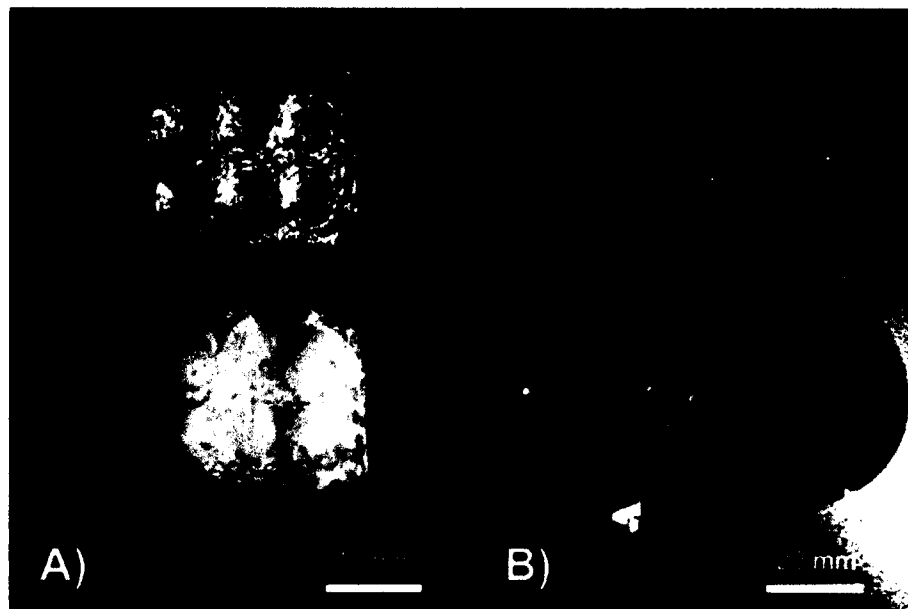
**Figure 4-117:** Elution profile 1wt% GS-PLA catheter

The elution profile lasted between 30-40 hours. This was when the maximum visualization was reached using the capabilities of the spectrophotometer.

#### 4.6.6.3 Antibiotic beads

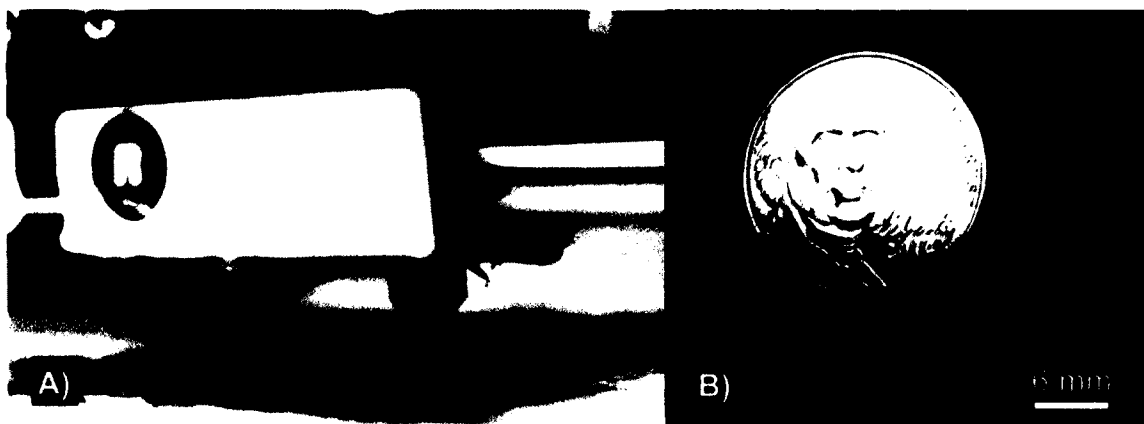
The current technology for antibiotic beads uses PMMA-based bone cements. These have cytotoxic components and do not break down in the body. A standard antibiotic bead size is 6 mm and must be hand molded onto a string. To test the potential for 3D fabricated antibiotic beads, it was necessary to compare them to the current gold standard of PMMA. Both control and 1 wt% PMMA beads were fabricated using commercial Wright Medical Orthoset® bone cement. A two-part mold for the PMMA beads was fabricated on the 3D printer. During the fabrication, the beads stuck to the 3D fabricated mold and could not be removed. To even open the 3D printed mold required a hammer and chisel. A solution was found by creating a silicone rubber molding material to make a mold using 3D-printed 6 mm beads. The molds are shown below in Figure 4-118 to illustrate some of the difficulties in working with PMMA.



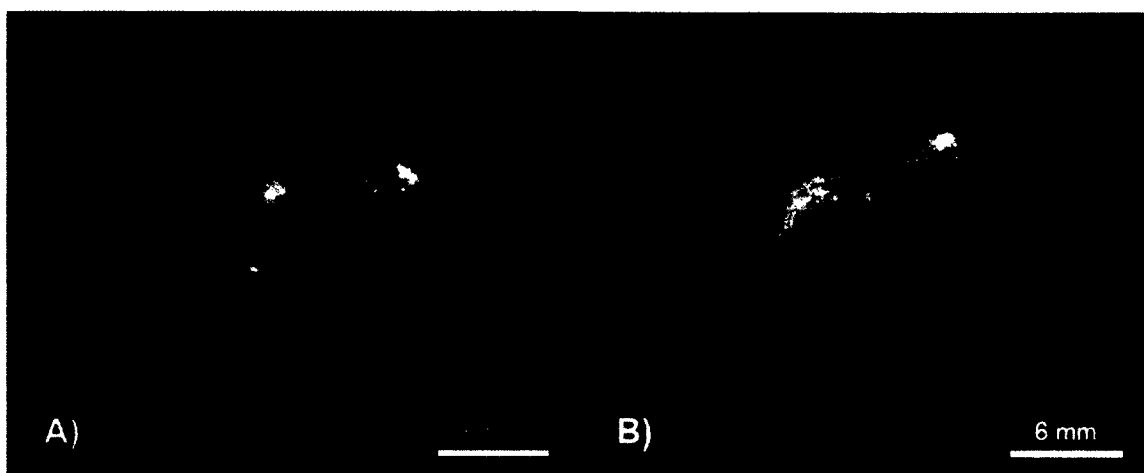


**Figure 4-118:** A) 3D printed mold B) Silicone rubber mold

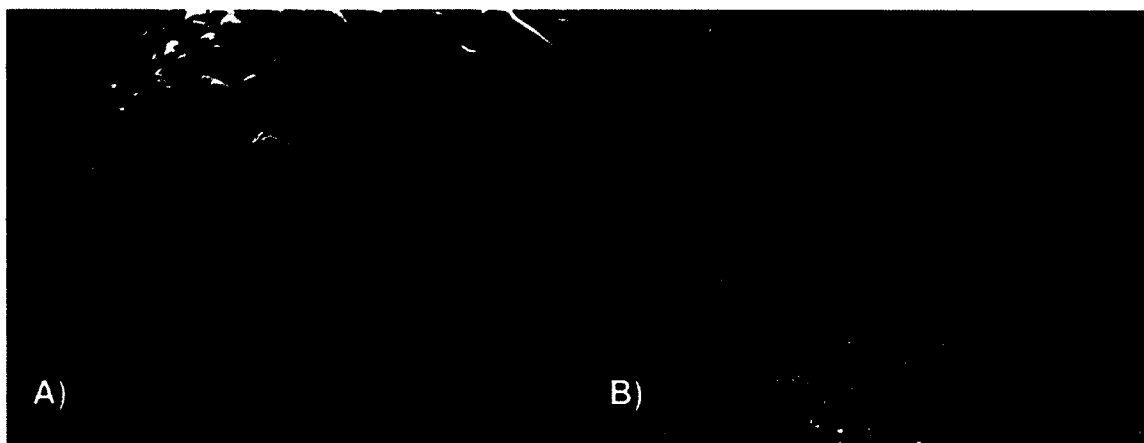
The 3D printed beads were fabricated using the 1wt% gentamicin filament. Photographs of the process, beads and SEM of the beads are shown in Figure 4-119, Figure 4-120 and Figure 4-121.



**Figure 4-119:** A) Printing antibiotic bead B) Antibiotic bead compared to coin

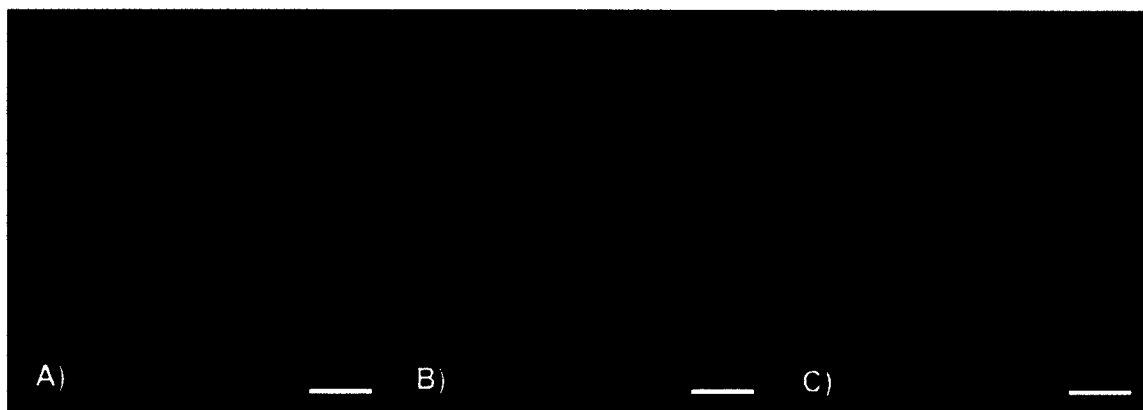


**Figure 4-120:** A) Control PLA 3D printed bead B) 1 wt% gentamicin PLA 3D printed bead



**Figure 4-121:** A-B) SEM 1 wt% gentamicin PLA 3D printed bead

The images show the fabrication of the 3D printed beads with gentamicin-laden filaments. The SEM image shows both the resolution of the layers at 300  $\mu\text{m}$  and the powders that can be seen on the surface of the bead at higher magnification. The control PMMA, control PLA, 1 wt% gentamicin PMMA and 1 wt% gentamicin PLA beads were tested on three Mueller Hinton plates and three Mueller Hinton broth cultures. The results are shown in Figure 4-122 to Figure 4-126.



**Figure 4-122:** A) Control beads B) 1 wt% gentamicin PLA 3D printed bead C) 1 wt% PMMA-molded bead



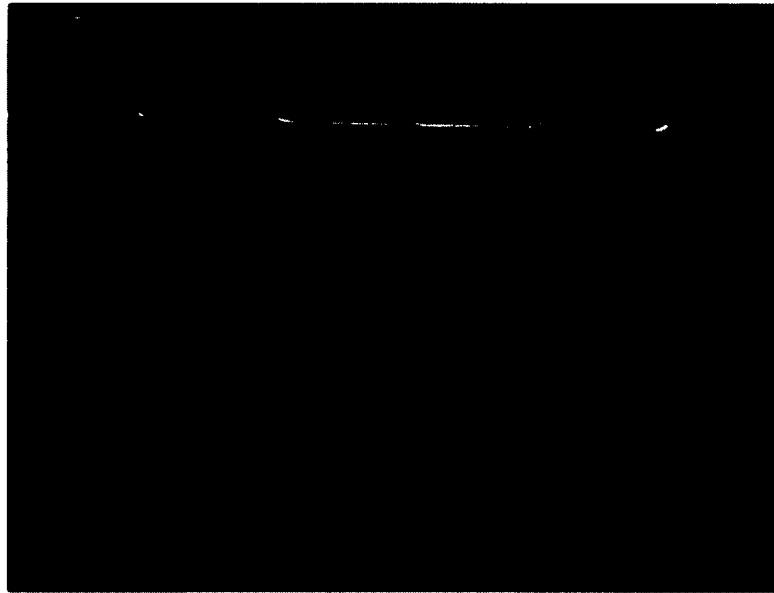
**Figure 4-123:** A) Sterile broth B) *E. coli* inoculated broth C-E) control PMMA-molded bead



**Figure 4-124:** A) Sterile broth B) *E. coli* inoculated broth C-E) 1 wt% gentamicin PMMA molded bead



**Figure 4-125:** A) Sterile broth B) *E. coli* inoculated broth C-E) control PLA 3D-fabricated beads

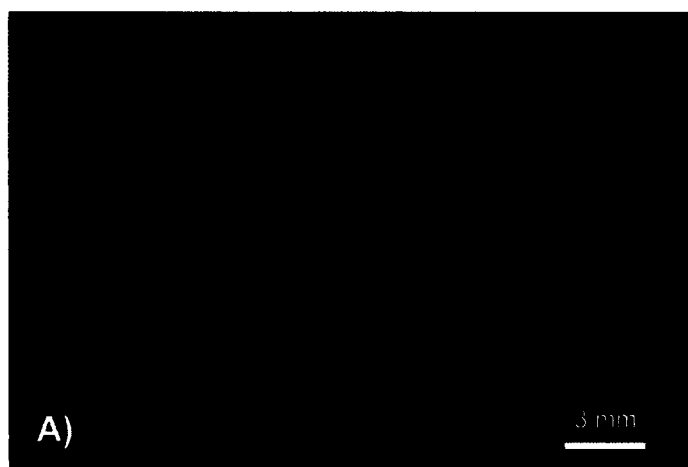


**Figure 4-126:** A) Sterile broth B) *E. coli* inoculated broth C-E) 1 wt% gentamicin PLA 3D fabricated bead

The bacterial plates show convincing evidence of the bioactive nature of the gentamicin laden 3D fabricated beads (Figure 4-122). The controls for both PMMA and PLA show no inhibition of bacterial growth on the plates. The 1wt% gentamicin PLA 3D printed beads have an average zone of inhibition of 19.62 mm (+/- 4.24 mm). This compares to the molded PLA beads which have an average zone of inhibition of 14.5 mm (+/- 1.11 mm). Statistical analysis shows a difference between the two groups. The broth cultures confirmed the bacterial plate results. The control broth cultures showed bacterial growth (Figure 4-123 and Figure 4-125). Both PMMA-molded beads and PLA 3D-printed beads inhibited bacterial growth in all tubes (Figure 4-124 and Figure 4-126). These results show the substantial potential that 3D printing bioactive constructs has to influence personalized medicine.

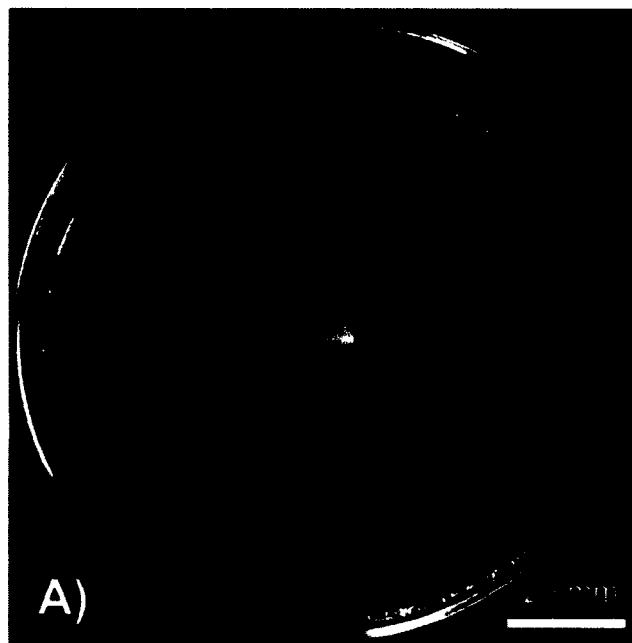
#### 4.6.6.4 Antibiotic beads with nanotubes

A proof of principle experiment was conducted to test the viability of HNTs to be included in the 3D fabrication process. This experiment was to show the potential of future work involving nanotechnologies. The importance of these technologies involves novel techniques for controlled or extended release of compounds. A 7.5 wt% HNT loaded with gentamicin PLA filament was fabricated into 6 mm beads. This bead is shown in Figure 4-127.

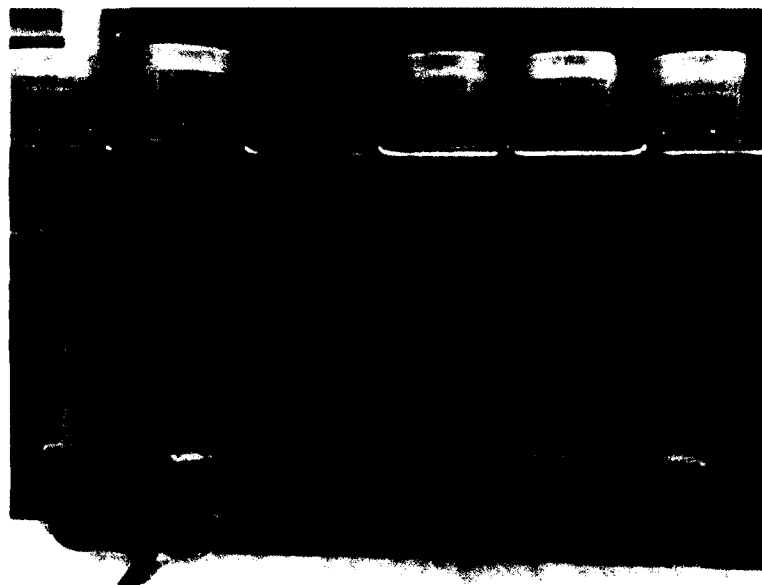


**Figure 4-127:** 7.5 wt% HNT loaded with gentamicin PLA 3D-printed bead

The beads printed consistently. Three beads were tested on bacterial Mueller Hinton plates and three were tested in Mueller Hinton broth cultures. These tests are shown in Figure 4-128 and Figure 4-129.



**Figure 4-128:** A) 7.5 wt% HNT loaded gentamicin PLA 3D-fabricated bead



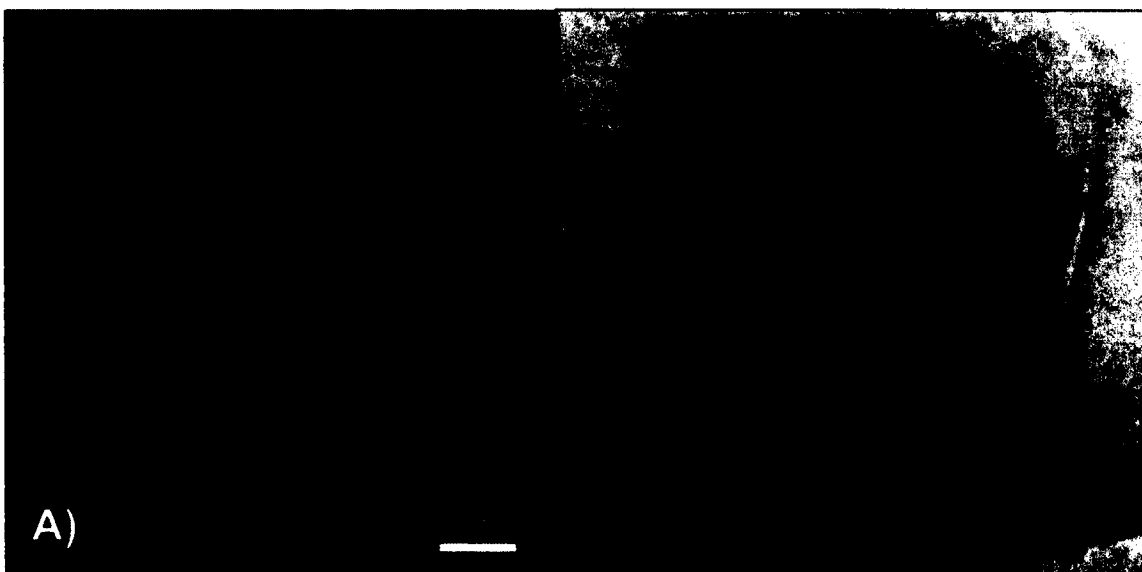
**Figure 4-129:** A) Sterile broth B) *E. coli* inoculated broth C-E) 7.5 wt% HNT loaded gentamicin PLA 3D-fabricated bead

The 7.5 wt% HNT loaded gentamicin PLA 3D printed beads inhibited growth on both the bacterial plate and in the broth cultures. The bacterial plate results were variable. The pictured plate had an average zone of inhibition of 15.7 mm. This size

contrasts the other two plates that had zones of inhibition ranging between 6 to 9 mm. The overall average was 9.64 mm (+/- 4.9 mm) This work shows the potential for nanotechnology to be included in printing.

#### 4.6.6.5 Scanning defects and printing custom inserts

One of the core advantages of being able to 3D fabricate custom shapes is the ability to work with organic or non-uniform structures. This ability opens up novel avenues of personal medicine. One concept is to scan a bone defect or area of the body and print a custom insert. This could apply to osteomyelitis requiring bone removal or a removed tumor's margins. A cow femur was used to model this concept. A standard 6 mm hole and material in the shape of an organic defect were removed from the cow femur on opposite sides, as shown in Figure 4-130.



**Figure 4-130:** A) Irregular shaped bone defect B) 6mm hole defects

The cow bone with defect was scanned using a 3D scanner. The defects were scanned with currently available technology. Figure 4-131 shows a full 360 degree view

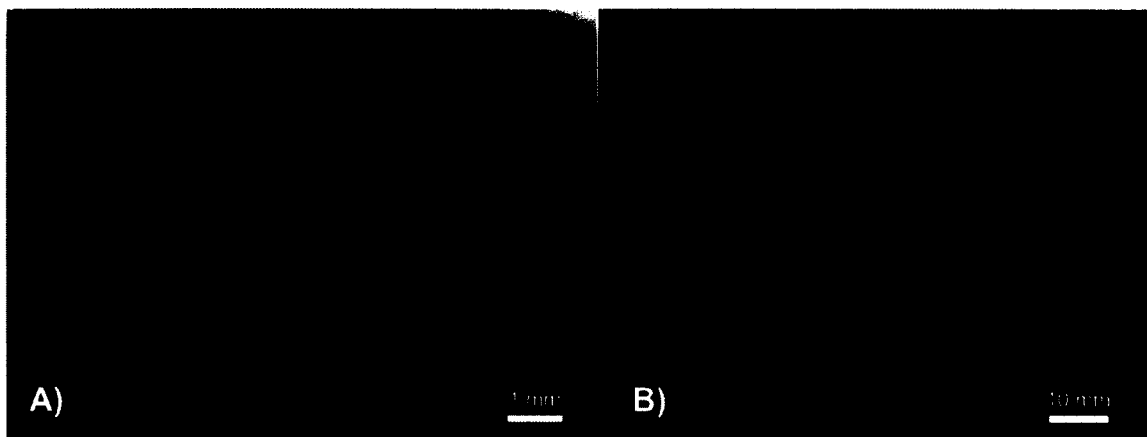


and both defects on the opposite sides of the bone in a single view such that they appear next to each other.



**Figure 4-131:** Bone 360 degree scan with all four defects

The bone defects were then manually modeled using solidworks and a proprietary method to generate plugs. The SolidWorks files of the plugs and original bone femur are shown in Figure 4-132 and Figure 4-133, respectively.

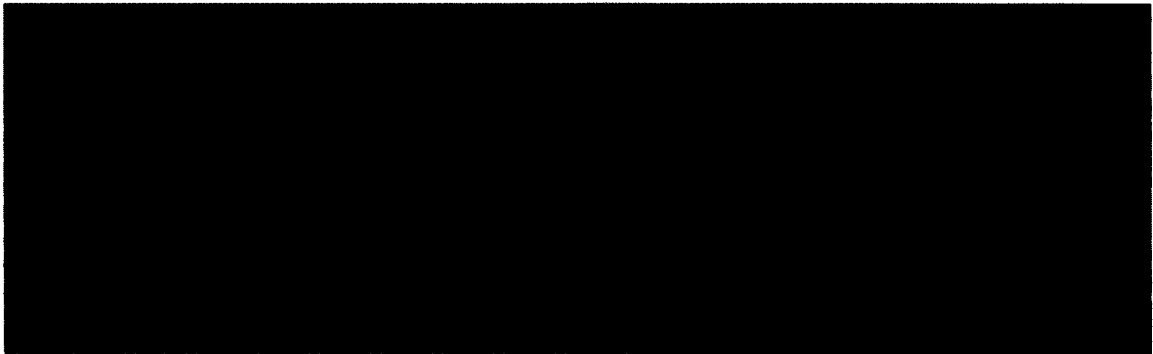


**Figure 4-132:** A) 6 mm bone defect B) Entire femur portion



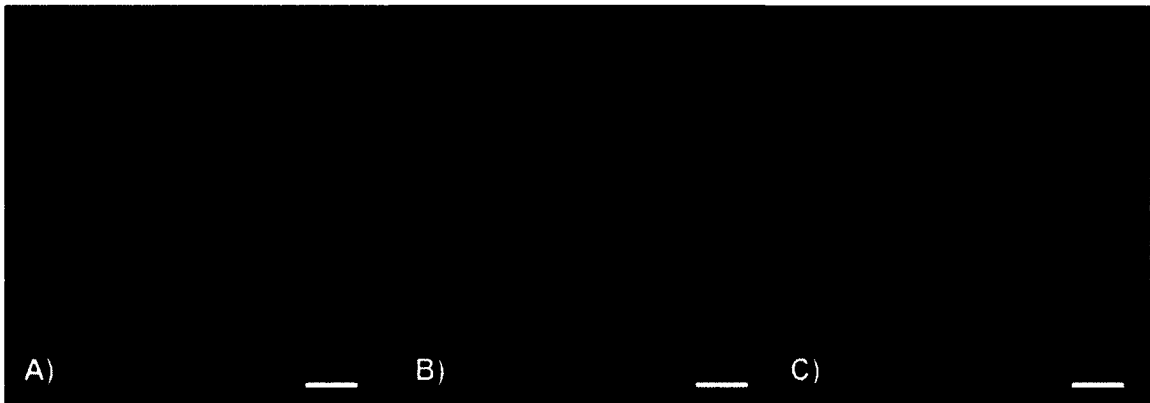
**Figure 4-133:** Irregular bone defect computer model

The irregular and 6 mm defect was printed with both control PLA and 1 wt% gentamicin PLA filament. The results are shown in Figure 4-134.



**Figure 4-134:** Printed irregular defect gentamicin (gray) control (white)

The irregular defect was test fitted in the cow femur with both a control PLA construct and 1 wt% gentamicin construct and as shown in Figure 4-135.



**Figure 4-135:** A) Femur with irregular defect B) Femur with 1 wt% gentamicin-PLA fitted insert C) Femur with control PLA fitted insert

The 3D-fabricated construct fit the irregular shapes well. It was so precise that it took some maneuvering to lock into place. However once in place, it would not easily move. This may prove medically important in the capability to use a MRI scan to then generate a precisely fitting implant. It could then be inserted through a minimally invasive procedure. The 6 mm cylindrical plug was also fabricated and tested for fit (Figure 4-136).



**Figure 4-136:** A) 6 mm control plug B) 6 mm control plug fitted into cow femur

## 4.7 Conclusion

Bioactive additives can be applied to 3D fabrication to create custom constructs for personalized medicine. Advances in additive manufacturing provide the potential to greatly increase the capabilities of personalized medicine in terms of drug delivery.

The bioactive compounds were shown to be thermally stable to the extent that they could be used in fused deposition modeling. This stability was shown for gentamicin, tobramycin and nitrofurantoin. A novel method of coating pellets for extrusion was developed. The pellets and process were tested in bacterial cultures to confirm. The results indicated that the bioactive compounds and not the coating process generated the effects seen. Visual inspection and SEM imaging confirmed this result.

PLA filaments were extruded for 3D fabrication. Bacterial testing of the filaments showed that bioactivity was present. Comparison testing was done with equivalently loaded PMMA bone cement filaments. This acted as a control to demonstrate expected effects using the industry gold standard. Gentamicin sulfate-laden filaments were equivalent or superior to the gentamicin sulfate laden-PMMA. Test discs were fabricated from PLA filaments or molded from PMMA bone cements. Again, gentamicin test discs of 1 wt% or 2.5 wt% showed equivalent activity to the PMMA standards.

More complex constructs such as beads or catheters were printed using 1 wt% gentamicin filaments. PMMA beads were molded for comparison. The antibiotic 3D printed beads showed equivalent or superior activity to PMMA molded ones. The 3D printing of gentamicin-laden catheters also showed bacterial inhibition in both broth and plate cultures.

Nanotechnology was used in this technology by creating halloysite-enhanced filaments. These filaments were proven to work with the 3D printers as well as maintain bioactivity through the fabrication process. The 1 wt% and 7.5 wt% HNT loaded with gentamicin were tested. Bioactivity of the gentamicin was seen and 7.5 wt% filaments, test discs and antibiotic printed beads showed bacterial inhibiting effects.

Finally, novel techniques were developed to scan and print custom inserts using bioactive filaments. These techniques show the potential of this technology to create new fields of personalized medicine.

## **CHAPTER 5**

### **3D PRINTING CHEMOTHERAPEUTICS AND BONE CEMENTS**

#### **5.1 Introduction**

This chapter will focus on chemotherapeutics and cytotoxicity. Previous results showed that antibiotic-laden constructs can be fabricated. The ability to fabricate an arbitrarily shaped construct that can be used as a biodegradable implant can allow for new concepts in personalized medicine.

In looking to 3D fabricate antibiotic constructs, the primary focus was on beads, catheters or organic shapes. In looking to create constructs with chemotherapeutics there is an additional demand for stents, thin filaments, or surgical site margin tracing. This can be done to prevent metastases or further growth in a sensitive area for palliative care.

Many antibiotics have high degradation points and can be stored in non-controlled environments. Other biological compounds, such as chemotherapeutics, are generally thought to be more fragile. Storage conditions are typically laboratory or hospital freezers. There is merit in establishing that these compounds can be used in additive manufacturing processes.

The cost and hazards of handling chemotherapeutic compounds present challenges in the testing of additives. The filament extrusion process currently has the potential to aerosolize quantities of the powders they are extruding. Chemotherapeutics

are designed to function at low concentrations. Additionally, chemotherapeutics can be costly. The prototype equipment for extrusion requires batches that use roughly one-gram quantities of bioactive additives at a time. This testing was possible only because the price of one chemotherapeutic recently dropped. For these reasons methotrexate was chosen as a model drug to be tested in the process.

These 3D printing filaments were tested on osteosarcoma cells. This *in vitro* testing shows the potential for future work including 3D tumor and animal studies to be done.

In addition to showing the cytotoxicity of chemotherapeutic enhanced prints, work was done to study how cytotoxicity of other materials could be enhanced or decreased by altering fabrication processes. PMMA bone cements were chosen as a material to check for enhancement since they have been the standard in biomaterials for the past fifty years. Alternative methods to process and fabricate this material with a goal of decreasing cytotoxicity were investigated.

This work and the information in proving the concept can lead to additional and alternative cancer treatments.

## **5.2 Design and Objectives**

The experimental design will look at proving further capabilities of filament extrusion and bioactive construct formation in light of chemotherapeutic delivery. It will also look at ways to develop less cytotoxic methods using current materials such as bone cements. The following section breaks down the objectives into specific areas.

### 5.2.1 Thermal Stability Objective

The first objective will be to confirm the thermal stability of methotrexate. This should be done at temperatures similar to the polymers used in the 3D fabrication process and optimal combinations should be found.

### 5.2.2 Filament Extrusion Objective

A method of consistently mixing chemotherapeutics into a 3D printing filament should be developed. This process should be optimized to allow for simple fabrication.

### 5.2.3 3D Printing and Additive Manufacturing Objective

The ability to achieve 3D fabrication with the custom designed chemotherapeutic filaments should be attempted. This would involve proving that the filaments operate with a standard 3D printer and creating simple constructs.

### 5.2.4 Cell Testing Objective

Cells should be cultured and tested with the filaments and constructs to prove *in vitro* capabilities of the technology. Only preliminary studies should be done since the technology will need to be optimized before animal modeling begins.

### 5.2.5 Elution Testing Objective

The ability to quantify the amount of chemotherapeutic elution from a filament should be conducted. This will yield valuable proof of principle information in determining dosing for animal trials.

### 5.2.6 Optimizing Existing Materials for 3D fabrication

Many existing biomaterials may benefit from 3D fabrication methods. Methods to 3D fabricate bone cements should be developed with a focus on limiting cytotoxicity.



### 5.3 Materials

The methotrexate used in this study was purchased from Sigma Aldrich (St. Louis, MO). PMMA bone cement was a Kyphon® Bone Cement from Medtronic (Memphis, TN). PMMA plain powder was from Original Truliner® – PMMA Denture Corrective Relining Material made by the Bosworth Company (Skokie, IL). The polylactic acid (PLA) beads used for the printing media were obtained from NatureWorks, LLC (Minnetonka, MN). The Polycaprolactone (PCL) pellets were purchased from Sigma Aldrich (St. Louis, MO). Cell culture plates and other lab plastics were purchased from MidSci, St. Louis, MO. Dulbecco's Phosphate Buffered Saline (DPBS), Dulbecco's Modified Eagle's Medium (DMEM), fetal bovine serum (FBS), penicillin-streptomycin-amphotericin (PSA) antibiotics, and Live/Dead Viability/Cytotoxicity kit were obtained from Life Technologies, Carlsbad, CA. Osteosarcoma cell line (CRL 2836) was purchased from ATCC (Manassas, VA). KJLC 705 silicone oil used for coating the beads prior to extrusion was purchased from Kurt J. Lesker Company (Jefferson Hills, PA). The 3D printing set-up consisted of an ExtrusionBot extruder purchased from ExtrusionBot, LLC (Phoenix, AZ) and a MakerBot 2X or Replicator 3D printer (Brooklyn, NY). The nanodrop spectrophotometer was from Thermo Scientific (Wilmington, DE). Heating of biomaterials was done with a Vulcan® A550 Series Benchtop Muffle Furnaces from Thomas Scientific (Swedesboro, NJ). The Solidworks 2014 student edition 3D CAD program Dassault Systèmes (Waltham, MA) was used for modeling. XTT assays were purchased from Sigma Aldrich (St. Louis, MO). The XTT assays were run using a Thermo Scientific Multiskan

Spectrum plate reader (Waltham, MA). The SEM was a Hitachi S-4800 (Schaumburg, IL).

The filament extrusion devices, 3D printers, modeling software detailed descriptions are similar to those of the materials section in chapter four. New materials are described in detail below.

### 5.3.1 Bioplastics and Polymers

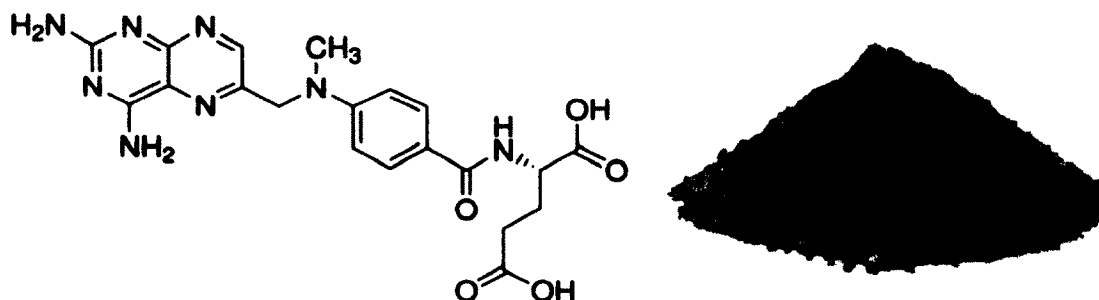
Polycaprolactone (PCL) was used as a polymer with a lower melting point. PCL begins to melt at 60 °C and undergoes a melt flow depending on pressure between 90 °C to 150 °C. The PCL structure is shown below in Figure 5-1.



**Figure 5-1:** PCL container, pellet and molecular structure[125]

### 5.3.2 Bioactive Materials

Methotrexate is an antifolate drug used in cancer or rheumatoid arthritis treatments. Methotrexate inhibits dihydrofolate reductase in a competitive manner. This results in a decrease in thymidine synthesis which is a required component of DNA. The cells are not able to generate the DNA needed to replicate. The molecule is considered to have a cytostatic effect that inhibits growth. The thermal stability according to the MSDS goes up to 190 °C. Methotrexate solutions can be quantified by spectrophotometry and absorbance levels at the 200 nm wavelength. The structure is shown below in Figure 5-2.

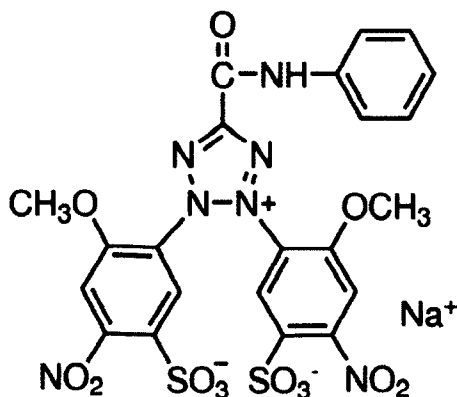


**Figure 5-2:** Methotrexate structure and powder [126]

### 5.3.3 XTT and Live/Dead Assay

XTT and Live/Dead assays were acquired to assess cytotoxicity of biomaterials. The Live/Dead viability assay operates by fluorescence. Two dyes are used that fluoresce different colors. They are chosen such that they bind or are present in the case of a cell being alive or being dead. The Life Technologies Inc. kit operates with calcein that is green at wavelengths 494/517 nm as well as ethidium homodimer-1 which is red at wavelengths 528/617 nm. The calcein dye stays inside the living cells by pump activity. The ethidium homodimer binds to unraveled DNA in dead cells and then

strongly fluoresces red. This technique can act as both a qualitative or quantitative indicator of cell metabolic activity. The XTT assay by Sigma Aldrich operates by addition of a sodium salt as shown below in Figure 5-3 being added to cell culture wells.

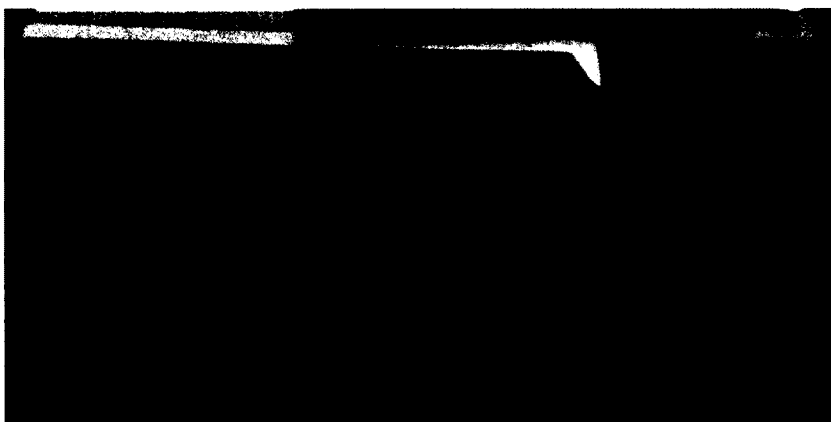


**Figure 5-3:** XTT reagent salt [127]

This salt is 2,3-bis-2-methoxy-4-nitro-5-sulfohenyl- 2H-tetrazolium-5-carboxyanilide and is converted by mitochondrial dehydrogenases to an orange solution which can be measured by spectrophotometry. The absorbance at the proper wavelength can be used to assess mitochondrial activity and thus cell number.

#### 5.3.4 Plate Reader

A thermo scientific multiskan spectrum plate reader was used to run XTT assays. The plate reader operates with 96 well cell culture plates and operates on the principle of spectroscopy to determine the absorbance at different wavelengths in the wells. This unit was operated at 450 nm and 690 nm. The plate reader is pictured in Figure 5-4.



**Figure 5-4: Thermo Scientific Plate Reader**

#### **5.4 Fabrication and Methods**

The 3D fabrication methods and elution profile testing were described in detail in chapter 5. However, there were differences in PCL extrusion. Cell culture techniques for cytotoxicity testing of the filaments are also described which include cell viability XTT and live/dead assays.

##### **5.4.1 PCL Extrusion and Methotrexate Printing**

PCL pellets were extruded in similar manner to PLA pellets. PCL however has a melting point of 60 °C and much lower melt-flow than PLA. The melt-flow according to the Sigma Aldrich specification sheet was 160 °C. [128] The pellets were malleable at substantially lower temperatures. The pressurized extrusion was done at temperatures ranging between 90 °C to 120 °C. The material extruded slower than PLA but would quickly enter a thermal “run-away” and extrude with more flexible properties than desired. For this reason the temperature was manually tuned during the entire extrusion process to gain the desired result.

Methotrexate enhanced filaments were printed at 190 °C. This involved using PCL or only doing small prints of pre-heated PLA filaments.

#### 5.4.2 Osteosarcoma Cell Cultures

Osteosarcoma cell line (CRL 2836) was purchased from ATCC (Manassas, VA). Osteosarcoma cells were plated in 25 cm<sup>2</sup> tissue culture flasks and incubated at 37°C under humidified 5% CO<sup>2</sup> and 95% air in complete DMEM containing 10% FBS and 1% PSA. Subconfluent cells were passaged with 0.25% Tryple-E, collected by centrifugation, resuspended in complete DMEM and subcultured at a 3:1 split into 25 cm<sup>2</sup> tissue culture flasks.

Confluent cultures were passaged and seeded onto filaments at uniform cell density. Test wells were tested for toxicity using an XTT assay and the Live/Dead Cytotoxicity assay on the third day of experiment.

#### 5.4.3 XTT Assay

This assay is based on the ability of the viable cells to reduce XTT dye. In these experiments, osteosarcoma cells were used. Cells were seeded in 96 well plates containing filaments with methotrexate along with other PLA filaments as controls. Cells were tested on day 3 when the wells were confluent.

The XTT assay protocol supplied by the manufacturer (Sigma-Aldrich) was followed. After aspiration of media, 100 µL buffer was added to each well along with 20 µL of XTT solution. Photometric absorption of each well was measured at 450 nm and 690 nm after 4 hours of incubation. After completing the XTT assay a Live/Dead assay was conducted on additional wells of each category on the same plate.

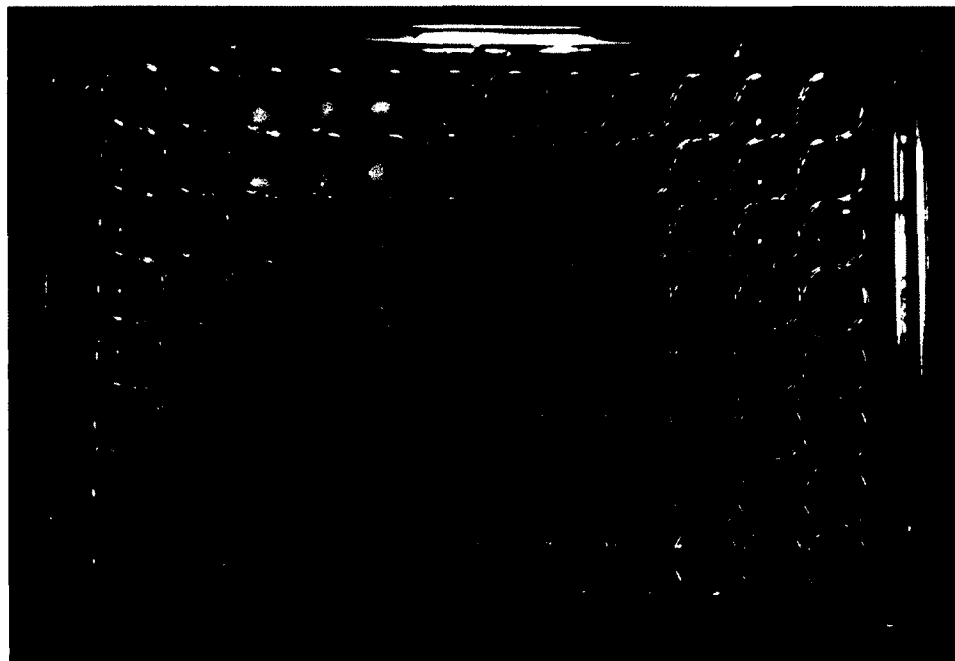
#### 5.4.4 Live/Dead Cytotoxicity Assay

A Live/Dead Cytotoxicity kit was used for testing. The protocol supplied by the manufacturer was used for the assay. The dyes were diluted to 2µM solutions and were

added to the test wells. Fluorescence microscopy was used to image live and dead cells after they were incubated for 30 minutes in the dye solutions.

#### 5.4.5 Cell Culture Well Inserts

Cell culture inserts can be used to limit movement of inserts that could damage the cells. This testing was meant to measure both the effect of drug elution and the effect of the scaffolding on cell growth. This would require a duplication of plates involving inserts and constructs directly inserted into the wells. Due to constraints on constructs and reagents it was necessary to measure both at the same time. A picture of a sample plate is shown in Figure 5-5 demonstrating the filaments, pellets or constructs that were placed into the wells.



**Figure 5-5:** 96 well with inserted pellets, filaments and discs

## 5.5 Testing and Controls

This testing required positive, negative and material controls to achieve reliable data. ANOVA statistical analysis was also done to confirm differences or similarities between experimental groups.

### 5.5.1 Pellet Coating and Extrusion Process

Pellets were visually inspected for a consistent coating. This was then confirmed with SEM. The extruded filaments were visually inspected for uniform coloring. A digital caliper was used to check for a uniform diameter of 1.75 mm +/- 0.1 mm. Pellets were used in XTT testing and the amount of inhibition of cell viability per well was checked for uniformity in relation to the amount of methotrexate coating per pellet.

Three Extrusionbot filament extruders were used during this project. Control filaments were created first on the machines to avoid any contamination. Bioactive coats of similar compounds were run initially on the same machines and in an increasing concentration. Additionally, after each batch of bioactive-coated pellets was run the equipment was cleaned. This resulted in substantial and sustained purges of the Extrusionbots with plain PLA pellets. The hoppers and tubing that led to the auger system we cleaned and vacuumed to pick up any loose particles. Specialized purges were done with more or less backpressure that was achieved by removing the metal die. Additionally, the machines were run at much higher temperatures up to 220 °C or with other polymers that are known to extrude more viscously and pick up leftover particulate.

### 5.5.2 Printer Testing and Controls

The 3D printers were carefully calibrated and returned to factory setting. The Makerbot 2X and Makerbot Replicator 5<sup>th</sup> generation were new and from the



manufacturer. All control constructs were printed on them before printing any bioactive constructs. The printer heads were purged for substantial periods of time between different filaments with control PLA filaments. Filaments of different levels of a bioactive compound were used from least to most concentrated. Before printing bioactive constructs the printers were used to make small random constructs and the weights were compared. The difference in construct weight was within 1%-5% when repetitive small prints were done.

#### 5.5.3 Heat of Decomposition Testing

The 3D printers were run at a temperature of 190 °C. The methotrexate was heated with Vulcan ovens for five minutes at 190 °C. They were then checked for effectiveness on osteosarcoma cells and compared with controls to show that there was no significant loss of properties during the heating process.

#### 5.5.4 Cell Culture Controls and Control Materials

During the cell culture testing process controls were always used. This included control media wells and control cell wells. This provided a negative and positive control for basic growth. Additionally all modified and tested materials were compared to controls. This included control filaments and pellets to those enhanced with bioactive additives. When possible differing steps of the fabrication process were tested. For example this would include testing a PLA pellet, PLA oil-coated pellets and PLA methotrexate-coated pellet by the oil coating process. This allowed proper conclusions to be drawn from the data.

### 5.5.5 Elution Testing Controls

Spectrophotometry must be checked with controls and properly calibrated. This must especially be done when using very low concentrations of a substrate of interest. The spectrophotometer was checked with plain deionized water regularly. This verified that the absorbance was zero with a control. Absorbance curves were calculated using known levels of a substrate.

## 5.6 **Results and Discussion**

The development of methods to demonstrate the benefits of 3D printing other biomaterials and the possibility of the creation of chemotherapeutic constructs was done in phases. The thermal stability of the methotrexate was proven. The coating method was demonstrated with methotrexate on both the PCL and PLA pellets. Filaments were extruded and simple test discs and constructs were printed. Photographs and SEM were taken during the process. Osteosarcoma testing was then undertaken with filaments and constructs to prove the effects. Elution testing was done.

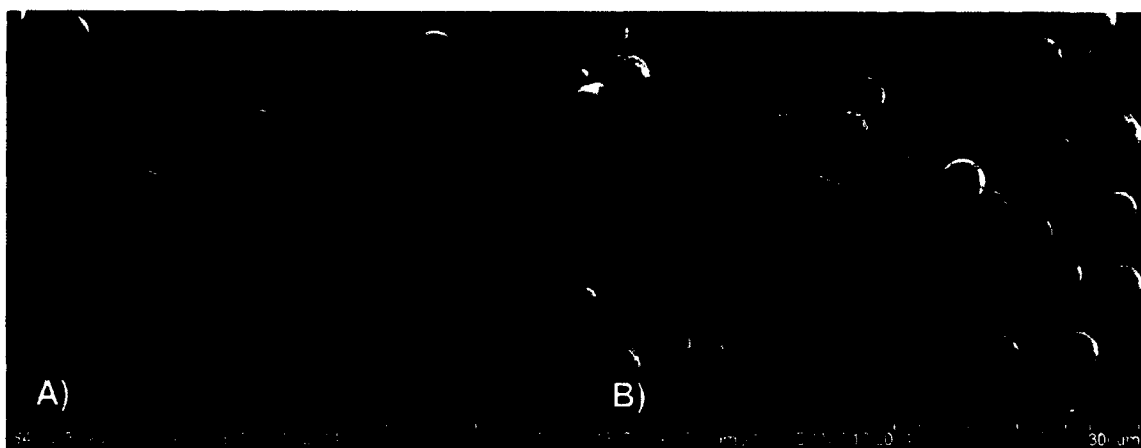
The results and discussion will first look at the 3D printing of PMMA based bone cements. Next, it will review the creation of PCL and PLA filaments. The filaments will be printed into test disc, constructs and tested with cell cultures.

### 5.6.1 3D Printing Bone Cements

The ability to use existing biomaterials for novel purposes could act to personalize medicine. PMMA bone cement was chosen for the fact that it was an existing standard.

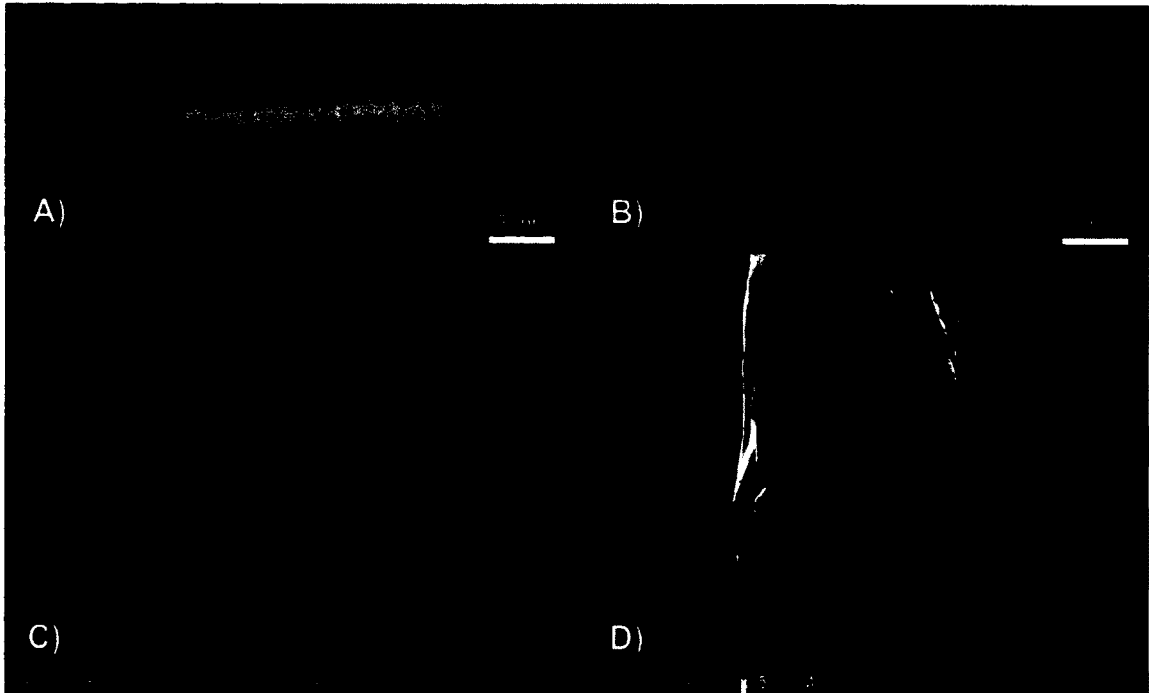
### 5.6.1.1 Bone cement filaments

Bone cement powders are a fine white powder on visual examination. A PMMA commercial bone cement powder with barium and Bosworth PMMA polymer-only powder was imaged by SEM. This is shown in Figure 5-6.



**Figure 5-6:** A) Bosworth PMMA only powder B) Commercial PMMA bone cement

The SEM shows that the PMMA are uniform spheres that vary slightly in diameter. The commercial bone cement has rough particulate that is barium. This is to provide contrast. The Bosworth PMMA powder was extruded via the Extrusionbot filament extruder at 220 °C in 20 gram batches. Several meters of filament were extruded at a 1.75mm +/- 0.1mm diameter. Kyphon bone cement was mixed per manufacturer instructions. This involved mixing the liquid monomer with the powdered polymer. It was loaded into a 5 mL syringe without a needle. The Luer-Lock tip of the syringe without a needle had a diameter of roughly 1.9 mm. The bone cement was extruded and allowed to dry. Sections of both filaments were then photographed and underwent SEM. This is shown in Figure 5-7.

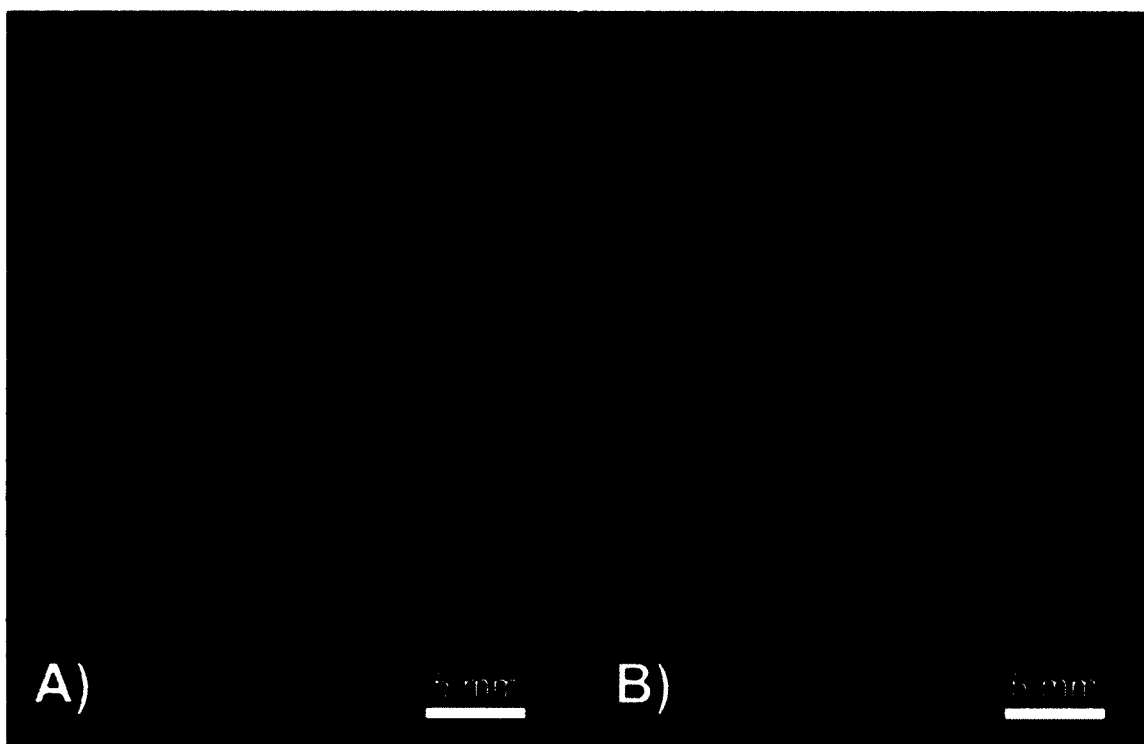


**Figure 5-7:** A) Kyphos bone cement filament B) Bosworth PMMA powder only filament C) SEM of Kyphos bone cement filament D) SEM of Bosworth PMMA powder only filament

On visual examination both filaments seem uniform. The filaments were made from white powders. The Bosworth PMMA filament was darker at some locations such as the piece shown. This was due to the higher temperature used for extrusion. This temperature was chosen due to a need for a melt-flow to occur in a low-pressure auger extruder and the fact that the 3D fabrication would require a similar temperature. The diameter was 1.75 mm +/- 0.1 mm as desired for substantial portions of the filament.

#### 5.6.1.2 3D printing bone cement filaments

The Bosworth PMMA filament was tested for 3D fabrication as a proof of principle. The shape of a 5 mm test disc and 6 mm hollow bead as shown in Chapter 5 were chosen. Both constructs were printed on a Makerbot at 220 °C and the disc was done at 100% in-fill while the bead was done at 10% in-fill. This is shown in Figure 5-8.

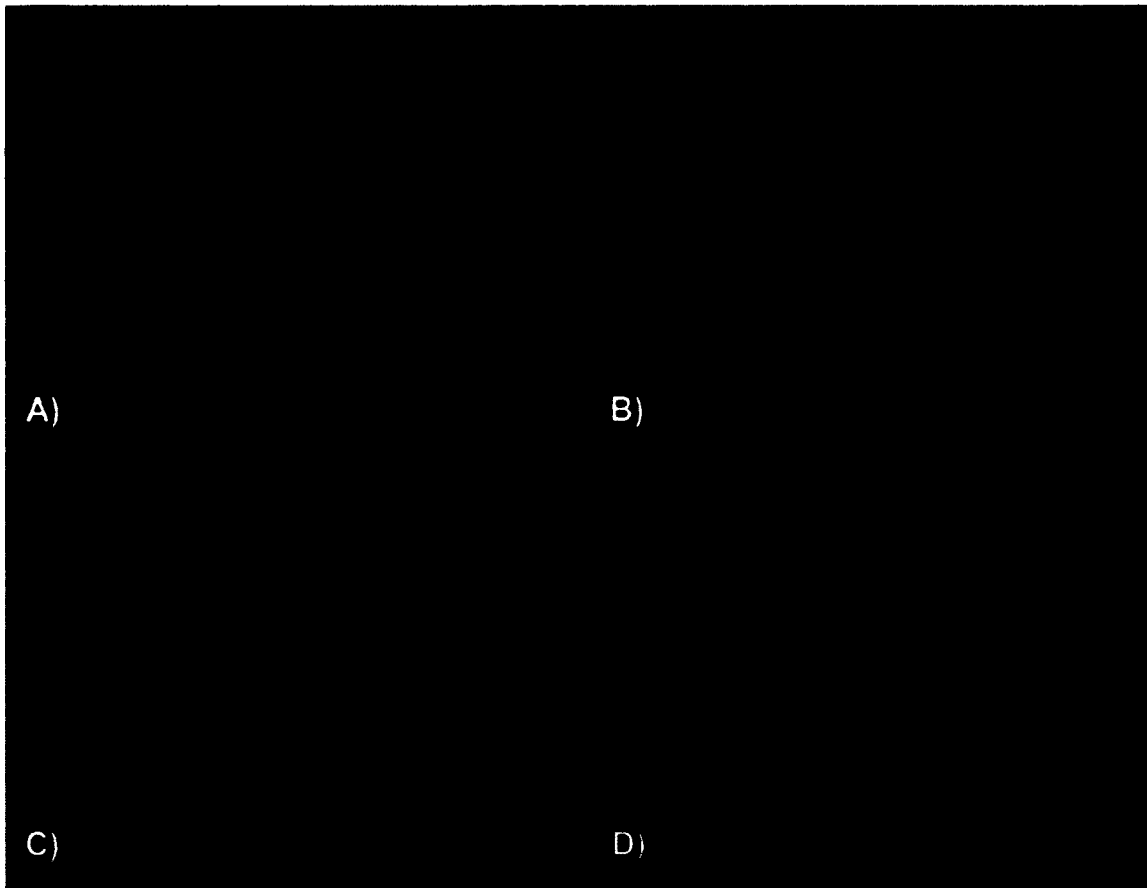


**Figure 5-8: A) Bosworth PMMA-only disc B) Bosworth PMMA-only bead**

The PMMA filament printed well at 220 °C. It was equivalent to printing with the PLA filaments. The constructs were uniform and it was possible to create multiple copies of each construct.

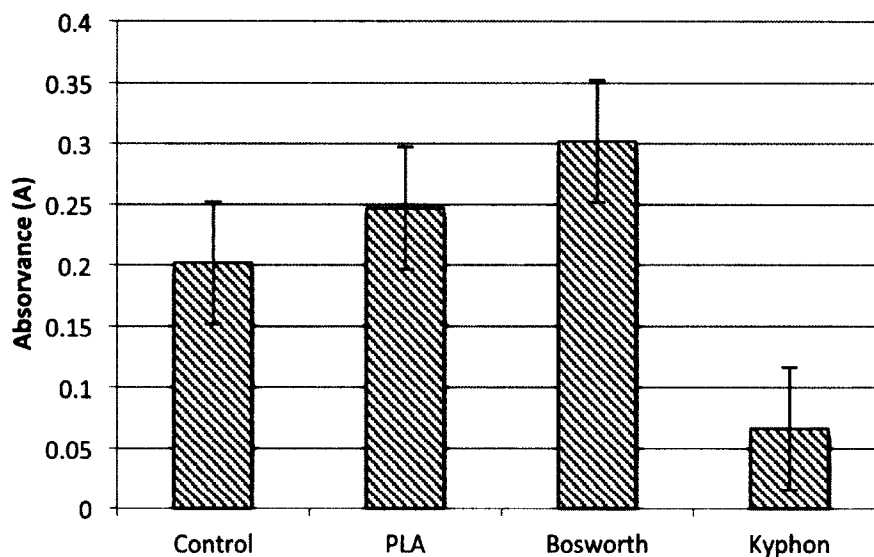
#### 5.6.1.3 *Cell viability assays with bone cement filaments*

The filaments were cut into 5 mm pieces. Osteosarcoma cells were cultured per the methods section. A 96 well plate was used that had control media wells, control osteosarcoma wells, PLA filament wells, Bosworth PMMA filament wells and Kyphon PMMA filament wells. After one day of growth the control well appeared confluent and a Live/Dead assay was performed on three wells from each category per the methods section. The results from that assay are shown in Figure 5-9 and Appendix A.



**Figure 5-9:** Live/Dead Assay A) Control well B) PLA filament well C) Bosworth PMMA-only filament well D) Kyphos commercial bone cement well

The control well is confluent with living green cells. The PLA filament and Bosworth powdered PMMA-only filaments are similar to the control. The Kyphos commercial bone cement has almost no green marked living cells. This is likely since the monomer in the commercial bone cement contains toxic substances that initiate the polymerization reaction. This figure strongly shows the potential that additive manufacturing can have in biomedical engineering by only changing the processing of established materials. An XTT assay was done on six wells of each group to provide analysis of the difference in cell metabolic activity between the wells (Figure 5-10).



**Figure 5-10: XTT assay of filaments**

The control well had confluent cell growth. On XTT assay it can be seen that the PLA and Bosworth PMMA filaments are acting as a scaffolding to allow for more growth or more metabolic activity. The PLA filament had 22.3% more activity and the Bosworth PMMA had 49.5% more activity than controls. This contrasts the Kyphos cement made with the monomer that had a drop in metabolic activity of 67.3% when compared to controls. It is highly likely that the toxic components of the monomer resulted in both cell death and a drop in metabolic activity. These results involve osteosarcoma cells that grow much faster than osteoblast cells. When used in a surgical procedure where there is a need for rapid healing, the effect of the toxins in bone cement may delay growth. This shows a proof of principle in 3D fabrication procedures providing improved methods for the use of existing biomaterials.

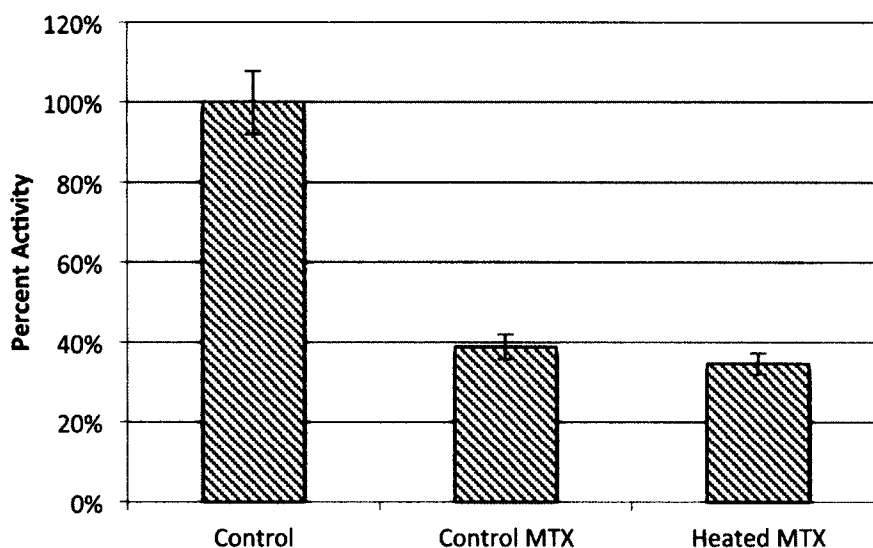
#### 5.6.2 Fabricating Methotrexate Laden Constructs

To test the capabilities of creating chemotherapeutic eluting constructs a similar process to antibiotic fabrication was followed. Methotrexate was heated and tested with

osteosarcoma cells to confirm bioactivity. Pellets were coated with methotrexate and imaged. Methotrexate filaments were fabricated and imaged. Elution profiles were tested to confirm a release profile. Any filaments with proper release profiles were tested with osteosarcoma cells.

#### 5.6.2.1 *Methotrexate thermal stability testing*

MSDS data indicated that the methotrexate would be thermally stable during the 3D printing process. The following process confirmed this process. MTX powder was heated in a Vulcan oven to 190 °C for five minutes. The heated MTX along with a control MTX powder was added to osteosarcoma cells that had been plated in a 96 well plate at 1%w/v. After a day, a XTT was completed to check cell activity. An inhibition of osteosarcoma growth by both heated and control MTX was found (Figure 5-11).

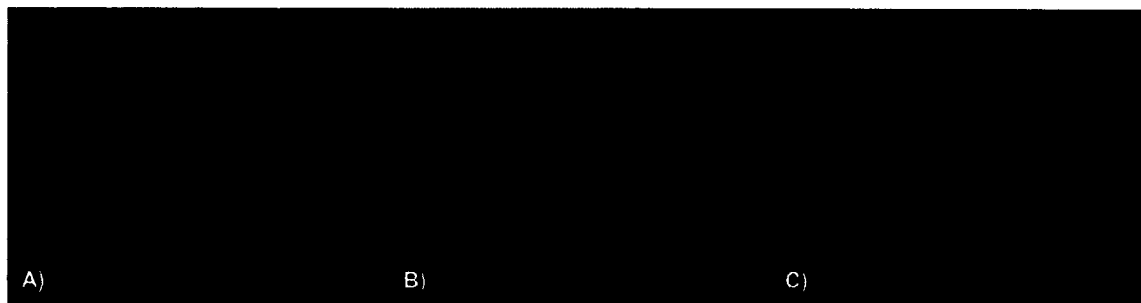


**Figure 5-11:** XTT table showing percent activity

Compared to controls, the inhibition of activity by heated and control MTX was 65.4% and 61.2%, respectively. Analysis was run to prove that there was both a statistical inhibition of growth and no statistical difference between groups. A Live/Dead assay was



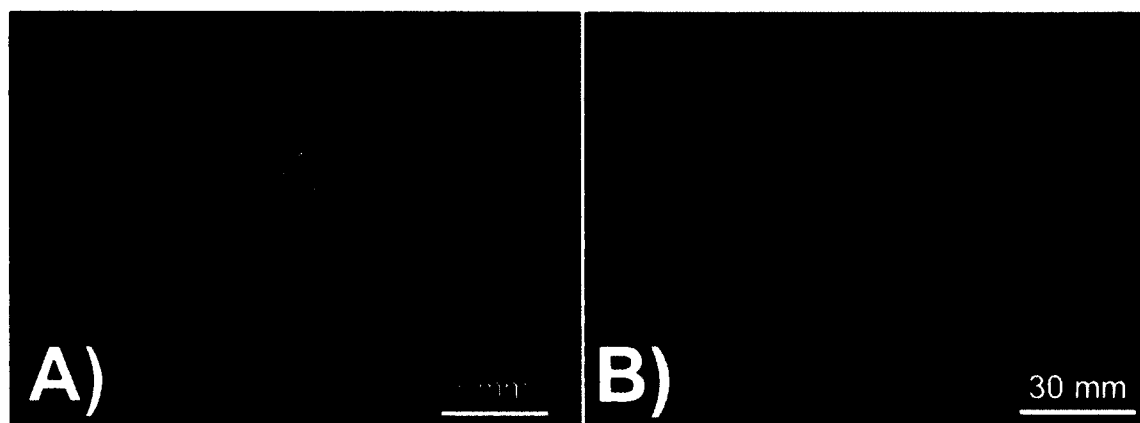
run to demonstrate any differences between the control, MTX control and MTX heated groups (Figure 5-12 and Appendix A).



**Figure 5-12:** Live/Dead cytotoxicity assays (A) Control well (B) Control methotrexate (C) Heated methotrexate

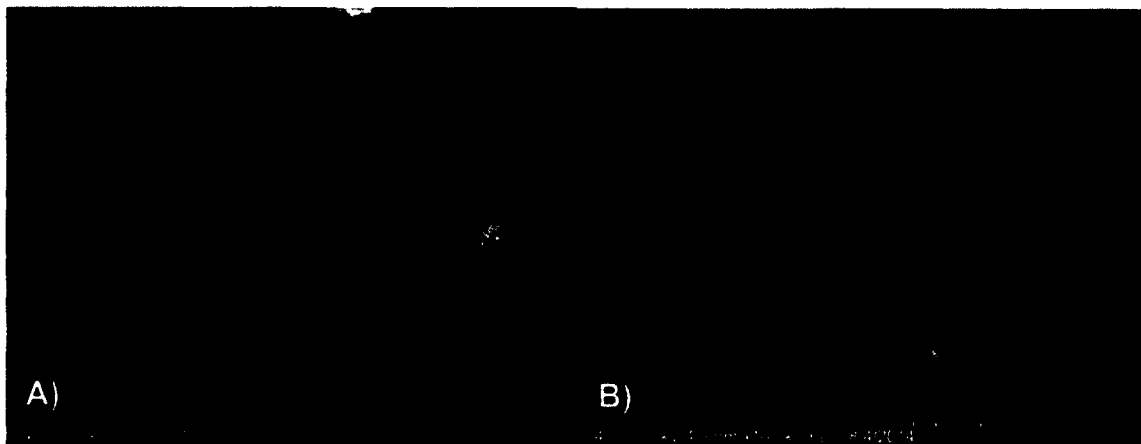
#### 5.6.2.2 *Methotrexate enhanced filaments*

The oil coating method described in Chapter 5 was used to coat both PCL and PLA pellets with methotrexate in 15 to 20 gram batches. A 1wt% PCL-coated batch of pellets and a 2.5 wt% PLA-coated batch of pellets was fabricated. This is shown in Figure 5-13.



**Figure 5-13:** A) 2.5 wt% PLA pellet B) 1 wt% PCL-coated pellets

The pellets were checked for a consistent coating with SEM. Imaging of the methotrexate powder and pellets were taken and are shown in Figure 5-14 and Figure 5-15.

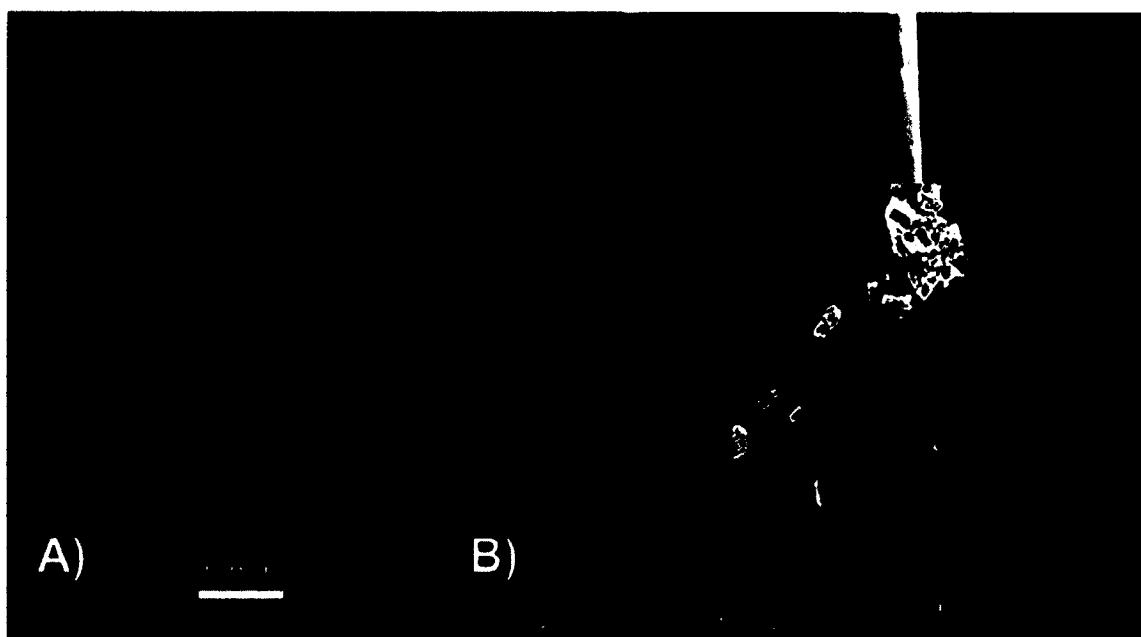


**Figure 5-14: A-B) Methotrexate powder SEM**

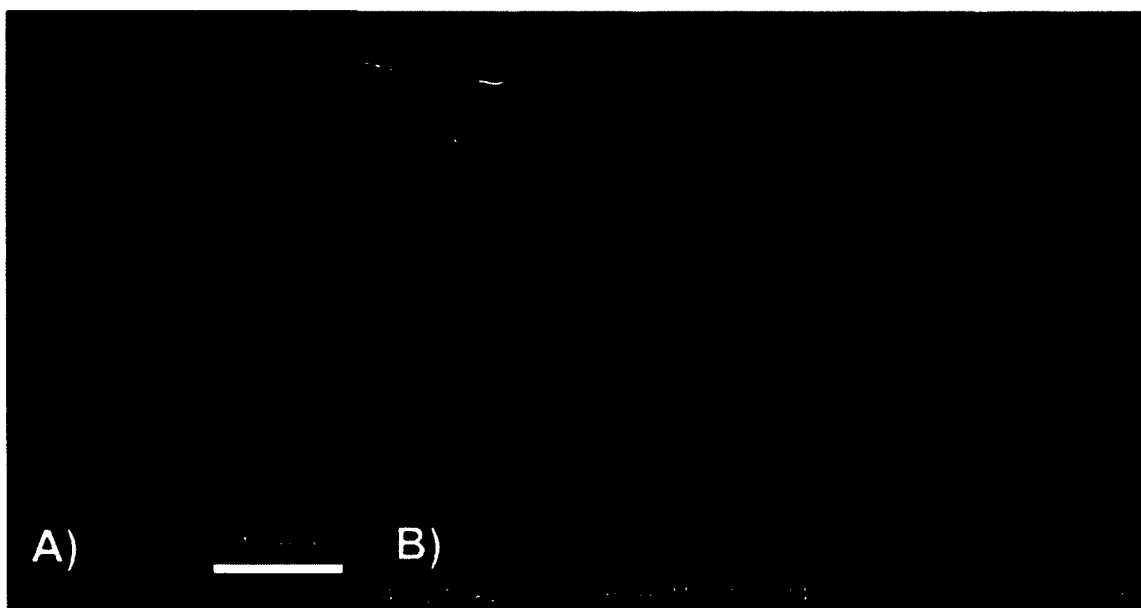


**Figure 5-15:** A) PLA pellet B) 2.5 wt% MTX-coated PLA pellet C) 1 wt% PCL pellet D) MTX-coated PCL pellet

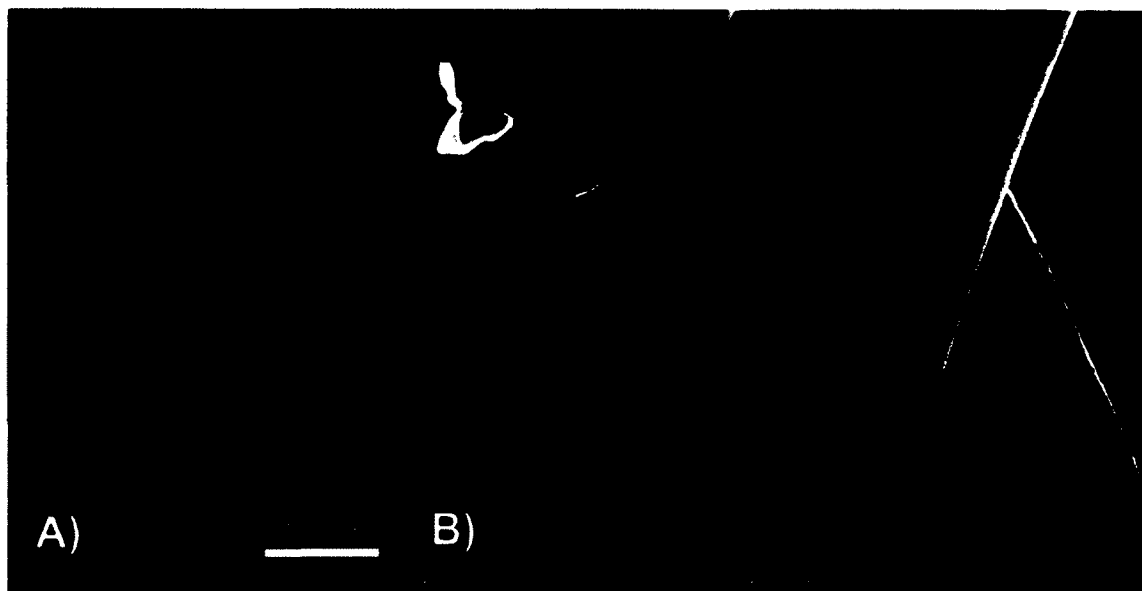
The methotrexate is an irregular crystal of roughly uniform size. The pellets were consistently coated as confirmed by SEM. Some of the coatings were lost by the compressed air needed to remove loose particulate before SEM was done. The pellets were then extruded with the Extrusionbot. The PLA was done at a standard temperature of 175 °C. However, the PCL pellets had a lower melting point and were done between 90-120 °C. A control PCL, 1wt% PCL and 2.5wt% PLA filaments were extruded then photographed and imaged by SEM. This is shown in Figure 5-16, Figure 5-17 and Figure 5-18.



**Figure 5-16:** (A) 2.5 wt% methotrexate PLA filament (B) SEM of 2.5 wt% methotrexate PLA filament



**Figure 5-17:** A) Control PCL filament B) SEM control PCL filament



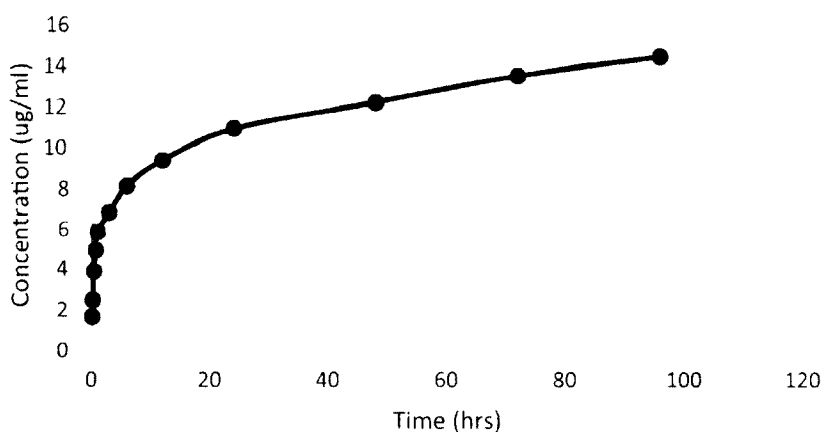
**Figure 5-18:** A) 1 wt% MTX PCL filament B) SEM of 1 wt% MTX PCL filament

Both the control PLA extruded in Chapter 5 and control PCL extruded here are clear or translucent (Figure 5-17). The PCL and PLA filaments are both yellow in color (Figure 5-16 and Figure 5-18). The PLA filament is slightly translucent yellow. The PCL filament is visually more solid and a deeper yellow even though it has less methotrexate than the PLA. The filaments were smooth and all 1.75 mm with a  $\pm 0.1$  mm variance. The PCL material was much more difficult to extrude and would likely require a more pressurized extruder to gain proper melt-flow. It should also be noted that trace amounts of halloysite can be seen on a high magnification in some images on the methotrexate--enhanced filaments. These are the small and long rectangular objects that appear in the image. These are trace amounts of halloysite resulting from trace amounts remaining after the cleaning purges.

#### 5.6.2.3 Methotrexate elution profiles

The methotrexate-enhanced PCL and PLA filaments were tested for elution of methotrexate. The filaments were cut into 1 cm section and placed in 1 mL Eppendorf

tubes. The elution was quickly tested to confirm release by allowing the filaments to soak for a few minutes to a few days. After a few minutes and a few days the 1wt% methotrexate PCL filament was tested on the nanodrop spectrophotometer. This was done at 200 nm. Trace amounts of methotrexate was found from the PCL filaments but not enough to run full elution profiles. PLA filaments had clear methotrexate elution so were processed for very preliminary cell culture work. The elution profile for the 2.5wt% methotrexate-laden PLA filament is shown below in Figure 5-19.



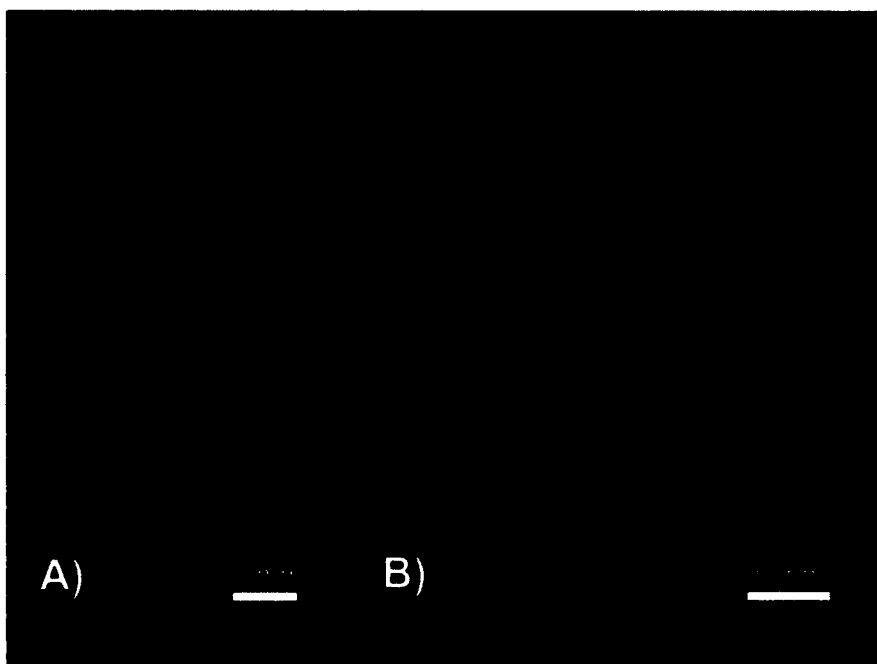
**Figure 5-19:** Elution Profile of 2.5wt% MTX-PLA filament

The elution profile lasted 100 hours when sampling was stopped. There profile appeared to be slowing down around the end of our sampling. This is likely due to a combination of the solubility of the methotrexate combined with a nominal degradation of the PLA or elution from pores.

#### 5.6.2.4 Fabrication of 3D printed methotrexate constructs

The 2.5wt% methotrexate PLA filament was test fabricated into constructs as a proof of principle. The PLA was printed at 190 °C which is below the more standard printing temperature of 220 °C. This can be done with added pressure or by only doing

small constructs. The need for a higher printing temperature is not always necessary. It may be that the material takes too much time to heat enough for melt-flow to occur. To demonstrate a proof of principle for the PLA filament, small amounts of PLA filament was loaded into the heating element and reservoir of the 3D printer head. The 5 mm disc, 6 mm bead and a 14 French stent/cylinder were printed to demonstrate the technology. The disc was at 100% in-fill and the bead and stent were at 10% in-fill (Figure 5-20 and Figure 5-21).



**Figure 5-20:** A) 2.5 wt% MTX PLA stent B) 2.5 wt% MTX PLA disc



**Figure 5-21:** Comparison between gentamicin and methotrexate laden beads. Left: gentamicin-laden bead; Right: methotrexate-laden bead

Methotrexate enhanced prints visually appeared equivalent to those of other bioactive laden filaments (Figure 5-20 and Figure 5-21). Temperature constraints made printing larger constructs difficult. The discs printed well and the bead/stent required external pressure. The prints were uniform on visual examination. SEM was done to conduct additional examination on the 6 mm bead as shown in Figure 5-22.



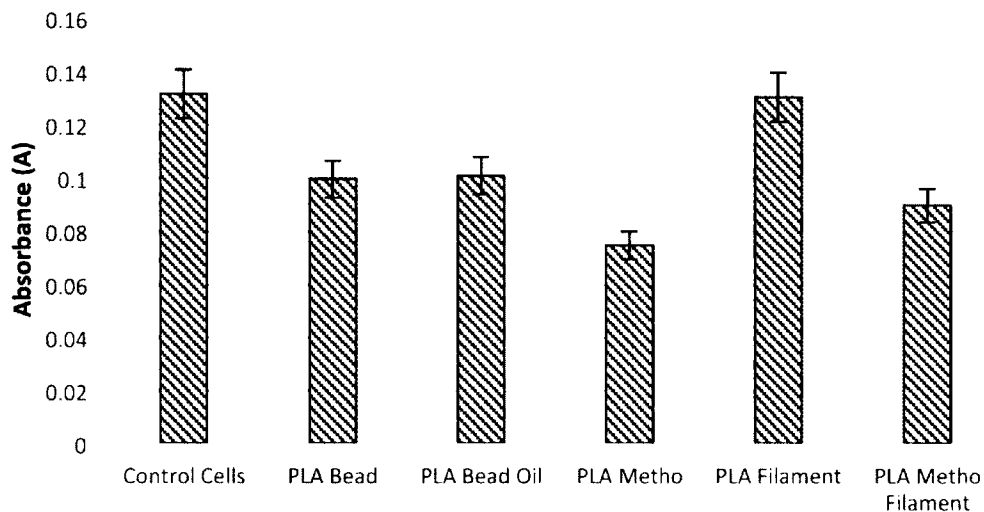


**Figure 5-22:** SEM of methotrexate laden 6 mm bead

The 3D fabricated 6 mm bead can be seen to have a layered construction with 300  $\mu\text{m}$  layer size. On higher resolution the additive methotrexate can be seen embedded in the PLA plastic.

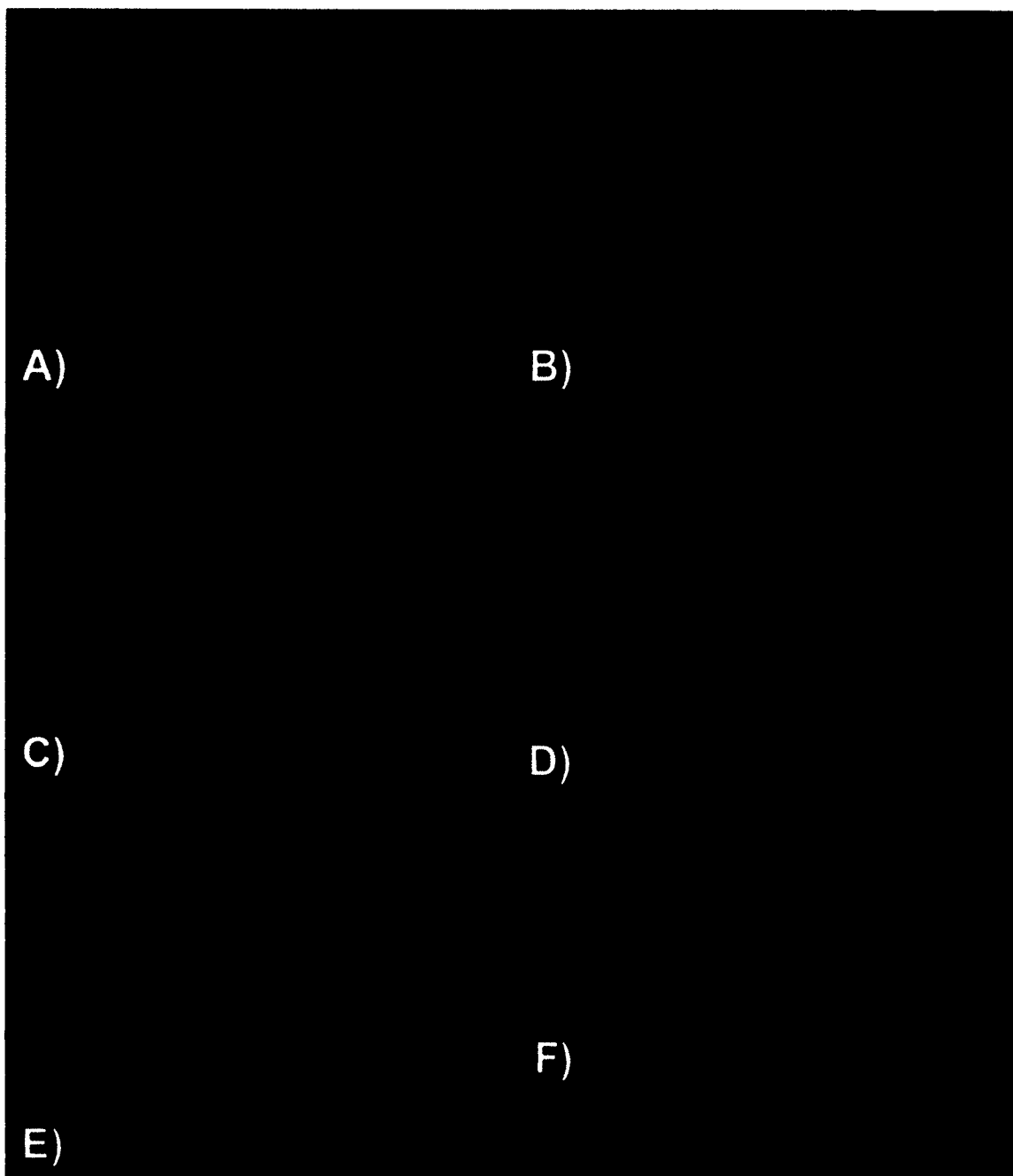
#### 5.6.2.5 Cell assays with methotrexate enhanced filaments

MTX enhanced PLA filaments were tested with osteosarcoma cells plated on 96 well plates. For this portion of the study eight test groups with five wells tested were used: control cells, control MTX, heated MTX, control PLA pellet, oil-coated PLA pellet, MTX-coated PLA pellet, control PLA filament, MTX PLA filament. After three days, once the control osteosarcoma well was confluent an XTT and Live/Dead assay were done. The XTT assay showed enhanced osteosarcoma growth in wells not containing MTX (Figure 5-23).

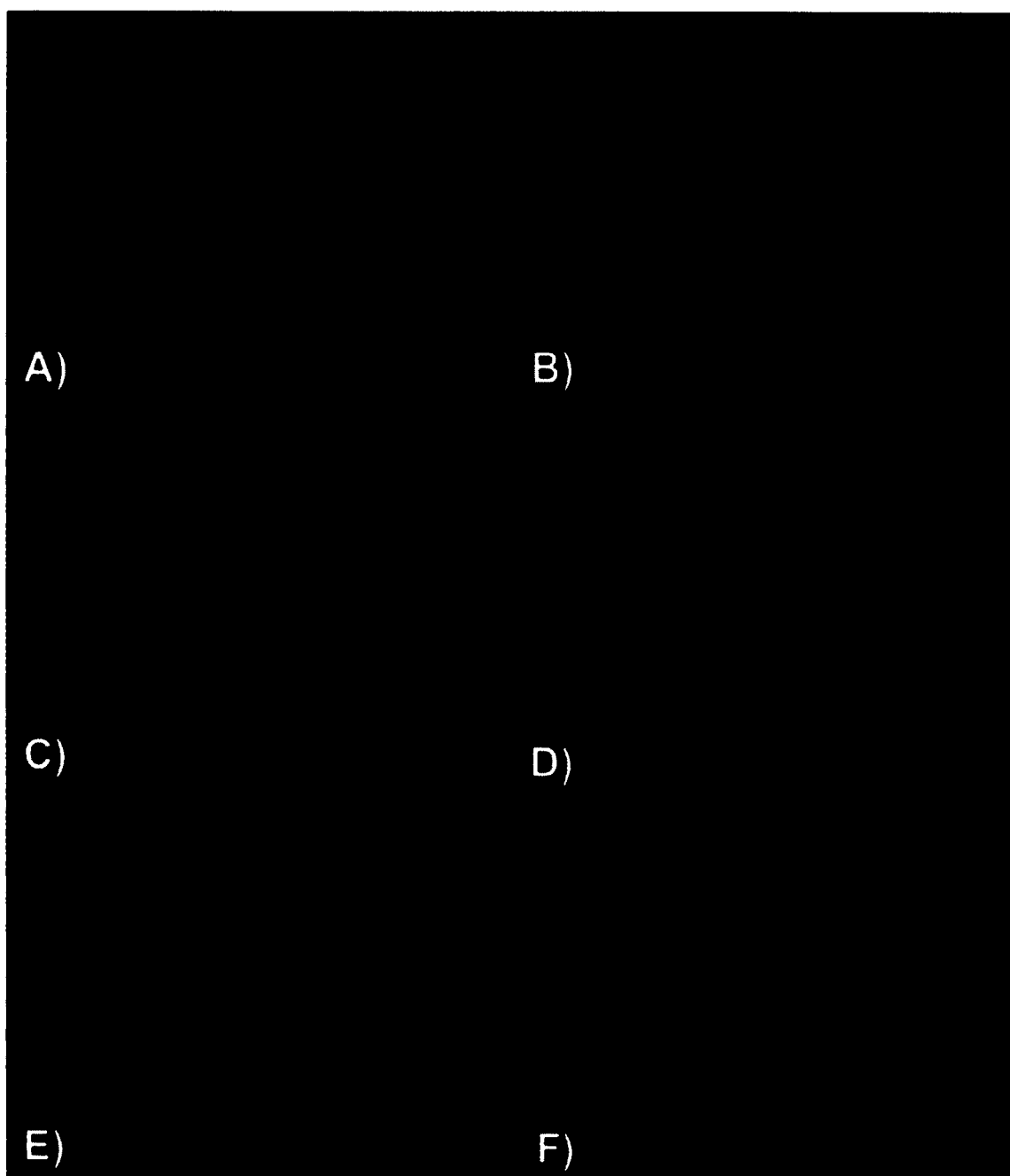


**Figure 5-23: XTT of 2.5 wt% methotrexate laden filament with osteosarcoma cells**

The silicon oil showed no effect on cell growth and was shown by comparing a control PLA pellet to a pellet coated in silicon oil. The control PLA filament had no difference in cell proliferation compared to the control well. There was a significant decrease in cell proliferation in the well with MTX enhanced PLA filament when compared to both the control well and PLA filament control well. Only 68.9% of the growth of control wells was shown in comparison in the presence of the MTX filaments. The PLA pellet coated in methotrexate was only 56.9% as metabolically active as the control well and 75.1% as active as the PLA control pellet well. Difference in activity between the PLA pellet and the control well were likely related to movement of the pellet that disturbed cells. The control well and PLA filament are nearly identical in activity. ANOVA analysis confirms statistical differences between XTT viability assays of the methotrexate enhanced filament/pellet and the respective control groups. The Live/Dead assay visually confirmed the XTT results (Figure 5-24, Figure 5-25 and Appendix A).



**Figure 5-24:** Live/Dead assay green live component A) Control B) PLA control pellet C) PLA pellet oil-coated D) PLA pellet coated MTX E) PLA filament F) 2.5 wt% MTX-PLA filament



**Figure 5-25:** Live/Dead assay red dead component A) Control B) PLA control pellet C) PLA pellet oil-coated D) PLA pellet coated MTX E) PLA filament F) 2.5 wt% MTX-PLA filament

The Live/Dead assay visually confirms the XTT results. The methotrexate-coated pellet and methotrexate filament both show reduced living cells and substantially more red labeled dead cells than the other wells. The oil-coated and control PLA pellet share

similar growth levels labeled green. The control well and PLA filament also share similar confluent growth levels. It should be noted again that methotrexate is cytostatic instead of cytotoxic. The methotrexate was added once cells became close to confluent. The Live/Dead assay would thus show wells looking fairly confluent. It is expected that differences would be subtler. The *in vitro* cell study results show the potential for the generation of bioactive chemotherapeutic 3D printing filaments.

### 5.7 Conclusion

Methotrexate laden filaments were created to show the potential for customized fabrication of chemotherapeutic eluting constructs. The XTT and Live/Dead kits showed comparable activity from methotrexate powders that had been heated similarly to the fabrication process. The MTX laden filaments prevented growth as was shown by ANOVA statistical analysis when compared to controls. Methotrexate is cytostatic as opposed to cytotoxic. Measurements were taken once the control wells had reached near confluence. Future work with cytotoxic compounds may show more significant reductions in cell activity on both the Live/Dead and XTT assays. As proof of principle small methotrexate-laden PLA constructs were fabricated. This included a stent and test disc. Additionally fabrication of hollow constructs would likely increase surface area and increase elution.

The 3D printing filament extrusion of PLA MTX filaments showed inhibition of cancer cell growth. Testing of the oil used to coat the PLA pellets showed that the effects are additive based. Applications of this fabrication process may enable fabrication of patient-specific treatment implants for targeted treatments of tumors or surgical margins. By using PLA, a well known biocompatible plastic, as the primary component of the

implants, normal body functions should prove to break down the implant after time, negating the necessity of additional procedures to remove the implant. Understanding of elution profiles of additives is necessary in order to fully comprehend patient treatment via this method and more involved studies should be included in future work.

The testing of bone cements fabricated as 3D printing filaments yielded results showing improved cytotoxicity when compared to the standard commercial fabrication process. This confirms the potential of additive manufacturing to have large effects even when using established biomaterials.

## **CHAPTER 6**

### **CONCLUSIONS AND FUTURE WORK**

#### **6.1 Conclusions**

It is clear that additive manufacturing can, even in the early stages, have a large effect on clinical medicine. The ability to 3D fabricate antibiotic laden beads or catheters for personal medicine yields great potential for new treatments and patient specific technologies. Combining these treatments with nanotechnology can make them even more customizable. The ability to use nanotubes in a modular fashion similar to 3D printing technology may yield unique and unforeseen results. Overall three core conclusions sum up the projects and objectives:

A modular nanotube technology was discovered and shows promise in use for sensors or customized treatments or experimental work. This was important in demonstrating low cost capabilities for custom nanotube construction that can easily be done anywhere. Imaging and EDAX analysis confirmed that it was possible to coat HNTs singularly or in combination with iron, gold, barium, copper, nickel and lithium. The iron-coated particles were shown to be magnetically susceptible. The particles were tested with osteoblast cells in culture to check for cytocompatibility. It was shown that control HNTs, iron-coated HNTs, gold-coated HNTs and barium-coated HNTs were relatively cytocompatible. In cell viability testing the iron-coated HNTs had 97.7% of the

number of viable cells compared to controls. In cell viability testing, the barium-coated HNTs had 90.1% of the number of viable cells compared to controls. The nickel-coated HNTs and copper-coated HNTs were found to be cytotoxic. Almost all cells in these wells died. In cell viability testing, the copper-coated HNTs had 0.04% of the number of viable cells compared to controls. In cell viability testing the nickel-coated HNTs had 0.12% of the number of viable cells compared to controls. The metal-coated HNTs were then coated in lipids or polyelectrolyte coatings. This was important since it demonstrated that biocompatible coatings could be added to these particles. The coated HNTs were also loaded with gentamicin, nitrofurantoin or methotrexate. Release profiles that lasted several hours to days were demonstrated. Finally, MRI imaging was done to bone cements enhanced with barium-coated HNTS.

Biomaterials were shown to be enhanced by the nanotechnology. Barium-coated halloysite nanotubes should value as a simple additive to bone cements that can increase both contrast and strength at a low cost.

A novel method of 3D fabricating antibiotic or chemotherapeutic eluting constructs was created and verified. As proof of principle of a novel technology, it demonstrates the capabilities of even the most basic fabrication devices. The ability to print bone cements and chemotherapeutic enhanced filaments was confirmed. The toxicity of commercial bone cements was confirmed by the XTT assay. This was shown by a 67.3% drop in metabolic activity seen in cells exposed to the commercial bone cement filament compared to controls. The thermal testing of methotrexate demonstrated that osteosarcoma inhibition only varied 4.2% between the control methotrexate group and thermally heated methotrexate group. Filaments were extruded and imaged.



Methotrexate crystals were visually confirmed in the images. Elution testing was then run and the 2.5wt% methotrexate enhanced filament was shown to elute for over 100 hours. Finally, cell viability assays were run with the filaments. Only 68.9% of the growth of control wells was shown in the presence of the MTX filaments.

## **6.2 Future Work**

The work that has been done is very preliminary and could best be classified as a proof of principle. While antibiotics and chemotherapeutics have been used in the 3D fabrication process, now other compounds must be researched. As an early stage technology there is much work to do.

All aspects of the process could be optimized and improved. Work on the optimization process has not begun yet. However everything from pellet coating methods to filament extrusion devices to novel 3D printers should be researched in advancing this technology. Additionally, animal studies must be done to prove these concepts.

## APPENDIX A

### IMAGEJ ANALYSIS LIVE/DEAD ASSAYS

It is important to note that Live/Dead assays are both quantitative and qualitative. The assays discussed in the body of the text were of the qualitative nature. However, pixel count, cell count, intensity and total area of pixels as well as ratios to the controls can be counted for qualitative analysis.

ImageJ analysis was done for the Live/Dead assays of the sintered nanoparticles Figure 3-31 and Figure 3-32. The green or red pixels were counted in images that had been color threshold adjusted and five well images were run for each category then averaged. This is shown in Table A-1.

**Table A-1:** ImageJ analysis of Live/Dead assay with metal-coated HNT categories

	<b>Green Pixel Count</b>	<b>Red Pixel Count</b>	<b>Ratio: R/G</b>	<b>Ratio R/Control R</b>	<b>Ratio G/Control G</b>
Control Cells	1,286,685	3,416	0.27%	100%	100.00%
<b>HNTs Raw Control</b>	<b>1,020,002</b>	<b>6,626</b>	<b>0.65%</b>	<b>100%</b>	<b>79.28%</b>
Lithium Coated HNTs	943,613	1,119	0.12%	33%	73.34%
<b>Iron Coated HNTs</b>	<b>1,256,443</b>	<b>4,746</b>	<b>0.38%</b>	<b>130%</b>	<b>97.65%</b>
Barium Coated HNTs	1,159,366	6,162	0.53%	180%	90.10%
<b>Copper Coated HNTs</b>	<b>486</b>	<b>0</b>	<b>0.00%</b>	<b>0%</b>	<b>0.04%</b>
Nickel Coated HNTs	1,486	428	28.80%	13%	0.12%

This table has several features that should be noted. The control wells have less than one percent of red cell death indicating pixels when compared to the green live stain. This follows through for control raw HNTs, lithium coated HNTs, iron coated HNTs and

barium coated HNTs. There were no red pixels above threshold for copper coated HNTs. This indicates almost a complete lack of cell growth, immediate cytotoxicity or degradation of the seeded cells red ethidium bromide stain binding points. The nickel coated HNTs had 29% of the internal group R/G ratio showing a high number of dead cells in relation to living. This correlates to a slower cell death or effect over time. The test group red stain compared to control red stain ratios resulted in most categories having a ratio greater than 100%. This meant that there were more red pixels or indicators of cell death in the test groups proportionally to the red cell death indicators in the control wells. This occurred for raw HNTs, iron HNTs and barium HNTs. The lithium HNTs had a ratio of 33% indicating that there was less cell death than in the controls. It should be noted that while copper and nickel coated HNTs had ratios below 100% as well, this was due to different causes. There was no cell growth to very minimal in these wells. This meant there were not enough cells to grow and then to later die to compare to the control group. The ratio of the groups green stained living cells to control stained living cells also provides substantial data on viability. There is no group that has more living cells than controls. Iron and barium coated HNTs prove most cytocompatible based on a respective 97% and 90% ratio. It should be noted that this was superior to raw HNTs which only had 79%. Copper and Nickel coated HNTs test groups had almost complete cell death and resulted in less than 1% of the viable cells as controls.

ImageJ analysis was done for the Live/Dead assays of the heated methotrexate (Figure 5-12). The green or red pixels were counted in images that had been color threshold adjusted and five well images were run for each category then averaged. This is shown in Table A-2.

**Table A-2: ImageJ analysis of Live/Dead assay with heated MTX categories**

	<b>Live-Green *Count</b>	<b>Red-Dead *Count</b>	<b>Ratio R/G</b>	<b>Ratio G/Control G</b>	<b>Ratio R/Control R</b>
<b>Control Cells</b>	<b>349648</b>	<b>34251</b>	<b>9.80%</b>	<b>100.00%</b>	<b>100.00%</b>
<b>Control MTX</b>	<b>27696</b>	<b>4485</b>	<b>16.20%</b>	<b>14.78%</b>	<b>13.05%</b>
<b>Heated MTX</b>	<b>73523</b>	<b>10197</b>	<b>13.87%</b>	<b>21.03%</b>	<b>29.77%</b>

This table has several notable features that enhance the discussion in the body of the text. The “\*” symbol represents the pixel count. The control cell green live cell pixel count is substantially higher as a raw number to both control and heated methotrexate groups. The number of red pixels indicating dead cells is higher in the control well since there are 10Xs the number of cells as the test groups and since confluence had been reached likely resulting in cell death. Methotrexate is cytostatic and not cytotoxic. The ratio of red to green indicating cell death is noted as 9.8% for the control group and 16.2% or 13.8% for the test groups. This fits the cytostatic nature of the tested drug. The ratio of test group green to control green shows the prevention of growth. Only 14.8% and 21% of the growth of the control group occurred in the control methotrexate and heated methotrexate groups, respectively. The test groups only had 13% and 29% of the cell death based on a red test group to red control group ratio for control methotrexate and heated methotrexate groups, respectively. This is to be expected as there are less cells which would be shown by the cytostatic nature of methotrexate.

ImageJ analysis was done for the Live/Dead assays of the heated methotrexate (Figure 5-23 and Figure 5-24). The green or red pixels were counted in images that had been color threshold adjusted and five well images were run for each category then averaged. This is shown in Table A-3.

**Table A-3: ImageJ analysis of Live/Dead assay with MTX filament categories**

	<b>Green Pixel Count</b>	<b>Red Pixel Count</b>	<b>Ratio: R/G</b>	<b>Ratio R/Control R</b>	<b>Ratio G/Control G</b>
Control	1,307,807.00	1,752.00	0.13%	100%	100%
PLA Pellet	1,336,499.00	6,672.00	0.67%	99%	102%
PLA Oil Coated Pellet	1,237,174.00	271.00	0.02%	15%	95%
PLA MTX Coated Pellet	335,495.00	28,935.00	10.50%	1907%	17%
Control PLA Filament	1,027,093.00	10,371.00	1.01%	592%	79%
2.5wt% MTX PLA Filament	492,292.00	18,513.00	3.76%	1957%	38%

This table has several notable features that enhance the discussion in the body of the text. The green pixel count for the control, PLA pellet, PLA oil coated pellet and Control PLA filament are all well over a million. This similarity is shown even more when doing a ratio analysis. The ratio of green sample group to control green is 102% and 95% for the control PLA pellet and oil coated PLA pellet, respectively. The control PLA filament is 79%. This contrasts greatly with the difference between the 17% and 38% ratio seen in the MTX coated pellet and MTX filament, respectively. The results carry over to the ratio of red dead cell pixel count in test groups to the control group red dead pixel count. The ratio for the groups with MTX are all above 1,000% or 10X increases compared to controls in relation to cell death. Now it should be noted that control PLA groups have 5X the amount of cell death as the control groups but this could relate to impurities in the PLA used.

## APPENDIX B

### SURFACE AREA RATIOS

The ratio of surface area of the cylinders to the zone of inhibition can be calculated if desired. This can be done as follows:

- Given that the diameter of the filaments is 1.75 mm, and the length of each is 10 mm, we can find the surface area of the cylinder as

$$SA = 2\pi rh + 2\pi r^2 = 2\pi * 1.75 * 10 + 2\pi * 1.75^2 = 129.198 \text{ mm}^2$$

- Next, we are able to use the average kill zone diameters measured to find the area of the zone of inhibition; for example we can use the 2.5wt% PLA and PMMA filaments. These are 23.13 mm for the PLA and 22.58 mm for the PMMA.

$$A = \pi r^2$$

$$A_{PLA} = \pi * 23.13^2 = 1686.74 \text{ mm}^2$$

$$A_{PMMA} = \pi * 22.58^2 = 1601.76 \text{ mm}^2$$

- Finally, putting these numbers into the desired ratio, we obtain

$$\frac{SA}{A_{PLA}} = \frac{129.198}{1686.74} = 0.07687$$

$$\frac{SA}{A_{PMMA}} = \frac{129.198}{1601.76} = 0.08066$$

## APPENDIX C

### EDGE EFFECTS BASIC MODEL

For Figure 4-109, inhibition can be modeled the same as the superposition of line and point charges in electromagnetics. Shown below is the equation of a line charge from electromagnetics:

$$E = \frac{Q}{4\pi\epsilon_0 r^2}.$$

If we take  $Q/4\pi\epsilon_0$  to be the concentration of the antibiotic within the material and place this at the corner, we obtain the desired  $1/r^2$  term needed to define the rounded nature and lessened inhibition of the corners. For the edges of the square, they can be treated as line charges with a  $1/r$  decay as shown below:

$$E = \frac{Q}{4\pi\epsilon_0 r}.$$

Again, the  $Q/4\pi\epsilon_0$  will be used to define the concentration of the antibiotic. For the following calculations, notation will come from the square shown below in Figure C-1.

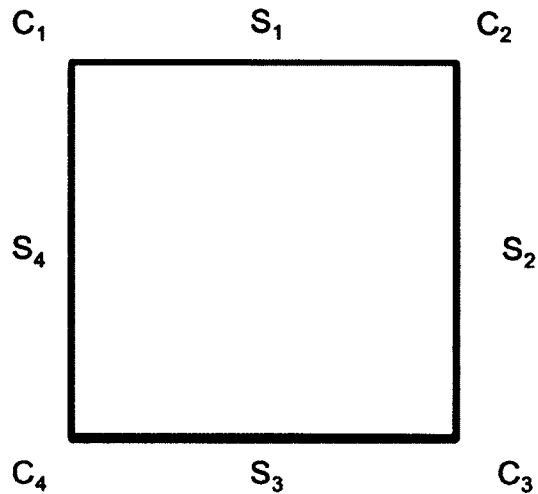


Figure C-1: Model of square sides and corners

By superimposing these together, we can find the given decay at any point away from the material. For cases where the point lies directly above a flat edge such as S<sub>1</sub>, the decay will be defined as:

$$\begin{aligned} \text{Concentration} &= \frac{\text{Concentration from } s_1}{r_{s_1}} + \frac{\text{Concentration from } c_1}{r_{c_1}^2} \\ &+ \frac{\text{Concentration from } c_2}{r_{c_2}^2} \end{aligned}$$

where the radii from the corners can be calculated using Pythagorean theorem, and the r from the side can be taken linearly. Instances where the point measured are removed from the corners will see very little contribution due to the  $1/r^2$  nature.

For instances where the point is very near the corner, the corner term will dominate close to the corner, however have a distinct rounded edge, explaining the edge effects seen in the defense. Using C<sub>1</sub> as an example, a point directly diagonal from C<sub>1</sub> can be characterized by



$$\begin{aligned} \text{Concentration} &= \frac{\text{Concentration from } c_1}{r_{c_1}^2} + \frac{\text{Concentration from } s_1}{r_{s_1}} \\ &+ \frac{\text{Concentration from } s_4}{r_{s_4}} \end{aligned}$$

As the minimum inhibition characteristics were not taken into account during the experiments, further calculations would require further experimental setups.

The above equations were modeled in Matlab to demonstrate the edge effects of a test wafer disc and 3D printed biosquare. The corners can be seen as rounded due to the edge effects from the line and point charges in Figure C-2.

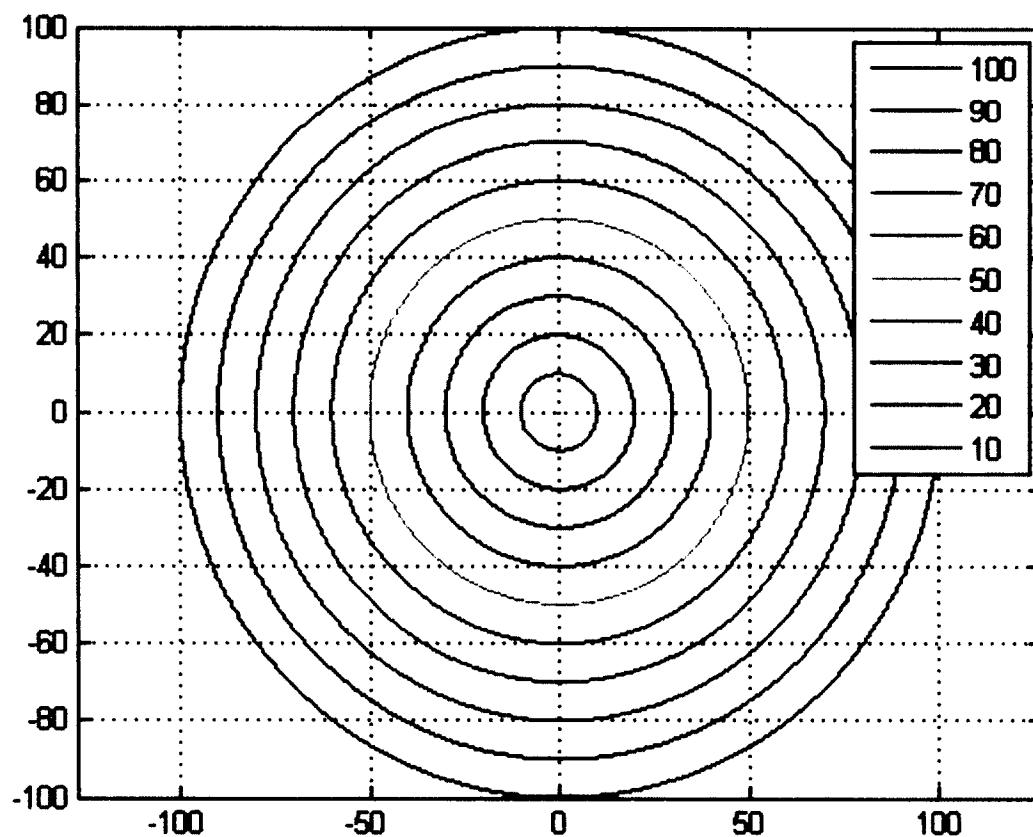


Figure C-2: Test Disc Elution Field

The test disc elution field is modeled and shown to not have edge effects. There are only edges and no corners to create a point from the intersection of two lines. This is seen in Figure C-3

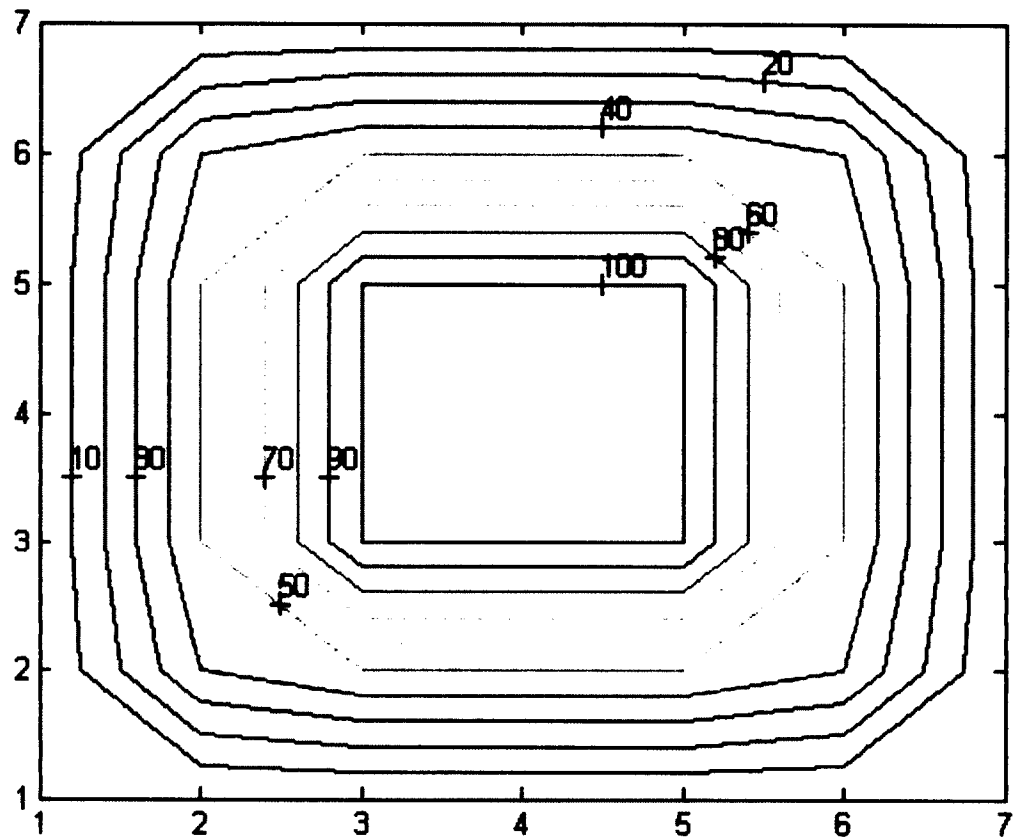


Figure C-3: Biosquare Elution Field

A square field would have to account for both line and point charges in an electric field. In this case the line and point charges result in different concentrations in elution. The minimum inhibitory concentration does not occur from the edges and thus results in a rounded corner.

This work demonstrates theoretical modeling and additional laboratory calculations of minimum inhibitory concentrations would be necessary to generate

additional data to model the precise distances of the zone of elution based upon size of construct.

## BIBLIOGRAPHY

- [1] S. Senthil, J. T. Munro, and R. P. Pitto, "Infection in total hip replacement: meta-analysis," *Int Orthop*, vol. 35, pp. 253-60, Feb 2011.
- [2] J. F. Crowe, T. P. Sculco, and B. Kahn, "Revision total hip arthroplasty: hospital cost and reimbursement analysis," *Clin Orthop Relat Res*, pp. 175-82, Aug 2003.
- [3] D. Nesteruk, K. Wertheim-Tysarowska, and J. Bal, "[Cystic fibrosis emerging therapies.]," *Dev Period Med*, vol. 18, pp. 256-265, 2014.
- [4] M. Dobbelstein and U. Moll, "Targeting tumour-supportive cellular machineries in anticancer drug development," *Nat Rev Drug Discov*, vol. 13, pp. 179-96, Mar 2014.
- [5] P. J. Bergen, C. B. Landersdorfer, H. J. Lee, J. Li, and R. L. Nation, "'Old' antibiotics for emerging multidrug-resistant bacteria," *Curr Opin Infect Dis*, vol. 25, pp. 626-33, Dec 2012.
- [6] T. Wirth, N. Parker, and S. Yla-Herttuala, "History of gene therapy," *Gene*, vol. 525, pp. 162-9, Aug 10 2013.
- [7] M. S. El-Ridy, A. Abdelbary, T. Essam, R. M. El-Salam, and A. A. Kassem, "Niosomes as a potential drug delivery system for increasing the efficacy and safety of nystatin," *Drug Dev Ind Pharm*, vol. 37, pp. 1491-508, Dec 2011.

- [8] M. C. Tanzi, S. Bozzini, G. Candiani, A. Cigada, L. De Nardo, S. Fare, *et al.*, "Trends in biomedical engineering: focus on Smart Bio-Materials and Drug Delivery," *J Appl Biomater Biomech*, vol. 9, pp. 87-97, May-Aug 2011.
- [9] B. Bayram, K. Araz, S. Uckan, and C. Balcik, "Comparison of fixation stability of resorbable versus titanium plate and screws in mandibular angle fractures," *J Oral Maxillofac Surg*, vol. 67, pp. 1644-8, Aug 2009.
- [10] N. A. Fonseca, A. C. Gregorio, A. Valerio-Fernandes, S. Simoes, and J. N. Moreira, "Bridging cancer biology and the patients' needs with nanotechnology-based approaches," *Cancer Treat Rev*, vol. 40, pp. 626-35, Jun 2014.
- [11] S. Ilbasmis-Tamer, S. Yilmaz, E. Banoglu, and I. T. Degim, "Carbon nanotubes to deliver drug molecules," *J Biomed Nanotechnol*, vol. 6, pp. 20-7, Feb 2010.
- [12] K. J. MacKenzie, O. M. Dunens, C. H. See, and A. T. Harris, "Large-scale carbon nanotube synthesis," *Recent Pat Nanotechnol*, vol. 2, pp. 25-40, 2008.
- [13] E. Abdullayev and Y. Lvov, "Halloysite clay nanotubes for controlled release of protective agents," *J Nanosci Nanotechnol*, vol. 11, pp. 10007-26, Nov 2011.
- [14] T. J. Horn and O. L. Harrysson, "Overview of current additive manufacturing technologies and selected applications," *Sci Prog*, vol. 95, pp. 255-82, 2012.
- [15] F. Marga, K. Jakab, C. Khatiwala, B. Shepherd, S. Dorfman, B. Hubbard, *et al.*, "Toward engineering functional organ modules by additive manufacturing," *Biofabrication*, vol. 4, p. 022001, Jun 2012.
- [16] National Academy of Engineering. (2012, February, 2014). *NAE Grand Challenges For Engineering*. Available: <http://www.engineeringchallenges.org/>

- [17] B. Berman, "3-D printing: The new industrial revolution," *Business horizons*, vol. 55, pp. 155-162, 2012.
- [18] S. P. Hunger, X. Lu, M. Devidas, B. M. Camitta, P. S. Gaynon, N. J. Winick, *et al.*, "Improved survival for children and adolescents with acute lymphoblastic leukemia between 1990 and 2005: a report from the children's oncology group," *Journal of Clinical Oncology*, p. JCO. 2011.37. 8018, 2012.
- [19] D. Li, K. Xie, R. Wolff, and J. L. Abbruzzese, "Pancreatic cancer," *The Lancet*, vol. 363, pp. 1049-1057, 2004.
- [20] E. S. Darley and A. P. MacGowan, "Antibiotic treatment of gram-positive bone and joint infections," *Journal of antimicrobial chemotherapy*, vol. 53, pp. 928-935, 2004.
- [21] M. Yamamoto and D. T. Curiel, "Current issues and future directions of oncolytic adenoviruses," *Mol Ther*, vol. 18, pp. 243-50, Feb 2010.
- [22] Y. Juan Juan, C. B. Pollock, and K. Kelly, "Mechanisms of cancer metastasis to the bone," *Cell research*, vol. 15, pp. 57-62, 2005.
- [23] J. M. Jimenez-Andrade, W. G. Mantyh, A. P. Bloom, A. S. Ferng, C. P. Geffre, and P. W. Mantyh, "Bone cancer pain," *Annals of the New York Academy of Sciences*, vol. 1198, pp. 173-181, 2010.
- [24] J. C. Wittig, J. Bickels, D. Priebat, J. Jelinek, K. Kellar-Graney, B. Shmookler, *et al.*, "Osteosarcoma: a multidisciplinary approach to diagnosis and treatment," *American family physician*, vol. 65, pp. 1123-1132, 2002.

- [25] A. Luetke, P. A. Meyers, I. Lewis, and H. Juergens, "Osteosarcoma treatment—where do we stand? A state of the art review," *Cancer treatment reviews*, vol. 40, pp. 523-532, 2014.
- [26] G. Ottaviani and N. Jaffe, "The epidemiology of osteosarcoma," in *Pediatric and Adolescent Osteosarcoma*, ed: Springer, 2010, pp. 3-13.
- [27] E. Hauben, J. Arends, J. Vandenbroucke, C. Van Asperen, E. Van Marck, and P. Hogendoorn, "Multiple primary malignancies in osteosarcoma patients. Incidence and predictive value of osteosarcoma subtype for cancer syndromes related with osteosarcoma," *European journal of human genetics*, vol. 11, pp. 611-618, 2003.
- [28] C. A. Arndt and W. M. Crist, "Common musculoskeletal tumors of childhood and adolescence," *New England Journal of Medicine*, vol. 341, pp. 342-352, 1999.
- [29] A. Berrington de Gonzalez, E. Gilbert, R. Curtis, P. Inskip, R. Kleinerman, L. Morton, *et al.*, "Second solid cancers after radiation therapy: a systematic review of the epidemiologic studies of the radiation dose-response relationship," *International Journal of Radiation Oncology Biology Physics*, vol. 86, pp. 224-233, 2013.
- [30] R. Grimer, S. Cannon, A. Taminiau, S. Bielack, B. Kempf-Bielack, R. Windhager, *et al.*, "Osteosarcoma over the age of forty," *European Journal of Cancer*, vol. 39, pp. 157-163, 2003.
- [31] B. Widhe and T. Widhe, "Initial Symptoms and Clinical Features in Osteosarcoma and Ewing Sarcoma\*," *The Journal of Bone and Joint Surgery*, vol. 82, pp. 667-667, 2000.

- [32] T. Mizowaki, N. Araki, Y. Nagata, Y. Negoro, T. Aoki, and M. Hiraoka, "The use of a permanent magnetic resonance imaging system for radiotherapy treatment planning of bone metastases," *International Journal of Radiation Oncology\* Biology\* Physics*, vol. 49, pp. 605-611, 2001.
- [33] G. Bacci, A. Longhi, S. Ferrari, S. Lari, M. Manfrini, D. Donati, *et al.*, "Prognostic significance of serum alkaline phosphatase in osteosarcoma of the extremity treated with neoadjuvant chemotherapy: recent experience at Rizzoli Institute," *Oncology reports*, vol. 9, pp. 171-175, 2002.
- [34] T. D. Peabody and M. A. Simon, "Making the diagnosis: keys to a successful biopsy in children with bone and soft-tissue tumors," *The Orthopedic clinics of North America*, vol. 27, pp. 453-459, 1996.
- [35] J. U. Ahrar and K. Ahrar, "Ultrasound-Guided Biopsy," in *Percutaneous Image-Guided Biopsy*, ed: Springer, 2014, pp. 39-47.
- [36] T. Bury, A. Barreto, F. Daenen, N. Barthelemy, B. Ghaye, and P. Rigo, "Fluorine-18 deoxyglucose positron emission tomography for the detection of bone metastases in patients with non-small cell lung cancer," *European journal of nuclear medicine*, vol. 25, pp. 1244-1247, 1998.
- [37] M. M. Malawer and K. A. Mchale, "Limb-sparing surgery for high-grade malignant tumors of the proximal tibia: surgical technique and a method of extensor mechanism reconstruction," *Clinical orthopaedics and related research*, vol. 239, pp. 231-248, 1989.
- [38] G. Rosen, "Preoperative (neoadjuvant) chemotherapy for osteogenic sarcoma: a ten year experience," *Orthopedics*, vol. 8, pp. 659-664, 1985.



- [39] M. P. Link, A. M. Goorin, M. Horowitz, W. H. Meyer, J. Belasco, A. Baker, *et al.*, "Adjuvant chemotherapy of high-grade osteosarcoma of the extremity: updated results of the Multi-Institutional Osteosarcoma Study," *Clinical orthopaedics and related research*, vol. 270, pp. 8-14, 1991.
- [40] D. Carrle and S. S. Bielack, "Current strategies of chemotherapy in osteosarcoma," *International orthopaedics*, vol. 30, pp. 445-451, 2006.
- [41] J. K. Anninga, H. Gelderblom, M. Fiocco, J. R. Kroep, A. H. Taminiau, P. C. Hogendoorn, *et al.*, "Chemotherapeutic adjuvant treatment for osteosarcoma: where do we stand?," *European journal of cancer*, vol. 47, pp. 2431-2445, 2011.
- [42] J.-p. Chu, W. Chen, J.-p. Li, W.-q. Zhuang, Y.-h. Huang, Z.-m. Huang, *et al.*, "Clinicopathologic features and results of transcatheter arterial chemoembolization for osteosarcoma," *Cardiovascular and interventional radiology*, vol. 30, pp. 201-206, 2007.
- [43] H.-J. Zhang, J.-J. Yang, J.-P. Lu, C.-J. Lai, J. Sheng, Y.-X. Li, *et al.*, "Use of intra-arterial chemotherapy and embolization before limb salvage surgery for osteosarcoma of the lower extremity," *Cardiovascular and interventional radiology*, vol. 32, pp. 672-678, 2009.
- [44] J. W. Cullen, B. A. Jamroz, S. L. Stevens, W. Madsen, I. Hinshaw, R. M. Wilkins, *et al.*, "The value of serial arteriography in osteosarcoma: delivery of chemotherapy, determination of therapy duration, and prediction of necrosis," *Journal of vascular and interventional radiology*, vol. 16, pp. 1107-1119, 2005.

- [45] M. Los and E. E. Voest, "The potential role of antivascular therapy in the adjuvant and neoadjuvant treatment of cancer," in *Seminars in oncology*, 2001, pp. 93-105.
- [46] K. Hamada, Y. Tomita, A. Inoue, T. Fujimoto, N. Hashimoto, A. Myoui, *et al.*, "Evaluation of chemotherapy response in osteosarcoma with FDG-PET," *Annals of nuclear medicine*, vol. 23, pp. 89-95, 2009.
- [47] W. Williard, S. I. Hajdu, E. S. Casper, and M. F. Brennan, "Comparison of amputation with limb-sparing operations for adult soft tissue sarcoma of the extremity," *Annals of surgery*, vol. 215, p. 269, 1992.
- [48] X. Li, V. M. Moretti, A. O. Ashana, and R. D. Lackman, "Impact of close surgical margin on local recurrence and survival in osteosarcoma," *International orthopaedics*, vol. 36, pp. 131-137, 2012.
- [49] S. Miura, Y. Mii, Y. Miyauchi, H. Ohgushi, T. Morishita, K. Hohnoki, *et al.*, "Efficacy of slow-releasing anticancer drug delivery systems on transplantable osteosarcomas in rats," *Japanese journal of clinical oncology*, vol. 25, pp. 61-71, 1995.
- [50] S. Natsugoe, T. Kumanohoso, K. Tokuda, M. Shimada, J. Mueller, K. Nakamura, *et al.*, "Controlled release of cisplatin incorporated into biodegradable poly-d, l-lactic acid," *Anticancer research*, vol. 17, pp. 1957-1960, 1996.
- [51] S. J. Withrow, J. M. Liptak, R. C. Straw, W. S. Dernell, V. J. Jameson, B. E. Powers, *et al.*, "Biodegradable cisplatin polymer in limb-sparing surgery for canine osteosarcoma," *Annals of surgical oncology*, vol. 11, pp. 705-713, 2004.

- [52] K. Gulati, S. Ramakrishnan, M. S. Aw, G. J. Atkins, D. M. Findlay, and D. Losic, "Biocompatible polymer coating of titania nanotube arrays for improved drug elution and osteoblast adhesion," *Acta biomaterialia*, vol. 8, pp. 449-456, 2012.
- [53] M. MacKinnon and K. Allen, "Long-term MRSA carriage in hospital patients," *Journal of Hospital Infection*, vol. 46, pp. 216-221, 2000.
- [54] V. G. Fowler, S. M. O'Brien, L. H. Muhlbaier, G. R. Corey, T. B. Ferguson, and E. D. Peterson, "Clinical predictors of major infections after cardiac surgery," *Circulation*, vol. 112, pp. I-358-I-365, 2005.
- [55] D. P. Lew and F. A. Waldvogel, "Osteomyelitis," *The Lancet*, vol. 364, pp. 369-379, 2004.
- [56] L. Lazzarini, J. T. Mader, and J. H. Calhoun, "Osteomyelitis in long bones," *The Journal of Bone and Joint Surgery*, vol. 86, pp. 2305-2318, 2004.
- [57] Ø. R. Riise, E. Kirkhus, K. S. Handeland, B. Flatø, T. Reiser, M. Cvancarova, *et al.*, "Childhood osteomyelitis-incidence and differentiation from other acute onset musculoskeletal features in a population-based study," *BMC pediatrics*, vol. 8, p. 45, 2008.
- [58] D. P. Lew and F. A. Waldvogel, "Osteomyelitis," *New England Journal of Medicine*, vol. 336, pp. 999-1007, 1997.
- [59] P. A. Mackowiak and J. W. Smith, "Polymicrobial infections in osteomyelitis," *Review of Infectious Diseases*, vol. 5, pp. 167-168, 1983.
- [60] D. R. Dirschl and L. C. Almekinders, "Osteomyelitis," *Drugs*, vol. 45, pp. 29-43, 1993.

- [61] R. David, B. Barron, and J. Madewell, "Osteomyelitis, acute and chronic," *Radiologic Clinics of North America*, vol. 25, pp. 1171-1201, 1987.
- [62] E. Goergens, A. McEvoy, M. Watson, and I. Barrett, "Acute osteomyelitis and septic arthritis in children," *Journal of paediatrics and child health*, vol. 41, pp. 59-62, 2005.
- [63] B. A. Lipsky, A. R. Berendt, H. G. Deery, J. M. Embil, W. S. Joseph, A. W. Karchmer, *et al.*, "Diagnosis and treatment of diabetic foot infections," *Clinical Infectious Diseases*, vol. 39, pp. 885-910, 2004.
- [64] J. Mader, J. Wang, M. Shirliff, J. Calhoun, and J. Tan, "Osteomyelitis," *Expert guide to infectious diseases*, pp. 585-604, 2002.
- [65] C. K. Chua, K. F. Leong, and C. S. Lim, *Rapid prototyping: principles and applications*: World Scientific, 2010.
- [66] J. Flowers and M. Moniz, "Rapid prototyping in technology education," *Technology Teacher*, vol. 62, pp. 7-25, 2002.
- [67] C. C. Kai, C. S. Meng, L. S. Ching, E. K. Hoe, and L. K. Fah, "Rapid prototyping assisted surgery planning," *The International Journal of Advanced Manufacturing Technology*, vol. 14, pp. 624-630, 1998.
- [68] J.-P. Kruth, "Material increment manufacturing by rapid prototyping techniques," *CIRP Annals-Manufacturing Technology*, vol. 40, pp. 603-614, 1991.
- [69] S. Morvan, R. Hochsmann, and A. CARRARO, "Rapid Manufacturing finally delivers: the Prometal RCT process, for the fabrication of complex sand molds and sand cores," in *RPD Conference*, 2004.

- [70] K. Thrimurthulu, P. M. Pandey, and N. Venkata Reddy, "Optimum part deposition orientation in fused deposition modeling," *International Journal of Machine Tools and Manufacture*, vol. 44, pp. 585-594, 2004.
- [71] R. Singh, "Process capability study of polyjet printing for plastic components," *Journal of mechanical science and technology*, vol. 25, pp. 1011-1015, 2011.
- [72] V. Petrovic, J. Vicente Haro Gonzalez, O. Jorda Ferrando, J. Delgado Gordillo, J. Ramon Blasco Puchades, and L. Portoles Grinan, "Additive layered manufacturing: sectors of industrial application shown through case studies," *International Journal of Production Research*, vol. 49, pp. 1061-1079, 2011.
- [73] K. Cooper, *Rapid prototyping technology: selection and application*: CRC press, 2001.
- [74] V. K. Balla, S. Bose, and A. Bandyopadhyay, "Processing of bulk alumina ceramics using laser engineered net shaping," *International Journal of Applied Ceramic Technology*, vol. 5, pp. 234-242, 2008.
- [75] Y. Liao, H. Li, and Y. Chiu, "Study of laminated object manufacturing with separately applied heating and pressing," *The International Journal of Advanced Manufacturing Technology*, vol. 27, pp. 703-707, 2006.
- [76] G. V. Salmoria, R. A. Paggi, A. Lago, and V. E. Beal, "Microstructural and mechanical characterization of PA12/MWCNTs nanocomposite manufactured by selective laser sintering," *Polymer Testing*, vol. 30, pp. 611-615, 2011.
- [77] J. W. Halloran, V. Tomeckova, S. Gentry, S. Das, P. Cilino, D. Yuan, *et al.*, "Photopolymerization of powder suspensions for shaping ceramics," *Journal of the European Ceramic Society*, vol. 31, pp. 2613-2619, 2011.

- [78] H.-H. Tang, M.-L. Chiu, and H.-C. Yen, "Slurry-based selective laser sintering of polymer-coated ceramic powders to fabricate high strength alumina parts," *Journal of the European Ceramic Society*, vol. 31, pp. 1383-1388, 2011.
- [79] M. J. Cima, J. S. Haggerty, E. M. Sachs, and P. A. Williams, "Three-dimensional printing techniques," ed: Google Patents, 1993.
- [80] D. Jijotiya and P. L. Verma, "A Survey of Performance based Advanced Rapid Prototyping Techniques."
- [81] D. Dimitrov, K. Schreve, and N. De Beer, "Advances in three dimensional printing-state of the art and future perspectives," *Journal for New Generation Sciences*, vol. 4, pp. p. 21-49, 2006.
- [82] P. J. Kitson, A. Macdonell, S. Tsuda, H. Zang, D.-L. Long, and L. Cronin, "Bringing Crystal Structures to Reality by Three-Dimensional Printing," *Crystal Growth and Design*, 2014.
- [83] S. J. Leigh, R. J. Bradley, C. P. Purcell, D. R. Billson, and D. A. Hutchins, "A simple, low-cost conductive composite material for 3D printing of electronic sensors," *PloS one*, vol. 7, p. e49365, 2012.
- [84] P. Z. PM, J. Cole, H. Lu, and W. Weise, "LITERATURE REVIEW 3D PRINTER," 2013.
- [85] M. Frauenfelder, *Make: Ultimate guide to 3D printing 2014*: Maker Media, Inc., 2013.
- [86] S. Bordeepong, D. Bhongsuwan, T. Pungrassami, and T. Bhongsuwan, "Characterization of halloysite from Thung Yai District, Nakhon Si Thammarat

- Province, in Southern Thailand," *Sonklanakarin Journal of Science and Technology*, vol. 33, p. 599, 2011.
- [87] M. Liu, B. Guo, M. Du, Y. Lei, and D. Jia, "Natural inorganic nanotubes reinforced epoxy resin nanocomposites," *Journal of Polymer Research*, vol. 15, pp. 205-212, 2008.
- [88] Y. M. Lvov, D. G. Shchukin, H. Mohwald, and R. R. Price, "Halloysite clay nanotubes for controlled release of protective agents," *Acs Nano*, vol. 2, pp. 814-820, 2008.
- [89] N. G. Veerabadrán, R. R. Price, and Y. M. Lvov, "Clay nanotubes for encapsulation and sustained release of drugs," *Nano*, vol. 2, pp. 115-120, 2007.
- [90] W. O. Yah, A. Takahara, and Y. M. Lvov, "Selective modification of halloysite lumen with octadecylphosphonic acid: new inorganic tubular micelle," *Journal of the American Chemical Society*, vol. 134, pp. 1853-1859, 2012.
- [91] G. Nitya, G. T. Nair, U. Mony, K. P. Chennazhi, and S. V. Nair, "In vitro evaluation of electrospun PCL/nanoclay composite scaffold for bone tissue engineering," *Journal of Materials Science: Materials in Medicine*, vol. 23, pp. 1749-1761, 2012.
- [92] E. Abdullayev and Y. Lvov, "Halloysite clay nanotubes for controlled release of protective agents," *Journal of nanoscience and nanotechnology*, vol. 11, pp. 10007-10026, 2011.
- [93] M. Liu, Z. Jia, D. Jia, and C. Zhou, "Recent advance in research on halloysite nanotubes-polymer nanocomposite," *Progress in Polymer Science*, 2014.

- [94] Y. Lvov and E. Abdullayev, "Functional polymer–clay nanotube composites with sustained release of chemical agents," *Progress in Polymer Science*, vol. 38, pp. 1690-1719, 2013.
- [95] D. Mills, "Biocompatibility of halloysite clay nanotubes in a rat dermal model (87.4)," *The FASEB Journal*, vol. 28, p. 87.4, 2014.
- [96] W. Wei, E. Abdullayev, A. Hollister, D. Mills, and Y. M. Lvov, "Clay nanotube/poly (methyl methacrylate) bone cement composites with sustained antibiotic release," *Macromolecular Materials and Engineering*, vol. 297, pp. 645-653, 2012.
- [97] J. V. Hoene, R. G. Charles, and W. M. Hickam, "Thermal decomposition of metal acetylacetonates: mass spectrometer studies," *The Journal of Physical Chemistry*, vol. 62, pp. 1098-1101, 1958.
- [98] J. R. Brody, E. S. Calhoun, E. Gallmeier, T. D. Creavalle, and S. E. Kern, "Ultra-fast high-resolution agarose electrophoresis of DNA and RNA using low-molarity conductive media," *Biotechniques*, vol. 37, pp. 598-602, 2004.
- [99] B. Pal and M. Sharon, "Preparation of iron oxide thin film by metal organic deposition from Fe (III)-acetylacetonate: a study of photocatalytic properties," *Thin Solid Films*, vol. 379, pp. 83-88, 2000.
- [100] F. R. DiMaio, "The science of bone cement: a historical review," *Orthopedics*, vol. 25, pp. 1399-407; quiz 1408-9, 2002.
- [101] S. Breusch and K. Kühn, "[Bone cements based on polymethylmethacrylate]," *Der Orthopade*, vol. 32, pp. 41-50, 2003.



- [102] G. Lewis, "Properties of acrylic bone cement: state of the art review," *Journal of biomedical materials research*, vol. 38, pp. 155-182, 1997.
- [103] J. E. Block and H. A. Stubbs, "Reducing the risk of deep wound infection in primary joint arthroplasty with antibiotic bone cement," *ORTHOPEDICS-NEW JERSEY*, vol. 28, p. 1334, 2005.
- [104] D. A. Wininger and R. J. Fass, "Antibiotic-impregnated cement and beads for orthopedic infections," *Antimicrobial agents and chemotherapy*, vol. 40, p. 2675, 1996.
- [105] D. Heck, A. Rosenberg, M. Schink-Ascani, S. Garbus, and T. Kiewitt, "Use of antibiotic-impregnated cement during hip and knee arthroplasty in the United States," *The Journal of arthroplasty*, vol. 10, pp. 470-475, 1995.
- [106] J. Leggett, S. Ebert, B. Fantin, and W. Craig, "Comparative dose-effect relations at several dosing intervals for beta-lactam, aminoglycoside and quinolone antibiotics against gram-negative bacilli in murine thigh-infection and pneumonitis models," *Scandinavian journal of infectious diseases. Supplementum*, vol. 74, pp. 179-184, 1989.
- [107] M. Rubin, J. W. Hathorn, D. Marshall, J. Gress, S. M. Steinberg, and P. A. Pizzo, "Gram-positive infections and the use of vancomycin in 550 episodes of fever and neutropenia," *Annals of internal medicine*, vol. 108, pp. 30-35, 1988.
- [108] E. Lautenschlager, G. Marshall, K. Marks, J. Schwartz, and C. Nelson, "Mechanical strength of acrylic bone cements impregnated with antibiotics," *Journal of biomedical materials research*, vol. 10, pp. 837-845, 1976.

- [109] P. Frutos Cabanillas, E. Díez Peña, J. Barrales-Rienda, and G. Frutos, "Validation and in vitro characterization of antibiotic-loaded bone cement release," *International journal of pharmaceutics*, vol. 209, pp. 15-26, 2000.
- [110] Sigma Aldrich. (February, 2014). *Iron(III) acetylacetonate*. Available: <http://www.sigmaaldrich.com/catalog/product/aldrich/f300?lang=en&region=US>
- [111] Avanti Polar Lipids Inc. (February, 2014). *18:1 TAP (DOTAP)*. Available: [http://avantilipids.com/index.php?option=com\\_content&view=article&id=946&Itemid=156&catnumber=890890](http://avantilipids.com/index.php?option=com_content&view=article&id=946&Itemid=156&catnumber=890890)
- [112] Sigma Aldrich. (February, 2014). *Polyvinylpyrrolidone* Available: <http://www.sigmaaldrich.com/catalog/product/sial/pvp40?lang=en&region=US>
- [113] E. Abdullayev, R. Price, D. Shchukin, and Y. Lvov, "Halloysite tubes as nanocontainers for anticorrosion coating with benzotriazole," *ACS applied materials & interfaces*, vol. 1, pp. 1437-1443, 2009.
- [114] Decoster, Mark. 2010. An Electromagnetic Probe Device. U.S. Patent US 7763175 filed May 17, 2005, and issued July 27, 2010
- [115] S. Deodhar, J. Huckaby, M. Delahoussaye, and M. A. DeCoster, "High-Aspect Ratio Bio-Metallic Nanocomposites for Cellular Interactions," in *IOP Conference Series: Materials Science and Engineering*, 2014, p. 012014.
- [116] G. Parekh, P. Pattekari, C. Joshi, T. Shutava, M. DeCoster, T. Levchenko, *et al.*, "Layer-by-layer nanoencapsulation of camptothecin with improved activity," *International journal of pharmaceutics*, vol. 465, pp. 218-227, 2014.
- [117] R. F. Egerton, *Electron energy-loss spectroscopy in the electron microscope* vol. 233: Springer, 1996.

- [118] Extrusionbot. (February, 2014). *PLA Pellets*. Available:  
<http://www.extrusionbot.com/products/>
- [119] Nature Works LLC. (February, 2014). *PLA Technical Data Sheet*. Available:  
<http://www.natureworksllc.com/Technical-Resources/Technical-Documentation>
- [120] Sigma Aldrich. (February, 2014). *PMMA Structure*. Available:  
<http://www.sigmaaldrich.com/materials-science/material-science-products.html?TablePage=113790840>
- [121] Sigma Aldrich. (February, 2014). *Gentamicin Sulfate*. Available:  
<http://www.sigmaaldrich.com/catalog/product/sigma/g1264?lang=en&region=US>
- [122] Sigma Aldrich. (February, 2014). *Gentamicin, Tobramycin and Nitrofurantoin Specification Sheet*.
- [123] Dassault Systemes. (May, 2014). *SolidWorks Screen*. Available:  
<http://www.solidworks.com/>
- [124] Makerbot Inc. (May, 2014). *Makerbot 3D Printers*. Available:  
<http://www.makerbot.com>
- [125] Sigma Aldrich. (February, 2014). *Polycaprolactone*. Available:  
<http://www.sigmaaldrich.com/catalog/product/aldrich/440744?lang=en&region=US>
- [126] Sigma Aldrich. (February, 2014). *Methotrexate*. Available:  
<http://www.sigmaaldrich.com/catalog/product/fluka/m1000000?lang=en&region=US>
- [127] Sigma Aldrich. (May, 2014). *XTT Reagent Image*. Available:  
<http://www.sigmaaldrich.com/catalog/product/sigma/x4626?lang=en&region=US>

[128] S. Aldrich, "Polycaprolactone Specification Sheet," 2014.